The development of protein-functionalised plasma polymer biointerfaces for orthopaedic applications

Callum Arthur Charles Stewart

A thesis submitted in fulfilment of the requirements for the degree of Doctor of Philosophy

School of Physics

The University of Sydney

2019

Statement of Originality

This is to certify that to the best of my knowledge, the content of this thesis is my own work. All the assistance received in preparing this thesis and sources have been acknowledged. This thesis has not been submitted for any degree or other purposes.

_____

Callum Arthur Charles Stewart

Thesis Abstract

Orthopaedic implants are an ever-growing global industry with hundreds of thousands of operations performed annually. Titanium alloys are the standard material for load-bearing orthopaedic devices because of their biocompatibility and favourable mechanical properties. Despite a variety of surgical strategies, a significant number of implants experience post-operative complications, such as bacterial-film formation and fibrotic encapsulation, or long-term implant loosening due to bone resorption. Biomolecule functionalisation with proteins or peptides is a promising approach to create a biologically-active surface that reduces the potential for adverse post-operative complications and encourages bone formation. The biomolecules commonly utilised for enhancing bone formation either increase cell recruitment by simulating the natural extracellular matrix or accelerating the bone formation through mineralisation. An optimum functionalisation would include multiple active biomolecules so that attachment and mineralisation would be enhanced simultaneously. Previously, biomolecule-functionalisation of titanium surfaces was performed through physical adsorption, chemical covalent linker molecules, or plasma-based technologies that require subsequent wet chemical processing. Few techniques have provided a simple, reproducible, and scalable approach to transition from the laboratory into a manufacturing setting. There is currently no approach that enables the covalent immobilisation of multiple biomolecules to a surface.

This thesis explores the application of radical-functionalised plasma polymers films (rPPFs) as multifunctional protein biointerfaces for orthopaedics. rPPFs are a dry, plasma deposited coating that modifies surfaces for covalent attachment of biomolecules through embedded unpaired electrons. The mechanical and biological properties of rPPF coatings were optimised for titanium substrates, and the effects of the radical fluxes on surface chemistry and cell behaviour were investigated. Two multifunctional protein surfaces were developed and comparatively examined against the component proteins for bone formation potential with primary osteoblasts and mesenchymal stem cells. Overall,

this work shows the versatility of rPPFs and opens a potential avenue for translating multiple biomolecule-functionalisation into the manufacturing environment.

Table of Contents

Acknowledgements

First and foremost, I would like to thank my supervisors Prof. Marcela Bilek, Dr Behnam Akhavan, and Dr Steven Wise for your sage advice, patience, and encouragement over the last 3.5 years of PhD. Without you, there would be no thesis. Thank you, Marcela, for letting me participate in the development of a unique and versatile project. Thank you, Behnam, for always being available for discussion on work and academic life alike. Dr Steve Wise providing advice and support in the biological reaches of this thesis. A special thanks to Dr Shisan 'Bob' Bao for allowing me to perform biochemical and cellular experiments in your laboratory.

The multidisciplinary nature of this thesis allowed me to collaborate with numerous departments across the university, without whom the project would not have been as interesting or successful. I would like to thank all the members of the Applied and Plasma Physics department, especially Thao Tran, Elena Kosobrodova, Lewis Martin, Enyi Guo, Miguel Santos, and Kosta Tsoukas. Each of you has been friendly, hospitable, and open to discussions on a variety of topics. I would like to thank Dr Wojciech Chrzanowski and his students, Sally Kim and Dipesh Kanal, in the school of Pharmacy for their friendship and assistance when I was starting my PhD. To JuiChien Hung, Richard Tran, Alex Chan, Bob Lee, and Praveesuda 'Joy' Michael at the Heart Research Institute, thank you for the all the help you have given during my time working with you. I wish you all the best as you head off into the world.

To all the staff at Physics, Pharmacy, Australian Centre for Microscopy and Microanalysis, Charles Perkins Centre, and the Heart Research Institute; your friendly assistance despite our foibles is greatly appreciated by not only myself but all the students and researchers.

I would like to thank my family and friends for putting up with the late hours and absences, smiling and nodding at my incomprehensible ramblings, the bad moods from failed tests, and for celebrating the wins with me. You are the reason I am not as 'mad scientist' as I could have been.

"Though one may be overpowered, two can defend themselves. A cord of three strands is not quickly broken." - Ecclesiastes 4:12

I would like to acknowledge the contributions of other researchers, fellow students, and staff members who assisted in this multidisciplinary work; Dr Behnam Akhavan for performing the X-Ray photoelectron spectroscopy measurements and plasma polymer deposition training, Miguel Santos and Dr Clare Hawkins for training on electron paramagnetic resonance (EPR), and JuiChien Hung for the harvesting and culturing of the primary cells used in the cell assays.

Academic output

Publications

Stewart, C., Akhavan, B., Wise, S., and Bilek, M. *A review of biomimetic surface functionalization for bone-integrating orthopedic implants: Mechanisms, current approaches, and future directions.* Progress in Materials Science. (Under review)

Stewart, C., Akhavan, B., Santos, M., Hung, J., Hawkins, C., Bao, S., Wise, S. and Bilek, M. **(2018)**. *Cellular responses to radical propagation from ion-implanted plasma polymer surfaces.* Applied Surface Science, 456, pp.701-710.

Stewart, C., Akhavan, B., Hung, J., Bao, S., Jang. J-H, Wise, S.G, and Bilek, M. **(2018)** *Multifunctional protein-immobilised plasma polymer coatings for orthopaedic applications.* ACS Biomaterials Science and Engineering. (Accepted).

Conference proceedings

The 9th Vacuum and Surface Science Conference of Asia and Australia, 13th-16th August 2018, **Technical support and Poster**: *Protein-functionalised Plasma Activated Coatings for Orthopaedic Applications*

Australian Nanotechnology Network Entrepreneur workshop, 12-13 July 2017, **Poster***: Protein-functionalised Plasma Activated Coatings for Orthopaedic Applications*

Advanced materials and Nanotechnology 8, 12-16 February 2017, **oral:** *Plasma polymer age and its effect on cell proliferation*

Authorship attribution statement

Chapter 1 of this thesis has been submitted as a review manuscript to Progress in Materials Science as:

Stewart, C., Akhavan, B., Wise, S., and Bilek, M. *A review of biomimetic surface functionalization for bone-integrating orthopedic implants: Mechanisms, current approaches, and future directions.* Progress in Materials Science. (Under review)

I performed the literature research and wrote the manuscript.

Chapter 4 of this thesis is published as:

Stewart, C., Akhavan, B., Santos, M., Hung, J., Hawkins, C., Bao, S., Wise, S. and Bilek, M. **(2018)**. *Cellular responses to radical propagation from ion-implanted plasma polymer surfaces.* Applied Surface Science, 456, pp.701-710.

I designed the study with help of supervisors, co-acquired, analysed and interpreted the data and wrote the manuscript.

Chapter 5 and 6 are partially published as:

Stewart, C., Akhavan, B., Hung, J., Bao, S., Jang. J-H, Wise, S.G, and Bilek, M. **(2018)** *Multifunctional protein-immobilised plasma polymer coatings for orthopaedic applications.* ACS Biomaterials Science and Engineering. (Accepted).

I designed the study with help of supervisors, co-acquired, analysed and interpreted the data and wrote the manuscript.

Callum A.C. Stewart: Date:

As supervisors for the candidature upon which this thesis is based, I can confirm that the authorship attribution statements above are correct.

Marcela M.M. Bilek: Date:

Behnam Akhavan: Date:

Abbreviations

HRI – Heart Research Institute

CPC – Charles Perkins Centre

ACMM – Australian Centre of Microscopic and microanalysis

rPPF – radical-functionalised plasma polymer film

cPPF – chemical-functionalised plasma polymer film

PECVD – Plasma enhanced chemical vapour deposition

SEM – Scanning electron microscopy/microscope

XPS – X-ray photoelectron spectroscopy

EPR – electron paramagnetic resonance

AFM – Atomic force microscopy/ microscope

DMEM – Dulbecco's Modified Eagle's Medium

FBS - Fetal bovine serum

PBS – Phosphate buffer solution

BSA – Bovine serum albumin

ELISA – Enzyme-Linked Immunosorbent Assay

ECM - Extracellular matrix

FN - Fibronectin

OCN - Osteocalcin

FN-OCN / fusion – a custom fibronectin (9,10)-OCN (22-49) fusion protein

MG63 – Osteosarcoma cell line (MG63)

OB – Osteoblast

MSC – mesenchymal stem cell

List of Figures

3.1. The atomic composition of rPPF coatings deposited with varying nitrogen and acetylene precursor gas ratios

3.2. High-resolution C1s fitting of rPPFs with increasing nitrogen content after 24 hours.

3.3. Scanning electron microscopy (SEM) images of cell formation and rPPF integrity on the varying N% at day 3 and day 7 growth time points compared to titanium.

3.4. Representative surface topology traces performed on AFM

3.5. MG63 cell proliferation assay results over one week on rPPFs with varying N%.

4.1. Elemental composition of the radical-functionalised PPFs as a function of time determined by XPS.

4.2. C1s XPS spectra recorded after various ageing times: 15 min, 4 h, 24 h, 48 h, 7 days, 11 days, and 14 days time points

4.3. ATR-FTIR spectra showing rPPFs surface chemistry after ageing times of 15 minutes, 4 hour, 11 days, and 14 days.

4.4. Surface energy and water contact angle for rPPF deposited on Ti foils as a function of time after deposition.

4.5. **a)** The EPR spectrum of fresh and aged rPPF deposited on polystyrene foils. **b)** The radical density decay curve fitted to the double exponential trend, $Y=A_0 + A_1*\exp(-x/t_1) + A_2*\exp(-x/t_2)$

4.6. Osteoblast cell attachment, spreading, and proliferation on Ti, fresh rPPF, and aged rPPF.

4.7. MG63 Cell attachment and proliferation on untreated Ti, and the fresh and aged rPPF surfaces.

5.1. Characterisation of the rPPF surface.

5.2. Fibronectin ELISA surface quantification.

5.3. OCN mid-sequence ELISA surface quantification.

5.4. ELISA optimisation and quantification of FN-OCN fusion protein surfaces.

5.5. ELISA quantification of the co-immobilised rPPF surfaces.

5.6. A visual representation of protein equilibrium on Ti and rPPF surfaces.

List of Tables

Chapter 1 – Introduction

The subject of biomolecule-functionalisation with applications in orthopaedic devices is examined in this chapter. The current materials used for orthopaedic devices and their limitations that drive the need for biomolecule-functionalisation are highlighted. The surface properties that govern protein-surface interactions are explained, before reviewing and discussing the progress in biomolecule-functionalisation of orthopaedic surfaces performed via adsorption, chemical covalent immobilisation, and physical covalent immobilisation. The immobilisation mechanisms for each approach are examined, and the strategies are evaluated according to their complexity, efficacy, reproducibility, and scalability. Finally, the motivation for the application of radical-functionalised plasma polymer coatings for bio-functionalisation of orthopaedic surfaces is outlined.

The chapter is adapted from a manuscript invited for submission at Progress in Materials science based on a prior editorial review: 'A review of biomimetic surface functionalization for bone-integrating orthopedic implants: Mechanisms, current approaches, and future directions', by Callum Stewart, Behnam Akhavan, Steven G. Wise, and Marcela M. M. Bilek.

1. Literature review

1.1 Biological interactions with orthopaedic implant surfaces

The prevalence of orthopaedic or bone implants has greatly increased worldwide. For example, in Australia alone, close to a million total hip and knee replacement operations have been performed since 1999, around 10% of which required revision surgeries due to problems associated with poor bone integration [1]. Despite strategies such as optimised surgical implant techniques, aseptic surgical conditions, and increased postoperative care [2], a significant proportion of implants fail due to poor

integration with adjacent bone tissue. Failure to rapidly promote the growth of new bone on their surface leaves implants susceptible to encapsulation by fibrotic tissue in a process known as the foreign body reaction [3-5], and bacterial colonisation leading to biofilm formation on the implant surface [6, 7]. Biofilm formation leads to infections that can often only be eliminated by surgical removal of the implant; whilst the presence of fibrotic tissue at the bone-implant interface often interferes with implant fixation and function, also often requiring repeat surgical intervention [2, 3]. The costs, risks, and patient discomfort of revision surgery provide a compelling need for surface modifications that facilitate rapid osseointegration or the growth of new natural bone on and around the implant surface. With the increasing number of orthopaedic implants performed annually worldwide and the need for longer implant lifetimes as lifespans increase, the need for optimally osseointegrating bone implants is becoming more significant.

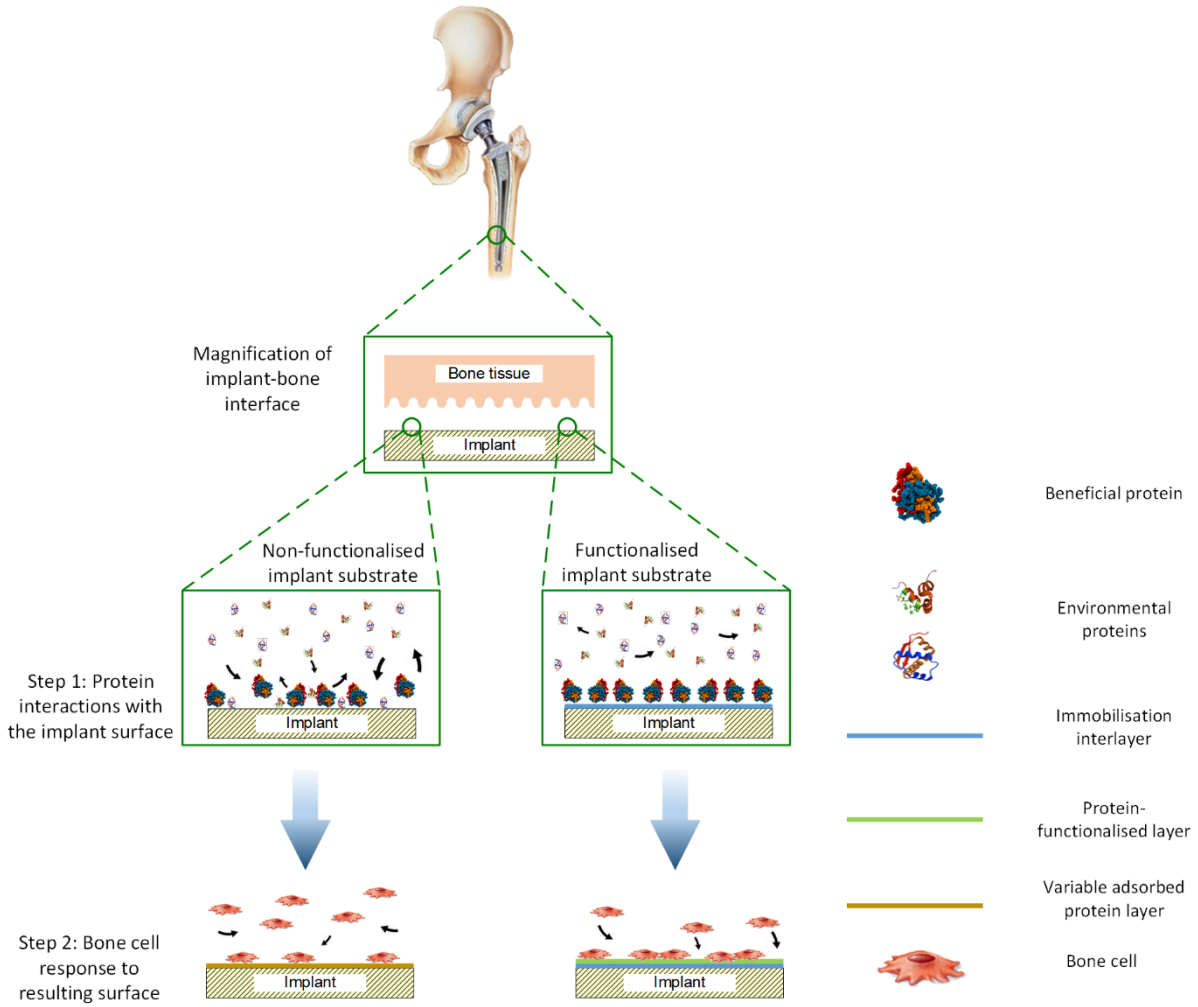

Figure 1.1. A diagrammatic representation of the initial stages of implant osseointegration for non-functionalised (current orthopaedic implants) and biomolecule functionalised implants. After implantation, the implant surface interacts with the biological environment. The surfaces of non-functionalised implants become coated in proteins from the environment forming a variable protein layer (as described by the Vroman effect). The cellular response to the variable protein layer changes with the composition leading to unfavourable immune response, infection, or failure to integrate. Biomolecule-functionalised surfaces produce a defined layer of biomolecules for a more controlled biological response leading to improved osseointegration.

Orthopaedic implants are categorised into non-load bearing and load bearing, depending on the application of the device. Non-load bearing implants are devices like screws or maxillofacial plates that provide structure but do not support weight. The preferred materials for non-load bearing devices

are resorbable ceramics chemically similar to bone, such as hydroxyapatite (HA) [8, 9], or biodegradable polymers, such as polycaprolactone (PCL) [10-12]. In this case, the role of the implant is to facilitate the formation of natural bone that gradually fills the volume of the implanted scaffold as it degrades. Load bearing implants, like artificial knees and hips, on the other hand, must be able to support the patient's weight during movement. Materials used for the fabrication of these implants must be capable of retaining their shape under significant mechanical forces applied repetitively. Polymeric materials are not generally strong enough to support repetitive loading without plastic deformation [13]. The exception is polyether (ether ketone) (PEEK) which has mechanical properties close to those of natural bone and has found applications in spinal implants [14-17]. Ceramic materials do not exhibit the necessary flexibility due to their high degree of ionic bonding [18]. Metallic materials, however, demonstrate the required mechanical strength to support physical loading and the level of elastic deformation needed to resist failure under cyclic physiological stresses.

Three metallic alloys have been widely investigated during the development of orthopaedic implants over the last century; stainless steel, cobalt chromium (CoCr), and titanium (Ti). Initially proposed in the 1940's [19], Ti and its alloys have been used almost exclusively for the latter half of the twentieth century. Numerous Ti alloys have been investigated for the fabrication of bone implants and have been thoroughly reviewed elsewhere [20-22]. One of the later developments has been the production of porous Ti alloys that show enhanced osseointegration [23], but possess lower mechanical strength because the pores act as stress concentrators [24, 25].

For orthopaedic implants, titanium alloys are superior to stainless steel and CoCr alloys due to their lower modulus of elasticity and greater biocompatibility. Titanium alloys have an elastic modulus of between 50 - 118 GPa as listed in **Table 1.1** [20-22]. This modulus is half that of stainless steel (216 GPa) and CoCr alloys (240 GPa) but is still 2 to 5 times higher than hard cortical bone (10-30 GPa) [26-28]. The disparity between the elastic moduli of bone and the implant results in a condition known as 'stress shielding', where the bone is resorbed from around the implant [29-31]. The structure of bone

tissue results from the forces experienced by the bone and undergoes a constant formation-resorption cycle, as dictated by Wolff's Law [32]. Upon the insertion of a titanium implant, the hard bone tissue no longer experiences the necessary mechanotransductive forces for bone formation, causing the surrounding hard tissue to be resorbed. The lack of physiological feedback leads to implant loosening that requires revision surgery to correct [33].

Titanium-based alloys are generally well tolerated *in vivo* [34, 35], whereas, stainless steel and CoCr alloys have detrimental effects on surrounding tissue due to the leaching of metallic ions [36-38]. Fe, Co, and Cr ions are strongly cytotoxic to the surrounding cells, while Ti ions are significantly less cytotoxic [39]. These advantages have made titanium-based alloys the dominant material used in modern load-bearing orthopaedic implants.

Table 1.1. Properties of Ti and its alloys applied for the fabrication of bone implants. The values for the mechanical properties are obtained from [20] unless otherwise cited.

Alloy	**Description**	**Elastic modulus (GPa)**	**Yield strength (MPa)**	**Tensile strength (MPa)**	**Biocompatibility**
Commercially pure (CP) -Ti	Pure titanium (α – phase) first used for the fabrication of implants.	101 – 110	170 – 485	240 – 550	Greater osseointegration than SS and CoCr alloys
Ti-6Al-4V Ti 6-4 Grade 23	α-β phase Ti alloy with higher strength than CP-Ti	101 – 110	729 – 847	954 – 976	Similar biocompatibility to CP-Ti. Leaching of Al and V may induce apoptosis in osteoblasts [37, 40].
Ti-29Nb-13Ta-4.6Zr (TNTz) "Gum metal"	β phase low modulus alloy [41]	50 – 80 [42]	547 – 864	596 – 911	Reduced bone atrophy due to stress shielding compared with stainless steel and Ti-6-4.[43-45]

Titanium is biologically inert due to the formation of an unreactive oxide layer with a thickness of ~ 5 nm on the surface (also referred to as the passive layer) [34, 39, 46, 47]. Although titanium is well tolerated *in vivo*, it fails to actively encourage osseointegration on the cellular level. Once titanium is placed inside the body, proteins from the biological environment rapidly adsorb on the implant surface to minimise the free energy of the interface [48, 49]. Adsorbing proteins reduce the free energy of an interface that is more hydrophobic than the local aqueous environment by unfolding to expose their inner hydrophobic regions to the surface and concentrating their hydrophilic domains in the aqueous medium. The proteins on the surface may aggregate with or be displaced by proteins arriving later, leading to a layer of varying composition and conformation. The adsorbed proteins act as markers and signalling agents, governing the interactions between the surface and the biological environment [50]. An unstable protein layer containing molecules with non-native conformations triggers a foreign body response in which the implant is encapsulated by fibrotic tissue [2, 3]. The functionalisation of a titanium implant via the immobilisation of desirable proteins or their bioactive fragments in their native conformations is a promising approach to overcome the bioinertness of the surface, leading to improved osseointegration. Protein immobilisation cannot eliminate the underlying problem of elastic modulus mismatch as the elastic modulus is a bulk material property. However, protein immobilisation can reduce the net impact of stress shielding in regions susceptible to bone resorption by encouraging more optimal bone integration.

Protein immobilisation, first performed on glass substrates, stemmed from peptide immobilisation. Originating in 1990 [51], a limited number of studies were published prior to the 2000's [52]. Protein immobilisation has since become a large field with a variety of processes and proteins investigated. The proteins considered for enhancing osseointegration can be categorised into two classes: (i) proteins that provide signals stimulating bone formation and (ii) extracellular matrix (ECM) proteins that provide adhesion sites for cells. BMP-2, known to stimulate cortical bone

formation in surgical procedures [53, 54], has been immobilised on Ti surfaces and found to stimulate the proliferation and differentiation of bone marrow stem cells and osteoblast-like cells [55-57]. Cell adhesion proteins, including fibronectin, collagen, tropoelastin [58], silk fibroin (SF) [59, 60], and sericin [61], are proteins immobilised to facilitate the indirect formation of bone tissue. These proteins create ECM adhesion sites allowing osteoblastic cells to attach and initiate the osseointegration process. The initial functionalisation investigations utilised simple methods, such as physisorption, for the immobilisation of proteins. However, the initially simple processes have developed into intricate systems as time progressed [2]. This chapter reviews the fundamentals of surface – protein interactions that underpin the techniques used for functionalisation of orthopaedics surfaces. Protein immobilisation techniques applied to orthopaedic surfaces are evaluated with respect to their complexity, reproducibility, scalability, and properties of the functionalised surfaces focussing on stability and biological efficacy.

1.2 Protein – surface interactions

Protein immobilisation mechanisms on orthopaedic surfaces are governed by a number of surface properties which influence the permanence, orientation, and conformation of the immobilised proteins. The fundamental properties of a surface that govern protein – surface interactions are topology and chemistry. These two properties together determine the surface free energy (SFE) and charge, which in turn controls the forces of interaction (hydrophobic/hydrophilic and electrostatic) between proteins and the surface, as depicted in **Figure 1.2**. Therefore, by manipulating the surface topology and chemistry, it becomes possible to tune the protein-surface interactions and achieve optimal bioactivity.

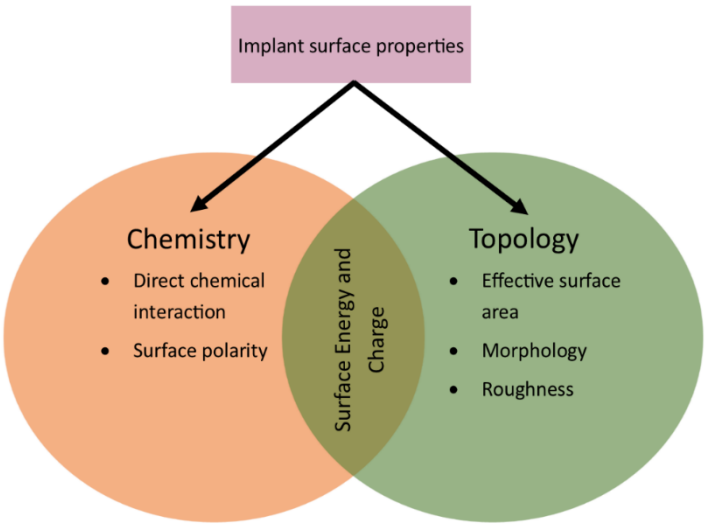

Figure 1.2. A visualisation of the contributing factors affecting the protein-surface interactions as derived from the surface chemistry and topology of an implant.

1.2.1 Surface chemistry

The chemical composition of any solid material at its interface with another phase, such as the aqueous environment of the human body, is referred to as surface chemistry. The surface chemistry determines the distribution of electric dipole moments and charges at the interface, which results in electrostatic interactions with proteins in the aqueous environment. The electron distribution within the bond determines the electric dipole moment of a chemical bond. Polar molecules are those with an electron bond density biased towards the more electronegative atoms (atoms that attract bonding electrons), that form net asymmetric positive (+Q or +δ) and negative (-Q or -δ) regions within the molecule [62]. Non-polar molecules, in contrast, demonstrate a symmetrical charge distribution, and therefore, no net dipole moment. Typical examples of polar and nonpolar molecules containing polar bonds are CO and CO_2. Both molecules contain polar bonds between the more electronegative O and less electronegative C. The C=O molecule has a single polar bond resulting in an asymmetrical distribution and, therefore, is a polar molecule; whereas the net charge distribution is symmetrical in the case of CO_2 (O=C=O), making the molecule overall nonpolar.

Surface charge at the interface is derived from the molecular groups that possess a net positive or negative charge due to the addition or removal of ionised species, such as a proton (H^+). The surface charge is thus affected by the environmental pH, i.e. proton concentration [63]. The isoelectric point (pI or IEP) of a chemical group is the pH where the group has no net charge in the statistical mean. The chemical groups become increasingly deprotonated (negatively charged at pH > pI) or protonated (positively charged at pH < pI) as the pH diverges from the pI [63]. For example, at the physiological pH 7.4, carboxylic acid groups (COOH) are negatively charged (COO^-), while amino (NH_2) groups are positively charged (NH_3^+) [64].

The surface free energy (SFE) depends on the chemical groups present and whether they are charged or have dipole moments. The chemical composition and resulting SFE, therefore, governs how the surface interacts with the aqueous biological environment and the proteins within, as schematically illustrated in **Figure 1.3**. The SFE determines the surface affinity with water and is typically measured by the water contact angle (WCA). The WCA is determined by the relative strength of the adhesive forces between the polar water molecules and the surface on the one hand, and the cohesive forces between water molecules on the other hand. A surface is classified as hydrophobic or hydrophilic based on WCA >90˚ and WCA <90˚, respectively [65, 66]. Surfaces with higher hydrophilicity (and SFE) possess greater adhesive interactions with the polar species *in vivo*, such as water molecules [62]. In addition, electrostatic interactions can assist in attracting and orienting proteins based on charged regions in the structure, as demonstrated by the electrophoretic deposition of silk fibroin [59, 60]. Proteins demonstrate a tendency to change conformation during interactions with surfaces [67]. The protein's environment changes from liquid to a solid-liquid interface once it encounters a solid surface. To accommodate the influences of the surface, the protein refolds from its native conformation which corresponds to a low free energy state in aqueous solution, to a new conformation to achieve a free energy minimum at the interface. The strongly bound layer of water molecules on a hydrophilic surface prevents strong interactions between the protein and the surface, allowing the protein to maintain its native conformation [68]. Highly hydrophilic surfaces, therefore,

are protein repellent and do not adsorb proteins from aqueous solutions [69, 70]. In contrast, the interface of a hydrophobic surface with water presents a significant energy penalty and the system will evolve to a lower energy state through the adsorption and unfolding of proteins. In such rearrangements, the hydrophobic groups are placed on the surface and the polar hydrophilic groups become the interface with the water. The new conformation will be significantly different from the native conformation, potentially rendering the protein useless for the desired biological signalling [71]. Highly hydrophobic surfaces, therefore, result in the irreversible build-up of non-functional, denatured proteins. This phenomenon is referred to as protein fouling and has been reviewed elsewhere [72].

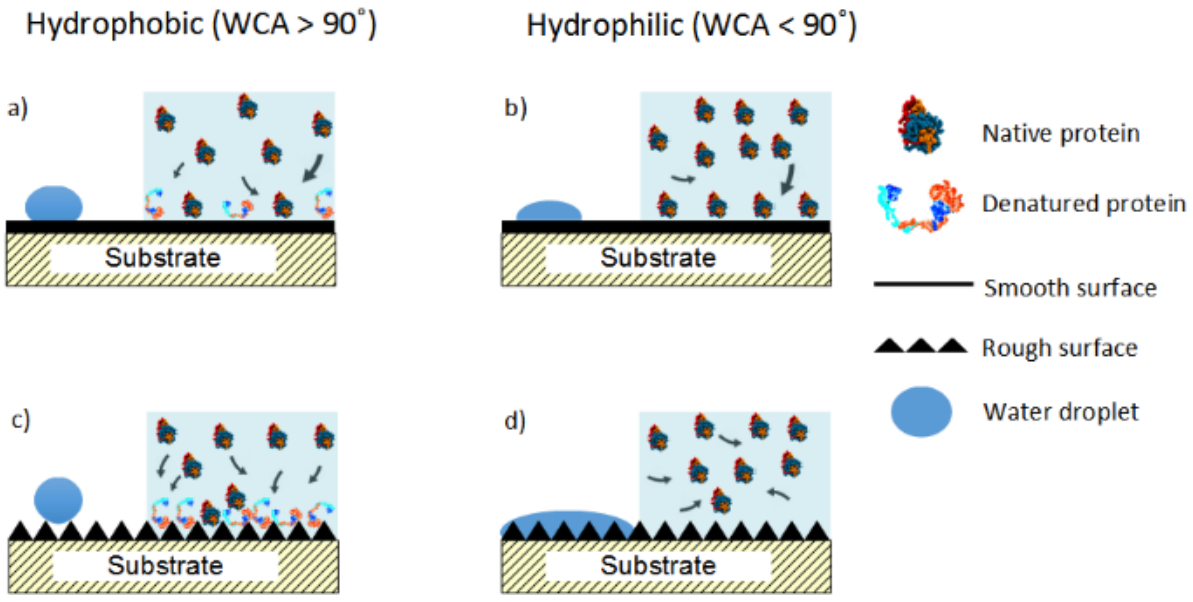

Figure 1.3. An illustration of protein-surface interactions for given hydrophobicities of smooth (**a, b**) and roughened (**c, d**) surfaces. The roughening of substrates enhances the pre-existing hydrophobicity. For hydrophobic surfaces (**a, c**) the roughened surface increases the protein adsorption quantity but results in protein fouling. Hydrophilic surfaces possess a water layer which impedes protein adsorption but maintains native protein conformation (**b**). Enhancement by roughening (**d**) produces a non-fouling surface due to the increased water attraction preventing protein adsorption.

1.2.2 Surface topology and roughness

Surface topology is defined as the physical roughness and morphology of the interface. Roughness is the height variation from the statistical mean across the interface and is reported as the average roughness (R_a) or root mean square roughness (R_{RMS}), while, morphology is the form the roughness takes, e.g. pores, grooves, or random formations. The process of altering the surface topology towards roughness and inducing morphological changes is referred to as roughening and can be performed through multiple means, e.g. grit blasting, acid etching, or plasma treatment [73]. Roughening processes increase the effective surface area at the interface, multiplying the quantity of chemical groups accessible to the contacting fluid, which in turn, enhances the pre-existing hydrophobicity/hydrophilicity of the interface. Accordingly, polymeric materials have been shown to become more hydrophobic as the surface roughness increases [74], whereas metallic surfaces experience an increase in hydrophilicity [66] (**Figure 1.3**).

The types of interactions that determine implant biocompatibility have been shown to occur at different roughness scales [75-77]. The micron-scale improves mechanical interlocking [78], the submicron scale affects cellular activity [75, 76, 78], and protein interactions are influenced by the nanoscale morphology [79-81]. Proteins of different molecular sizes, charges, and surface affinities will interact differently with identical nanoscale topologies. [82]. The effect of surface roughness on protein adsorption has been investigated only for a limited number of proteins. Nanoscale surface topology accommodates protein attachment greater than could be accounted for by an increase in the surface area alone, and the mechanism is believed to be through protein conformational changes [79, 80]. It has also been shown that roughening on the submicron scale will affect the attachment of proteins based on the interactions between the individual protein and the enhanced hydrophobic/hydrophilic nature of the surface [83]. Surface roughening has been incorporated into current titanium orthopaedic devices to take advantage of the increase in biological interactions it affords.

1.3 Protein immobilisation approaches

Protein immobilisation on an orthopaedic surface allows greater control over the biological interactions between the implant and the body. Several methodologies have been investigated since the inception of protein functionalisation for orthopaedics. The following section reviews the mechanisms of methodologies investigated and evaluates their complexity, reproducibility, and scalability. The properties of the functionalised surfaces, specifically their stability and biological efficacy, are also discussed. Titanium-based alloys are the standard for orthopaedic implants, and as such, the body of work on protein immobilisation methodologies for orthopaedic applications are focussed on titanium substrates. Immobilisation techniques that have been applied to PEEK are also addressed due to its potential to replace titanium in some orthopaedic devices.

1.3.1 Physical Adsorption

Physical adsorption, also referred to as physisorption, is the simplest method to immobilise proteins on substrates. It utilises hydrophobic and electrostatic interactions to non-covalently attach proteins to the surface. The adsorption of proteins occurs whenever a surface is placed in contact with a protein-containing medium, whether intentionally through incubation in a specific protein solution, e.g. BMP-2 in buffer solution, or unintentionally through exposure to serum-containing cell media or an *in vivo* physiological environment. The unintentional adsorption of serum proteins is usually neglected in the case of cellular studies, despite the fact it always occurs. The literature suggests that surface pretreatment of metals via acid or alkali solutions (e.g. HNO_3 or NaOH) or treatment through electrochemical methods [84-86], primarily used for cleaning, are beneficial for cell attachment. This improvement is due to the increased hydrophilicity resulting from polar groups formed at the protein – surface interface. The increased hydrophilicity allows adsorbed protein molecules to retain native-like conformations. The beneficial effects of pretreatment are also likely to be related, in part, to the

increase in available surface area due to a change in nanoscale topology. Similar advantages can be achieved on polymers, such as PEEK, using chemical modifications that introduce COOH and OH groups [87, 88]. The physisorption process is also utilised for the intentional attachment of selected proteins to influence the biological response. The pre-treated substrates are immersed in a protein solution for a given time before being transferred into the biological environment. Currently, research is focused primarily on the adsorption of proteins onto porous alloys and other porous structures, usually with a view to achieving controlled protein release rather than permanent immobilisation [89, 90].

The main advantage of non-covalent protein immobilisation is the simplicity of the process, making it attractive for manufacturing [91]. However, the non-covalent nature of adsorption presents a number of disadvantages including low effective protein concentrations, protein denaturing, and unfolding. The effective concentration of a protein is the quantity that interacts with the physiological environment per unit of area. Physisorption does not usually perform well in this respect because attachment strength is low on hydrophilic surfaces; while proteins tend to unfold and spread on hydrophobic surfaces where the forces of interaction are strongest [68, 71].

Two chemical modification strategies have been developed for the adsorption process in an attempt to address the issues of low effective protein attachment, steric effects, and denaturing. The first strategy is the substitution of buffer solutions with hydrogels to deposit proteins. The desired protein is loaded into a hydrogel, the substrate is immersed and then removed to be air dried [2]. This approach increases protein deposition and retention on an interface and overcomes protein denaturing through enclosure within the hydrophilic environment of the hydrogel [92]. However, once placed within the aqueous environment, the hydrogel rehydrates and swells allowing the proteins to become displaced from the hydrogel via diffusion or hydrogel erosion, depending on the size ratio between the hydrogel pores and the protein [93]. Hydrogels are not widely utilised in orthopaedic devices for protein immobilisation due to the potential for mechanical removal. They have, however,

become popular in tissue engineering scaffolds and for drug and protein release applications [94-97]. The application of hydrogels for biomolecule delivery and release has been reviewed elsewhere [98, 99].

The second strategy aiming to improve the performance of adsorption-based processes is the introduction of alternative chemical groups on the substrate, resulting in Chemisorption (adsorption through the formation of temporary chemical bonds). Surfaces presenting hydroxyl groups, such as titanium, can be modified using a process known as tresylation. In this process, schematically depicted in **Figure 1.4**, trifluoromethane sulfonyl (Tresyl) chloride molecules are chemisorbed to the hydroxyl groups on the surface. Tresyl molecules ($SO_2CH_2CF_3$) are attached to the surface through ionic chemical bonding between the terminal sulphur and a surface hydroxyl [100-103]. During the protein immobilisation process, the tresyl group acts as a molecular guide being displaced via nucleophilic substitution by the incoming protein resulting in a strong electrostatic bond between the positive amine of a protein and the negative surface hydroxyl.

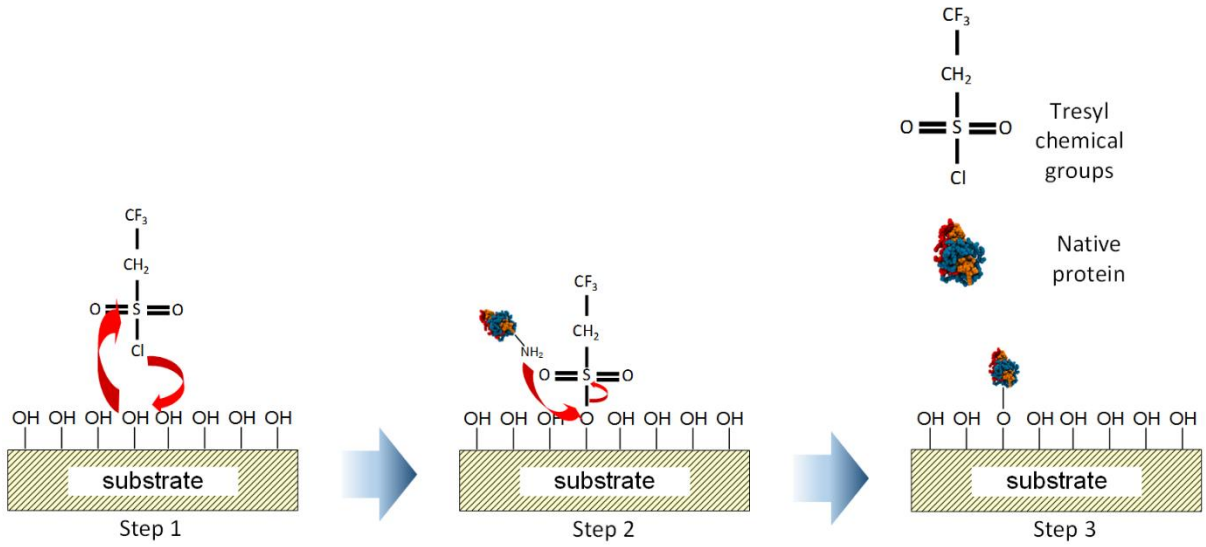

Figure 1.4. Protein chemisorption via tresylation. **Step 1**: The tresyl groups attach to the substrate and release Cl, forming a temporary O-S bond. **Step 2**: The incoming protein undergoes S_N2 nucleophilic substitution via an amino group, disrupting the O-S bond. **Step 3**: Protein is chemisorbed to the surface through an O-N bond.

Hayakawa *et al.* have demonstrated that the concentration of protein adsorbed to a tresylated substrate is greatly increased over a non-treated surface. The ionic bonding forms a more rigid protein layer that is less susceptible to protein desorption [104-107] and surfaces functionalised with proteins via tresylation have indicated a beneficial response both *in vitro [108]* and *in vivo* [109, 110]. However, the reversibility of this form of bonding leads to three disadvantages. Firstly, Tresyl groups can be removed through hydrolysis at the S-O bond [102, 103] potentially reducing the number of binding sites for protein immobilisation. Secondly, care must be taken to avoid the presence of other nucleophilic groups during protein incubation, as they would compete with the protein in the substitution reaction [105, 106]. Finally, adsorbed proteins could potentially be replaced *in vitro/vivo* by proteins with higher affinities in a similar nucleophilic substitution.

While each adsorption approach has particular strengths, a major disadvantage of all physical and chemical adsorption processes is that proteins are susceptible to competitive replacement, also known as the Vroman effect (depicted in **Figure 1.5**). Vroman *et al.* [111] noted that clean surfaces placed in contact with blood first adsorb a layer of low molecular weight proteins present in high concentrations, such as albumin. The adsorbed proteins are replaced over time by higher molecular weight proteins, such as fibrinogen, which have a greater affinity for the surface. Although the process of the Vroman effect is not fully understood, the formation of a transitional protein complex that rotates to release the originally adsorbed protein has been observed [112]. Physisorbed protein layers would be expected to experience similar displacement through competition with other proteins in a physiological environment. The likelihood of displacement is a function of relative protein concentrations and surface affinities [113, 114]. The primary application of physisorbed protein layers has, therefore, focussed on applications requiring protein release.

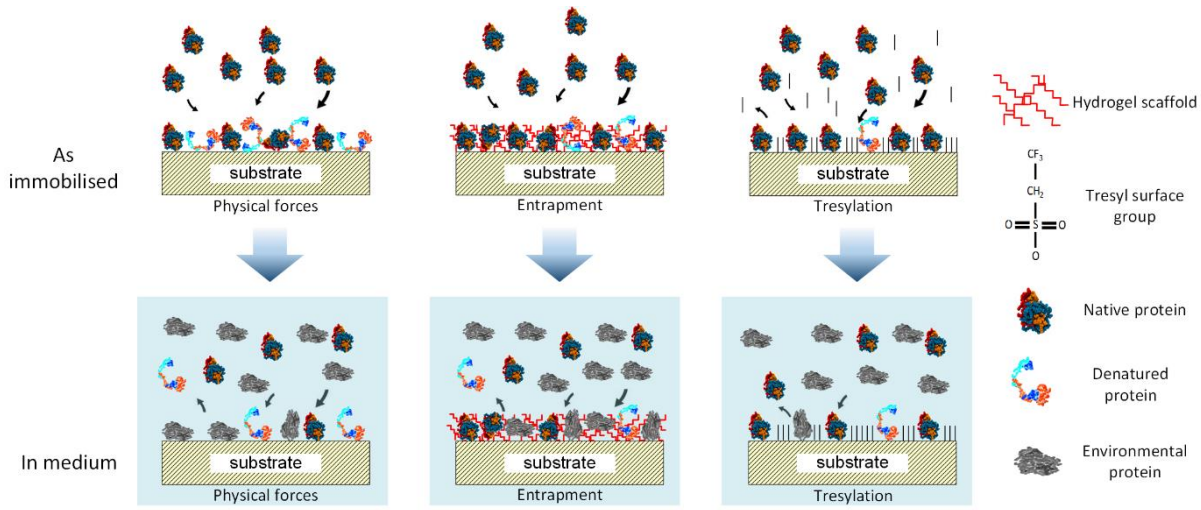

Figure 1.5. Protein adsorption to substrates via physical forces, scaffold entrapment through hydrogels, and tresylation. Substrates adsorbing protein via physical forces rely on electrostatic and hydrophobic interactions. The effectiveness will vary depending on the surface chemistry and topology. The adsorbed proteins are readily displaced in the medium through interactions with environmental proteins. Protein entrapment within hydrogels increases protein quantity. However, hydrogels experience degradation and swelling in medium, resulting in the exchange of proteins. Tresylated substrates attach protein through nucleophilic substitution, producing a strong, non-covalent bond between the protein and substrate. The proteins are still susceptible to displacement via nucleophilic substitution and desorption.

1.3.2 Covalent immobilisation via chemical methods

The inability of adsorption processes to permanently attach proteins to an orthopaedic surface highlighted the need for an alternative approach to protein functionalisation. For permanent attachment to occur, the surface chemistry of both metallic and polymeric substrates must be altered to facilitate covalent reactions between the surface and the desired protein. The covalent attachment can be achieved either directly via surface functional groups or indirectly through a separate linker molecule that mediates the binding between the substrate and the desired protein.

1.3.2.1 Direct Chemical immobilisation

PEEK substrates have demonstrated the potential to be chemically modified to allow direct covalent protein immobilisation. Chemical modifications must be performed before proteins can be covalently bonded to the surface due to PEEK's chemical inertness [115]. Hydroxyl functionalisation (PEEK-OH) is the first step for all the chemical modification reactions. The untreated PEEK is refluxed in dimethyl sulfoxide (DMSO) and sodium borohydride ($NaBH_4$) at 120˚C for 3 hours and subsequently washed with water, acid, and alcohol [87, 115]. The PEEK-OH can be further reacted to produce other surface functional groups such as amines [115], isocyanates [87], and carboxyl groups [116]. Isocyanate (NCO) functionalised PEEK is synthesised by further treating PEEK-OH with hexamethylene diisocyanate and diazabicyclooctane in toluene for three days. PEEK polymers functionalised with NCO are able to directly bind proteins covalently through a nucleophilic addition mechanism [87]. PEEK-NCO can be further hydrolysed with NaOH and dioxane to bear amine groups. PEEK has also been functionalised with carboxylic acids and aldehyde groups. To produce carboxylic acid or aldehyde groups, the surface must be reacted with methylhydroquinone to form methylated PEEK (MePEEK). After bromination under UV light, the aldehyde functionalisation is formed through dehydration [116]. The aldehyde groups are then treated with sodium chlorite solutions to achieve oxidation to carboxylic acids as mild oxidative conditions are needed. The potential of chemically functionalised PEEK for the covalent attachment of biomolecules has not yet been explored for biomedical applications. This might be due to the complexity of the reactions and difficulties in scaling the process to apply to the 3D structures used in implantable devices. Nevertheless, the carboxylic acid and aldehyde groups presented at the chemically modified PEEK surface can be used to covalently tether biomolecules to the surface through subsequent chemical reactions.

1.3.2.2 Chemical linker-mediated immobilisation

Both PEEK and titanium have been functionalised with biomolecules through linker-mediated immobilisation. Chemical linkers represent the most common method used for covalent immobilisation on titanium surfaces to date as opposed to direct chemical functionalisation potenitally due to reaction time and complex chemistry outlined in section 1.3.2.1(see **Figure 1.6**). A pre-treatment step is required to expose the native oxide layer terminated by hydroxyl groups for the covalent attachment of the linker molecules via dehydration/condensation reactions [57, 117]. Linker molecules are generally carbon chain molecules either synthetic, like silane and polyethylene glycol (PEG), or biologically derived, like heparin, dopamine, and chitosan.

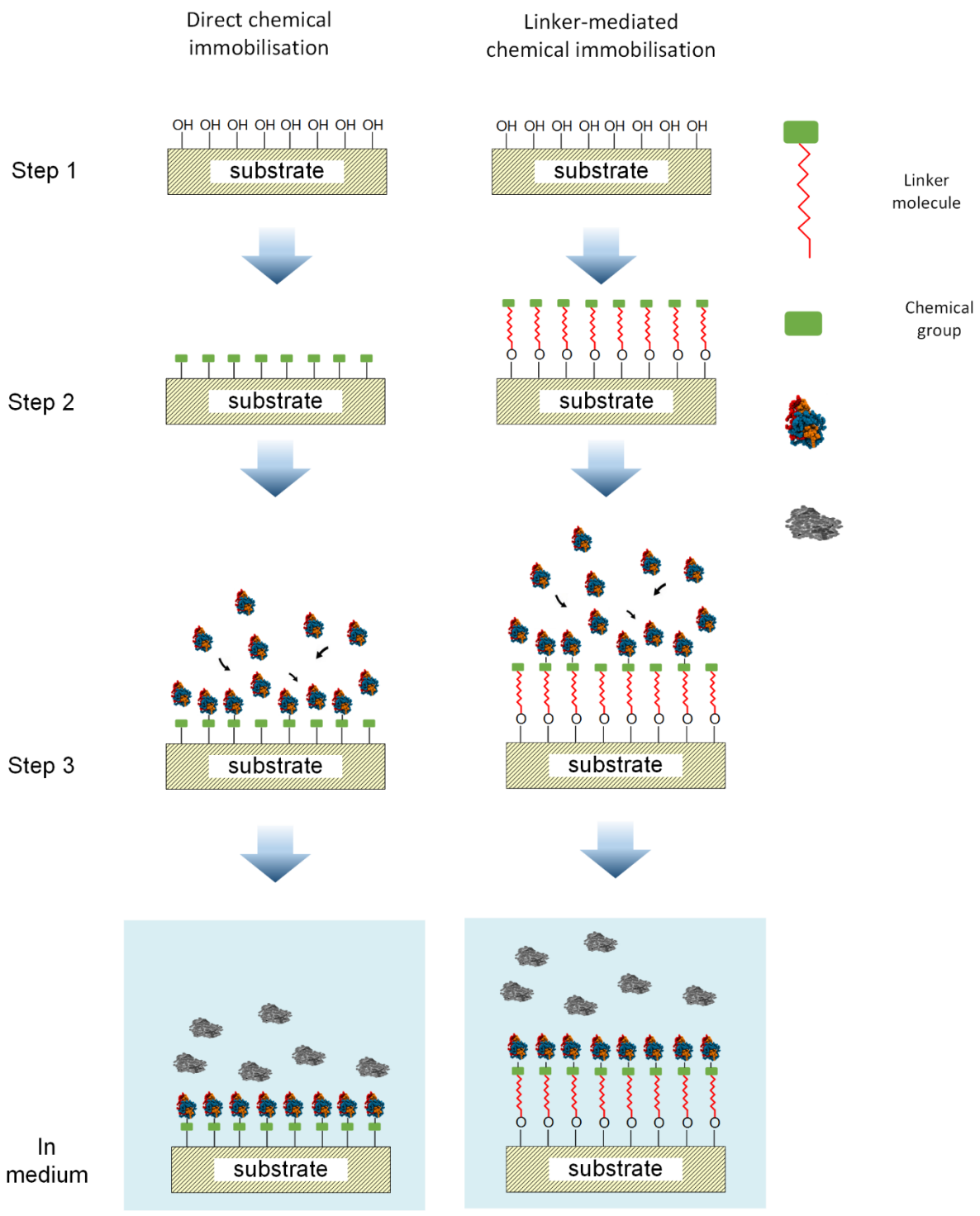

Figure 1.6. A schematic of protein immobilisation via direct and linker-mediated covalent chemical attachment. Linker-mediated covalent immobilisation has been performed on Ti and PEEK substrates. Direct chemical immobilisation has been performed on PEEK only. Direct chemical immobilisation starts with a hydroxylated surface *(step 1)* and undergoes sequential chemical reactions to produce a reactive chemical functional group *(step 2)*. Linker-mediated chemical immobilisation also starts with a hydroxylated substrate. The linker

molecules are added and undergo a condensation reaction with the hydroxyl groups and attach to the surface (step 2). The surfaces functionalised with chemical groups are exposed to the desired protein solution and treated with the required chemicals for immobilisation, e.g. EDC/NHS *(step 3)*. Chemical covalent immobilisation has been shown to prevent protein displacement in the medium.

The two most commonly used synthetic linker molecules for protein immobilisation in orthopaedics are silane and PEG. Silanisation of orthopaedic substrates, first reported in 1995, has become the most widely applied method for the immobilisation of proteins and is still currently in use [118-120]. Alkylsilane linkers attach to hydroxylated substrates via a condensation reaction between the head groups of the alkylsilane and the OH groups on the surface, resulting in an O-Si bond, as shown in **Figure 1.7**. Alkylsilane compounds are chemically versatile with many variations having been developed over the last two decades to provide further functionalisation. These variants are classified by the functional groups used to immobilise biomolecules, located either on the head groups or the alkyl tail: Aminosilanes (containing primary or secondary amines), glycidoxysilanes (containing an epoxide group), and mercaptosilanes (containing a thiol functional group) [121]. An initial *in vivo* study by Voggenreiter *et al.* [122] demonstrated covalent immobilisation and retention of BMP-2 biological activity through silanisation. The histological analysis showed new bone formation on the 150-200 ng BMP-2 immobilised substrates was equal to that formed in the presence of 1 µg solubilised BMP-2 (**Figure 1.8**) [122]. Silanes have also been used to immobilised type I collagen [123] and a branched adhesion biomolecule [124] both inducing a significant improvement in osseoconduction and osseointegration *in vivo*.

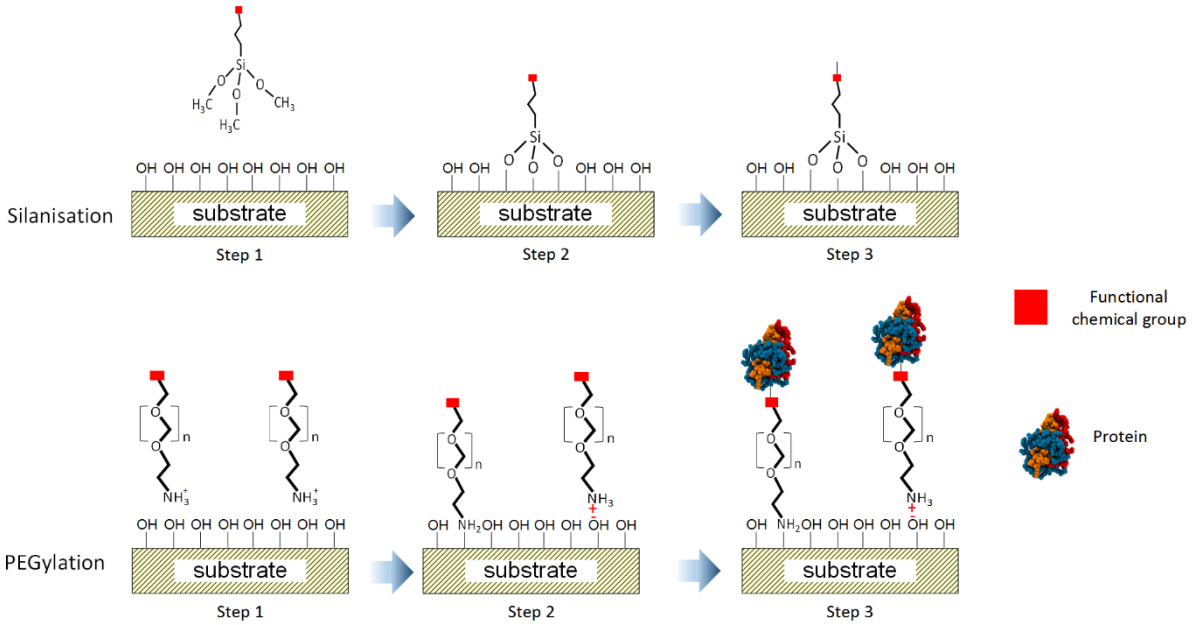

Figure 1.7. An outline of surface functionalisation with the chemical linkers silane and PEG, examining an individual molecule. *Step 1:* the hydroxylated substrate is exposed to the linkers in solution. *Step 2:* Silane linkers undergo a condensation reaction with the surface hydroxyl groups, releasing H_3COH, to form Si-O bonds. PEG will attach to the surface either via a condensation reaction, releasing water, or electrostatic attraction. The type of surface bonding is derived by the available surface charges, thus, condensation reactions can be preferentially increased by a strongly basic pH or through the use of electrodeposition [125-127]. The presence of multiple linker molecules will result in cross-linking of self-assembled monolayers. *Step 3:* The desired protein is attached to the surface via the chemical functional group on the linker, i.e. carbodiimide, Schiff-base, or disulphide.

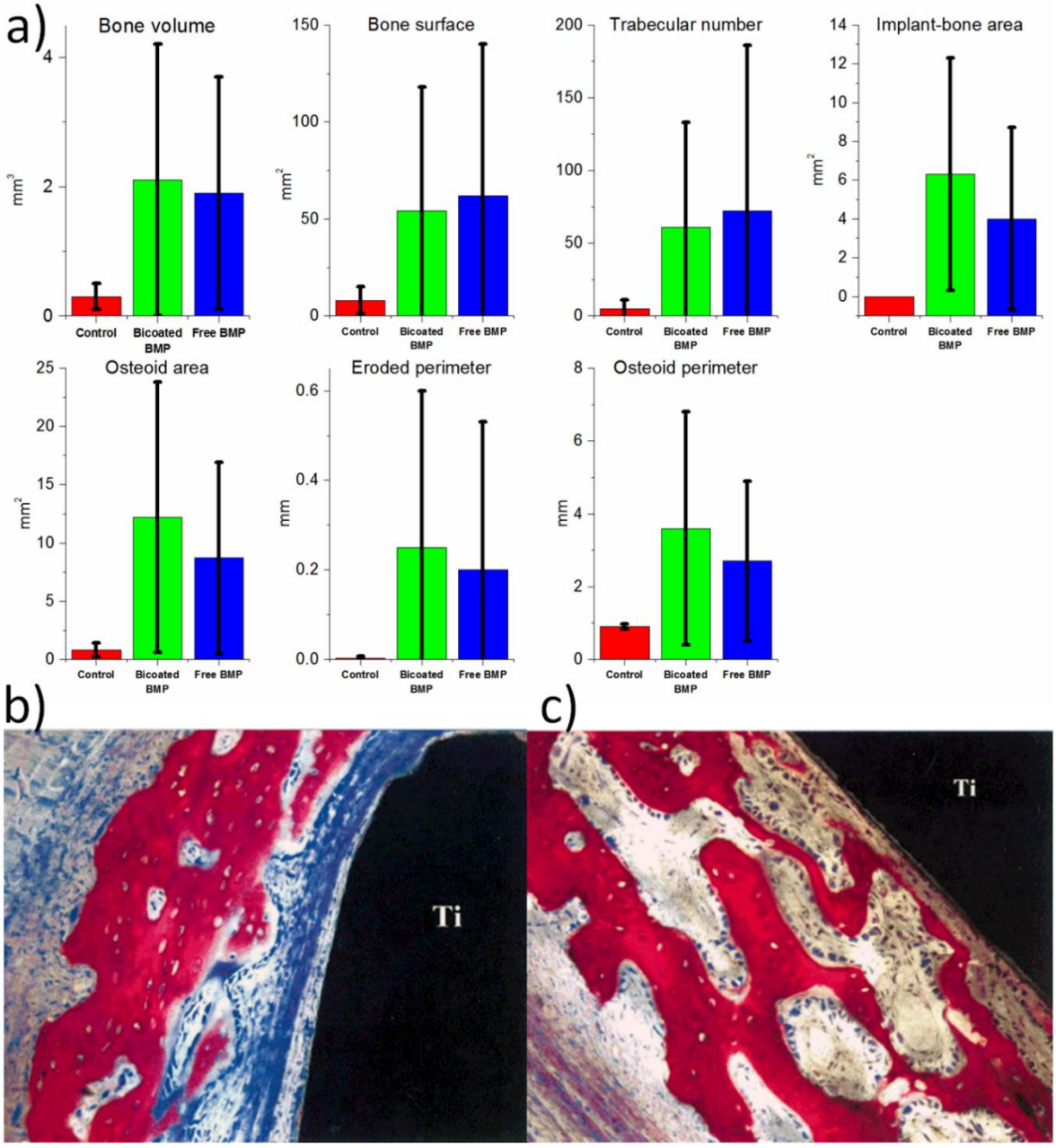

Figure 1.8. a) A graphical representation of the examined histological parameters; bone volume, bone surface, trabecular number, implant-bone area, osteoid area, eroded perimeter and osteoid perimeter, for the titanium control (red), 150-200 ng BMP-2 coated implant (green), and 1 µg free-solution BMP-2 (blue). Microphotographical comparison of stained implant preparations implanted with soluble free **(b)** and chemically immobilised **(c)** rhBMP-2. The histological information demonstrated equal bond formation under both conditions, proving that smaller quantities of BMP-2 can be surface immobilised to produce the same biological effect. Reprinted with permission from [122].

PEGylation of orthopaedic substrates has previously been used to immobilise proteins but the main focus of the last decade has moved towards utilising PEG's highly hydrophilic nature to improve the antifouling properties of surfaces [128-130]. The standard approach to surface PEGylation makes use of the pre-existing hydroxyl terminals to chemisorb the PEG molecules to the substrate, as schematically illustrated in **Figure 1.7**. Recently, terminally modified PEG molecules have been used in place of unmodified PEG for immersion and electrodeposition relying on the presence of electrostatic interactions between the selected terminal groups and the hydroxylated surface [131]. Amine- (NH_2 – PEG- NH_2) and carboxyl- (COOH–PEG-NH_2) functionalised PEG are used for protein immobilisation via carbodiimide reactions. These modified PEG molecules are used either individually or together with a co-linker, such as an alkylsilane, to immobilise biomolecules [132, 133]. Further exploration of PEGylation can be found within [92].

Recently, research focus has shifted from silane and PEG towards other biologically - derived linkers that have individual biofunctionality. In theory, the use of such molecules would provide a beneficial effect from unconjugated regions in addition to the immobilised proteins, as chemical linkers do not always provide 100% surface immobilisation. The biologically active molecules widely used as linkers include; dopamine (DOPA) [134, 135], chitosan [136], and heparin (HEP) [137-139]. These molecules have been investigated both as individual and copolymer linkers. The deposition of these biomolecules on substrates predominantly occurs through immersion reactions, as listed in **Table 1.2**, requiring at least 12 hours to initiate the protein immobilisation.

Dopamine which shows activity in extracellular matrix (ECM) signalling, is a strong mineralisation inducer [134] and has been used to immobilise a number of proteins since the early 2000's [134, 135, 140-144]. Chitosan is a recently discovered biopolymer that has been used in biochemical linker immobilisation due to its antibacterial properties [136, 145-147]. First published by Dodane *et al.*, this biopolymer is extracted from exoskeletal structures of arthropods, i.e. crustaceans, as well as fungi and insects [148]. Carboxymethyl-functionalised chitosan is commonly used for orthopaedic

applications relying on the presence of COOH groups for carbodiimide reactions. This variation has also been used for tissue engineering scaffolds [98, 148, 149] and nanomaterials [150]. DOPA and chitosan attachment utilises condensation reactions with the hydroxyl-functionalised surface. Chitosan-functionalisation of a substrate requires exposure to the protein solution via immersion or electrodeposition (see **Table 1.2**). The original synthesis method for DOPA was complex, as the reactive oxygen catchetol side chains had to be protected from oxidation and cross-linking when applied as a self-assembled monolayer [151]. However, an easier alternative approach has been developed, requiring an overnight immersion in a DOPA/HCl - Tris buffer solution [142, 152-154]. The Tris buffer attachment process results in crosslinking of dopamine and the formation of an interconnected scaffold layer with exposed amine groups [152]. *In vivo* studies have been performed for DOPA functionalised with lovastatin, a bone-forming drug, and bacitracin, an antibiotic. Lovastatin-functionalised DOPA demonstrated an increased bone formation (as shown in **Figure 1.9** below) [155], while bacitracin greatly impeded biofilm formation *in vivo* on the surface of the implant [156]. Investigations into *in vivo* Ti/Chitosan conjugated with biomolecules remains to be performed.

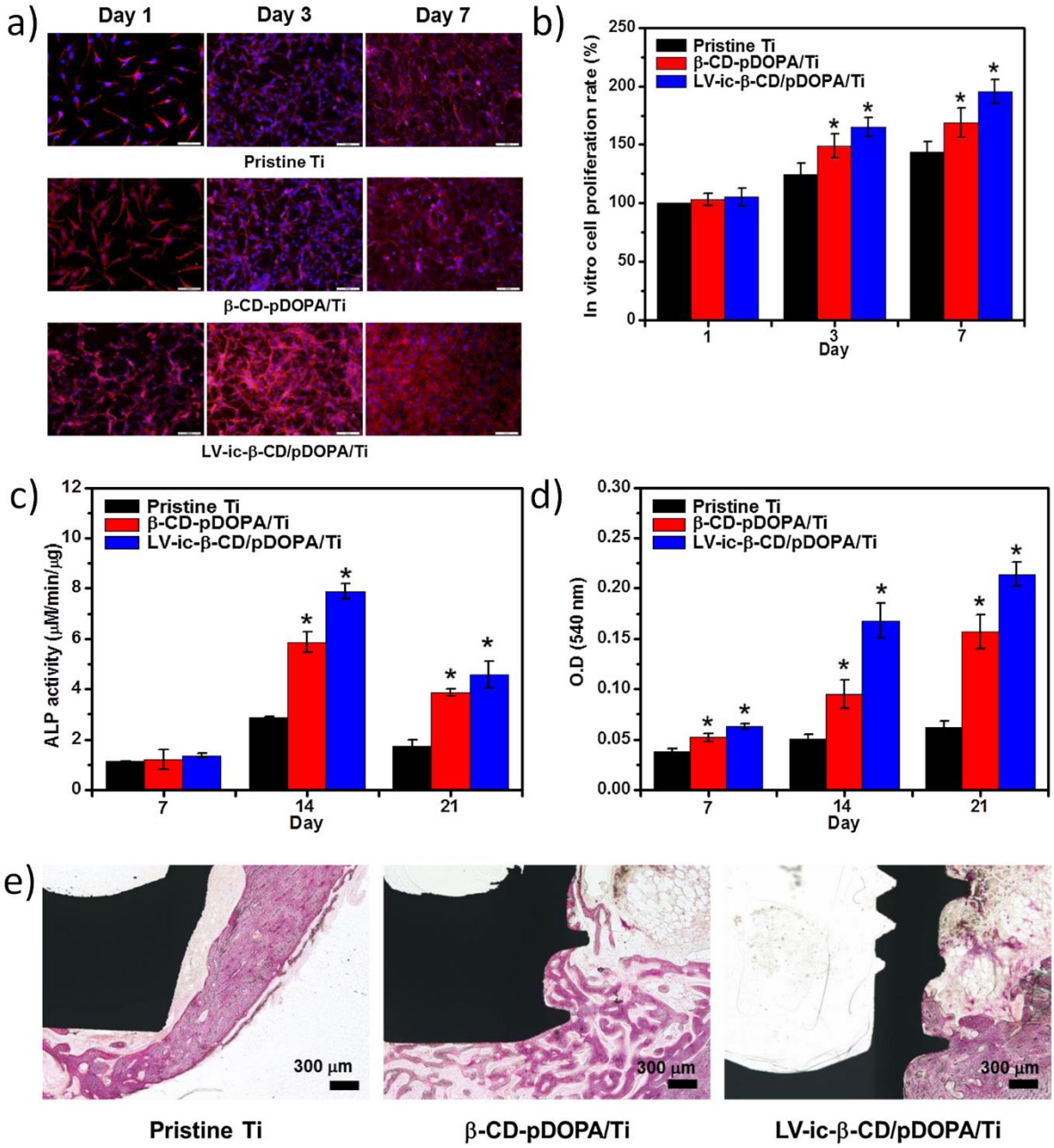

Figure 1.9. **a)** Fluorescence microscopy images of DAPI and F-actin stained MC3T3 cells on pristine, β-CD-DOPA, and lovastatin-functionalised Ti at 1, 3, and 7 days. Proliferation rates **(b)**, alkaline phosphatase activity **(c)**, and calcium deposition **(d)** of MC3T3 cells on the investigated surfaces were compared to tissue culture plastic. The β-CD-DOPA and lovastatin-functionalised Ti demonstrated a significant increase compared to pristine control, with lovastatin-functionalised Ti exhibiting consistently higher activities than the β CD-DOPA. **e)** Histological imaging of Ti screws revealed the formation of lamella bone and bone ingrowth in β-CD-DOPA-, and lovastatin-functionalised Ti not present in the pristine titanium. Reprinted with permission from [155].

Heparin is an anti-thrombogenic protein originally used in cardiovascular applications for bypass circuits, synthetic vascular grafts, and coronary stents [157]. Heparin does not react directly with the hydroxylated surface. Instead, it requires an aminated surface to attach via a condensation reaction. As such, heparin has been immobilised with other compounds such as DOPA [56] or silane [158] that provide an amine terminal. Alternatively, Kim *et al.* outlined a click chemistry procedure utilising propargyl bromide and 2-azidoethanamine for amine-functionalising titanium substrates before attaching the heparin [139]. *In vitro* and *in vivo* studies of orthopaedic implant surfaces and scaffolds have been performed using heparin to immobilise BMP-2 [159-161]. Kim *et al.* have shown that the impermanent nature of the heparin-protein bond allowed the BMP-2 to be released into the biological environment which results in greater bone formation than controls in an *in vivo* dog model (**Figure 1.10**)[56].

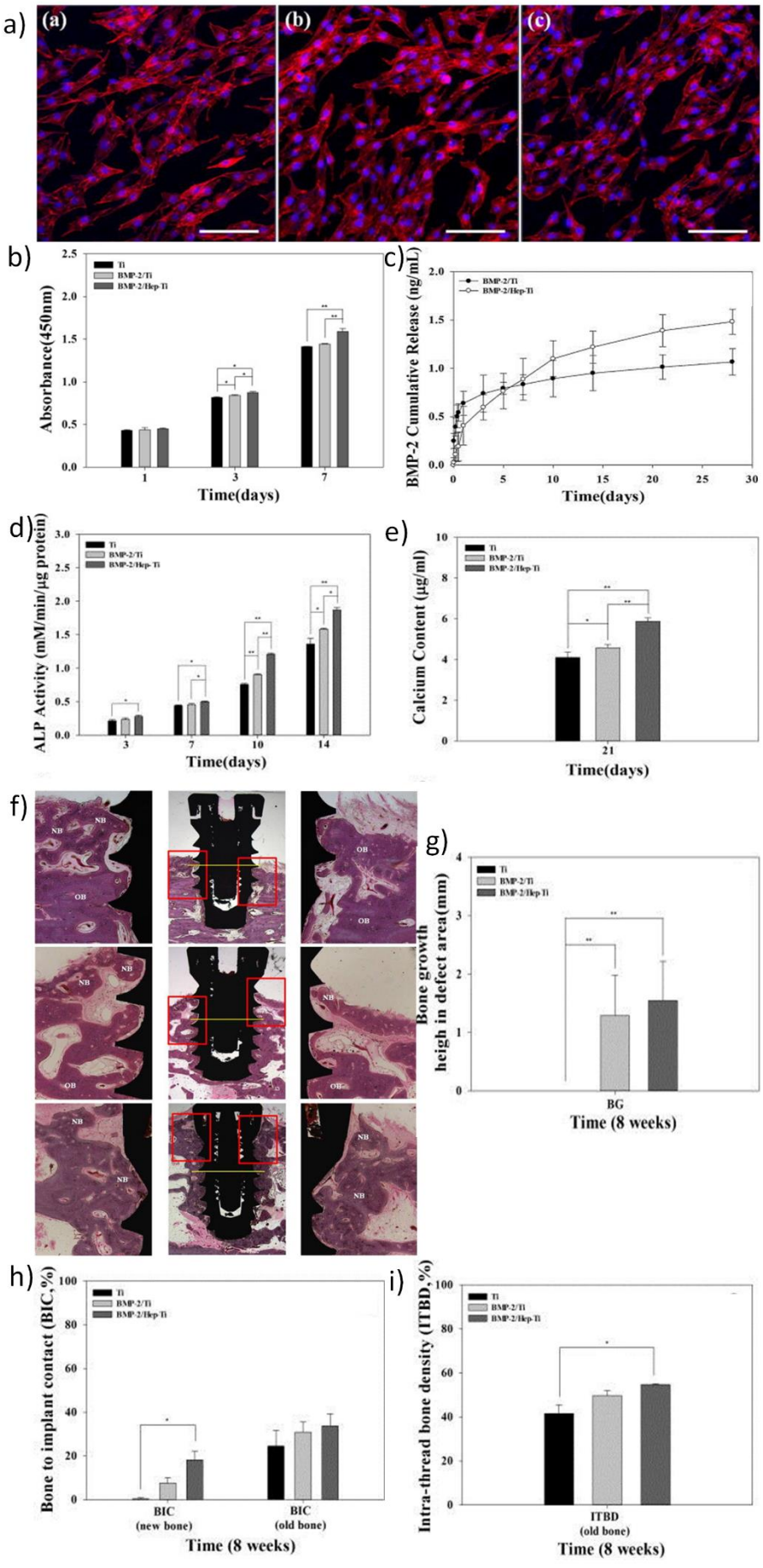
a)
(a)
(b)
(c)
b)
Absorbance(450nm)
Time(days)
Ti
BMP-2/Ti
BMP-2/Hep-Ti
c)
BMP-2 Cumulative Release (ng/mL)
Time(days)
BMP-2/Ti
BMP-2/Hep-Ti
d)
ALP Activity (mM/min/μg protein)
Time(days)
e)
Calcium Content (μg/ml)
Time(days)
f)
NB
OB
g)
Bone growth heigh in defect area(mm)
BG
Time (8 weeks)
h)
Bone to implant contact (BIC,%)
BIC (new bone)
BIC (old bone)
Time (8 weeks)
i)
Intra-thread bone density (ITBD,%)
ITBD (old bone)
Time (8 weeks)

Figure 1.10. **a**) F-actin and DAPI stained fluorescence images of MG63 cells on Ti (**a.a**), adsorbed BMP-2 (**a.b**), and BMP-2/heparin/Ti (**a.c**). **b**) Cell proliferation of cells grown on the investigated surfaces at 1, 3, and 7 day time points as determined by CCK-8 assays. **c**) The release kinetics of adsorbed BMP-2 on titanium and heparin/Ti, respectively. The degree of mineralisation for MG63 cells was determined via alkaline phosphatase (ALP) levels (**d**) and calcium content (**e**). The BMP-2/Heparin/Ti surface demonstrate statistical increases over both the untreated Ti and the adsorbed BMP-2 Ti. *In vivo* investigations revealed significant increases in bone formation for the BMP-2 releasing surfaces, as shown in (**f**). In descending order: Ti (top row), BMP-2/Ti (middle row), and BMP-2/Heparin/Ti (bottom). Analysis of the histological results showed significant increases in bone growth in defect areas (**g**), bone-implant contact (BIC) angle of new bone (**h**), and bone density between the screw threads (**i**). Reprinted with permission from [56].

1.3.2.3 The chemistries of protein immobilisation

There are three main types of chemistries utilised for direct and linker-mediated protein immobilisation: disulfide, Schiff-base, and carbodiimide reactions. The chemical reactions are outlined in **Figure 1.11.** In each case, the particular functional groups as shown must be present at the surface for the immobilisation to proceed. Surfaces functionalised with epoxy groups, although not widely applied, have been reported to immobilise proteins via nucleophilic substitution ring opening reactions involving the amine groups on the amino acid (AA) side chains [162].

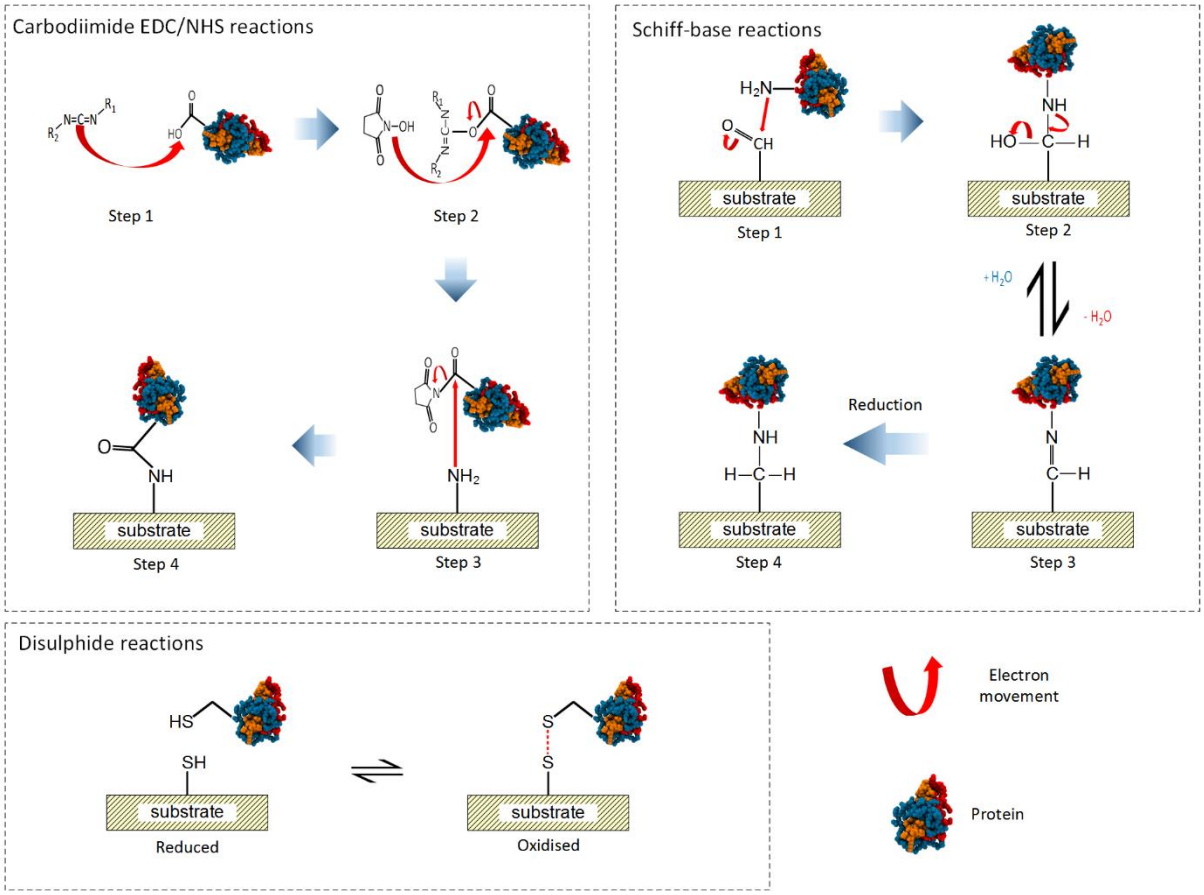

Figure 1.11. An outline of the reaction steps for EDC/NHS carbodiimide, Schiff-base, and disulfide reactions commonly utilised in biomolecule immobilisation chemistry. **EDC/NHS carbodiimide reactions:** The desired protein, EDC, and NHS are exposed to the substrate in an optimised molar ratio. EDC attaches to the OH of a carboxylic acid on the protein (step 1) before being substituted with NHS (step 2). The NHS is replaced with the amine group at the surface (step 3) resulting in covalent immobilisation (step 4). Carbodiimide reactions will also occur with the locations of the amine and carboxylic acid groups interchanged. **Schiff-base reactions:** Protein amines undergo nucleophilic addition to an aldehyde group on the surface (step 1) forming a temporary imine bond (step 2 and 3). The imine can be chemically reduced to form a covalent N-C bond (step 4). **Disulfide reactions:** A sulfuric functional group can form a temporary S-S bond with a cysteine amino acid in the protein structure through oxidation. The bond can be reduced in mildly acidic conditions, as often occurs in aqueous environments.

Thiol functional groups can be utilised for protein immobilisation through the formation of disulphide bonds (R-S-S-R') with cysteine amino acids. The use of the disulphide chemical process in protein immobilisation allows for specific attachment, as cysteine is the only amino acid capable of forming disulphide bonds. Mercaptosilane linker molecules can utilise disulphide bonds to attach

proteins through the cysteine [163] or undergo sulfo-SMCC linker modification to immobilise proteins via carbodiimide reactions [164]. Disulphide bonds are reducible in mildly acidic conditions [165] and, therefore, may not provide sufficiently persistent protein functionalisation for use in implantable biomedical devices.

Schiff-base reactions involve the formation of an imine (R/R'-C=N-R") via nucleophilic substitution of an amine group on the double bonded carbon-oxygen (-C=O) of an aldehyde or carboxylic acid, resulting in the release of water [166]. This process targets amino acids with nucleophilic amines in their structure, such as histidine. Imine bonds are, however, hydrolysable and reduction of the C=N bond to a C-N bond is required for permanent immobilisation [165, 166]. Hence, Schiff-base chemistry may be useful for delayed release applications. For example, Kim *et al.* immobilised BMP-2 protein to a heparinised surface through Schiff-base chemistry and observed the gradual release of BMP-2 together with significantly increased mineralisation of MG63 cells [56].

The most common linker chemistry utilised for protein immobilisation is the carbodiimide reaction, which forms an imide bond (R-N=C=N-R') between amine and carboxylic acids groups. Carbodiimide chemistry employs 1-ethyl-3-(3-dimethylaminopropyl) carbodiimide/*N*-hydroxysuccinimide (EDC/NHS) or glutaraldehyde (GA) to attach proteins via the positively-charged lysine and arginine amino acid or the negatively-charged glutamic and aspartic acids, through surface attached carboxyl or amine groups, respectively. The synthetic linker molecules, amino silanes [61, 103, 167-171], and NH_2-PEG and COOH-PEG [133], are typical examples of linkers that immobilise proteins through carbodiimide chemistry (**Figure 1.11**).

PEEK has been functionalised with Gly-Arg-Gly-Asp (GRGD) peptides through EDC/NHS reactions to the 7-Oct-1-enyltrichlorosilane (OETS) linker surface monolayer [117]. Titanium has been functionalised with collagen using EDC/NHS with the linkers aminopropyl-triethoxysilane (APS) [120], and a two-step attachment process linking (3-Aminopropyl) trimethoxysilane to COOH-PEG [133]. The biologically-derived linkers, dopamine and chitosan, almost exclusively utilise EDC/NHS chemistry to

covalently immobilise proteins through their presented amine groups. Biomolecules that have been immobilised through this chemistry include BMP-2 [136, 142, 172], heparin [56], and collagen [134]. EDC/NHS chemistry has also been used to cross-link immobilised collagen to improve the stability of the layer [173]. The cross-linking of collagen does not appear to negatively affect cell growth [134].

EDC/NHS has also proved effective in stabilising self-assembled monolayers (SAMs) by cross-linking. SAMs rely on physical interactions to produce a layer with well-defined structure and surface chemistry [174, 175]. They consist of surfactant molecules containing an alkyl chain tail and a functional head group that self-assemble on the substrate to form organised monolayers through electrostatic and hydrophobic/hydrophilic interactions [176, 177]. A variety of monolayer coatings can be assembled with different functional groups for the structural inclusion of the protein [174], or covalent immobilisation through chemical reactions, such as epoxy ring opening [178] and carbodiimide chemistry [179]. Covalent attachment of a SAM to a surface offering improved stability can be achieved by chemical reactions between the substrate and the contacting region of the individual SAM molecules. Such chemical attachment requires appropriate chemical modification of the substrate and the external end of the SAM surfactant molecules. Nevertheless, the physical interactions underpinning the SAM structure may result in insufficient stability for demanding applications such as in implantable biomedical devices. Stabilisation can be achieved through EDC/NHS cross-linking of the SAM itself [174, 179].

1.3.2.4 Evaluation of chemical linker-mediated immobilisation approaches

Chemical immobilisation methods successfully mitigate the problems of protein exchange via the Vroman effect after implantation, as shown in several *in vivo* studies [56, 122, 123, 155, 156]. However, direct and linker-mediated chemical attachment introduces several issues. The main issues arise from process complexity, reaction time, the toxicity of reactants, and the lack of scalability and reproducibility. The chemistry behind both direct and linker-mediated chemical immobilisation is

often complex and time-consuming, with each step of the process needing to be confirmed through characterisation. A linker-mediated protein immobilisation process requires a minimum of three steps: (i) preparation of the surface to present the required chemical groups (e.g. hydroxylation); (ii) reaction of the prepared surface with the linker molecule; and (iii) immobilisation of the protein to the linker. The total processing time is typically in the order of days as listed in **Table 1.2**. Direct chemical immobilisation of proteins to PEEK surfaces eliminates the required steps for linker molecule surface attachment. However, the chemical modification required to prepare the surface often takes longer to perform than the attachment of the linker and protein [115, 116]. The chemical reactions involved are sensitive to slight variations in environmental conditions, reactant quantities, and handling for each step, which may compound into much larger fluctuations in yield between batches. Additional side reactions also occur with each step further reducing the overall yield and reproducibility [180].

The majority of techniques utilised for chemical protein immobilisation are not scalable. Many of these techniques have shown success under laboratory conditions by skilled chemists, a situation that is not common in manufacturing environments. The chemicals required are potentially hazardous, expensive, or currently unavailable to be purchased in the bulk quantities required for manufacturing. For example, γ-aminopropyl-triethoxysilane used for silanisation is corrosive and flammable. EDC, which appears in multiple linking chemistries, causes skin irritation, eye damage, and organ damage, according to the Safety Data Sheet. The use of such chemicals would also require additional safety facilities and equipment under work safety regulations and introduces significant hurdles concerning waste disposal and regulatory approval.

Table 1.2. Protein-functionalisation of titanium surfaces through linker-chemistry methods. A summary of deposition processes, synthesis times, investigated proteins, and biological testing.

Linker molecule(s)	**Application/ deposition processes**	**Synthesis Time (excluding substrate preparation)**	**Proteins immobilised**	***In vitro/vivo testing***
Silanisation [121] e.g. Aminosilanes Glycidoxysilanes Mercaptosilanes	1) Immersion [61, 103, 167, 168, 170, 171] 2) Self Assembling Monolayer (SAM) [179]	1) Immersion: 3 hours [103] to 10 hours [61] immersion and drying overnight - Followed by the required chemistry. 2) SAM: Silane was added and allowed to react for 3 hours, followed by washing and overnight drying. Protein immobilisation was then performed (2 hours).	Collagen [120, 123, 181, 182] Bovine Serum Albumin (BSA) Trypsin A branched adhesion biomolecule [124] BMP-2 [57] Heparin	Bone marrow stem cells [57] Rat Osteoblasts [103] h-Mesenchymal stem cells and *in vivo* rabbit model [120, 123]
PEGylation [92]	**1) Individual** i) Electrodeposition ii) Immersion **2) Copolymer** Conjugated with Silanes [133]/ Ethyl 3-Mercaptopropionyl-Succinic Acid (EMPSA) [132]	**1) Individual** i) 300s for electrodeposition excluding the drying step [131]. ii) (time) incubation in PEG buffer solution **2) Copolymer** Step 1: 42 hours for the synthesis of silane-PEG-Col. Step2: 3 days for the preparation of EMPSA conjugated PEG [132]	Collagen BMP-2	HUVEC ECV304 endothelial cells Platelets [133]
Heparinisation [138]	**1) Individual** Click reaction [139] **2) Copolymer** Solution incubation with DOPA	**1) Individual** Amine-functionalisation of substrate required for heparin attachment, followed by incubation in buffer and protein immobilisation. 5-6 days [139, 184]	BMP-2 [56] Lactoferrin [135]	MG63 Osteosarcoma [135] *In vivo* Dog model (13 - 15 kg) [56]

	[56, 135, 138, 139] Solution with Collagen [183]	**2) Copolymer** Immersion in DOPA solution for 24 hours, followed by exposure to an EDC/NHS/Heparin solution (time unspecified). Protein immobilisation was then performed for 6-24 hours depending on the protein.		
Polydopamine	**1) Individual** Tris(hydroxymethyl) aminomethane (Tris) – hydrochloric acid solution overnight. [134, 152-154] **2) Copolymer** See Heparinisation [56, 135, 138, 139]	**1) Individual** Overnight immersion in DOPA – Tris/HCl buffer, followed by protein immobilisation. **2) Copolymer** Refer to heparin co-polymerisation synthesis time above.	BMP-2 [142, 172], Chitosan [136] Fibronectin [185] collagen [134] RGD peptide and nanoparticles [142]	Rat bone marrow-derived osteoblast-like cells MC3T3-E1 transformed mouse osteoblast-like cells Immortalized human mesenchymal 3A6 Cells [142] Rabbit model [155, 156]
Chitosan	**1) Individual** Electrodeposition [186] **2) Copolymer** Solution with DOPA [136, 145-147, 187]	**1) Individual** Electrodeposition: Stirring in water-acetic acid solution for 24 hours. Deposition for 400 seconds at 10 V/cm.[186] **2) Copolymer** DOPA was first deposited overnight and allowed to dry. Carboxymethyl chitosan was prepared and added in EDC/NHS solution for 16 hours, followed by protein immobilisation.	BMP-2	In vitro: *S. aureus* *S.epidermidis* Osteoblasts Human Mesenchymal stem cells (hMSCs) [136] Sarcoma osteogenic SaOS-2 [146]
Self-assembling monolayers (SAMs) [175]	1) Electrodeposition [176] 2) Incubation and Protein inclusion in SAM structure [174]	1) Electrodeposition: 250 - 400 seconds after 24 hours surface preparation [176, 188] 2) Immersion time depends on the monomer used: Alkyl Phosphonic Acid (1-5 days) [176, 189], Silane (2 days- see above) [179]. Protein inclusion in SAM requires 4 hours preparation plus lyophilisation, followed by 5 hours deposition [174].	Bovine serum albumin (BSA) [179]	Mesenchymal stem cells [179]

1.3.3 Covalent immobilisation via dry and plasma methods

Chemical immobilisation proved that it was possible to covalently immobilise proteins to orthopaedic substrates, overcoming the unintentional protein release observed in adsorption approaches due to the Vroman effect. However, the complexity of the wet chemistry, time requirements, batch variability, and waste disposal issues have encouraged the development of dry plasma-based approaches to the biological functionalisation of surfaces.

1.3.3.1 Physical surface treatment procedures

A variety of plasma-based processes have been applied for surface engineering of orthopaedic implants. These techniques utilise plasma, referred to as the fourth state of matter, to treat the surface of the implant. Plasma discharges produce a partially ionised gas comprising of electrons, photons, and ionised and neutral species [190]. Plasmas are considered "quasi-neutral" due to an overall charge neutrality between electrons and ionised species [191, 192]. However, local regions of like-charges can form and influence the random motion of charged species. Electrons, ions, and neutral particles undergo collisions and energy transfer, giving rise to a thermodynamic equilibrium. Plasmas referred to as "hot plasma" are those where all the electrons, ions, and neutrals are in equilibrium, such as in the Sun. Plasmas referred to as "cold plasma" are those where the electrons, ions, and neutrals are not in equilibrium. Cold plasmas are typically used for surface modification [193-195]. As outlined in **Figure 1.12**, there are two general categories of plasma-based technologies: i) non-depositing plasma treatments which implant ionic species into a surface to modify it, e.g. plasma immersion ion implantation (PIII or PI^3), and ii) depositing plasmas that coat the surface with an additional layer of new material. This section will focus on the depositing processes suitable for the modification of orthopaedic devices, and the use of the non-depositing technique, plasma immersion ion implantation (PIII or PI^3), to modify the surfaces of PEEK substrates.

There are two plasma enhanced (PE) deposition techniques for coating orthopaedic implants: physical vapour deposition (PVD) and chemical vapour deposition (CVD). Physical vapour deposition uses physical processes to generate a vapour from a solid or liquid source such as electron or laser beam ablations, sputtering, or thermal evaporation. The vapour is transported *in vacuo* to the substrate, where it recondenses into a thin film [196]. PVD is used for the deposition of calcium phosphates (CaP)/ hydroxyapatite (HA) coatings for orthopaedic applications and has been applied to commercial products [197-199]. CaP and HA layers have not been used for covalent protein immobilisation. However, it is possible to immobilise proteins through Schiff-base reactions on hydrazine modified calcium phosphonates [200]. The use of CaP as orthopaedic coatings has been reviewed elsewhere [201, 202].

Chemical vapour deposition generates reagent vapours from liquid or gaseous sources and relies on chemistry occurring on the substrate surface to form a thin film coating. A substrate is exposed to volatile reactant gases under vacuum. The process uses heat as a source of energy, typically between 600˚C - 1200˚C, to initiate chemical reactions in the gas phase. The condensable chemical species deposit on the substrate where they form a thin film [196]. The application of high temperatures increases the mobility of species at the interface promoting the formation of an interfacial mixing layer between the substrate and the thin film. However, high temperatures restrict the number of suitable substrates and coating materials to those with high thermal tolerance [202]. CVD and its variants have become increasingly popular for biointerface applications and have been reviewed elsewhere [196, 202].

Plasma enhancement is used to provide additional energy in the PVD and CVD processes. The additional energy creates more reactive, excited, or ionised species and is often used to reduce the operating temperature. In both processes, the precursor vapour is excited into the plasma state. The electrons in the plasma are used as the form of energy input and excite the reactant gases, resulting in ionisation, radical fragmentation, and enhanced plasma phase chemistry. Plasma enhanced physical

vapour deposition (PEPVD) has been used to deposit CaP layers onto orthopaedics [203-205]. However, these layers have not been used for protein immobilisation. The processes and applications of PEPVD have been reviewed elsewhere [206].

PECVD is used to produce plasma polymer interlayers commonly used for biointerfaces [196, 207]. A nano-thin layer of coating, comprising primarily of carbon, is deposited on any substrate exposed to the plasma. Highly cross-linked polymer structures are formed through a radical fragmentation-recombination process [193]. The PECVD process is versatile, allowing the production of coatings with a range of surface chemistries, SFEs, and charge by tuning the precursor gas composition and deposition parameters, such as precursor gas pressure and energy coupled into the plasma. The carbon-based thin film interlayers are typically biocompatible and functionalisable with subsequent plasma or wet chemical treatments to incorporate additional surface chemical groups suitable for protein immobilisation (see **Figure 1.12**). The surface modification achieved by plasma polymerisation is substrate independent [208], and therefore, plasma polymer (PP) interlayers, thin films (PPFs), and coatings deposited on substrates other than titanium are also reviewed here as they could potentially be applied to orthopaedic materials. Further explanations of PECVD processes and mechanisms can be found within [196, 207].

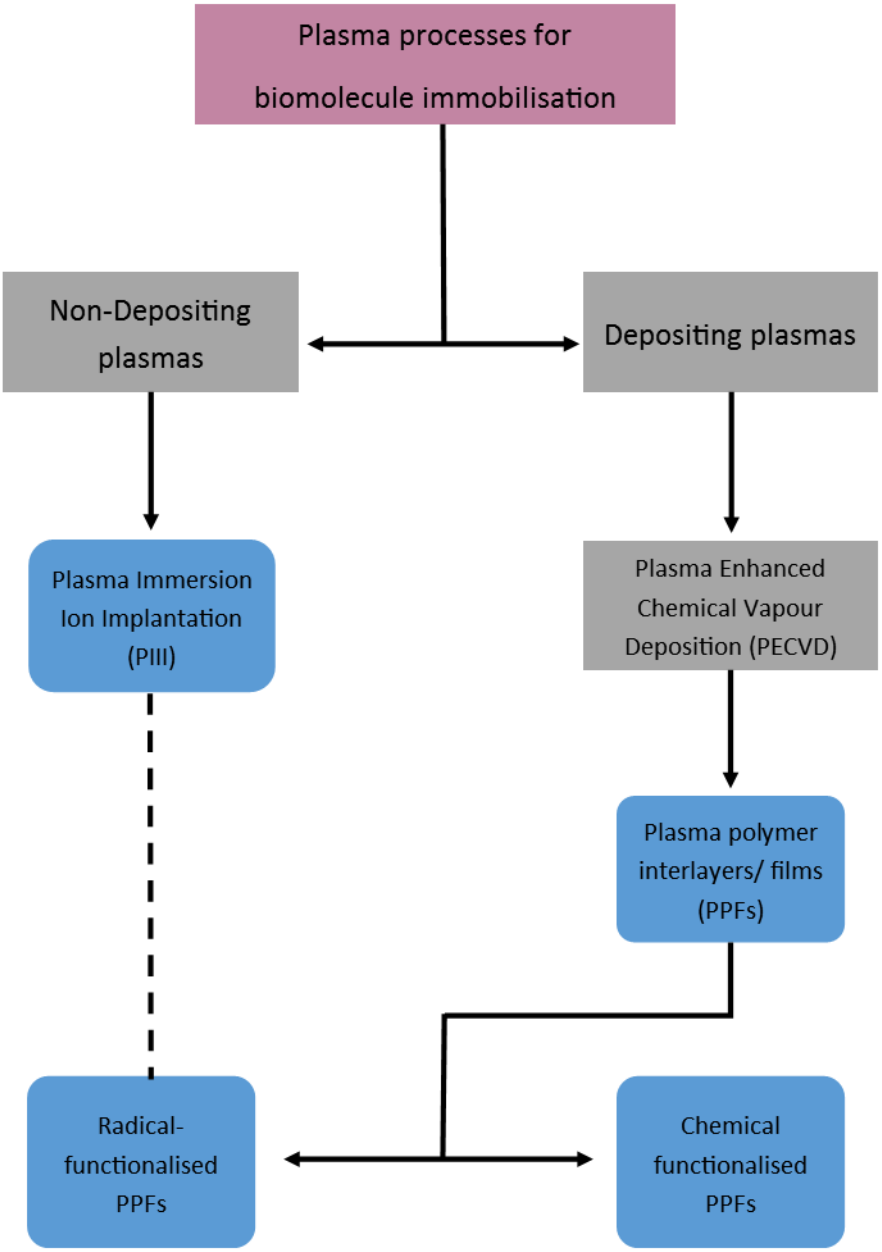

Figure 1.12. An outline of plasma processes used for biomolecule immobilisation. Plasmas used for treatments are categorised as non-depositing and depositing plasmas. Non-depositing plasmas generate radicals in the existing substrate which are then used for covalent biomolecule immobilisation. The depositing plasmas used for biomolecule immobilisation focus on the deposition of polymeric thin film coatings. These can then be used to immobilise proteins through further wet chemical reactions (chemically functionalised PPFs) or through radicals embedded in the coatings (plasma activated coatings).

1.3.3.2 Protein immobilisation onto plasma polymer interlayers

Functional molecules can be immobilised on PP films through two approaches: multi-step attachment through chemical linkers or direct attachment. Multi-step attachment by means of chemical linker molecules is applied through an intermediate wet chemistry step [209-214]. The linkers may also include polymer brushes [207, 215]. Direct immobilisation of the biomolecule to the PP surface is achieved through radicals and/or surface functional groups present on the coating, referred to as "moieties" here [216, 217].

Multi-step immobilisation on PP films through chemical linkers

Post-synthesis grafting of functional molecules onto PP films can be performed through chemical linkers. The attachment of chemical linkers still requires subsequent wet chemistry steps to covalently bind the target proteins, but the use of PP films eliminates the need for substrate pretreatment and broadens the range of functionalisable substrates. Surface moieties can also be included as to improve the surface chemistry. The first use of post-synthesis linkers for protein immobilisation on PPFs for an orthopaedic application was by Puleo *et al.* [218]. The authors grafted BMP-4 onto an allylamine PP (ppAAm) through two chemical modification approaches: (i) a method based on the one-step EDC/NHS carbodiimide reactions (as depicted in **Figure 1.11**); and (ii) a two-step succinic anhydride and EDC carbodiimide process utilizing the amine groups on the PP surface (**Figure 1.13**) [218]. The authors proposed that the two-step approach was more effective in binding the test lysosome enzyme, and therefore BMP-2, due to the sequential exposure to the cross-linking components. This strategy removes the potential for protein-protein cross-linking reactions observed in the one-step process. This was demonstrated by the enzymatic activity which showed complete enzyme deactivation from the one-step method, while the two-step immobilisation retained 75-80% of the enzyme functionality.

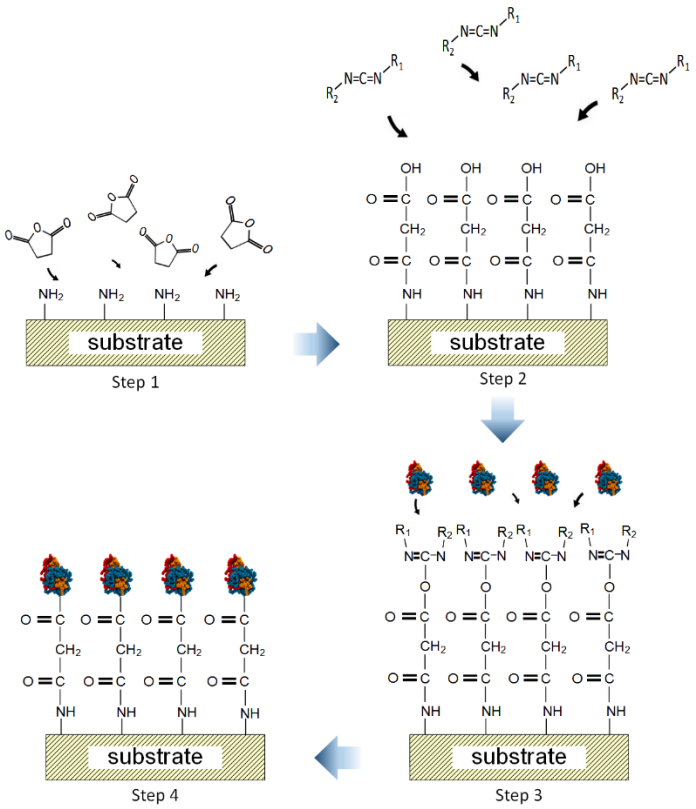

Figure 1.13. A schematic illustration of the chemical reactions for the 2-Step carbodiimide chemistry. The 2-step immobilisation chemistry incorporates succinic anhydride to modify the amine-functionalised surface into a carboxyl-functionalised surface before commencing EDC/NHS reactions, as per the traditional 1-step approach outlined in **Figure 1.11**. The process changes the focus of the chemistry from modifying the proteins to modifying the surface moieties. The authors report an accompanying increase in biological activity and decrease in protein cross-linking. Adapted with permission from [218].

Following this application of PPFs, the field has developed multiple techniques capable of binding proteins. An extensive range of proteins and attachment procedures have been investigated, primarily using alkyl (carbon) PP interlayers [209-214]. Briefly, the polymer is deposited on the substrate by PECVD. The appropriate moieties on the coatings are then reacted with a chemical linker (e.g. silane or PEG), followed by further chemical reactions for protein immobilisation, as described previously in Section 3.2.

Protein immobilisation via plasma polymer brushes

Polymeric molecules tethered to the surface to form brush-like structures are referred to as polymer brushes. These structures can be synthesised on PP coatings and attached to the substrate by means of either chemical reactions in solvents [219] or free radicals (atom transfer radical polymerisation) [220, 221]. Simply, a PP film is deposited onto the desired substrate which is then exposed to the brush monomer reagent, either as vapour [220, 221] or in solution [219]. Energy to promote the reactions is supplied as either heat or UV radiation. Polymer brushes have been synthesised primarily to prevent protein adsorption to surfaces as reviewed by Keating [222] and Krishnamoorthy [223]. Such structures can also be used for protein release applications [224, 225]. Polymer brushes could potentially be used for covalent protein immobilisation if the antifouling end groups were replaced by reactive groups such as those used for chemical linker-mediated immobilisation.

Direct immobilisation on PP films

Proteins can also be directly immobilised on plasma polymer coated substrates through covalent bonding with reactive functionalities present on the surface, as schematically illustrated in **Figure 1.14**. PP films that present reactive functionalities, such as amine or carboxyl groups, are known in the field as “functionalised PPFs” [195]. They have been developed over the last three decades and include those functionalised with specific chemical reactive groups and highly-reactive, non-specific radicals.

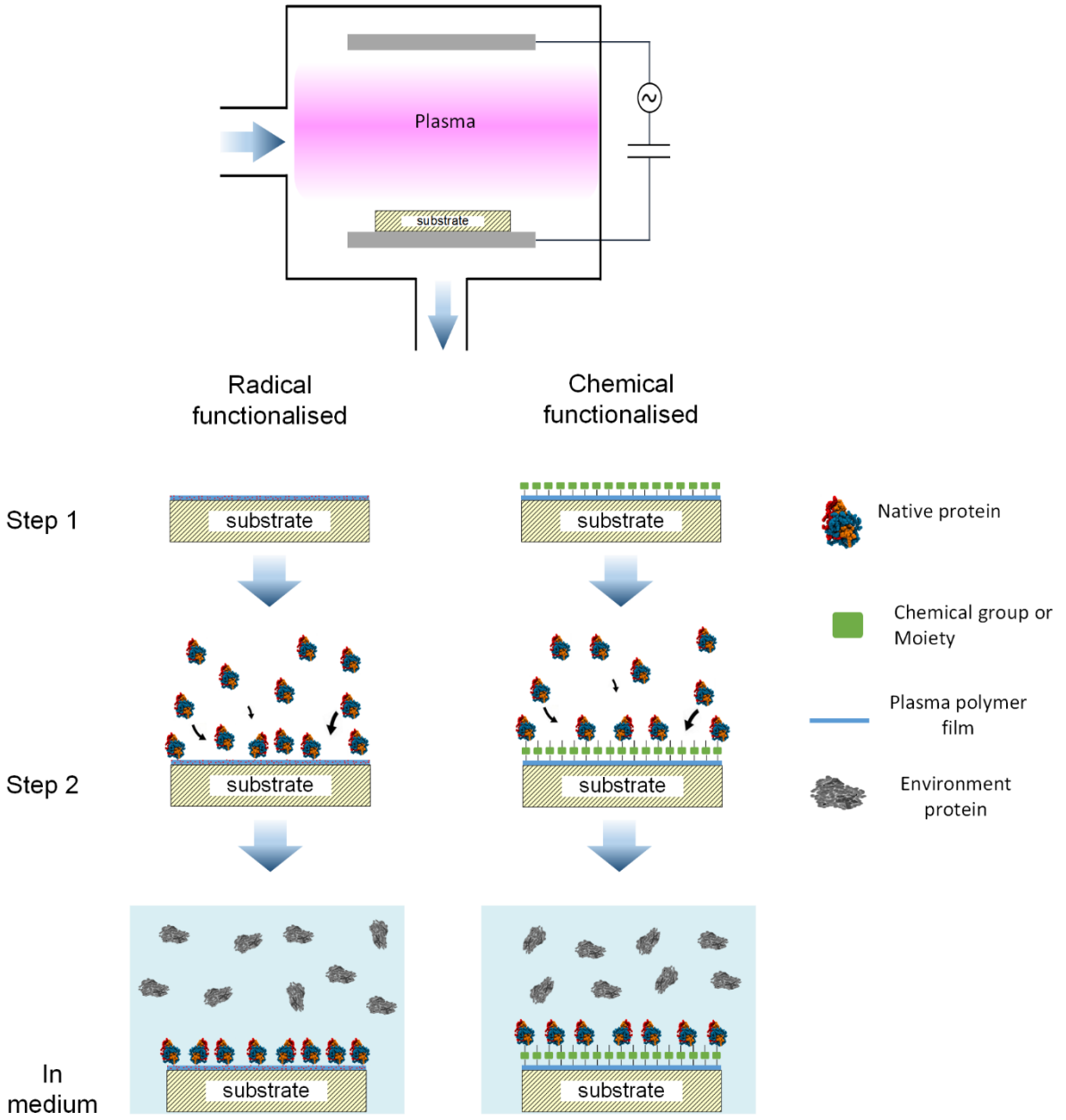

Figure 1.14. An outline of the biomolecule immobilisation procedure for free radical functionalised and chemically functionalised plasma polymer thin films (cPPFs). The PPFs are deposited on substrates inside a vacuum chamber either by a single or multi-step deposition (step 1). The PPF substrates are removed and undergo the required immobilisation procedures (step 2). For cPPFs, this includes wet chemical carbodiimide, Schiff-base, or disulfide reactions. For radical-functionalised PPFs (rPPFs), covalent protein coupling is achieved by a simple incubation step in the protein-buffer solution.

Direct Immobilisation through Specific Chemical Groups

The inclusion of functional groups or moieties in the surface coating that can be reacted directly with groups on the protein facilitates direct covalent immobilisation without the need for a linker molecule **(Figure 1.14**). A variety of moieties have been integrated into plasma polymer coatings for this purpose, with the most common being amine [226, 227], carboxyl [228], and aldehyde [229, 230] moieties. More recently, epoxy moieties have also been used to achieve covalent coupling of proteins to PPF surfaces through ring opening reactions [212]. The chemically functionalised PPs films (cPPFs) are produced through single or multi-step deposition procedures before protein immobilisation, as listed in **Table 1.3**. The first stage involves the deposition of a carbon-rich PP thin film. The following step(s) may include exposure to vapours (which may be in the form of another plasma) containing reactive fragments which form the desired functional groups on the surface. The synthesis of PP coatings functionalised with reactive moieties is generally performed at low plasma specific energies to avoid extensive fragmentation and thereby retaining the chemical functional group of the precursor monomer [231-234]. The plasma specific energy (W/F) is the available energy per unit volume of monomer as denoted by the ratio of plasma input power (W) to monomer flow rate (F) [235, 236]. The surface functional groups allow for directed protein immobilisation by chemical reactions with specific groups on the proteins, such as carboxyl or amine groups.

Amine and carboxyl moieties are the most studied surface functional groups in the literature. The amine and carboxyl moieties are produced through various procedures listed in **Table 1.3**, with the secondary treatments including N_2 gas and nitrogen-rich compounds for amine groups and Ar gas with carbon-oxygen (alkyl) compounds to obtain carboxyl functional groups. Amine- and carboxyl-functionalised PP films have been reported to considerably enhance cell attachment and proliferation without protein immobilisation via chemical coupling [237-242]. Specific to bone-forming cells, Jung *et al.* compared amine-, carboxyl-, and hydroxyl functionalised PPFs seeded with MC3T3-E1 cells [243]. They showed that the amine groups resulted in higher day 4 proliferation, whereas carboxyl groups

outperformed amine groups by day 7, as shown in **Figure 1.15**. It was proposed that the amino groups enhanced cellular adhesion, but the negatively charged carboxyl groups enhanced cell proliferation.

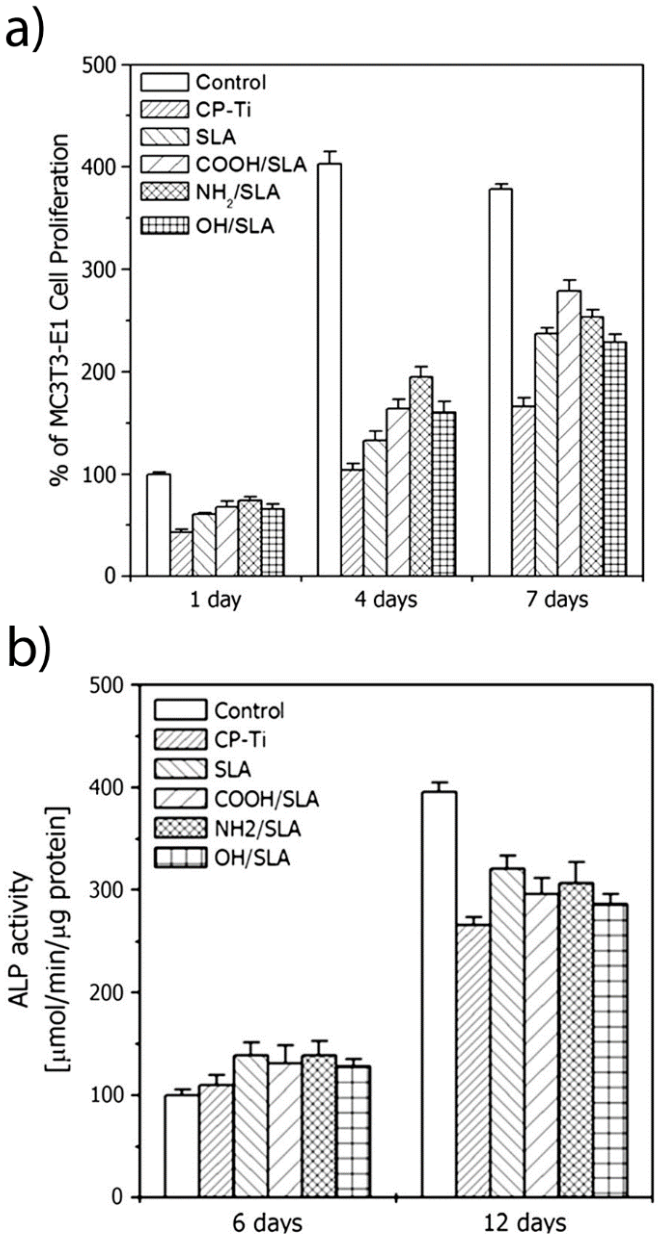

Figure 1.15. Proliferation (**a**) and alkaline phosphatase production (**b**) of MC3T3-E1 osteoblast-like cells on tissue culture plastic (Control), smooth Ti (CP-Ti), roughened (SLA), and PPFs functionalised with COOH, NH_2, and OH. Proliferation results showed an increase in cell number on COOH and NH_2 coatings at all time points, while ALP production was found to be approximately equal, suggesting no significant increases in mineralisation. Reprinted with permission from [243].

Liu *et al.* observed increased mineralisation in adipose-derived stem cells deposited on amine-functionalised PPs, due to the upregulation of osteoblast-specific markers and positive surface charge [244]. It is generally accepted that such improvements in cell behaviour on surfaces are mediated by surface adsorbed proteins from the medium [50]. Both carboxyl and amine groups acquire surface charge in the medium and therefore enhance the surface hydrophilicity, which in turn results in better retention of the native conformation of adsorbed proteins (as outlined in Section 2). The ability to preserve native protein conformations is also essential for surfaces used for covalent immobilisation of proteins. Covalent protein immobilisation on amine- and carboxyl-functionalised surfaces require the use of EDC/NHS chemistry to form carbodiimide bonds [214]. Heller *et al.* used an amine-functionalised PP film deposited from allylamine to compare the cellular response of human osteoblasts (HOBs) and umbilical cord cells (HUVACs) to fibrinogen, collagen, laminin, and osteopontin immobilised onto the PP surfaces [214]. Fibrinogen and collagen resulted in significantly higher cell coverage for HUVACs and HOBs compared to titanium as shown in **Figure 1.16**.

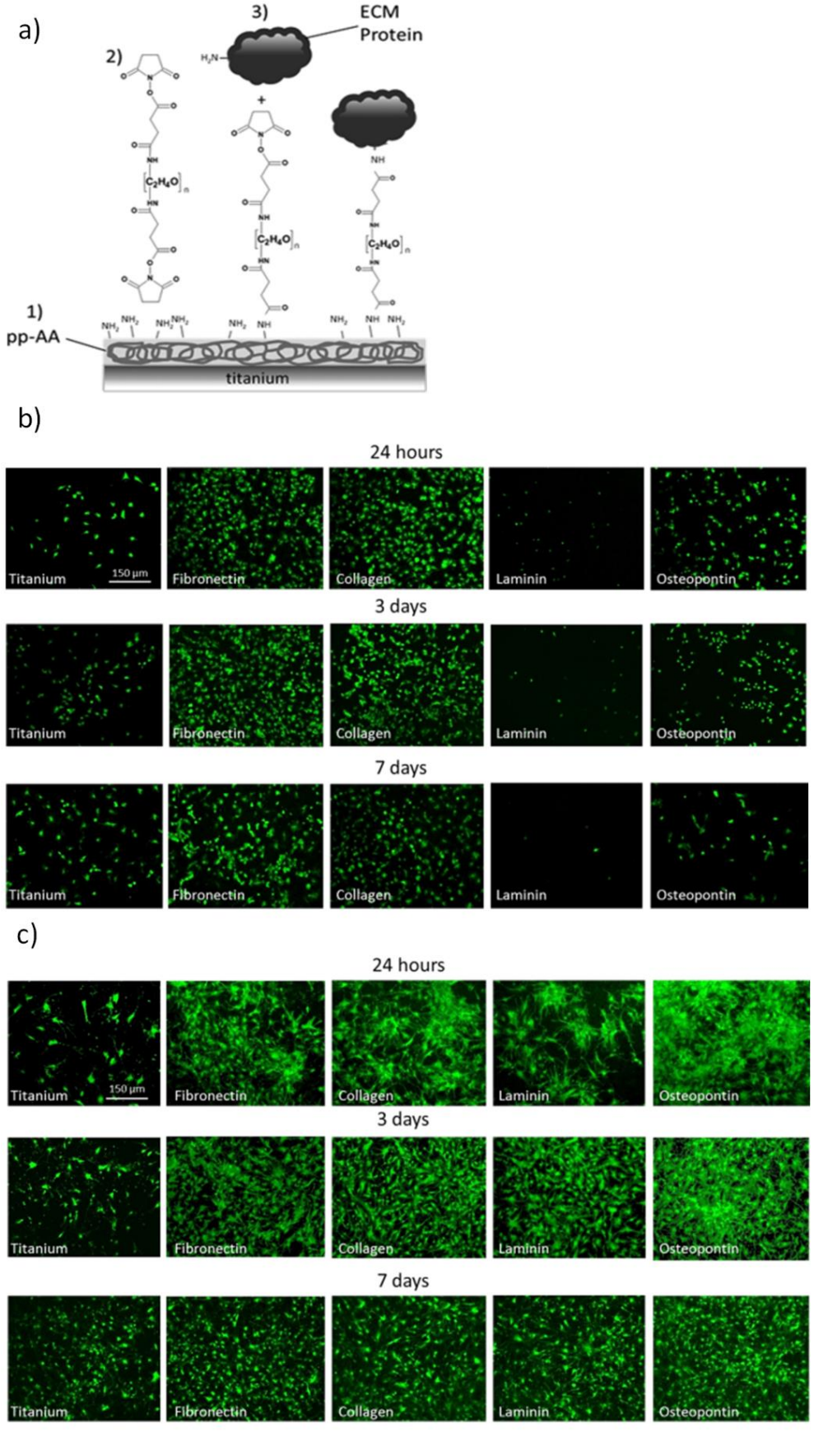
a)
3)
ECM
Protein
2)
1)
pp-AA
titanium
b)
24 hours
Titanium
150 µm
Fibronectin
Collagen
Laminin
Osteopontin
3 days
Titanium
Fibronectin
Collagen
Laminin
Osteopontin
7 days
Titanium
Fibronectin
Collagen
Laminin
Osteopontin
c)
24 hours
Titanium
150 µm
Fibronectin
Collagen
Laminin
Osteopontin
3 days
Titanium
Fibronectin
Collagen
Laminin
Osteopontin
7 days
Titanium
Fibronectin
Collagen
Laminin
Osteopontin

Figure 1.16. Fibronectin, collagen, laminin, and osteopontin were covalently immobilised to the amine-functionalised plasma polymer film via EDC/NHS chemistry, as outlined in (a) and **Figure 1.11**. The cell growth of HUVACS (b) and HOBs (c) was fluorescently imaged with calcein-AM. HUVACs demonstrated a distinct preference for fibronectin and collagen producing consistently elevated proliferation compared to the untreated Ti control (b). The authors attribute the discrepancy between fibronectin, collagen, and laminin to be the expression of the RGD adhesion sequence and the absence of the laminin integrin sequence on the HUVACs. Osteopontin also possesses this RGD sequence but the concentration may have been insufficient for HUVACs stimulation. The authors suggest that the HOBs possess binding sites for both the RGD sequence and the laminin-integrins thereby explaining increased attachment and proliferation across all functionalised surfaces compared to the control (c). Reprinted with permission from [214].

Aldehyde-functionalised PP films have not been studied as widely as their amine and carboxyl counterparts. These functional groups form hydrolysable covalent bonds with the target proteins through Schiff-base reactions that can be stabilised through a subsequent reduction reaction [165, 166, 208]. Aldehyde moieties can be produced by the deposition of aldehyde-containing precursor monomers, such as acetylaldehyde, benzylaldehyde [208], and propionaldehyde [245]. Direct protein immobilisation to aldehyde-functionalised PP has been achieved with streptavidin [245, 246] and heparin [247]. These PPFs have also been used as platforms for the immobilisation of non-fouling [248] and antifungal agents [249].

The first epoxy-functionalised PP film was developed by Inagaki *et al.* using allyl glycidyl ether monomer through a one-step deposition [250]. Oehr *et al.* [251] and Tarducci *et al.* [252] suggested that the reactive chemistry of the epoxy rings can be used to immobilise proteins through ring opening S_N2 reactions [162]. Experimental examination of protein immobilisation was performed by Thierry *et al.* [212], who immobilised lysozyme to an epoxy-functionalised PP film. Further biomolecule immobilisation applications, such as DNA probes [253, 254], have been explored but this PPF has not been applied to orthopaedics.

Table 1.3. Summary of direct immobilisation of proteins on functionalised plasma polymer films

"Functionalised" PP	Surface groups/moieties	Polymerisation method	Immobilised biomolecules	In vitro/ vivo testing
Amine	Amine (-NH_2) Amides (-N-R'/R")	Plasma polymerisation of allylamine [243], heptylamine [255] Addition of diamino cyclohexane (DACH) [216, 256]	fibrinogen, collagen, laminin, osteopontin [214]	MC3T3-E1 cells [243] Human osteoblast (HOB) and umbilical cord cells (HUVACs) [214] Adipose-derived stem cells [244]
Carboxyl	COOH CO_x	Plasma polymerisation: Deposition of Acrylic acid [236, 243, 257], and propanoic acid [255, 258]. Grafting with polyethylene oxide [259]	Collagen PtA-AF546 [257]	MC3T3-E1 cells [243]
Aldehyde	R-C=O	Plasma polymerisation of Alkyl/allyl aldehydes: acetylaldehyde, benzylaldehyde, propionaldehyde [208, 246, 248] ethylbutyraldehyde, capronaldehyde, nonylaldehyde [229]	Collagen, streptavidin [245, 246], heparin [247], antifungal agents [249]]	
Epoxy		Plasma polymerisation of allyl glycidyl ether [250]	Lysosome [212] DNA probes [253, 254]	

Direct immobilisation through non-specific reactive radicals

Direct immobilisation of proteins by means of radicals can be performed through two techniques depending on the substrate: (i) plasma immersion ion implantation (PIII or PI^3) for carbon-rich substrates such as most polymers [260-264], and (ii) a combination of plasma polymerisation and PIII treatment for the fabrication of radical-functionalised PP films on other substrates such as metals and ceramics [265-267]. Covalent immobilisation through reactions with radicals following these

processes is achieved upon contact with biomolecules in buffer solution without the need for chemical treatments [264].

PIII is a non-depositing technique that utilises energetic ions to generate radicals for covalent immobilisation of biomolecules [268]. Simply, the substrate is mounted on a negatively biased holder inside a reactor and exposed to the plasma. A negative bias of several kV is pulsed as a function of time with the resulting electric field repelling electrons and attracting ionic species. This pulsed bias forms an ion sheath around the sample holder and implants the ions into the substrate at a depth dependent on the bias. A detailed explanation can be found within [217]. This process has been investigated extensively for PEEK, with a range of treatment conditions and immobilised biomolecules examined [264, 269-271]. The PIII technique has also been used to implant N, C, O, and other elements into the surface of titanium [272-276]. This research focussed on titanium surface hardening with nitrogen [276, 277] and the addition of antibacterial properties with the implantation of Cu [278]. However, this procedure does not allow for direct radical-mediated immobilisation of biomolecules. Radical-mediated immobilisation of biomolecules to metallic orthopaedic substrates can be performed through radical-functionalised PPFs.

All PP interlayers contain radicals in the coatings as they are inherent to the fragmentation-recombination mechanisms of plasma polymerisation [221, 279]. The immobilisation of compounds through radicals embedded in PP films has been investigated outside of protein immobilisation, mainly focussing on the formation and grafting of polymer brushes for non-fouling applications [220, 221]. Covalent immobilisation of proteins through embedded radicals in a PP film was first reported by Kondyurin *et al.* [280] using n-hexane as a precursor. Subsequent work showed that alternative carbon-containing precursors, such as acetylene [264], can be used. Radical-functionalised PP films, also referred to as plasma activated coatings (PAC), are deposited from carbon-rich monomers while the substrate is negatively pulsed biased. The pulsed biasing of the substrate enhances the ion-bombardment, leading to PP structures with greater concentrations of radicals [58, 281, 282]. These

coatings have shown radical retention in aerobic environments for at least 15 days [58] and can still contain reactive radicals 4.5 months after deposition [283]. It is also possible to restore radical-functionality to a polymer film by driving off the oxygen via annealing [283]. The chemistry and properties of radical-functionalised PPFs can be tuned by the addition of other reactive gases, such as N_2, H_2, and O_2 during deposition [264, 266]. The immobilised biomolecules have also been shown to retain their bioactivity after immobilisation and also after freeze-drying [284]. Mechanical analysis of the PAC/protein system showed excellent mechanical stability through the formation of a graded interface between a stainless-steel substrate and PAC using magnetron sputtering during PAC deposition [264, 285]. In the case of carbide forming substrates, such as titanium and zirconium, the graded interface is not required due to the formation of covalent bonds between the substrate and the PAC layer [286]. Chrzanowski *et al.* created an adherent polymer layer by ion implanting a thin spin-coated polystyrene film on a NiTi substrate [287]. The samples were washed with 5% sodium dodecyl sulfate (SDS) (w/v) at 100˚C for 1 hour to evaluate the covalent binding capability of the radical-functionalised polymer layer. The radical-functionalised sample demonstrated an initial protein attachment of 1782 ± 110.0 ng/cm^2 and a 63 ± 7% retention of a fibronectin-osteocalcin fusion protein (FN-OCN) post-SDS washing, while the non-functionalised polystyrene control presented an initial protein attachment of 880.0 ± 22.2 ng/cm^2 and a 21 ± 2% protein retention, as shown in **Figure 1.17**. The significant retention of protein on the radical-functionalised substrate indicated covalent immobilisation.

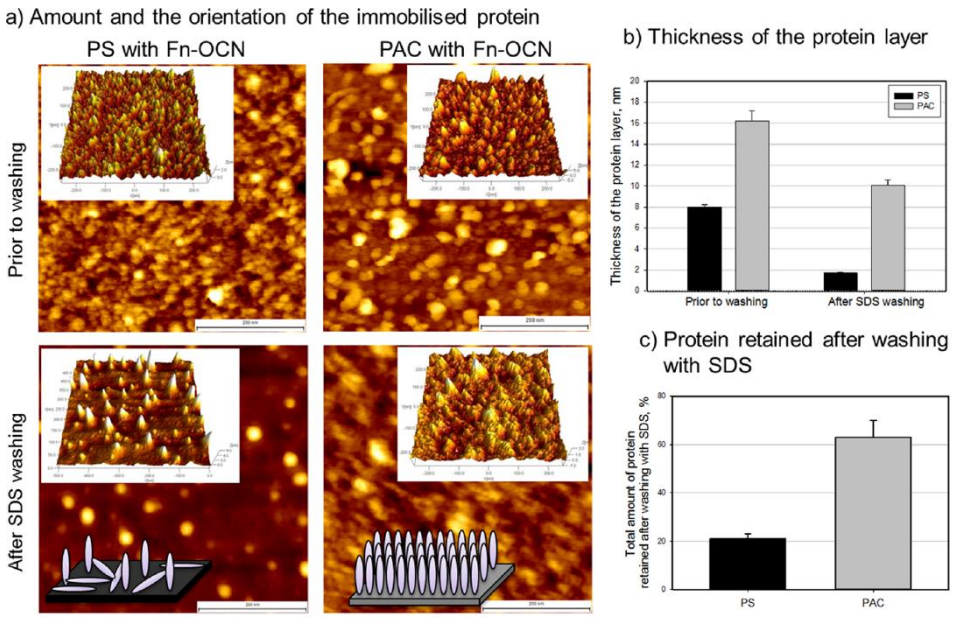

Figure 1.17. Atomic force microscopy (AFM) assessment of the immobilised FN-OCN protein on radical-functionalised and non-functionalised polystyrene (PS) coated silicon pre- and post- SDS washing. **a)** AFM topographical images of the unwashed and SDS-washed substrates. The PIII-treated substrates demonstrate a higher density of proteins both pre- and post- SDS washing, while the non-functionalised PS retained a significantly lower concentration, suggesting non-covalent protein binding. Graphical depictions of the protein layer thickness, and thereby, protein quantity is shown in (**b** and **c**). The authors state that the radical-functionalised PS demonstrated minimal changes to the protein layer thickness while a significant removal of protein is observed on the non-functionalised PS. Reprinted with permission from [287].

The authors also showed an increase in MSC differentiation into osteoblasts after 21-days through the immobilisation of the fibronectin-osteocalcin fusion protein compared to the bare and fibronectin controls. This was demonstrated by the elevated cell density, focal adhesion points (FAK), and osteopontin (OPN) as shown in **Figure 1.18**. More recently, Yeo *et al.* [58] demonstrated a significant increase in osteoblast-like cell proliferation and mineralisation using tropoelastin-functionalised PAC on zirconium. These works show that radical-functionalised surfaces facilitate direct covalent biological functionalisation of a range of orthopaedic implant materials (**Figure 1.19**).

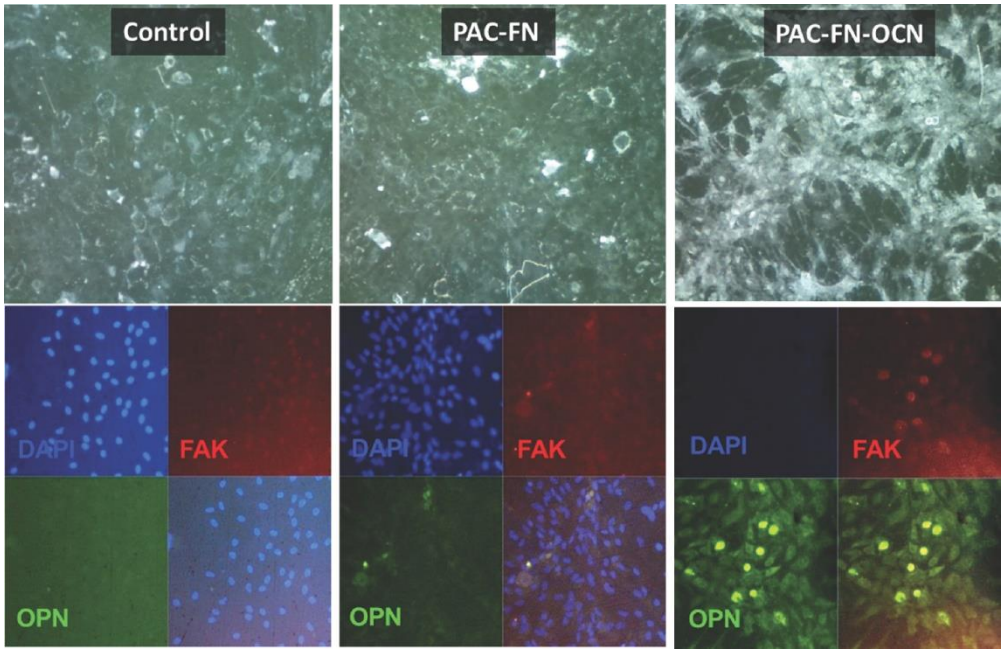

Figure 1.18. Phase contrast and immunostaining images of mesenchymal stem cells (MSCs) on control nickel-titanium (CON), fibronectin immobilised PAC (FN), and fusion-protein immobilised PAC (FN-OCN). Phase contrast images (top row) show a significantly greater attachment of MSCs on the FN-OCN samples compared to FN and Control. The immunostaining images on the bottom row demonstrate an increased quantity of focal adhesion points (FAK) and osteopontin expression (OPN), indicating more cell differentiation into osteoblasts on the FN-OCN functionalised substrates. Reprinted with permission from [287].

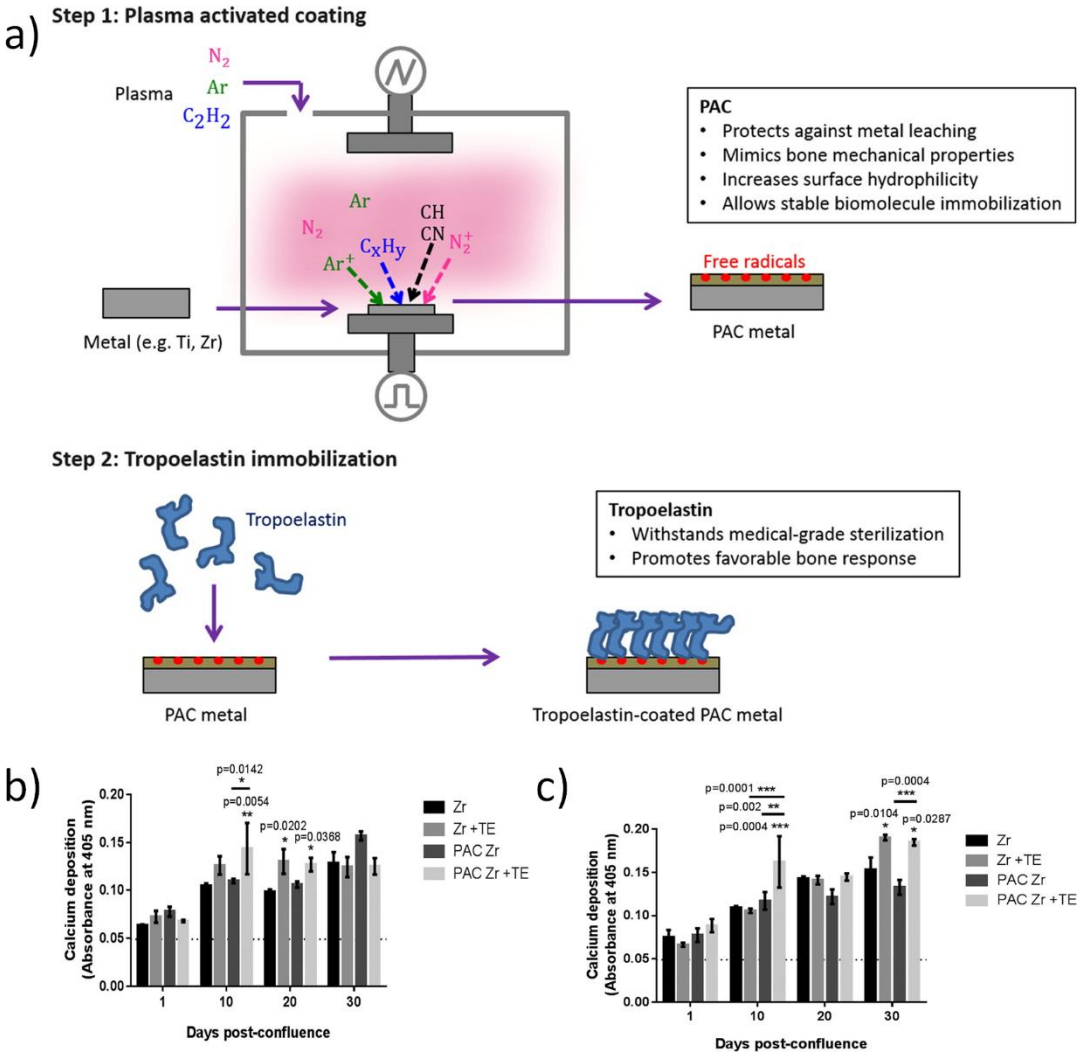

Figure 1.19. a) PAC deposition and protein immobilisation schematic of tropoelastin (also outlined in **Figure 1.14)**. The calcium deposition of MG63 cells at 1, 10, 20, and 30 days post-confluence in non-osteogenic **(b)**, and osteogenic **(c)** media was quantified with alizarinRed staining. Significant increases were recorded for substrates possessing tropoelastin, with the upregulation of ALP resulting in increased mineralisation at 20 days post-confluence in (b) and 30 days post-confluence in **(c)**. Reprinted with permission from [58].

1.3.3.3 Evaluation of physical immobilisation approaches

Physical covalent immobilisation of biomolecules is the most recent approach to orthopaedic biomimetic functionalisation and possesses advantages over adsorption and chemical covalent immobilisation. The PIII treatment or the deposition of radical-functionalised PP films together with the subsequent protein immobilisation step can be performed in a few hours rather than the days

required for chemical immobilisation. Radical-functionalised PPFs (rPPFs) covalently immobilise biomolecules upon contact providing the strength of covalent attachment with a simple process more akin to adsorption. These plasma-based methods are relatively “green” and produce minimal waste compared to chemical approaches [288]. Protein immobilisation on conventional chemically functionalised PPFs (cPPFs) is not entirely waste-free due to the use of EDC/NHS for carbodiimide chemistry or other agents for Schiff-base reduction. The synthesis methods of PPFs can be effectively scaled up as PIII, PEPVD, and PECVD methods are extensively used in a range of industrial environments [288, 289].

The disadvantages of physical covalent immobilisation techniques are primarily associated with the capital costs of the power supplies and vacuum systems. The deposition techniques make use of volatile chemicals and pressurised gases which require the installation of compliant gas management facilities [288]. In a manufacturing context, this is likely to be offset by costs associated with the multi-step complexity, monitoring, and purification required in wet chemical approaches for covalent coupling to ensure compliance with regulatory standards for implantable biomedical devices.

Ageing of plasma modified surfaces is a potential problem for applications where biomolecules are to be immobilised in a separate process after long-term storage. All plasma polymers contain radicals and, therefore, undergo radical recombination and autoxidation (reaction with air) [207]. The recombination of radicals is the reaction of the radical with an electron accepting molecule. While the principle of recombination appears simple, the recombination behaviour can be complex depending on the conditions of PP film synthesis [290, 291]. Autoxidation is the oxidation of the PPF due to interactions between reactive species at the air-surface interface [207, 292, 293]. This effect is greatest over the first few hours and stabilises with time, as shown by dramatic initial changes in contact angle and surface oxygen concentration [292]. Polymer chain diffusion can also lead to ageing in PP films that are not sufficiently cross-linked to prevent individual polymer chains at the surface from diffusing into the bulk [294]. These processes, together, lead to a phenomenon known as

'hydrophobic recovery' in which high-energy species are removed from the surface leading to an increase in the water contact angle [295-298]. These mechanisms are responsible for ageing in radical-functionalised surfaces resulting in the eventual loss of radicals and hence the capacity for direct covalent binding of biomolecules [264]. In addition, cPPFs experience moiety decomposition. Amine groups can decompose into amides (R-N-R') or NO_x groups [299, 300] and have been shown to lose 70% of the initial surface functionalisation over 7 days [240]. Carboxyl and aldehyde groups follow the same decomposition route, fragmenting into aldehydes, alcohols, and CO_x groups. More detailed examinations have been published outlining the mechanisms and effects of amine, carboxyl, and aldehyde decomposition [208, 216]. The ageing of epoxy-functionalised PPFs has been observed. Camporeale *et al.* present surface group composition of an epoxy-functionalised PP under a series of conditions, two of which correspond to a 50-day time lapse [254]. The epoxy surface signal decreased from 18% to 9% over 50 days in air. An increase of carbon-oxygen single bonds was observed, suggesting the rings underwent opening reactions. The protein bonding ability of rPPFs is dependent on the quantity of imbedded radicals migrating to the coating surface to form covalent bonds with proteins rather than the presence of specific chemical groups at the interface.

Implantation of orthopaedic devices is a highly mechanical process and the surface is likely to be damaged during the insertion. Scratching of the biofunctionalised surface will locally remove the biomolecules regardless of the immobilisation approach used. In the case of biomolecules immobilisation on surface coatings, there is an additional risk of delamination of the thin film coating following the exposure of the coating-substrate interface to the aqueous medium. Although plasma polymerisation is often referred to as a substrate independent process, the structure of the initially deposited layers depends on the chemistry of the PP-substrate interface [301-306]. The possibility of coating delamination *in-vivo* highlights the importance of interface engineering to ensure robust adhesion of the coating to the substrate.

Stability of the biofunctionalised surface in the long term depends on the stability of the protein molecules and the strength of the coupling to the surface. Physically immobilised biomolecules will be rapidly lost by substitution of molecules from the physiological environment [111, 112]. Covalently coupled molecules are susceptible to degradation or bond cleavage over the longer term [307]. The timescales for these phenomena will depend on the nature of the biomolecule and the linking chemistry used for immobilisation. Biomolecule immobilisation onto coatings may also suffer from swelling of the coating after exposure to the aqueous environment. This problem can be mitigated by ensuring a high degree of crosslinking within the coating by applying greater plasma input energies per unit volume of the precursor monomer [301, 308]. It has recently been shown that formation of a highly cross-linked layer close to the substrate provides enhanced stability in aqueous environments [309] (**Figure 1.20**). A limited number of studies report the mechanical and chemical stability of the linker layers. Stability studies were performed using pH 7.4 buffer and fluorescent dyes to evaluate the retention of adsorbed and covalently immobilised proteins [120, 169]. PP interlayer stability reports are more abundant than their linker-mediated counterparts [282, 286, 310-312]. The evaluation of stability typically includes exposure of the biofunctionalised substrate to a solution, e.g. water or buffer, followed by a surface analysis using techniques such as XPS [312], quartz crystal microbalance (QCM) [287], or an enzyme-linked immunosorbent assay (ELISA) [58]. Simulated body fluids (SBF) and sodium dodecyl sulfate (SDS or NaDS) have also been used to provide more aggressive environments for protein and coating stability assessments [58, 281, 286]. The stability assay time frame should be of considerable length given the decades spent in the body, but the majority of studies state short exposure times [120, 313-315].

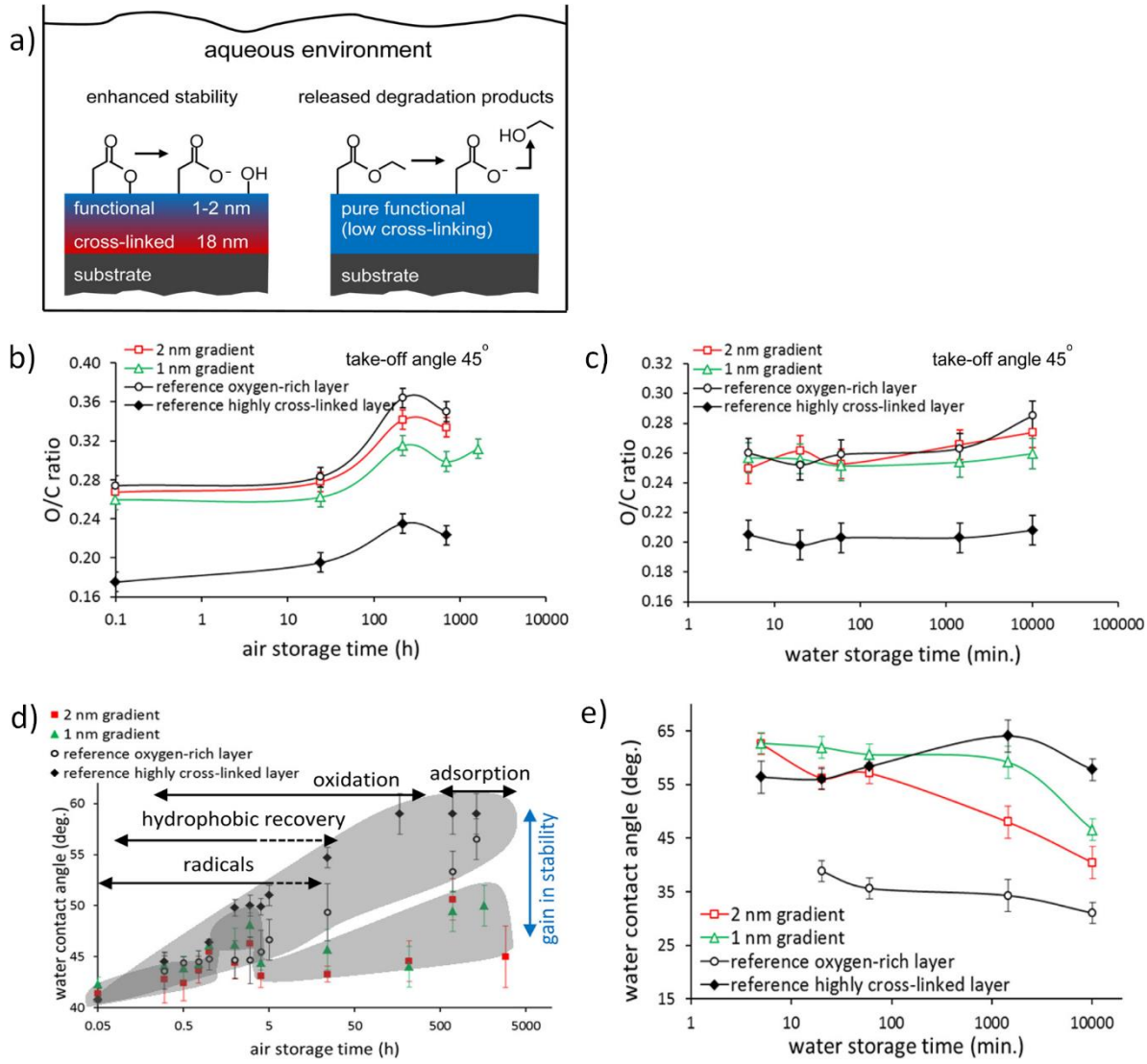

Figure 1.20. **a**) A diagrammatic representation of the gradient approach to enhance stability through cross-linking and retain chemical functionality. The ageing behaviour of 1 and 2 nm vertical gradient structures and non-gradient highly cross-linked or oxygen-rich structures in water at pH ≈ 6.2. Oxygen-to-carbon concentration ratio (O/C) of the plasma polymerised structures as a function of time as stored in air (**b**) and water (**c**). Water contact angle (WCA), are displayed as a function of the storage time in air up to 5000 hours (30 weeks) (**d**) and water up to 10 000 min (1 week) (**e**). Therefore, by depositing a highly cross-linked initial layer followed by a functional, the authors obtained chemical functionality (**b, c**) while retaining structural stability (**d, e**). Reprinted with permission from [309].

1.4 Project Aims and Thesis Structure

Load bearing titanium orthopaedic implants are mechanically strong and flexible, and well tolerated by the body [26-28, 34, 35, 39]. However, a number of short and long term problems still exist due to the biological inertness of the surface [3-7] and mechanical mismatch between the implant and bone [29-31]. Protein-functionalisation promises a bioactive surface capable of mitigating these effects by stimulating bone formation [57, 123, 184, 214], but current wet chemistry approaches are difficult to translate from the laboratory into cost-effective manufacturing due to the number of reagents and process steps required, as well as the potential for incomplete or side reactions.

This thesis aims to develop commercially translatable, multifunctional biointerfaces for orthopaedic applications utilising radical-functionalised plasma polymer films (rPPFs). rPPFs can be deposited onto any substrate and are fabricated through a simple, reproducible, and scalable approach to enable protein-functionalisation of orthopaedic devices [264, 288, 289]. Chapter 2 describes the techniques, including plasma deposition, physical and chemical surface characterisation methods, and cell culture assays, employed to investigate the utility of rPPFs for the biological functionalisation of titanium-based orthopaedics. The use of rPPFs in orthopaedics requires a coating that is mechanically robust, as coating failure (delamination) could have serious consequences. A series of coatings with varied N:C ratios in their surface chemistry are examined in Chapter 3 to determine the optimal coating conditions. Free radicals have been associated with numerous diseases, including osteoarthritis. Chapter 4 investigates the effects of radical flux migrating from the rPPFs on the surface chemistry and tests for potential radical-induced cytotoxicity with bone lineage cells. The single protein approach to biomolecule-functionalisation has shown some success. However, an evaluation of the bone integration process shows that a multifunctional surface is required for optimal integration. Fibronectin (FN), osteocalcin (OCN), and a custom osteocalcin-fibronectin fusion protein (FN-OCN) are optimised for immobilisation on rPPFs, alongside a co-immobilised ratio of FN and OCN (Chapter 5). The bone-integration potential of the multifunctional

and single protein functionalised rPPF surfaces were comparatively evaluated with primary osteoblasts and mesenchymal stem cells in Chapter 6.

Chapter 2 – Methods and materials

A range of techniques from multiple disciplines were utilised for the synthesis, optimisation, and examination of protein-functionalised plasma polymer film (rPPF) biointerfaces. This chapter contains the experimental procedures utilised for the synthesis and characterisation of surfaces in multiple chapters. The experimental procedures unique to an individual study are presented in the chapter describing that study. The experimental protocols described within are subdivided into materials preparation and characterisation, cell maintenance and substrate seeding, and microscopy techniques.

2.1 Material preparation and characterisation

2.1.1 Substrate preparation

Titanium – 6% aluminium – 4% vanadium (Ti-6Al-4V or Ti 6-4) was purchased from Firmetal (China) in thicknesses of 1 mm and 70 µm. The 1 mm Ti was subsequently cut into 0.8 cm x 0.8 cm pieces, referred to as 'sheets', prior to being polished. The 70 µm thick titanium was cut to the required size, referred to as 'foils', and remained unpolished so not to compromise its structural integrity. The Ti sheets and foils are collectively referred to as 'substrates' when describing processes common to both.

Polishing was performed at the Australian Centre for Microscopy and Microanalysis (ACMM). A total of four Ti sheets were carefully affixed per epoxy block with superglue and left to dry overnight. The epoxy blocks were inserted into the multi-sample holder before undergoing sanding and polishing with a Struers Rotopol-22 polisher and an IntegralPol-25 polisher, respectively. The sanding and polishing conditions are listed in **Table 2.1**. The Rotopol-22 utilised increasingly fine-grained sandpaper disks to sand back the surface using water as the lubricant, while the integralPol-25 rotating platform with attached abrasive disks utilised lubricants containing fine particulates. Water was used

to wash the integralPol-25 platform between runs to prevent cross-contamination between the fine polishing lubricants. The sample holder was positioned off-centre relative to the abrasive disk to produce the desired surface polishing upon rotation.

The polished sheets were immersed in acetone overnight to dissolve the super glue before washing in fresh acetone for 4-6 x 10 min as required to remove any remaining traces of the glue and other organic contaminants from the surface. The Ti sheets were then washed in milliQ water for 2 x 10 min followed by immersion for 30 min in 35% nitric acid solution. The titanium sheets were then washed in 2 x milliQ water for 10 min followed by 2 x 70% ethanol for 10 min. The 70 µm thick titanium foils were cut to the required total size for the respective procedures before undergoing the nitric acid cleaning protocol described, minus the overnight acetone immersion to remove superglue.

Table 2-1: RotoPol-22 and IntegralPol-25 sanding and polishing protocols

<table>
<tr><td colspan="5">RotoPol-22</td></tr>
<tr><td>ISO/FEPA Grit designation (P) (Grit size)</td><td>Normal Force applied during rotation (N)</td><td>Time (min)</td><td>Rotation speeds of the abrasive disks and the sample holder (RPM)</td><td>Lubricant</td></tr>
<tr><td rowspan="3">P 80 / 201 µm grit size</td><td>30</td><td>1</td><td rowspan="6">Abrasive disk = 150
Sample holder rotation = 150</td><td rowspan="6">Water</td></tr>
<tr><td>50</td><td>1</td></tr>
<tr><td>70</td><td>15</td></tr>
<tr><td>P 120 / 125 µm grit size</td><td>70</td><td>2</td></tr>
<tr><td>P 220 / 68 µm grit size</td><td>70</td><td>1</td></tr>
<tr><td>P 500 / 30 µm grit size</td><td>70</td><td>1</td></tr>
<tr><td>P 1200 / 15 µm grit size</td><td>70</td><td>1</td></tr>
<tr><td colspan="5">IntegralPol-25</td></tr>
<tr><td>MD Largo – 9 µm grit size</td><td>180</td><td>10</td><td>Abrasive disk = 150
Sample holder rotation = 150</td><td>Water – based diamond solution</td></tr>
<tr><td>MD Chem - 0.09 µm grit size</td><td>180</td><td>10</td><td>Abrasive disk = 150
Sample holder rotation = 150
(Counter rotation)</td><td>OP-S colloidal silica</td></tr>
</table>

2.1.2 Plasma polymer coating deposition

Titanium substrates (foils and sheets, collectively) were coated with radical-functionalised plasma polymer films (rPPFs) in the centre chamber of a three-chamber vacuum deposition system, shown schematically in **Figure 2.1**. Capacitively coupled radio-frequency (RF) power, produced by an RF generator (13.56 MHz Eni OEM-6) with a matching network (RFPP AM-5), and a DC pulsed substrate bias, produced by a RUP-6 DC pulsed voltage source (GBS-Electronik), were delivered to the lid-mounted RF electrode (10 cm diameter) and the sample mounting plate (10 x 10 cm) inside the chamber, respectively. An InfiniiVision oscilloscope (DS-X 3024A, Agilent Technologies) was used to monitor the RUP-6 output. The gas flow rates were monitored via Alicat flow controllers and the 'Flow vision' software (Alicat Scientific, version 1.1.35). The reagent gasses were introduced via a shower-head gas inlet, and the pressure was monitored by a Pfeiffer SingleGuage pressure gauge. The high purity N_2, Ar, and C_2H_2 reagent gasses were obtained from BOC Australia.

The Ti substrates and internal components of the deposition system were always handled with gloves as to prevent contamination with the oil from human skin. The Ti substrates were fixed to the sample mounting plate via double-sided conductive carbon or copper tape. The substrates were secured by applying gentle pressure with tweezers and the sample mounting plate slowly inverted to confirm attachment before being placed inside the chamber. The chamber was evacuated to below 1 Torr with a screw backup pump (Ebara PDV250). The turbomolecular pump gate valve was then opened, and the turbomolecular pump (Edwards NEXT400) was used to evacuate the chamber to a base pressure below $5x10^{-5}$ Torr.

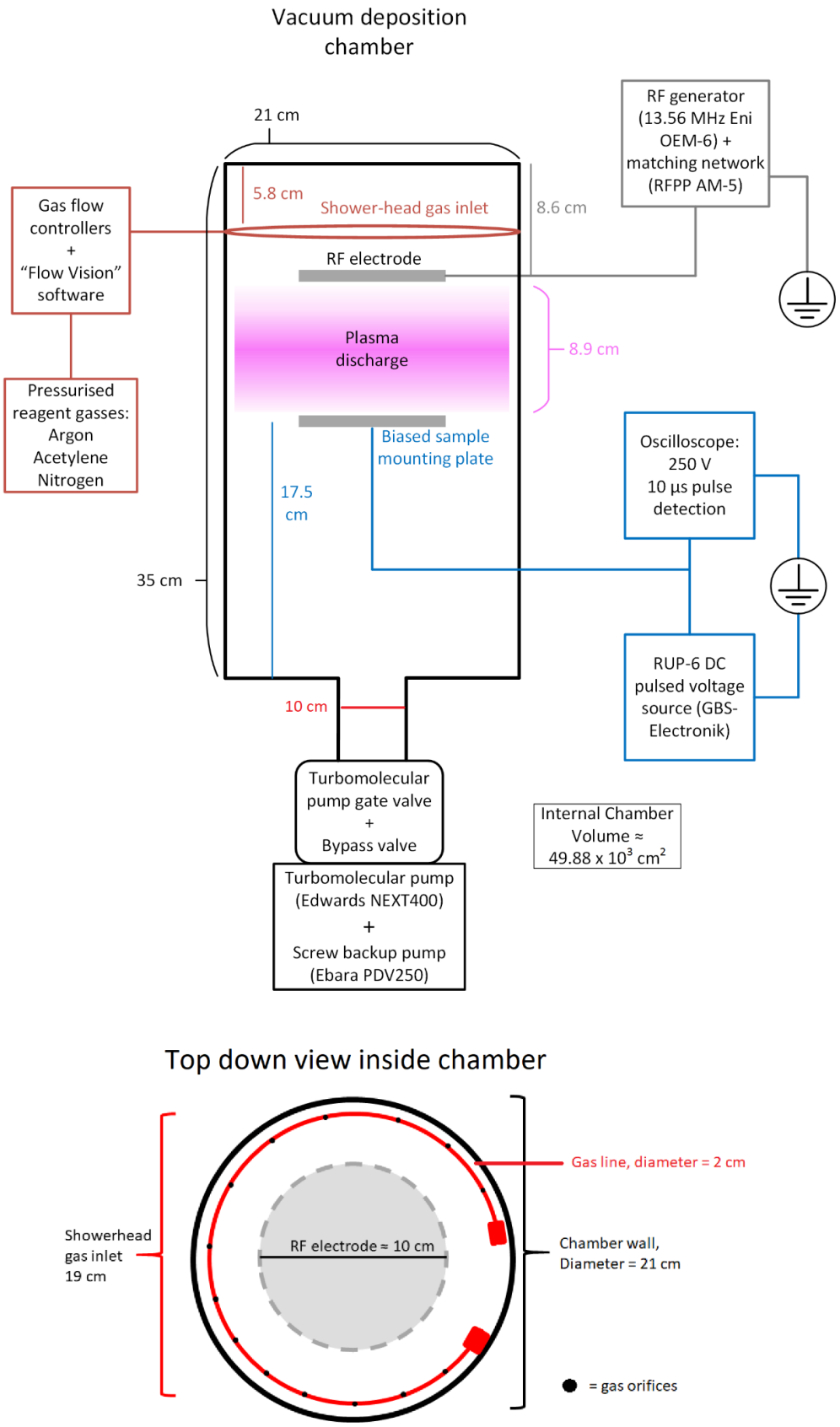

Figure 2.1. A schematic representation of the rPPF vacuum deposition chamber system. Insert: A top down view of the deposition chamber.

The substrates were plasma cleaned with argon at a gas flow rate of 40 standard cubic centimetres per minute (sccm). The turbomolecular pump gate valve was closed once the flow rate was stable to produce a working pressure of around $7x10^{-2}$ Torr. The pulsed high voltage RUP-6 was activated, and the output was adjusted to -500 V, with a frequency of 3 kHz and a pulse width of 20 µs. An RF forward input power of 75 W was applied while the reflected power was minimised using the matching network (approximately 10 W). The argon cleaning was performed for 10 min, and the chamber returned to base pressure.

Once the background pressure was reached, the gas flow rates of N_2, acetylene, and argon were adjusted using the Alicat controllers to obtain the desired N:C ratios. The turbomolecular pump gate valve was closed, and the chamber pressure was adjusted to 1.1×10^{-1} Torr via the bypass valve. The deposition time was adjusted according to the desired coating thickness and the reagent gas ratios. The RUP-6 output remained at 500 V, pulse frequency of 3 kHz, and pulse width of 20 µs and the RF power was set to 50 W with a reflected power < 5 W. The timer was started immediately after the RF input power was matched. Finer adjustments to the RUP-6 voltage were performed during the deposition as necessary. The RF power, RUP-6 voltage, and gas flow were stopped after the required time, and the vacuum chamber vented for sample retrieval.

2.1.3 Protein handling

All protein stocks were prepared under sterile conditions to reduce the potential of contamination in quantification and cell assays. Fibronectin (FN) and osteocalcin (OCN) lyophilised powders were purchased from Sigma Aldrich (F2006 - purity > 85% and O5761 - purity >94%, respectively). Fibronectin was made into main stock solutions of 100 µg/mL (2.3×10^{-7} M) and 500 µg/mL (1.1×10^{-6} M). Osteocalcin stocks were made to 100 µg/mL (1.7×10^{-6} M). The protein stock solutions were aliquoted into 1 mL volumes to limit freeze-thaw cycling and stored at -30˚C to extend

their lifetime. The FN-OCN fusion protein was supplied by Dr Jun-Hyeog Jang (School of Medicine, Inha University, Korea) in a 1000 µg/mL stock (2.5 x 10^{-5} M). The protein was left in the imidazole buffer and stored at 4˚C as instructed.

To produce a working solution for protein immobilisation or cell assays, the desired protein was recovered from storage and equilibrated to 37˚C. The main protein stock was transferred into a sterile biological safety cabinet (BSC) as per proper aseptic technique. The required volume of main protein stock (V_1) was calculated using the dilution equation (Equation 2.1) and added to the PBS to form the working solution. Any unused protein removed from the main stock was discarded.

$$C_1V_1 = C_2V_2 \qquad \textit{Equation 2.1}$$

Where: C_1 is the main stock concentration, V_1 is the required volume of the main stock, C_2 is the working solution concentration, and V_2 is the desired total working solution volume.

2.1.4 Fibronectin – Osteocalcin fusion protein synthesis

The FN-OCN fusion protein was produced by Jang *et al*. as previously described [287, 316]. The synthesis was initiated via polymerase chain reaction (PCR) amplification of the OCN and FN sequences. The OCN forward and reverse primers were 5’-TAGGAGCCCTCACACTCCTC-3 and 5’-CTGGAGAGGAGCAGAACTGG-3’, respectively. A restriction site was generated using the forward primer 5’-AACAGATCTTACCTGTATCAATGGCTGGGA-3, for *Bgl*II site, and the reverse primer 5’-AATGGTACCGACCGGGCCGTAGAAGCGCCG-3’, for *Kpn*I site. The FN sequence was generated with the forward and reverse primers, 5’-GGTACCGGTCTTGATTCCCCAACTGG-3’ and 5’-AAGCTTTGGTTTGTCAATTTCTGTTCGG-3’, respectively. PCR was conducted over 30 cycles; annealing at 55 °C for 1 min; extension at 72 °C for 1 min, and denaturation at 94 °C for 1 min. The amplified PCR products were digested using *Bgl*II, *Kpn*I and *Kpn*I, *Hind*III then ligated into pBAD-HisB vector (Invitrogen, Carlsbad, CA), giving rise to a pBAD-HisB-FN-OCN. TOP10 cells were cultured at 37˚C

overnight in LB medium containing ampicillin after transformation. The bacteria were harvested and pelleted by centrifugation at 6000 g for 10 min, lysed in NaCl-Tris-EDTA (STE) buffer, and sonicated. The soluble extract was centrifuged at 13,000 g for 2 x 10 min. The supernatant containing the fusion protein was then purified by passing through a chromatography column containing a nickel-nitrilotriacetic acid resin (Invitrogen, Carlsbad, CA) to 90% purity by sodium dodecyl sulphate polyacrylamide gel electrophoresis (SDS-PAGE) analysis

2.1.5 X-ray Photoelectron Spectroscopy procedure

X-ray photoelectron spectroscopy (XPS) is a surface analysis technique used to measure the elemental composition of the surface of a solid material by probing it with high-energy x-ray photons [317, 318]. Incident photons of known energy cause electron to be ejected from the atomic orbitals. Only electrons within ~ 10 nm from the surface have sufficient energy to escape the solid (**Figure 2.2**). The energy of the detected electrons is that of the photon minus the energy required to escape the atomic orbital and hence it provides information about the chemical identity and the chemical bonding of the atom from which the electron originates. The quantity of the ejected electrons is recorded as a function of electron kinetic energy loss. Since the incident radiation energy is known, the binding energy of the electrons can be determined using the following equation:

$$E_{binding} = E_{photon} - (E_{kinetic} + \phi) \qquad \textit{Equation 2.2}$$

Where the $E_{binding}$, or binding energy (BE), of the electron correlates to the energy required to eject the electron from the atomic orbital position, E_{photon} is the known energy input from the incident photons (hν), $E_{kinetic}$ is the resultant detected energy of the ejected electrons by the detector, and ϕ is the work function of the detector itself. The chemical composition is then determined by comparing the resulting electron binding energies and quantities to the known atomic orbitals electron structures of the elements.

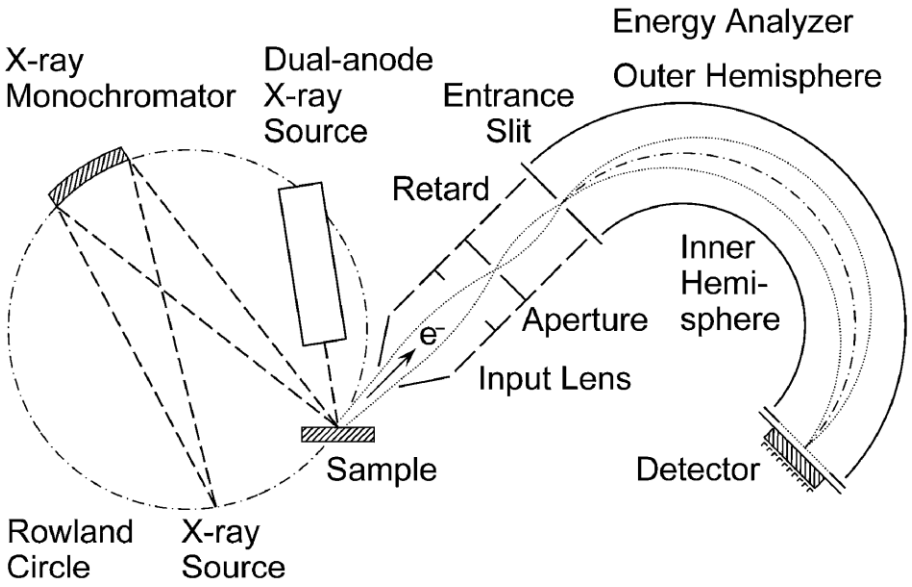

Figure 2.2. X-ray photoelectron spectroscope schematic. Reprinted with permission from [317].

The surface composition of rPPF-coated foil samples (0.8 cm x 1 cm) were examined using a SPECS SAGE spectrometer. The system was equipped with a monochromatic Al Kα (hν = 1486.7 eV) radiation source, a hemispherical analyser (PHOIBOS 150), and an MCD9 electron detector. The radiation source operated at 200 W (10 kV and 20 mA). The electron take-off angle was 90° with respect to the sample surface. The foils were affixed to copper sample holders and loaded into the examination chamber, which was evacuated to pressures below 5.0×10^{-8} mbar. The survey spectra were collected in an energy range of 0 − 1000 eV at a pass energy of 30 eV and a resolution of 0.5 eV. The resulting spectra were then analysed with the CasaXPS software (version 2.3.18PR1.0).

The spectra were calibrated with reference to the 284.6 eV C1s peak and the peak regions isolated with the elemental detection function. The element peaks underwent linear baseline removal and area integration to determine the surface composition. The uncertainty associated with the elemental composition comes from the manual peak definition and baseline procedure.

A high-resolution (0.1 eV) C 1s was collected at a pass energy of 20 eV and fitted to determine the ratios of different carbon-containing bonds. The peak baseline was subtracted, and the

component curves were fitted and added. The full width at half maximum (FWHM) and relative position constraints were applied to guide the fitting for the component curves. The predicted envelop was compared to the detected peak and the fitted component curves adjusted to obtain the closest possible match. An average of multiple 'optimal' fit values with uncertainty was reported for the high-resolution component peaks.

2.1.6 Fourier transform infrared spectroscopy (FTIR)

Fourier-transformed infrared (FTIR) spectroscopy investigates chemical composition by measuring the infrared absorbances corresponding to vibrational and rotational oscillations of bonds in compounds with dipoles [319]. The Infrared (IR) region is commonly divided into near IR (400 to 10 cm^{-1}), mid-IR (4000 to 400 cm^{-1}) and far IR (14000 – 4000 cm^{-1}). The instrumentation in this study utilised attenuated total reflectance (ATR) through a germanium crystal to measure the rPPF surface composition. IR light is passed through a crystal in physical contact with the surface under conditions creating total internal reflection within the crystal. However, at the site of contact, the IR beam partially penetrates into the sample in the form of an evanescent (or spatially decaying) wave [320]. A general schematic for this process is shown in **Figure 2.3**. The specific frequencies corresponding to the excitation energies of the bond vibrations in the sample at the interface are absorbed, and the remaining IR frequencies are transmitted.

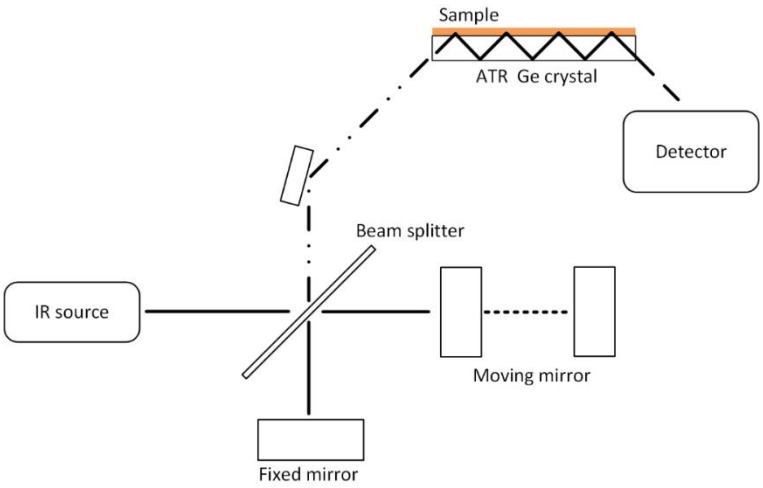

Figure 2.3. Schematic diagram of the ATR-FTIR spectrometer.

The FTIR in attenuated total reflectance mode (FTIR-ATR) spectra from the Ti and rPPF samples were recorded using a DigiLabFTS7000 FTIR spectrometer fitted with a multibounce ATR accessory and a trapezium germanium crystal at an incidence angle of 45˚. The titanium and rPPF- coated foils (1.5 cm x 2 cm) were measured at a resolution of 4 cm^{-1} within the mid-IR range of 4000 – 850 cm^{-1} and averaged over 500 scans. Pressure was applied evenly along the foil to ensure a firm crystal-foil interfacial contact. The contributions from Ti, CO_2, H_2O, and the air-crystal interface spectra were subtracted from the rPPF spectra using 'Digilab Resolutions Pro 4.0' software to leave only contributions from the rPPF coating. The spectral subtraction and baseline correction were carefully performed as over/under subtracting or incorrect baseline correction can introduce or remove spectral peaks.

2.1.7 Contact angle and surface energy measurements

The surface free energy (SFE) and wettability of an interface are important predictors of the biological interactions between a surface and the body, as discussed in Chapter 1, and can be determined by measuring the contact angles between solutions with different polarities and a surface (**Figure 2.4**). A common approach to calculating the SFE is to measure the contact angles of polar and

non-polar solutions and analyse the contact angles with the Owens–Wendt–Rabel–Kaelble (OWRK) model. The contact angle of a droplet is a result of the cohesive surface tension and the adhesive forces between the solution molecules and the surface. The internal angle produced at the liquid-solid interface is calculated from the reciprocal external angle formed by the vapour interfaces, and is substituted into Young's Equation [321, 322]:

$$\gamma_{sv} = \gamma_{sl} + \gamma_{lv} \cos\theta \qquad \textit{Equation 2.3}$$

Where: γ_{sv} is the surface energy of the solid-gas interface, γ_{sl} is the surface energy at the liquid-solid interface, γ_{lv} is the surface energy of the liquid-gas interface, with cos θ being the internal contact angle. The OWRK model is used to calculate the γ_{sl} based on the polar and dispersive (non-polar) components of liquid-solid interface [323].

$$\gamma_{sl} = \gamma_{sv} + \gamma_{lv} - 2\left(\sqrt{\gamma_{sv}^{D}\gamma_{lv}^{D}} + \sqrt{\gamma_{lv}^{P}\gamma_{sv}^{P}}\right) \qquad \textit{Equation 2.4}$$

Where the γ^{D} and γ^{P} refer to the dispersive and polar components of a given surface, respectively. To calculate the surface free energy of the substrate (γ_{sv}) the accepted surface energy components for multiple test liquids are substituted into equation 2.4 and rearranging for γ_{sv}.

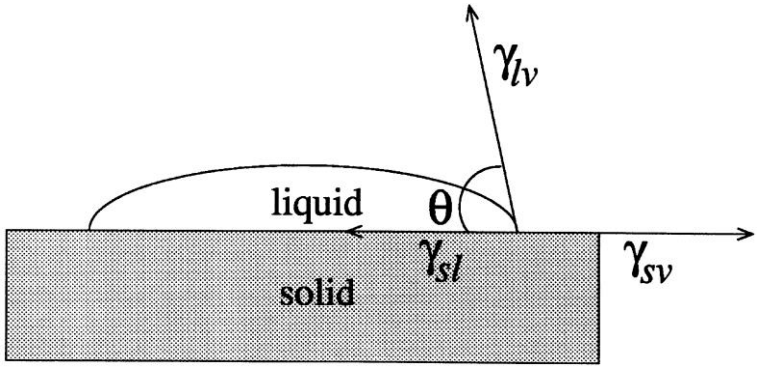

Figure 2.4. Surface energy components of contact angle droplets. Reprinted with permission [321].

The surface energy of the PPF was examined using a Krüss DS10 analyser equipped with a CCD camera. The contact angles of water (polar) and diiodomethane (non-polar) droplets (5 µL) were

measured on rPPF-coated foils. The contact angles were extracted from the captured images using the Krüss drop shape analysis software (version 1.90.0.11) and averaged over multiple readings (n = 5) with the sessile-drop method. The total, dispersive, and polar surface energies were then calculated by the Owens–Wendt–Rabel–Kaelble model.

2.1.8 Electron paramagnetic resonance (EPR) spectroscopy

Electron paramagnetic resonance (EPR) spectroscopy, also known as electron spin resonance (ESR) spectroscopy, measures unpaired electrons in a process similar to nuclear magnetic resonance (NMR) spectroscopy. EPR measures the change in electron magnetic moment (μ_e) under the presence of constant microwave energy and varying external magnetic field strength (B). The unpaired electron energy levels are shifted to produce Zeeman splitting [324, 325] according to:

$$E_{\pm\frac{1}{2}} = (\pm)\frac{1}{2}g\mu_B B \qquad \textit{Equation 2.5}$$

Where the energy of a spin state ($E_{\pm 1/2}$) is determined by the g-factor, the Bohr magneton (μ_B), and the applied magnetic field (B). The sample is scanned with an increasing magnetic field until the constant microwave radiation causes photoelectric excitation of the electron. The positions and intensities of the spectral peaks allow for the determination of unpaired electron species and quantities.

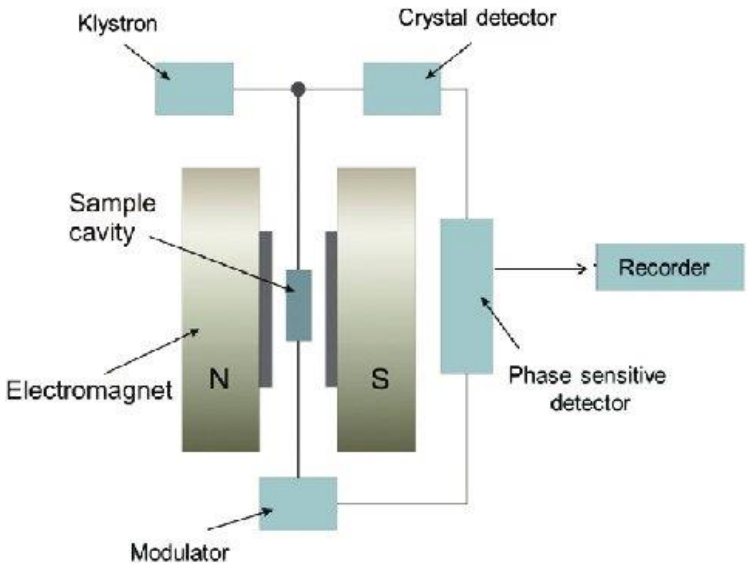

Figure 2.5. A general schematic of an electron paramagnetic resonance spectrometer. Reprinted from [326].

The concentration of unpaired electrons in the rPPFs deposited on polystyrene (PS) (25 µm, Goodfellow) were examined with a Bruker EMX PremiumX EPR spectrometer at room temperature. Polystyrene was used as metallic substrates are not compatible with the EPR detection process. The films deposited on PS were considered to be representative of those on titanium as PPFs are known to be substrate independent except for interface layers with a thickness less than approximately 10 nm [286, 291, 327]. The PS control and rPPF – coated PS samples (7 cm x 8 cm) were rolled and inserted into quartz NMR tubes. The spectra for each time point (n = 6) were examined with a scan time of 60.06 s using a centre field of 3513 G, modulation amplitude of 1.998 G, frequency of 100 kHz, and microwave frequency and power of 9.83 GHz and 0.025 W, respectively. The resonator detection cavity had a minimum signal to noise ratio of 400:1. A weak pitch (WP) control of known radical density ($\sim 1 \times 10^{13}$ spins/cm) was measured in conjunction with each sample set. The resulting spectrum was doubly integrated using Origin 8.5 to correlate the known linear radical density for the control within the 4 cm cavity to the area under the curve. This relationship was then used to determine the radical

density of the rPPF samples in the 4 cm x 8 cm examination region. The rPPF radial density was normalised to units of spins/cm^3.

2.1.9 Atomic force microscopy analysis

Atomic force microscopy is a surface analysis technique that examines the 3D topology of a surface [328, 329]. A cantilever of a given shape and sharpness is traced along the surface (x-y plane) and the deflection of the tip (z plane) is measured via laser-induced current on the position-sensitive detector array (**Figure 2.6**). The signal is transferred through a feedback system where the laser deflection is converted into a physical height measurement. The cantilever tip can be tapped or remain stationary as the surface is being scanned. The cantilever tips can be modified with particular shapes, sharpness, and chemically-functionalities to investigate specific structures, compositions, or physical properties from the micro to nanoscales [328]. AFM can also be performed in aqueous or vacuum conditions and can be used for various nanolithography procedures.

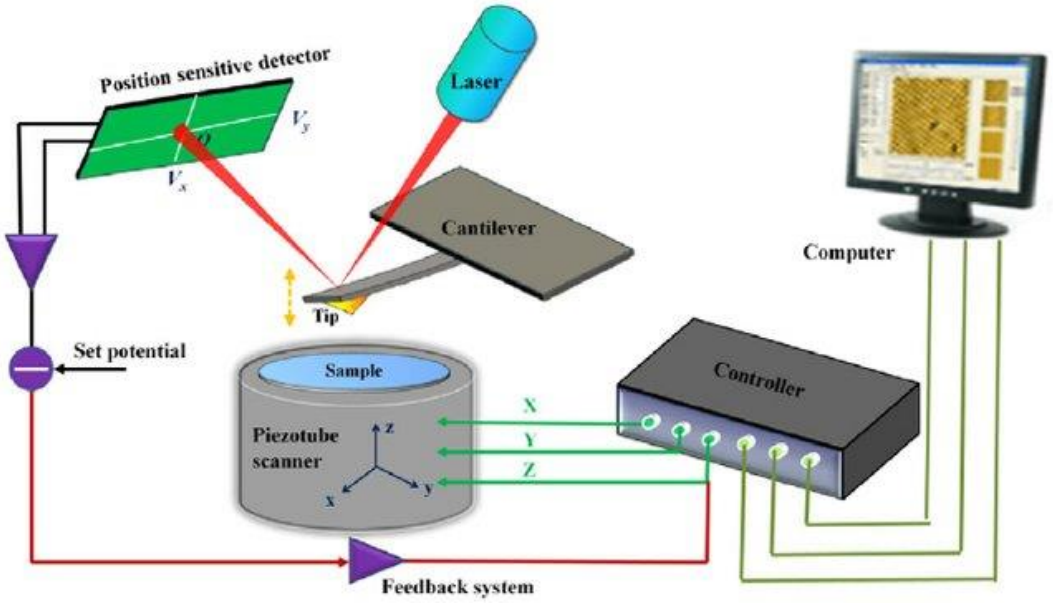

Figure 2.6. A representative schematic of an atomic force microscope [329].

AFM was performed on Ti substrates to determine if surface topology was altered during the nitric acid cleaning or the rPPF deposition processes. The toluene and nitric acid cleaned Ti sheets and bare and rPPF-coated foils were examined with a molecular imaging PicoSPM atomic force microscope (AFM) at the Australian centre for microscopy and microanalysis (ACMM). The samples were examined as close to the preparation as possible to reduce the effects of surface artefact contamination (e.g. dust). The individual samples were attached to the sample plate for examination. A 0.6 µm sharp microlever (Park Scientific Instruments) was inserted into the probe and the cantilever laser was aligned to the tip. A random 30 µm x 30 µm section of the surface was selected, the detection and feedback parameters were optimised, and the surface traced for topology and roughness. The results were analysed with the 'WSxM 5.0 Develop 8.5' software as developed by Horcas *et al.* [330].

2.1.10 Enzyme-linked immunosorbent assay detection

Enzyme-linked immunosorbent assay (ELISA) is a biochemical detection method for determining protein concentrations based on the specific interactions between antibodies, or immunoglobulins (Igs), and unique amino acid sequences in the target proteins [331]. The ELISA methodology in this study utilises a primary Ig that binds specifically to the target protein and a complementary secondary Ig conjugated with HRP that generates a colourimetric signal via the enzymatic breakdown of a TMB liquid substrate. A schematic outline of the ELISA process is shown in **Figure 2.7**. The samples were loaded into individual wells of a tissue culture well plate. Each ELISA test contained a negative bovine serum albumin (BSA) (Sigma Aldrich) control surface in triplicate to measure the background signal and an unblocked tissue culture plastic positive control surface to confirm successful ELISA detection. Each step is preceded by washing in PBS buffer to remove excess reagents. **Step 1:** Protein-immobilised and negative control surfaces were incubated in a 5% w/v BSA blocking protein solution for 1 hr to block the non-functionalised parts of the surface. **Step 2:** The surfaces were incubated in primary antibody solution (1 hr). **Step 3:** The substrates were exposed to the secondary antibody

conjugated with HRP for 1 hr. **Step 4:** The samples were transferred to a clean well plate to eliminate signal contributions from antibodies adsorbed onto the well plate. The TMB substrate solution was added for 30 min. A colourimetric change from clear to blue was produced through the reduction reaction between TMB and peroxide catalysed by HRP. An equal volume of 0.2 M sulphuric acid was added to stop the reaction and the absorbance was read at 450 nm.

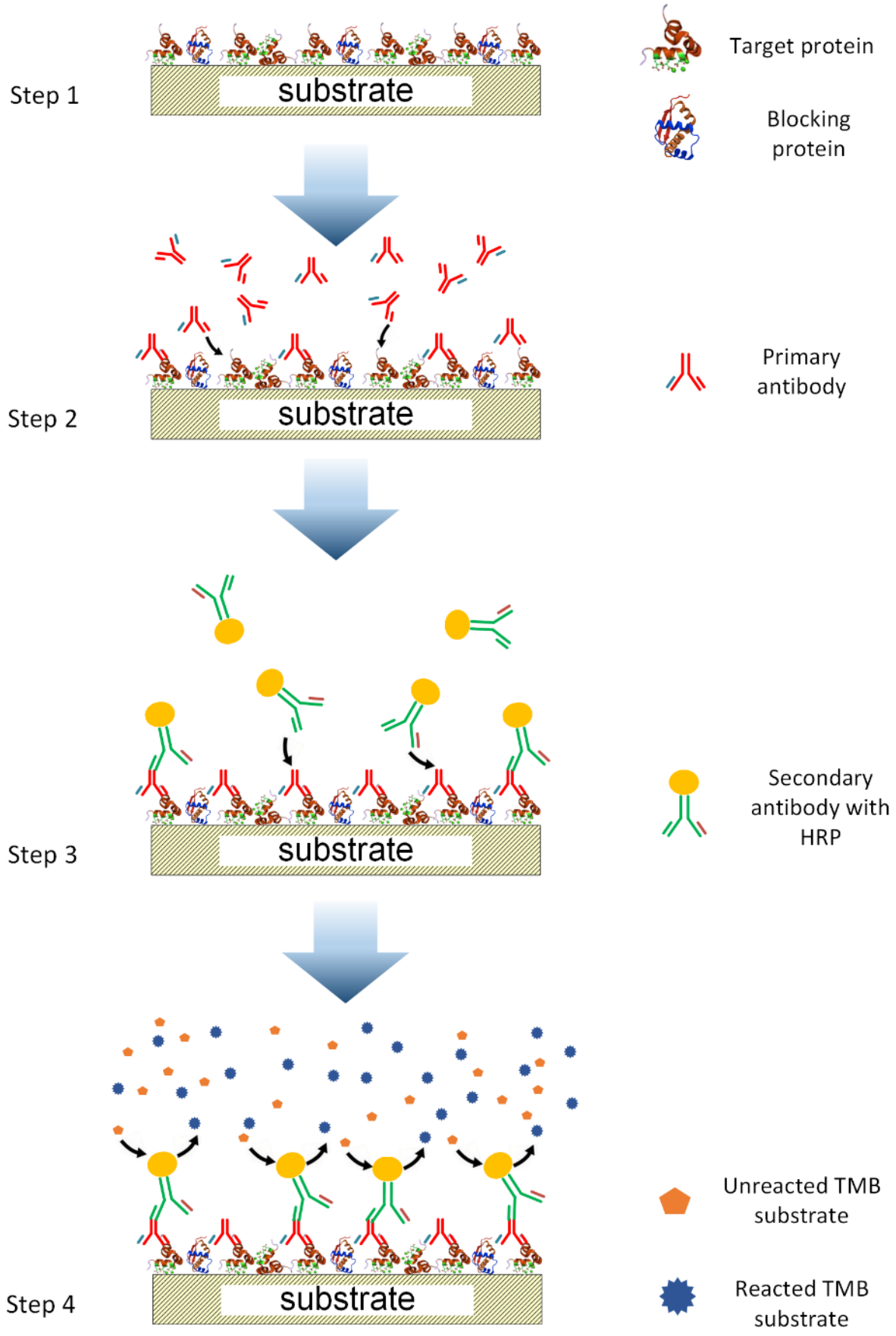

Figure 2.7. A schematic outline of the ELISA protein quantification process.

2.2 Cell maintenance and handling

2.2.1 Cell media and buffer preparation

Ham's F12 media (51651C, Sigma Aldrich) was supplemented with fetal bovine serum (FBS) (12003C, Invitrogen), and Penicillin-Streptomycin (P.S) (P4333, Sigma Aldrich), were used to make complete cell media (c-media) for the Osteosarcoma MG63 tumour cells. The media was prepared in under sterile conditions inside a biological safety cabinet (BSC). FBS was heated to 56˚C for 1 hr for heat inactivation. Ham's F12 and P.S were warmed to 37 ˚C. 50 mL of FBS (10% v/v) and 5 mL of 100 µg/mL P.S (1% v/v) were added to the Ham's F12 using a fresh pipette for each solution as to prevent cross-contamination. A 5 mL aliquot of c-media was transferred into a T25 cm^2 cell culture flask (Corning) to test for contamination. The c-media was sealed with parafilm and stored in cold conditions (refrigerator). The remaining FBS and P.S were aliquoted into 50 mL and 15 mL volumes, respectively, and stored at -30 ˚C.

Primary osteoblasts required a low glucose Dulbecco's Modified Eagle's medium (DMEM) (D5546, Sigma Aldrich). Non-osteogenic and osteogenic recipes of completed-DMEM (c-DMEM) were used for osteoblast maintenance. Both c-DMEM recipes contained 20% (v/v) FBS (100 mL) and 1% (v/v) P.S. (5 mL). 50 µg/mL ascorbic acid (vitamin C) was added to the osteogenic media to promote osteoblast differentiation.

Phosphate buffered saline solution without magnesium and calcium (PBS) was purchased from Sigma Aldrich (cat.56064C). 9.5 g of PBS powder was dissolved in 1L of deionised or milliQ water. The PBS solution was then sterilised by either a standard 2 hr 'wet run' autoclave routine or vacuum filtration with a 0.22 µm filter bottle-top vacuum filter (Corning). The sterilised PBS was stored under cold conditions.

2.2.2 MG63 osteosarcoma cell line culturing

MG63 osteosarcoma cells are a permanent malignant cell line derived from a bone tumour. They are one of the three common cell lines used for orthopaedic research, along with the human-derived Sarcoma Osteogenic (SAOS-2) and the transformed mouse pre-osteoblast MC3T3-E1 cell lines [332]. MG63 cells were provided by Dr W. Chrzanowski (Pharmacy) and Dr G. Yeo (CPC). A vial of frozen cells was retrieved from cryogenic storage in liquid nitrogen, equilibrated to 37˚C, and transferred into a 15 mL tube with 5 mL of media. The cell suspension was spun down in a centrifuge at 1200 rpm for 5 min. The supernatant was removed, the cell pellet resuspended in 2 mL of media, and transferred into T75 cm^2 tissue culture flask (Falcon, Sigma Aldrich) with 20 mL of media.

The cells were grown until they covered 80-90% of the surface, referred to as 80-90% confluence. The cells were washed twice with 5 mL PBS before the addition of 5 mL TrypLE express trypsin solution (Thermofisher Scientific). After the cells had detached from the flask (approximately 2-5 min), 5 mL of media was added to quench the TrypLE. The cell solution was transferred into a 15 mL tube and spun down at 1200 rpm for 5 min. The resulting pellet was resuspended in 2 mL of media and the cell concentration was determined via manual counting. 80 µL of 0.4% Trypan blue stain solution was transferred into a 1.5 mL Eppendorf tube followed by 20 µL of cell suspension. 10 µL of the mixed stained cell solution was transferred into one side of a haemocytometer and examined under a microscope. The average cell number per mL was calculated with equation 2.2 using the average cell number per square (0.1 µL) from 5 squares of the counting grid (**Figure 2.8**). Both sides of the haemocytometer were used to determine the cell suspension density for cell assays. Cell culture flasks containing complete media were then seeded at the required density for continued proliferation.

$$\text{Cell concentration } \left(\frac{cell}{mL}\right) = \text{ Cell average per } 0.1 \text{ µL region xTrypan Blue dilution x } 10{,}000 \quad \textit{Equation 2.2}$$

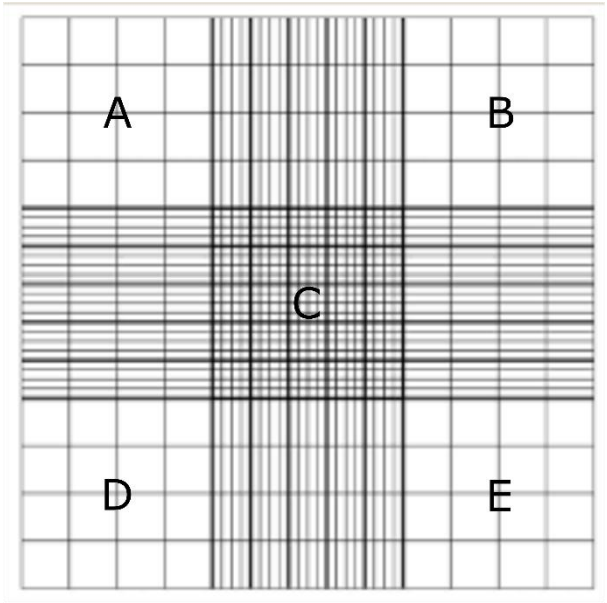

Figure 2.8. Standard Haemocytometer grid layout labelled with regions sampled for cell counting (A-E)

2.2.3 Primary Osteoblast collection and culturing

Primary osteoblasts were collected from sacrificed 7-week-old C57BL/6 mice following the accepted procedure [333, 334] at the Heart Research Institute (HRI). The experiments were conducted in accordance with the Australian Code of Practice for the Care and Use of Animals for Scientific Purposes. All personnel involved in the animal procedures have completed an approved animal care and ethics course. The abdomen was washed with ethanol. The femur, tibia, and fibula were cleaned and placed in a sterile Petri dish with PBS. The bones were transferred to a tube with 10 mL of collagenase II solution (heated to 37˚C) and mixed via shaking for 20 min. The samples were transferred to a fresh Petri dish where the epiphyses (ends of the bone) were opened and the marrow flushed out. The bone diaphysis (central parts of the bone) were cut into 1-2 mm^2 pieces, washed several times with PBS, and incubated in 4 mL collagenase II solution at 37˚C. The solution was shaken vigorously every 30 min for 2 hr. The bone pieces were rinsed 3 times with media and the supernatant discarded. The bone fragments were transferred to a 6-well plate at 20-30 bone pieces per well. Non-osteogenic media was added and the pieces were left to allow for osteoblast outgrowth. The cells typically migrated from the bone pieces after 3-5 days, being careful to avoid over-confluence around

the bone pieces, and were ready to be transferred after 11-15 days. The cells were trypsinated at 70 - 80% confluence and transferred to a larger culture flask for cell expansion (seeding density 60 – 80 x 10^4 cells /T175 flask). The OB cell subcultures were monitored through visual examination of the cellular morphology and staining with alizarin red. Any subcultures that indicated ingrowth of other cell types were discarded.

2.2.4 Substrate seeding

The Ti and rPPF coated 1 mm thick sheets, used for MG63 cell assays, were sterilised with UV light for 15 min on either side and transferred into individual wells of a 24-well plate (Corning). MG63 cells were suspended and seeded at a density of 10,000 cells/cm^2, or 6500 cells per sheet, using a droplet seeding method. The droplet (approx. 80 µL) was left on the substrate surface for 2 hr to allow for cell attachment [335]. The well was gently filled to 1 mL and examined under a light microscope to visualise any cells displaced from the sheets. The samples were incubated at 37˚C and 4% CO_2.

The bare and rPPF-coated titanium foils were used for primary osteoblast investigations. The foils were cut to size (0.8 cm x 1 cm) and sterilised with UV light before being transferred into an 8-well chamber slide (Nunc®154534, Life technologies). Primary osteoblasts were seeded on foils at 4000 cells per substrate in 0.4 mL of media, or 5000 cells/cm^2. The media was replaced every 3 days. The end chamber of each row was seeded as a control to monitor cell health.

2.2.5 Cellular proliferation assays

MG63 cellular proliferation was measured at 1, 3, and 7 days post seeding using three cell assays: AlamarBlue (AB) metabolic assay, cell counting kit – 8 (CCK-8) proliferation assay, and cyQUANT DNA detection. The three tests were performed under dark conditions to reduce photobleaching and loss of signal specificity. Blank samples were run in conjunction with each assay for background

subtraction. The results were presented as background subtracted absorbances and proliferation ratios of day 1.

AlamarBlue™ cell viability reagent (DAL1025, Thermofisher Scientific) is a non-toxic resazurin salt solution that acts as a cell metabolite, changing from blue resazurin to red resorufin as it is reduced. The cell media was removed, and the samples were incubated in 1 mL of AB solution (10% v/v in Ham's F12 media) for 2 hr. After the allotted time, 150 µL aliquots were taken from each sample and the absorbance measured at 570 nm.

The active compound in the CCK-8 proliferation assay is a non-toxic, soluble tetrazolium salt, WST-8 (2-(2-methoxy-4-nitrophenyl)-3-(4-nitrophenyl)-5-(2,4-disulfophenyl)-2H-tetrazolium, monosodium salt) (96992, Sigma Aldrich). The salt undergoes reduction reactions by dehydrogenase activities ($NADP/NADPH^+$) within cells to produce a yellow formazan dye. The media was removed from the samples and replaced with 500 µL of 10% (v/v) CCK-8 solution. Aliquots from each sample were removed after incubation for 3 hr, and the absorbance was measured at 450 nm.

CyQUANT NF is an endpoint assay that measures DNA quantity. The assay came as a multi-reagent kit (#96992, Sigma Aldrich) and was mixed per the included instructions. Briefly, 11 mL of 1x buffer was made from milliQ water and the 5x Hank's balanced salt solution (HBSS) concentrate provided. Next, a 22 µL aliquot of 'component A' DNA-binding dye reagent was added to the buffer (1 / 5,000 dilution). The cells were washed with PBS, 500 µL of cyQUANT solution was added to each well, and the samples were incubated for 30 min. 150 µL aliquots were removed, and the fluorescence was read at 485 nm excitation /530 nm emission.

The primary osteoblasts were examined with the 3-(4,5-dimethylthiazol-2-yl)-5-(3-carboxymethoxyphenyl)-2-(4-sulfophenyl)-2H-tetrazolium (MTS) endpoint cell assay due to the slow proliferation rates of the cells. The MTS assay produces yellow formazan through reaction with $NADP/NADPH^+$ like the CCK-8 assay. MTS was made up to 40 mM concentration and frozen into 1 mL aliquots. Following cell growth for the allotted time, the media was removed from the samples

followed by the addition of 160 µL of non-supplemented DMEM and 40 µL of MTS solution. The samples were incubated for 2 hr under dark conditions followed by the transfer of 100 µL of each sample into a 96 well plate. The absorbance was read at 490 nm.

2.2.6 Alizarin red mineralisation assays

The mineralisation capacity of the different protein conditions was examined with the AlizarinRed stain (ARS), which binds to calcium. ARS was purchased from Sigma Aldrich (#A5533) and the solution made up via the standard protocol [155, 336, 337]. 0.7 g of ARS powder was dissolved in 25 mL of distilled water. The pH of the solution was measured and adjusted to the final pH range of 4.1-4.3 with 0.5% (v/v) ammonium hydroxide solution. The solution was made up to 50 mL with distilled water, adjusting the pH as required. Phosphoric acid was used to increase the pH if excess ammonium hydroxide was added. The final solution was stored in a 50 mL falcon tube and wrapped in aluminium foil to prevent light exposure.

The Ti, rPPF, and protein-functionalised surfaces were prepared as described in Chapters 2 and 5, and primary osteoblasts were seeded at 10,000 cells per well. The cells were incubated up to 1 month, and the media was replaced every 3 days. After gentle washing in PBS, the respective samples were stained with ARS for 2 hr. The excess was removed, and the samples washed gently before being placed into individual Eppendorf tubes. 400 µL of 10% (v/v) acetic acid was added before vortexing and heating to 85˚C for 10 min. The samples were then centrifuged at 16000 g for 15 min, and 50 µL of ammonia hydroxide added to each sample. 200 µL aliquots were transferred to a 96 well plate, and the absorbance read at 405 nm.

2.2.7 Mesenchymal stem cell differentiation

The upregulation of the alkaline phosphatase (ALP) enzyme in mesenchymal stem cells (MSCs) is a common approach for detecting osteoblastic differentiation, as MSCs do not produce the enzyme in their undifferentiated state. The detection can be performed through a variety of methodologies, such as enzyme-linked immunosorbent assays (ELISAs), polymerase chain reactions (PCR), and fluorescence imaging [336, 338-340]. ALP production in MSCs was measured via fluorescent microscopy following a similar protocol to cell attachment and spreading (Chapter 2).

MSC harvesting and culturing were performed as described in the standard protocol [341]. Long bones were collected from 7-week-old mice and washed with 70% EtOH. The ends of the bone were removed as for the primary osteoblast extraction. The bone marrow was flushed out with DMEM solution and collected. The marrow solution was resuspended and filtered through a 70 µm cell sieve before being transferred to a well plate for culturing. The cells were cultured in complete DMEM without ascorbic acid as not to stimulate osteoblast differentiation and the media changed every 3 days. The cells were expanded to working stocks and closely monitored for differentiation or ingrowth of other cell types. MSCs were seeded at 8000 cells/well on the protein-functionalised rPPF surfaces in an 8-well chamber slide. The media was changed every 3 days to ensure sufficient nutrients. After 10 and 20 days, the cells were fixed to the foils with EtOH and washed in 0.1% Triton solution. The surfaces were stained with Vector Red Alkaline Phosphatase dye (Vector) and DAPI fluorescent mounting media (Agilent). The surfaces were then examined with a Zeiss Axio Imager.Z2 fluorescence microscope at 365/560 nm for the ALP dye and 358⁄461 nm for the DAPI. The images were analysed with the 'ImageJ' software. The degree of differentiation was determined by dividing the total area of the Vector Red (μm^2) by the number of cells (blue nuclei).

2.3 Microscope procedures

2.3.1 Cell preparation for scanning electron microscopy examination

Titanium sheets were prepared for examination with a scanning electron microscope (SEM) to visualise the effects of cell growth on the coating integrity. MG63 osteosarcoma cells were grown on Ti sheets according to the proliferation protocols (Chapter 2) for 3 days and 7 days. The samples were washed with PBS, incubated in a 4% paraformaldehyde (PFA) solution for 1 hr, and stored in PBS buffer at 4˚C until visual examination. The SEM imaging was performed at the Australian Centre for Microscopy and Microanalysis (ACMM). The samples were immersed for 1 hr in a 1% Osmium tetroxide (OsO_4) solution for secondary fixation and image contrast and washed with milliQ water. The samples were then dehydrated with increasing concentrations of ethanol from 30% to 100% (v/v) for 3 x 5 min. A pre-made solution of 2% (v/v) hexamethyldisilazane (HDMS) was pipetted onto the sample in minimal volumes and any remaining solution was removed after 2 min. The samples were affixed to SEM mounting stubs with carbon tape and coated with a 20 nm layer of gold via sputtering (Emiteck K550X sputter coater). The samples were imaged with secondary emission detection using a neoscope JEOL tabletop SEM at a 10 V electron acceleration and working height of 48 mm. Three samples for each condition were examined at multiple sites (minimum n = 5) for each surface.

2.3.2 Fluorescence microscopy for cellular attachment

Cellular attachment after 1 hr was examined via fluorescent staining. Ti foils were cut to 0.8 cm x 1 cm and sterilised under UV light before being transferred to an 8 well multichannel slide (Nunc®154534, Lifetechnologies). Primary osteoblasts and MG63 cells were seeded at the density of 10,000 or 24,000 cells per well, respectively [171, 342, 343]. After 60 min, the seeding media was removed, the foils gently washed with PBS, and the attached cells fixed with 70% ethanol for 10 min. The samples were stored in PBS under cold conditions if imaging could not be performed on the same

day. After storage as required, the foils were exposed to a 0.1% Triton-x100 (Sigma Aldrich) solution for 10 min to remove potential contaminants. The cytoskeleton of the attached cells was stained with approximately 200 µL of an actinRED555™ (Invitrogen) solution per well for 10 min; 2 drops of actinRED555™ per mL of PBS. The nuclei were stained with 4',6-Diamidino-2-Phenylindole dihydrochloride (DAPI) fluorescent mounting media (Agilent) and the cells were placed between two glass slides for examination. Direct handling of the surfaces was minimised to reduce artefacts.

The samples were examined at 540/565nm excitation/emission for actinRED555™ and 358/461nm for DAPI with a Zeiss Axio Imager.Z2 fluorescence microscope. The magnification and fluorescence exposure time were kept constant between samples. The surfaces were examined under 5x (≈ 4mm^2) and 10x (≈ 1 mm^2) magnifications. Minor post-capture adjustments were made uniformly to the colour intensity of all images using the "best fit" colour adjustment in 'ZEN Pro' software (Zeiss).

The image analysis software "ImageJ" was used to calculate the average cell quantities and sizes. The images were split into the red and blue component colours and thresholded for the maximum distinction between cells. The image was further processed to fill holes and watershed connected cells. The resulting image was analysed for the number of cells and their average area. A minimum size limitation of 40 and 20 pixels was applied for cell size (red - cytoskeleton) and cell number (blue - DAPI) measurements, respectively, to exclude background artefacts. These results were tabulated and averaged over a series of images ($n > 9$) for the respective samples. A visual representation of the image analysis process is outlined in **Figure 2.9.**

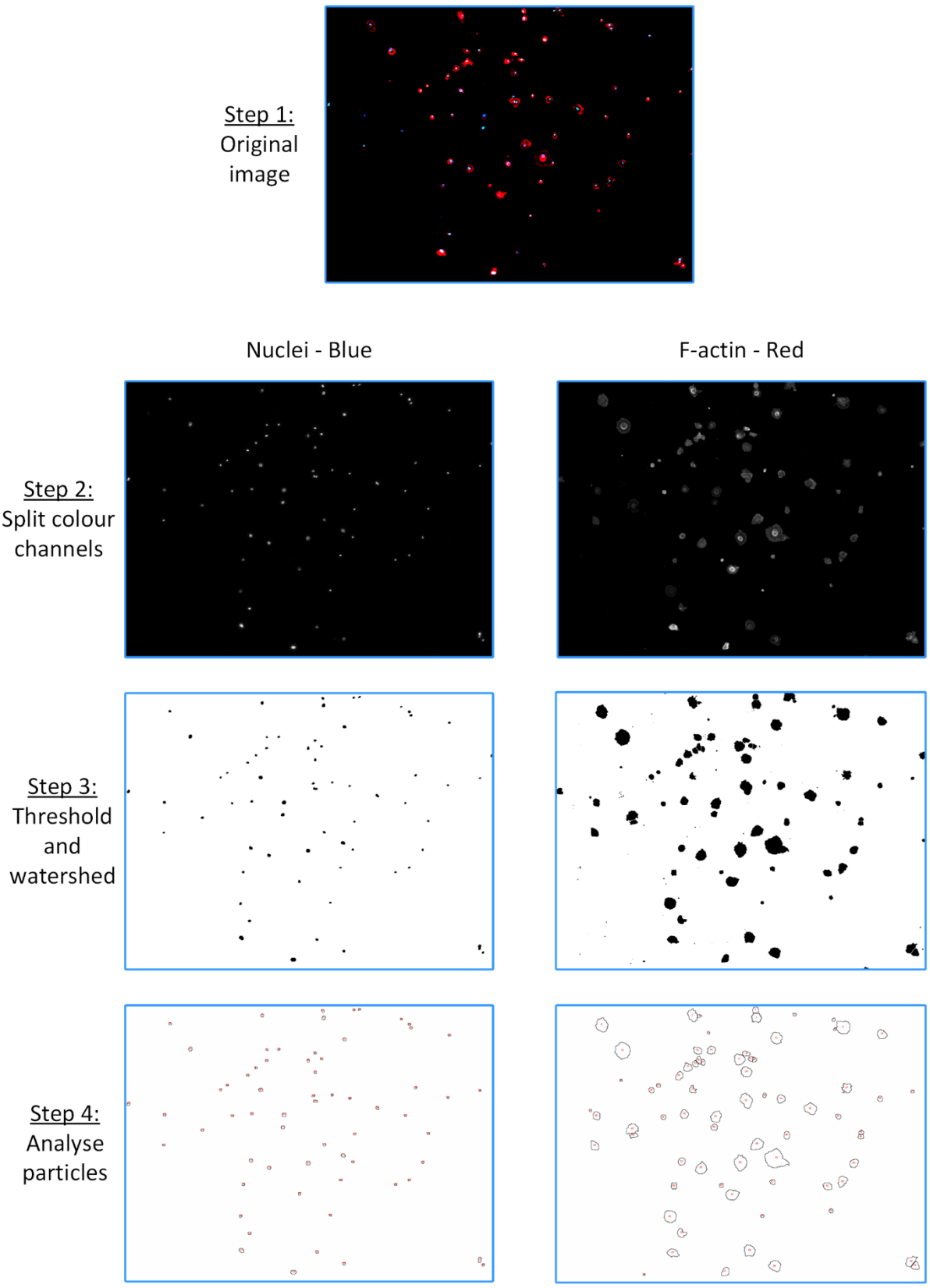

Figure 2.9. Pictographic flow of ImageJ analysis process.

Chapter 3 – Material optimisation and biological screening

In this chapter, the mechanical and biological properties of radical-functionalised plasma polymer films (rPPFs) deposited with nitrogen atomic concentrations ranging from 0 -30%N are investigated. The rPPF coated titanium sheets were seeded with MG63 osteosarcoma cells for in vitro *examinations of coating stability under cellular proliferation conditions. Scanning electron microscopy images demonstrated significantly greater robustness on the coatings with higher nitrogen content, with a preference towards the 30%N rPPF. Cellular proliferation assays showed little difference between the rPPF coatings, with a slight preference for the 20%N over the 30%N. Hence, both the biologically favoured 20%N rPPFs and mechanically favoured 30%N rPPFs were selected for further investigations.*

3.1 Introduction

The primary requirements for orthopaedic surface coatings are a strong coating-substrate interfacial adhesion and coating robustness sufficient to resist the partial or complete removal of the coating, referred to as delamination. The products of a delamination event can trigger adverse immune reactions similar to that of metallic and ceramic wear [344-348], thereby, reducing the effectiveness and lifetime of the implant. Recently, plasma polymer films (PPFs) have garnered great interest in biomaterials and biointerfaces applications, such as orthopaedic implants, because of their versatile and substrate-independent surface chemistry [208, 243, 244, 253, 254, 349-352]. The resistance to delamination of PPFs depends on the initial layer formation and can vary based on the mechanical and chemical properties of the underlying substrate [286, 304]. For a constant precursor gas composition and other plasma deposition conditions, such as plasma input power, the PPFs can have vastly different mechanical adhesion on silica, stainless steel, and titanium. Radical-functionalised PPFs (rPPFs) have been characterised on silicon wafers [283] and applied to stainless steel for cardiovascular stents [353-355], but had not been deposited on titanium before this work

[58, 356, 357]. Therefore, a new set of deposition parameters are needed for the deposition of a robust rPPF onto titanium surfaces that is capable of resisting delamination.

Two approaches can be taken to improve the mechanical properties of PPFs: i) The formation of graded PPF layers, and ii) the incorporation of nitrogen. Graded layers eliminate a sharp substrate-film interface prone to failure by creating a region through which the properties of the substrate gradually transfer to those of the film. Dramatically improved adhesion has been achieved through either compositional grading [264, 285], where the film deposition begins with deposition of the underlying metal onto a argon plasma cleaned substrate with the precursors gradually changing to the composition of the carbon-based film, or through structural grading [309], where a highly cross-linked polymer layer is deposited onto the substrate to form a mechanically stiffer and robust foundation followed by the less cross-linked soft layers that contain the desired chemical functionalities. The graded layers approach is commonly applied to chemically-functionalised PPFs (cPPFs) due to the poor interfacial adhesion resulting from the low plasma specific energies used to deposit the desired chemical functionalities [231-234]. The second approach for improving the PPF mechanical properties is by the incorporation of nitrogen as applied typically to diamond-like carbon (DLC) coatings [358-360]. Nitrogen introduces a series of trigonal chemical structures, such as imines, amides, imides, and enamines, that possess a lower bonding energy configuration and increase the ratio of sp^2:sp^3 (double: single) bonded carbon [361, 362], improving the elasticity and robustness of the coating. The deposition of rPPFs utilises pulse bias voltages applied to the substrate for the embedding of radicals in the form of dangling bonds created via enhanced ion bombardment. At the initial stages of film growth these energetic ions implant into the substrate producing a small "ion-stitched" graded layer at the interface that provides strong rPPF adhesion [285]. The energetic deposition and extensive cross-linking also results in higher degrees of internal coating stress. The incorporation of nitrogen into the structure of rPPFs increases the coating elasticity, reducing stress and producing robust rPPF coatings capable of withstanding the abrasive surgical implantation procedures.

The inclusion of nitrogen groups has also been shown to increase the biological affinity of PPFs [237-243]. The nitrogen-containing groups can become protonated under physiological pH conditions (pH 7.4), e.g. NH_3^+, and increase cell attachment and proliferation [237, 238, 243]. They can also increase the mineralisation of bone lineage cells and encourage the osteoblastic differentiation of stem cells [243, 244]. In this chapter, rPPF coatings are deposited on titanium surfaces from a variety of N_2:C_2H_2 reagent gas ratios. The resulting coatings were examined with bone lineage cells to identify the reagent gas ratio that produces the most robust coating and any biological preferences.

3.2 Methods

3.2.1 Substrate preparation and rPPF deposition

Titanium substrates were cleaned with the nitric acid protocol outlined in Chapter 2 and with an organic solvent protocol [58, 356, 357]. For nitric acid cleaning, the sheets were washed in acetone and water (2 x 10 min each) followed by a 30 min immersion in a 35% nitric acid solution. The sheets were then washed with water and ethanol (2 x 10 min each). In the organic solvent protocol, the sheets were sonicated for 1 x 10 minutes in 10-15 mL of toluene, acetone, and 70% ethanol (v/v), rPPF coatings were deposited on Ti substrates as outlined in Chapter 2. Briefly, the cleaned titanium substrates were treated with argon (Ar) plasma for 10 minutes (flow rate = 40 standard cubic centimetres per minute (sccm), RF power = 75 W, substrate bias voltage = −500 V, pulse width = 20 µs, pulse frequency = 3 kHz). The rPPF coatings were then deposited with varying reagent gas ratios. The flow rate of argon was kept constant at 15 sccm while the flow rates of acetylene (C_2H_2) and nitrogen (N_2) were varied as shown in **Table 3.1**. The chamber working pressure was adjusted to 0.11 Torr and the coatings deposited to a thickness of approximately 60 ± 7 nm (RF power = 50 W, substrate bias voltage = −500 V, pulse width = 20 µs, pulse frequency = 3 kHz)**.** The chamber was vented, and the samples were stored under aerobic conditions.

Table 3-1. Plasma deposition gas ratio conditions

Nitrogen (sccm)	Acetylene (sccm)	Argon (sccm)	Deposition time for 60 ± 7 nm layer (min, sec)
0	15	15	1 min, 30 sec
5	10	15	1 min, 44 sec
10	5	15	2 min, 50 sec
12.5	2.5	15	6 min, 32 sec

3.2.2 X-ray photoelectron spectroscopy

The surface composition of rPPF coated substrates with varying N:C ratios were examined after 24 hours, according to the x-ray photoelectron spectroscopy (XPS) protocol outlined in Chapter 2. Briefly, the survey spectra were collected in an energy range of 0−1000 eV at a pass energy of 30 eV and a resolution of 0.5 eV. High-resolution (0.1 eV) C 1s spectra were collected at a pass energy of 20 eV. The chamber pressure was below 5.0×10^{-8} mbar. The resulting spectra were then analysed with the CasaXPS software.

3.2.3 Cell preparation for scanning electron microscopy examination

Titanium sheets were prepared for examination with a scanning electron microscope (SEM) to visualise the effects of cell growth on the coating integrity as outlined in Chapter 2. MG63 osteosarcoma cells were grown on Ti sheets according to the proliferation protocols (Chapter 2) for 3 days and 7 days. The samples were washed with PBS, incubated in a 4% paraformaldehyde (PFA) solution for 1 hr, and stored in PBS buffer at 4˚C until visual examination. The samples were fixed with 1% Osmium tetroxide (OsO_4) solution then dehydrated with increasing concentrations of ethanol and a pre-made solution of 2% (v/v) hexamethyldisilazane (HDMS). The samples were affixed to SEM mounting stubs with carbon tape and coated with a 20 nm layer of gold via sputtering (Emiteck K550X sputter coater). The samples were imaged with secondary emission detection using a neoscope JEOL

tabletop SEM at a 10 V electron acceleration and working height of 48 mm. Three samples for each condition were examined at multiple sites (minimum n = 5) for each surface.

3.2.4 Atomic force microscopy analysis

AFM was performed on Ti substrates to determine if surface topology was altered during the nitric acid cleaning or the rPPF deposition processes, as described in Chapter 2.1.8. Briefly, the toluene and nitric acid cleaned Ti sheets and bare and rPPF-coated foils were prepared as close to the examination date as possible and examined with a molecular imaging PicoSPM atomic force microscope (AFM). The individual samples were attached to the sample plate, a 0.6 µm sharp microlever (Park Scientific Instruments) was inserted into the probe, and the cantilever laser was aligned to the tip. A random 30 µm x 30 µm section of the surface was selected, the detection and feedback parameters were optimised, and the surface traced for topology and roughness. The results were analysed with the 'WSxM 5.0 Develop 8.5' software as developed by Horcas *et al.* [330].

3.2.5 Cell proliferation assays

The MG63 cellular proliferation was measured with the AlamarBlue (AB), cell counting kit – 8 (CCK-8), and cyQUANT proliferation assays as per the protocols in Chapter 2. Briefly, the Ti and rPPF coated sheets were sterilised with UV light for 15 min per side and transferred into individual wells of a 24-well plate (Corning). The MG63 cells were seeded at a density of 10,000 cells/cm^2, or 6500 cells per sheet, using a droplet seeding method. The droplet was left on the substrate surface for 2 hr to allow for cell attachment. The well was gently filled with 1 mL of cell media and placed in the incubator. Cellular proliferation was measured at day 1, day 3, and day 7 post seeding. The proliferation assays were performed under dark conditions to reduce photobleaching. Blank samples were run in

conjunction with each assay for background subtraction. The results were examined as background subtracted signal intensity and proliferation ratios compared to day 1.

3.3 Results and Discussion

3.3.1 rPPF deposition parameters and the resulting C:N ratios

The rPPF coatings with varying N_2: C_2H_2 gas ratios were deposited to a thickness of 60 ± 7 nm as determined by ellipsometry. The reagent gas ratios and deposition times are shown in **Table 3-1**. By increasing the N_2: C_2H_2 ratio from 0: 15 to 12.5: 2.5, the incorporated nitrogen increased from 0 at% to 28 at% while the carbon content decreased from 93 at% to 66 at% (**Figure 3.1**). The majority concentration of carbon is typical for amorphous films deposited from carbon-based monomers that have been highly cross-linked through ion bombardment. Nitrogen is incorporated predominantly through the radical fragmentation-recombination reactions in the plasma before deposition and can also be included through ion implantation mechanisms. The presence of oxygen suggests that the rPPF-coatings have undergone autoxidation reactions between carbon-centred radicals and atmospheric oxygen [207, 292, 363].

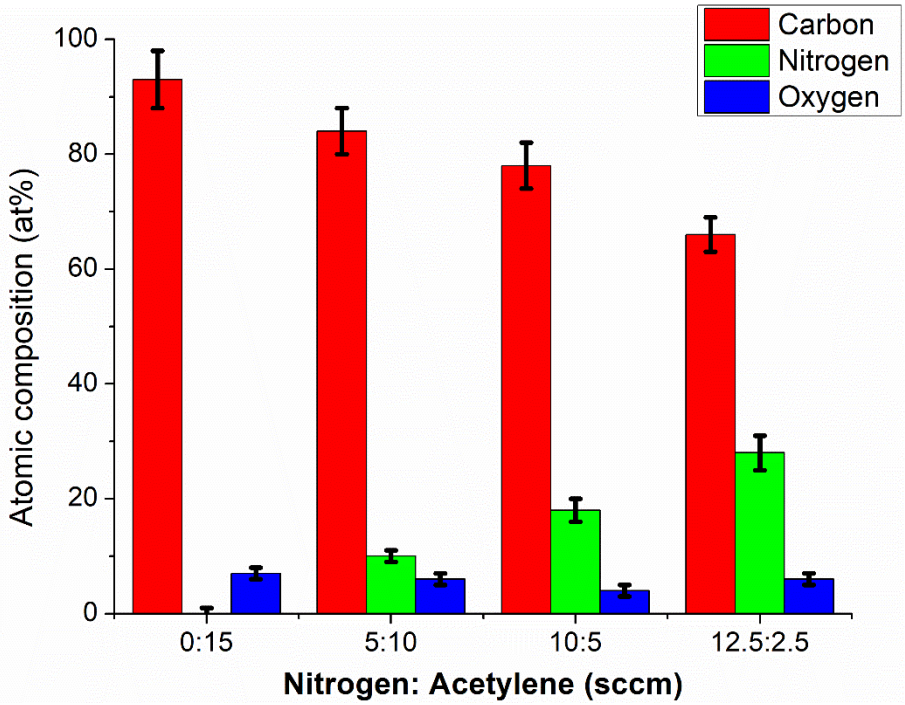

Figure 3.1. The atomic composition of rPPF coatings deposited with varying nitrogen and acetylene precursor gas ratios.

The C1s high-resolution peaks were curve-fitted with components at binding energies corresponding to C−C/C−H (284.6 ± 0.5 eV), C−O/C−N (286.5 ± 0.5 eV), C=O/N−C=O (287.5 ± 0.5 eV), and COOH (289 ± 0.5 eV) [309, 353, 364]. The C-H/C-C groups are the dominant component of C 1s spectra (red peak at 284.6 eV in **figure 3.2**). The C-O/C-N components increased relative to the C-H/C-C components with the N_2:C_2H_2 reagent gas ratios. The C-N/C-O peak fittings, along with the minor contributions of the COOH functionalities (green peak at 289 ± 0.5 eV), also illustrated autoxidation of the rPPF surfaces through the formation of predominately singly bonded carbon-oxygen groups. The organic polar groups formed as autoxidative products are known to be beneficial for cellular attachment and proliferation [243]. Overall, the nitrogen content in the rPPF coatings was shown to increase proportionally to the N_2:C_2H_2 ratio and these coatings were further examined for robustness and biocompatibility.

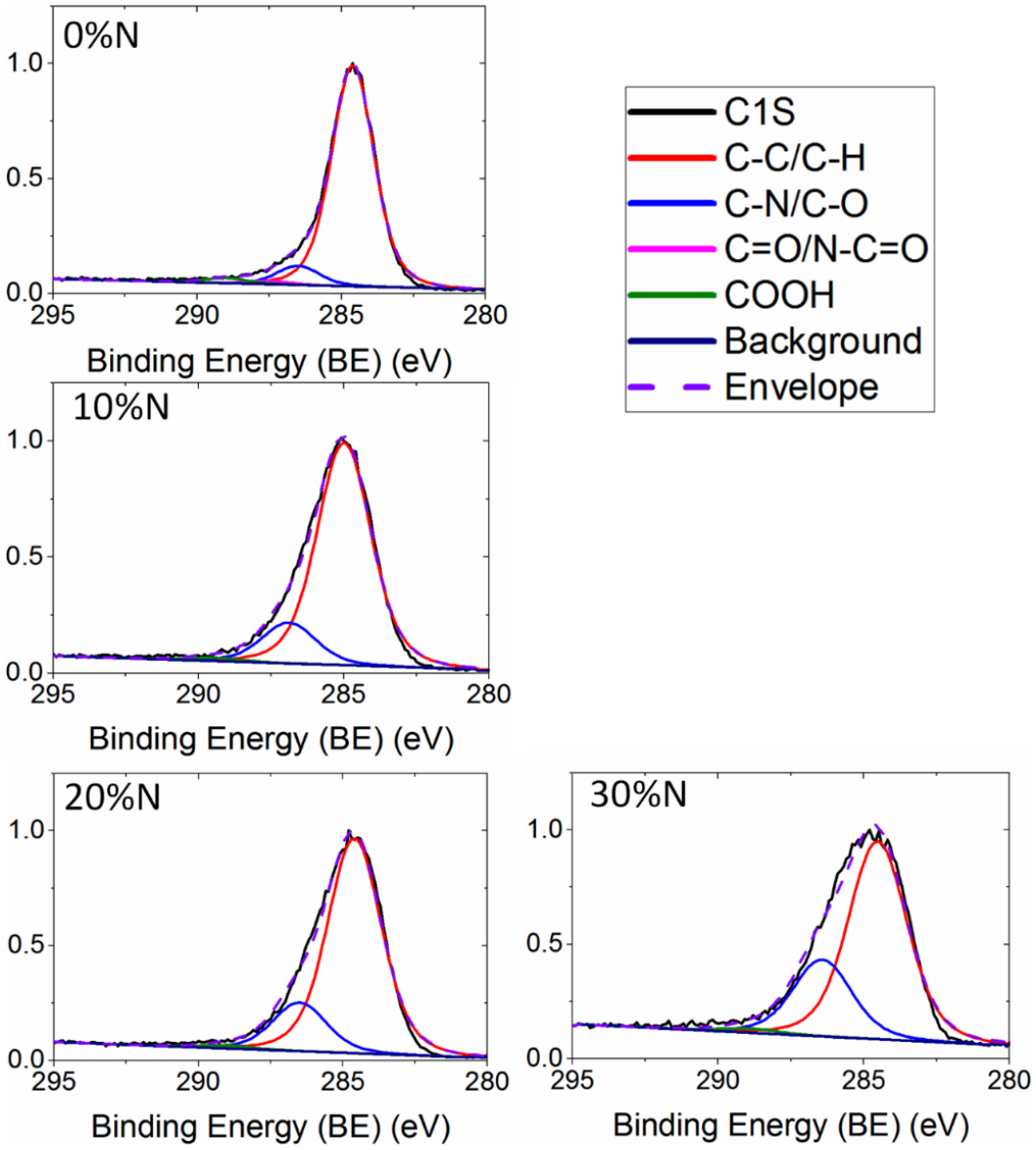

Figure 3.2. High-resolution C1s fitting of rPPFs with increasing nitrogen content after 24 hours of atmospheric exposure post deposition. The increase in the C-N/C-O fitted peak (blue) compared to the C-H/C-C fitted peak (red) indicates the incorporation of nitrogen roughly proportional to initial reagent gas ratios. The presence of the COOH fitted peaks (green) in conjunction with the C-N/C-O peak in the 0%N coating indicates autoxidation of the rPPF-coatings.

3.3.2 rPPF robustness in biological environments

To test the mechanical suitability of the varying N:C ratio rPPF coatings in biological environments, bare and rPPF coated Ti sheets were seeded with MG63 cells and examined for coating failure with a scanning electron microscope at the day 3 and day 7. The day 3 images demonstrated a

predominately homogenous cell distributed on the bare Ti surfaces, while all rPPF surfaces produced cell clustering. A closer x600 magnification examination showed more pronounced coating swelling and creases on the 0%N and 10%N surfaces compared to the 20%N and 30%N surfaces (**Figure 3.3**). The day 7 images showed the formation of cell multilayers across all surfaces. The multilayers produced on the Ti surfaces were homogenously distributed while the multilayers on rPPFs resembled converging grain boundaries as suggested by the day 3 cell distributions. Cell loss was observed on all surfaces due to the preparation procedures. However, coating and cell layer delamination were frequently observed on the lower nitrogen rPPF coated surfaces. The higher 20%N and 30%N rPPF coated surfaces experienced considerably less cell loss and virtually no coating delamination.

Overall, the incorporation of nitrogen and the strong adhesion at the rPPF-titanium interface, through the formation of titanium carbide bonds [286], resulted in a more robust film for the 20%N and 30%N rPPFs, with a slight improvement in the case of the 30%N coating.

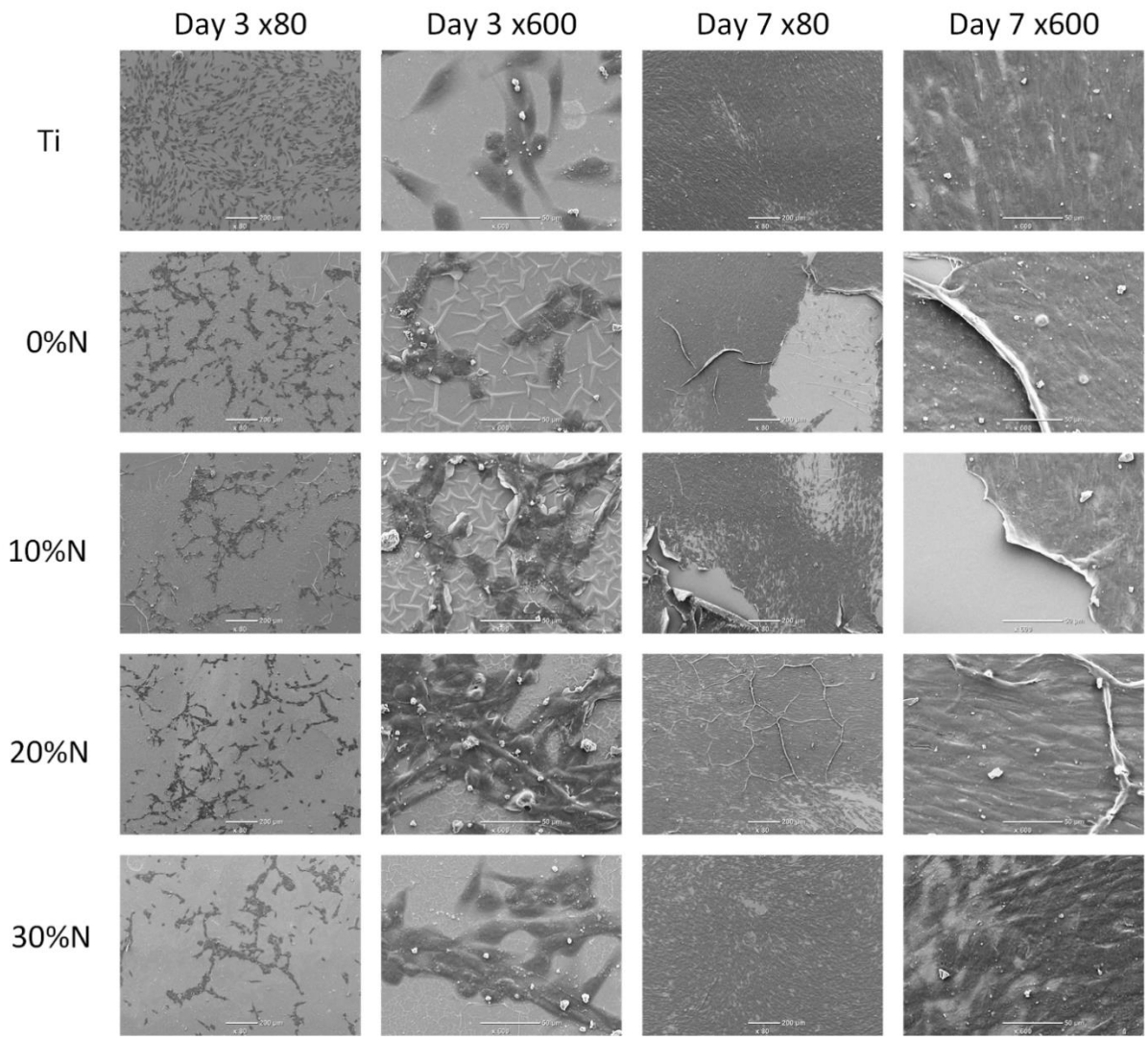

Figure 3.3. Representative scanning electron microscopy (SEM) images of cell formation and rPPF integrity on the varying N% coatings at day 3 and day 7 growth time points compared to titanium. Day 3 x80 magnification shows clustered cell growth on all rPPF surfaces. rPPF swelling is visible for the 0%N and 10%N coatings under x80 (scale = 200 µm) and x600 (scale = 50 µm) magnifications. Day 7 SEM examination showed coating delamination on the 0%N and 10%N rPPFs.

3.3.3 Surface topology analysis

An increased surface roughness produced through surface modification techniques, such as acid and plasma treatments [365], has been shown to produce statistically significant improvements in the attachment, proliferation, differentiation, and mineralisation of bone lineage and stem cells over their smoother counterparts [76, 243, 366, 367]. Therefore, any potential difference in surface roughness produced from the nitric acid cleaning or rPPF deposition must be taken into account to determine if any biological preference exists for particular rPPF N:C ratios. The nitric acid and toluene cleaned Ti sheets produced a root mean square (RMS) roughness of 32 ± 6 nm and 34 ± 8 nm in a 30 µm x 30 µm square, respectively. Both nitric acid (**Figure 3.4.a**) and toluene (**Figure 3.4.b**) cleaned sheets showed pitting from the manufacturing, and skewness and kurtosis from polishing processes (**Figure 3.4 c,d**). The uncoated and 20%N rPPF-coated Ti foils showed no significant differences in measured roughness, with both possessing an RMS roughness between 7-18 nm as measured over 1 μm^2. Therefore, surface roughness changes through cleaning treatments or coating deposition can be eliminated from consideration as contributing factors to the observed differences in cell behaviour. Any observed differences can, therefore, be attributed to the effects of the changes in nitrogen incorporation.

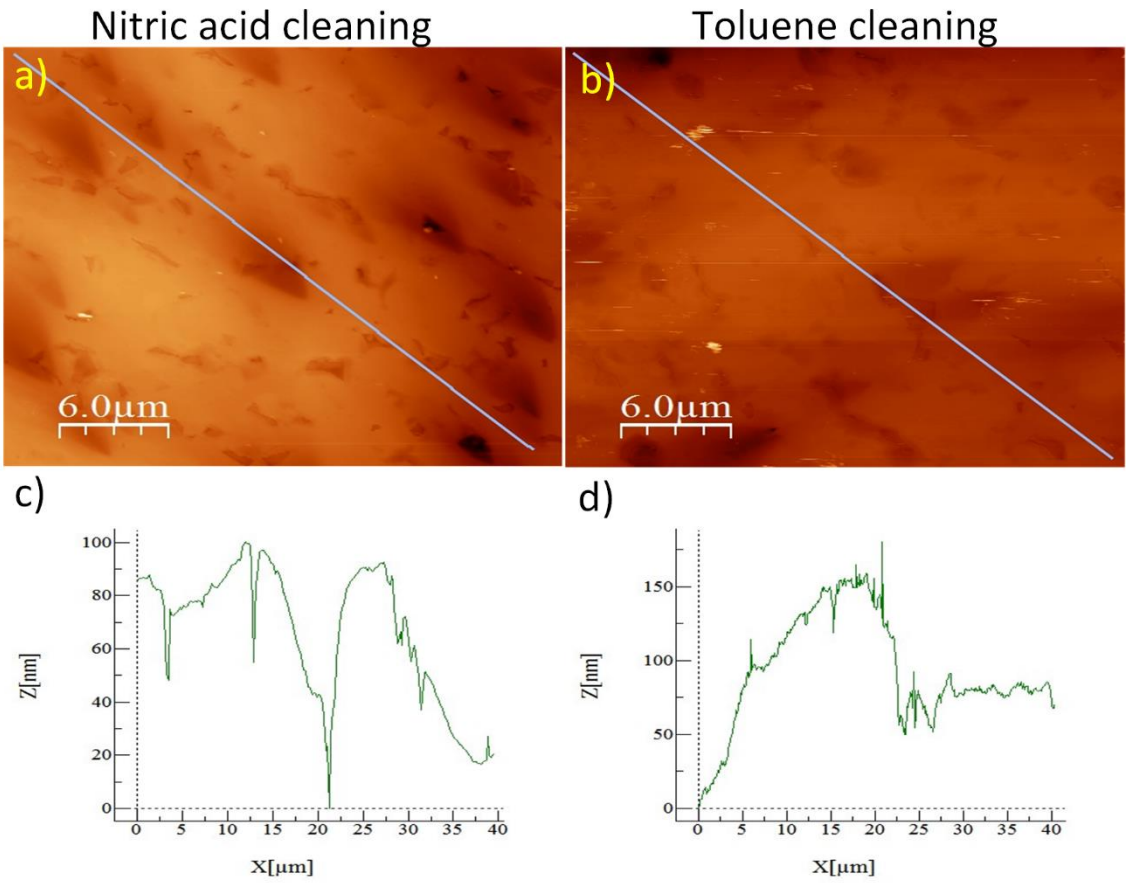

Figure 3.4. Representative surface topology traces obtained by AFM. The surface traces of polished Ti sheets cleaned via the nitric acid protocol (**a**) and the toluene protocol (**b**) showed little topological differences between the two surfaces. The surface profiles of nitric acid (**c**) and toluene (**d**) show similar height variations across the surface taking into account the kurtosis. No significant difference was found between the average surface RMS roughnesses.

3.3.4 *In vitro* biological evaluation

The biological compatibility of the varying N:C ratio rPPFs was examined with the AlamarBlue (AB), cell counting kit 8 (CCK-8), and cyQUANT NF cell assays. The cellular proliferation followed similar trends across the three assays with some deviation based on the targeted compound or detection pathway, as shown in **Figure 3.5**. Coating delamination was occasionally observed on the lower N% rPPF samples.

The AB absorbances and growth ratios are shown in **Figure 3.5.a** and **Figure 3.5.b**, respectively. The day 1 assay showed no significant difference between Ti and the rPPFs except for a lower absorbance on the 30%N surfaces. The day 3 absorbances again showed no statistically significant differences except for an increase on the 10%N rPPF. The day 3 growth ratios had statistically significant increases over Ti for the 10 - 30%N rPPFs. The day 7 absorbance results showed reductions in signal for the rPPF surfaces but no statistically significant differences in growth rate. Cell number determination by CCK-8 assay (**Figure 3.5. c,d**) showed similar levels of $NADPH^{+}$ expression across all time points for all surfaces. No significant variation was found between the Ti and 0%N - 20%N rPPFs. The 30%N rPPFs produced a statistically significant reduction in absorbance signal relative to the bare Ti surfaces at the day 3 and day 7 time points. The cell growth rates also showed a lower ratio for the 30%N rPPF coatings. The CyQUANT assays were used to determine the DNA quantity in each sample (**Figure 3.5. e, f**). The day 1 fluorescence results were equal within uncertainty across all surfaces. The day 3 results deviated from the previous assays and showed a reduction of DNA on the 0%N and 30%N surfaces relative to the Ti and 10 - 20%N rPPFs. No statistically significant differences in DNA quantity were observed by day 7 compared to the titanium surfaces. The MG63 growth rates of the surfaces were equivalent within uncertainty across all time points except for a significant increase on day 3 for the 10%N rPPF only.

The coating stability is of primary importance for implantable devices, but the biological compatibility must also be examined as to prevent adverse immune responses. The incorporation of nitrogen has been shown to increase the biological acceptance through the presence of positively charged nitrogen-containing groups at the interface [237-243], and as such, the 20%N and 30%N were expected to be the most biologically beneficial. However, the proliferation assays showed that the 30%N coating produced somewhat lower cell signals than the other surfaces. No significant differences in cell growth rates were observed between the 0 - 20%N rPPFs and the 30%N rPPFs. The lower cellular proliferation behaviour can be attributed to the lower initial cell attachment compared to the other surfaces observed in the day 1 measurements. Overall, by combining the SEM imaging of

coating robustness, which showed that only the coatings with over 20% nitrogen content had appropriate robustness, and the general biocompatibility observed across all rPPF coatings, the biologically favoured 20%N and the mechanically favoured 30%N rPPF coatings were selected for continued examination as potential orthopaedic coatings.

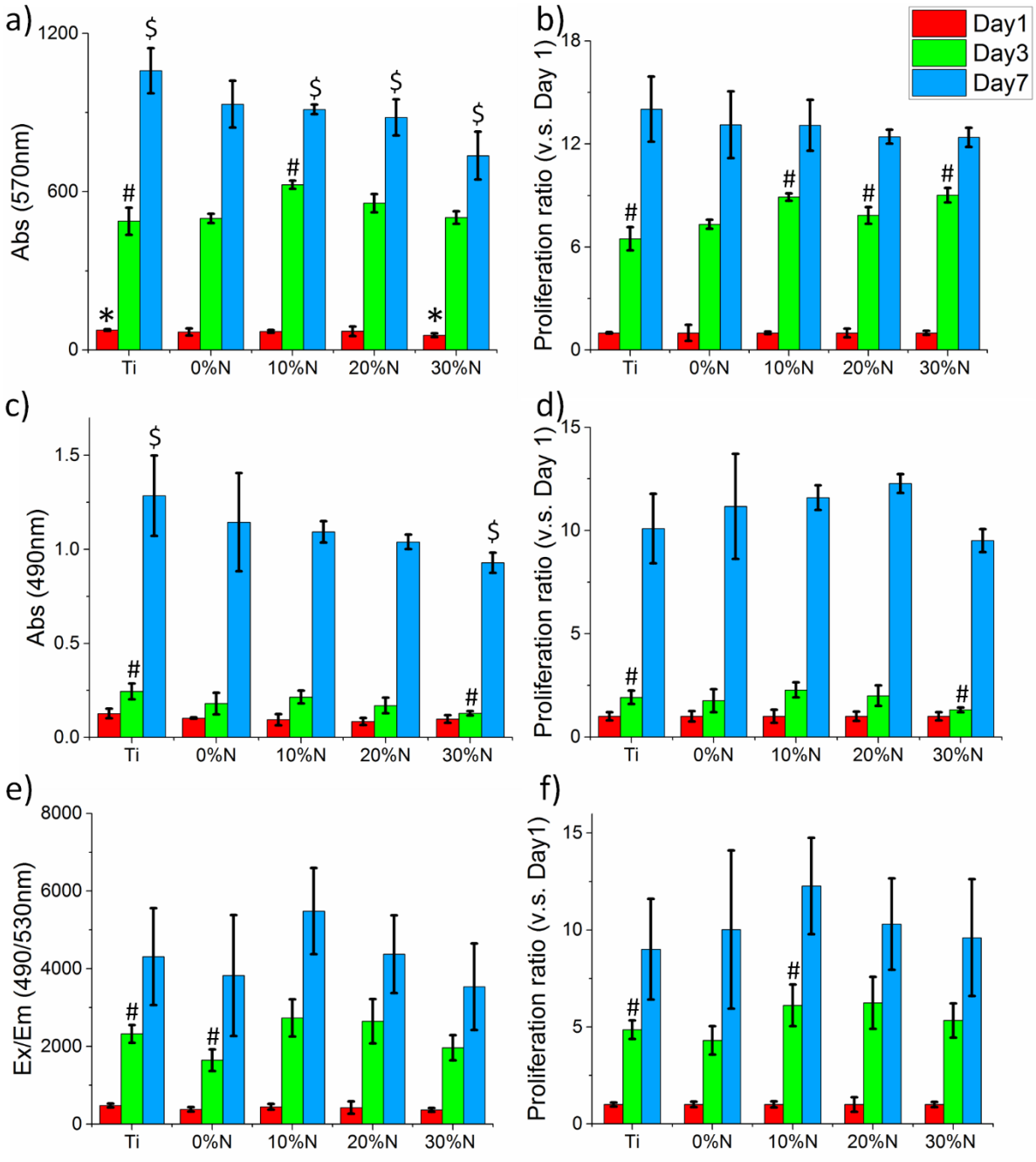

Figure 3.5. MG63 cell proliferation assay results over one week. AlamarBlue measurements of cell metabolism showing the absorbance (**a**) and proliferation ratio (**b**) over 7 days. Cell counting kit -8 measurements of the $NADP/NADPH^+$ energy production indicating the relative live cell quantities as absorbance (**c**) and the growth rate (**d**). The DNA quantity was investigated with cyQUANT NF measuring the relative increases in cell mitosis shown as fluorescence data (**e**) and proliferation ratio (**f**). Mean values ($n < 6$) are shown. Uncertainties are determined by the standard deviations. Statistical significance ($p < 0.05$) against titanium is shown for day 1 (*), day 3 (#), and day 7 ($). No significant trends were found with the exception of a reduction in the cell quantity initially attached on the 30%N coating.

3.4 Conclusion

A primary requirement for an orthopaedic coating is the ability to resist delamination during the surgical implantation process and the extended time in the body. In this chapter, a series of ratios for nitrogen: acetylene reagent gases were investigated to determine the precursor gas composition that produced robust and biologically compatible rPPF surfaces. The XPS results showed that increasing the N_2:C_2H_2 gas ratio resulted in greater surface atomic concentrations of nitrogen. The SEM images demonstrated that the 20%N and 30%N rPPF coatings were more mechanically stable than the 0%N and 10%N. All rPPF surfaces demonstrated biocompatibility with the 30%N producing less initial cell proliferation compared to the 20%N, potentially due to a reduced cell attachment. Overall, the biologically favoured 20%N coating and mechanically favoured 30%N coating were selected for further examination.

Chapter 4: The effect of plasma polymer ageing on rPPF elemental composition and cellular activity

In this chapter, the potential for radical-induced cytotoxicity originating from rPPF surfaces with high radical flux occurring soon after deposition was investigated. The surface properties of rPPFs were examined over the course of two weeks, and the changes were shown to be derived from the radical decay. rPPF surfaces with low and high radical fluxes showed no cytotoxicity to MG63 osteosarcoma cells or primary osteoblasts.

Results from this chapter have been published in "Cellular responses to radical propagation from ion-implanted plasma polymer surfaces" by Callum A.C. Stewart, Behnam Akhavan, Miguel Santos, JuiChien Hung, Clare L. Hawkins, Shisan Bao, Steven G. Wise, Marcela .M.M. Bilek, 2018, Applied Surface Science, https://doi.org/10.1016/j.apsusc.2018.06.111 [343].

4.1 Introduction

Biomolecule-functionalisation has the potential to vastly improve the biocompatibility and longevity of implanted medical devices, with significant improvements to patients' quality of life [368, 369]. Plasma polymers represent a promising method to bio-functionalise devices on the manufacturing scale [288]. Chemical-functionalised and radical-functionalised plasma polymer films, (cPPFs and rPPFs, respectively) have been proven to possess reproducible surface chemical composition regardless of the substrate chemistry, geometry, and size [286, 308, 353, 370-372] allowing for the biomolecule-functionalisation of any underlying surface.

Both classes of PPFs are affected by a process known as ageing in which the surface chemistry changes over time [292, 300]. PPF ageing occurs due to the oxidation of carbon-centred radicals (referred to as autoxidation) [207, 292], chemical group oxidation [208, 254], and polymer chain

diffusion (hydrophobic recovery) [309, 373]. These ageing phenomena are explained in detail in Chapter 1.3.3.3. When relying on surface chemical groups for functionalisation, chemical instability from functional group oxidation [208, 212, 216, 240, 253, 254, 299, 300] and hydrophobic recovery [309, 373] may limit the applications in practice, and can greatly impact the long-term functionality of cPPFs and cellular interactions [374]. Although strategies have been developed to mitigate hydrophobic recovery [375], cPPFs should be used immediately after deposition for best performance of biomolecule functionalisation.

In the case of rPPFs, ageing does not directly affect the ability to immobilise biomolecules providing that sufficient reactive radicals are available in the coating structure [264, 355, 356, 376]. Biomolecule-functionalisation can be performed immediately after deposition or after various ageing periods (e.g. 15 days [58] or up to 4.5 months [283]) with only minimal changes in immobilisation time to account for variations in the flux of radicals diffusing to the surface. Hydrophobic recovery occurs over time, initially due to the conversion of radicals to polar groups upon reaction with atmospheric constituents at the surface. The polar groups possess lower free energy than the radicals they replace, and as such, the surface becomes more hydrophobic but stabilises in a mildly hydrophilic state [377]. In previous works, the rPPFs were aged to allow for the stabilisation of surface chemistry prior to biomolecule functionalisation and use in a biological context.

The higher concentration of radicals at short ageing times, however, may have adverse biological consequences. Radical species are produced naturally as a consequence of cellular metabolism, and cells have antioxidative countermeasures to prevent oxidative damage [378, 379]. However, high concentrations of radicals are known to be cytotoxic. An imbalance favouring radical species production compared to their removal can induce oxidative stress within the cell, which can lead to DNA, protein, and lipid damage, dysregulation of signalling cascades, and cell death through apoptosis or necrosis [380, 381]. Radical-mediated cellular damage and dysfunction have been implicated in ageing and the pathology of numerous diseases, including osteoarthritis and osteoporosis [381, 382].

Therefore, there are concerns about the potential radical-induced cytotoxicity of fresh rPPFs. The high flux of radicals emerging from fresh rPPFs may induce oxidative stress in the attached cells, resulting in cell death and/or detrimental biological activity.

This chapter investigates the effects of radical flux and rPPF ageing on cells by comparing cellular responses to fresh and aged rPPFs. The surface chemistry, surface energy, and radical density of rPPFs were characterised at a series of time points from 15 min. to 2 weeks. Titanium was used as the substrate due to its extensive application in biomedical devices [34, 383]. Bone lineage cells, i.e. primary mouse osteoblasts and the MG63 bone osteosarcoma cell line, were chosen to reflect the prominence of Ti in orthopaedic devices [35, 383, 384]. The time points of 4 hours (fresh) and 11 days (aged) post-deposition were selected for cell studies as they represent the earliest possible implant time following surface treatment and the ageing conditions for rPPFs used without inducing cytotoxicity in prior experiments, respectively [58, 353, 356].

4.2 Methods

4.2.1 Substrate preparation

rPPF coatings were deposited onto Ti sheets (0.8 mm x 0.8 mm x 1 mm) and foils (70µm thickness) as described in Chapter 2. In short, the Ti substrates were cleaned with the nitric acid protocol before rPPF deposition. The surfaces were plasma cleaned with Ar for 10 min (Mass flow rate = 40 sccm, working pressure = 7 x 10^{-2} Torr, RF power = 75 W, substrate bias voltage = -500V, pulse frequency = 3 kHz, pulse width = 20 µs), followed by coating with 30%N rPPF. The rPPF was deposited for 6.5 min with mass flow rates of 2.5 sccm for acetylene, 12.5 sccm for nitrogen, and 15 sccm for argon. The RF power was 50 W and the working pressure was 0.11 Torr. The rPPF coated substrates were stored in air as required.

4.2.2 X-ray photoelectron spectroscopy (XPS)

A more comprehensive explanation of the XPS procedure is presented in Chapter 2. Briefly, the survey spectra were collected in an energy range of 0–1000 eV at a pass energy of 30 eV and a resolution of 0.5 eV. High-resolution (0.1 eV) C 1s spectra were collected at a pass energy of 20 eV. Pressures during measurement were below 5.0×10^{-8} mbar. The resulting spectra from the rPPF-coated samples (0.8 cm x 1 cm) were then analysed with the CasaXPS software (version 2.3.18PR1.0).

4.2.3 Fourier transform infrared spectroscopy (FTIR)

The surface chemistry of the uncoated and rPPF coated Ti sheets was performed via FTIR as described in Chapter 2. Briefly, the FTIR spectra of the Ti and rPPF samples were recorded using a DigiLabFTS7000 FTIR spectrometer fitted with a multibounce ATR accessory and a trapezium germanium crystal at an incidence angle of 45˚. The titanium and rPPF- coated foils (1.5 cm x 2 cm) were measured at a resolution of 4 cm^{-1} within the mid-IR range of 4000 – 850 cm^{-1} and averaged over 500 scans. The contributions from Ti, CO_2, H_2O, and the air-crystal interface spectra were subtracted using 'Digilab Resolutions Pro 4.0' software.

4.2.4 Contact angle measurements and surface energy calculations

The surface energy was measured as described in chapter 2. Briefly, the contact angles of water (polar) and diiodomethane (non-polar) droplets were measured (drop volume ≈ 5 µL). The contact angles were measured from captured images (n = 5), and the total, dispersive, and polar surface energies were calculated by the Owens–Wendt–Rabel–Kaelble model.

4.2.5 Electron paramagnetic resonance (EPR)

The measurement of the concentration of unpaired electrons in the rPPF coating is described in detail in Chapter 2. Briefly, the rPPF was deposited on 25 µm polystyrene (PS) (7 cm x 8 cm). The spectra for each time point (n = 6) were examined alongside a weak pitch (WP) control of known radical density (~1 × 10^{13} spins/cm) for calibration. The radical density of the rPPF samples was calculated in spins/cm^3.

4.2.6 Cell maintenance and examination

The responses of MG63 cells and primary osteoblasts to extended contact with the bare Ti and coated substrates were examined. The cells were collected and maintained using the procedures outlined in Chapter 2. The rPPF substrates were prepared and sterilised before cells were seeded onto the surface, as per the protocols described there. Cell attachment fluorescent microscopy assays for both cell lineages on bare Ti foils, 4 hours (fresh) and 11 days (aged) rPPF surfaces were performed as described in Chapter 2. MG63 cell proliferation was examined with AlamarBlue assays at day 1, 3, and 7 for comparison against previous publications, while, the proliferation of primary osteoblasts was examined with the MTS assay because of the slow doubling time of the cells and the consequent need to detect subtle proliferation differences.

4.3 Results

4.3.1 Surface analyses

The surface chemistry as a function of ageing time was studied using XPS and FTIR spectroscopy. The composition of the rPPF, measured by XPS survey elemental scans as a function of ageing time is shown in **Figure 4.1**. The carbon content remained relatively unchanged, fluctuating around approximately 70%. Comparing the chemical composition of the fresh sample with that of a sample

aged for 14 days highlights the increase in oxygen concentration and the decrease in nitrogen. The nitrogen atomic concentration decreased from 24.69% for the as-deposited coating (15 min. after deposition) to 19.01% after 14 days of ageing; while the oxygen content increased from 5.96% to 10.23%. These changes in surface chemistry derive from the well-documented autoxidation processes initiated from carbon-centred radicals [207, 292]. It has been shown in previous publications for ion-implanted polymer substrates [385, 386] as well as rPPF surfaces [353], that nitrogen groups, such as the nitrile ions [283, 353], can react with air to form volatiles, e.g. nitroxide gasses (NO_x), that diffuse out of the polymer [385]. The thermally activated production of nitrogen-containing volatiles during ageing could account for the loss of nitrogen over time.

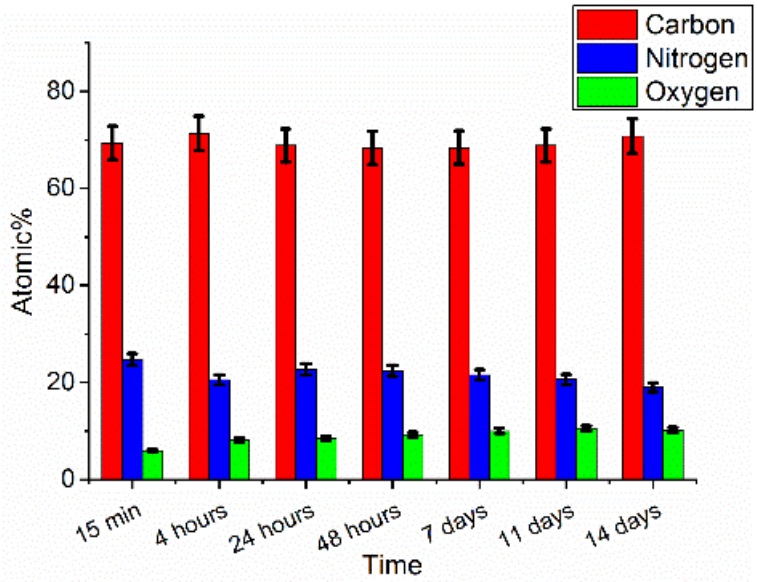

Figure 4.1. Elemental composition of the radical-functionalised PPFs as a function of time determined by XPS. The spectral analysis indicates a stable carbon atomic concentration of approximately 70% within error across all time points, while the oxygen atomic concentration increased considerably over the 14 days period (6% to 10%). The corresponding decrease in nitrogen atomic concentration from 25% to 19% suggests the release of nitrogen from the rPPF during the oxidative process. The measurement uncertainty shown is derived from instrument sensitivity together with the accuracy of integration range selection in the CasaXPS software.

Comparative analysis of curve-fitted high-resolution C1s spectra of the coatings with different ageing times, shown in **Figure 4.2**, further elucidates the variations of oxygen- and nitrogen-

containing carbon species. The C-C/C-H, C-N/C-O, N-C=O/C=O, and COOH chemical bond peaks are fitted at energies 284.6 ± 0.5, 286.5 ± 0.5, 287.4 ± 0.5 eV, and 289 ± 0.5 eV, respectively [286, 309, 353]. The proportion of the total carbon counts attributed to each fitted component as a function of ageing time is summarised in **Table 4.1**. The increase in the N-C=O/C=O and COOH components as a function of ageing time is in agreement with the increase of atomic oxygen concentration measured in the survey spectra (**Figure 4.2**). The notable increase between the as-deposited and day 14 conditions reiterates the significant changes to the surface chemistry through autoxidation.

These element composition changes resemble those observed for cPPFs. The changes observed in XPS oxygen after 24 hours is consistent with those observed for ethylene/ ammonia and allylamine cPPFs [240, 387], which showed an oxygen increase of approximately 11% along with a nitrogen reduction of approximately 5.5% [240]. Amine-containing cPPFs lost up to 70% of the functional NH_2 groups over two weeks, although the total nitrogen content did not vary significantly due to the formation of amides and other oxidative products [234, 240]. The loss of nitrogen and autoxidation in the rPPF-coatings follow similar overall trends [388].

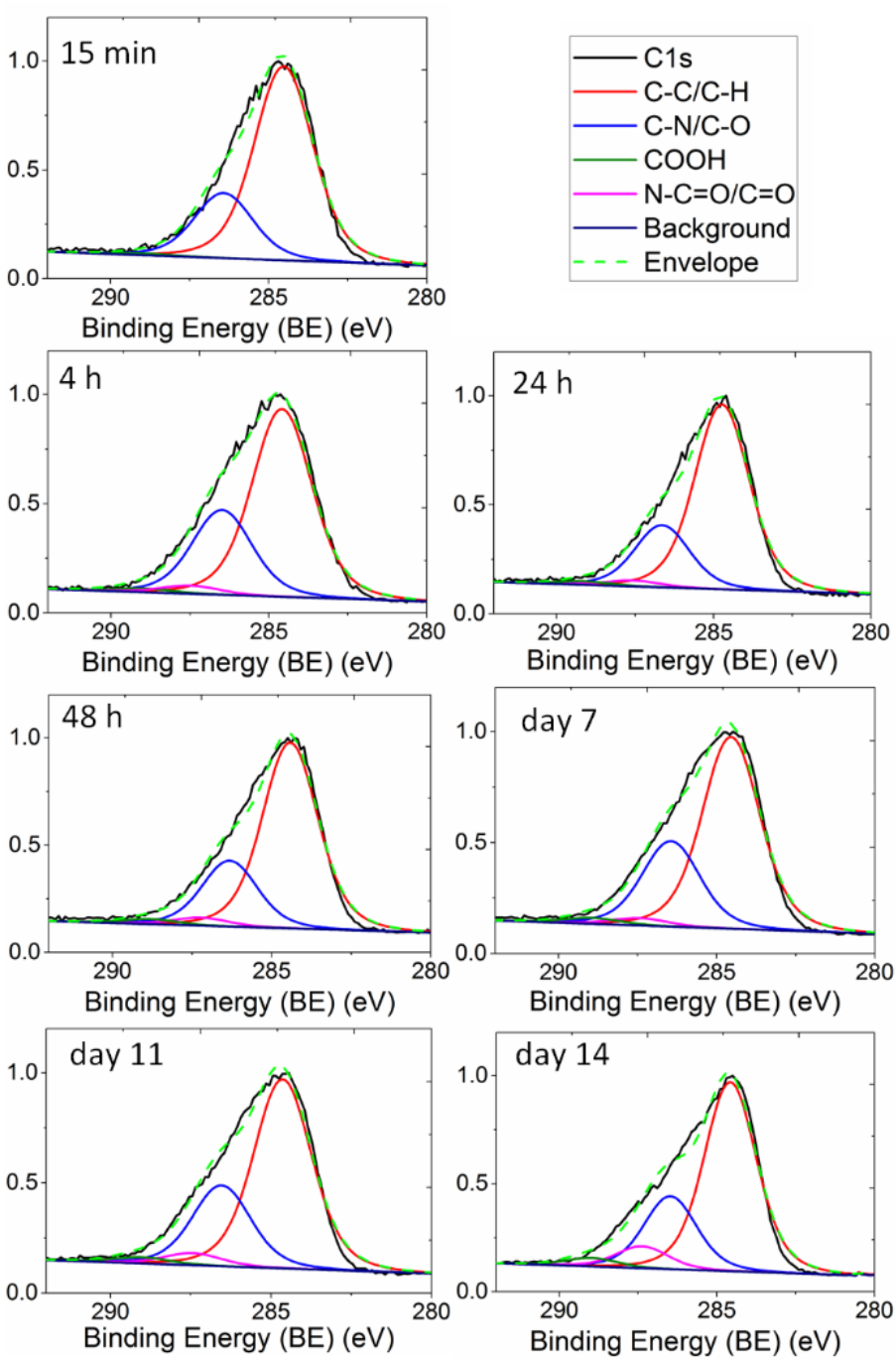

Figure 4.2. C1s XPS spectra recorded after various ageing times: 15 min, 4 h, 24 h, 48 h, 7 days, 11 days, and 14 days time points. The red, blue, magenta and green lines represent the fitted component peaks: C-C/C-H, C-N/C-O, N-C=O/C=O, and COOH bond energy spectra. C-C/C-H at 284.6 eV, C-N/C-O at 286.5 eV, N-C=O/C=O at 287.4, and COOH at 289.0 [286, 309, 353]. The percentage contributions of the total C 1s peak for each component at each time point is shown in **Table 4.1**. The percentage contribution of the N-C=O/C=O component (magenta) increases substantially over time from approximately 1.2% of the total area after 15 min of ageing to almost 10 % by 14 days. The COOH component (olive/green) drastically increases from 1.1% of the total area after 15 min ageing to 2.4% after 14 days.

Table 4.1. The percentage concentration of the four fitted peaks to the C1s high-resolution peak.

Percentage contribution to C1s peak	15 min	4 Hr	24 Hr	48 Hr	7 days	11 days	14 days
C-C/C-H	76.3 ± 0.9	66.1 ± 3.3	71.8 ± 0.2	69.7 ± 3.5	66.0 ± 0.7	66.2 ± 0.6	64.4 ± 0.3
C-N/C-O	21.0 ± 1.6	29.7 ± 1.5	24.9 ± 1.2	25.7 ± 1.5	28.4 ± 1.0	27.3 ± 0.5	24.8 ± 0.5
N-C=O/C=O	1.2 ± 0.3	2.7 ± 0.3	1.6 ± 1.2	2.1 ± 1.8	3.5 ± 0.9	4.3 ± 1.1	8.4 ± 1.4
COOH	1.1 ± 0.4	1.5 ± 0.2	1.5 ± 0.3	2.4 ± 0.6	2.1 ± 0.5	2.2 ± 0.6	2.4 ± 0.7

Figure 4.3 presents the FTIR spectra of rPPFs at various times after deposition, recorded over the spectral range of 3500 - 1000 cm^{-1}. The broad peak observed in the region 1690 – 1450 cm^{-1} originates from the rPPF [58] and consists of C=O, C=C, C=N, N-H, and potentially also aromatic chemical groups. The peaks observed in the 1450 – 1250 cm^{-1} region derive from C-C, N-O, C-H, NH_3^+, and NO_3^- group vibrations, while C-O and C-N peaks are located in the 1200 – 1000 cm^{-1} range [58, 283, 389, 390]. The fluctuation in baseline signal from 3500 – 2500 cm^{-1} appears due to the subtraction of water and other background components, exacerbated by the differences in signal strengths. A relative increase in the intensity of oxygen species in the rPPF is observed when comparing the spectra of the as-deposited coatings (15 min.) to those of samples aged for various times (**Figure 4.3**). The separation of the nitrogen and carbon species peaks, observed between 1690 – 1450 cm^{-1} in the as-deposited spectrum, is lost as the rPPF ages. The emergence of peaks in the 1450 – 1250 cm^{-1} and 1200 – 1000 cm^{-1} regions compared to the as-deposited coating, corresponding to C-O, C-H, and C-C groups, further shows the formation of oxygen-containing groups as a function of ageing time. The increase in oxygen group vibrations in the FTIR spectra agrees with the changes in surface chemistry indicated by the XPS data (**Figure 4.1**, **4.2** and **Table 4.1**). These FTIR spectral changes as a function of time are similar to those observed in the ageing of amine- and carboxyl- functionalised cPPFs deposited from ethylene, excluding the signature of the specific chemical functional groups [388, 391, 392].

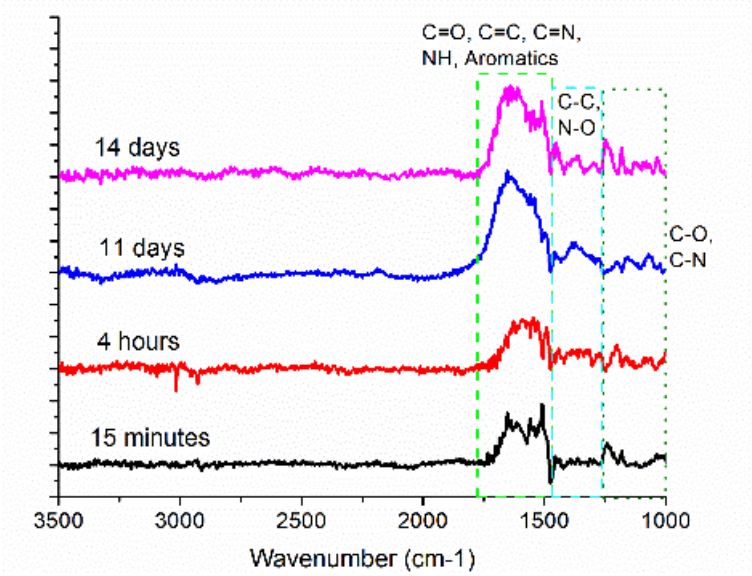

Figure 4.3. ATR-FTIR spectra showing rPPFs surface chemistry after ageing times of 15 minutes, 4 hours, 11 days, and 14 days. Increasing quantities of oxygen-containing species are observed in the aged coatings, as demonstrated by an initial increase in double bonded oxygen groups at 4 hours (1690 – 1450 cm^{-1}) and the subsequent increase in singly bonded groups at 11 days (1450 – 1250 cm^{-1}). The labels showing the chemical groups are noted at their reported wavenumbers. Three dashed boxes have been used to separate the 1690 – 1450 cm^{-1}, 1450 – 1250 cm^{-1}, and 1200 – 1000 cm^{-1} regions.

The varying surface energy (SE) of the rPPFs was monitored via contact angle measurements. The water contact angle (WCA) and corresponding SE values are plotted as a function of ageing time in **Figure 4.5**. The WCA increased sharply from the as-deposited 41.5˚ ± 1.0˚ to 56.0˚ ± 1.0˚ at 48 hours, after which the WCA plateaued with fluctuations within uncertainty (blue curve in **Figure 4.4**). The diiodomethane contact angle increased continually from the as-deposited 27.0˚ ± 1.5˚ to 40.5˚ ± 0.5˚ at day 14. The contact angles for both water and diiodomethane were used to calculate the surface energy of the rPPFs. The total SE, shown in red in **Figure 4.4**, decreased overall as a function of time from an as-deposited 66.8 ± 0.5 mN/m^2 to 54.5 ± 0.3 mN/m^2 at 14 days. The reduction in surface energy and resulting decrease in wettability is a well-studied process called hydrophobic recovery, and it is also observed for cPPFs [295, 373, 387, 393-395]. The surface energy reduction observed in cPPFs is attributed to the oxidation of the chemical-functional groups [208, 240]. Over long time scales (t > week), the contact angles of cPPFs and rPPFs stabilise at similar values, however, there are

differences in the short time scale (t < week) water contact angle behaviour. In the case of cPPFs, the chemical degradation processes of the functional groups may lead to temporary reductions in WCA, such as amine functionalities converting to amides and imines [396]. In contrast, rPPFs typically have lower initial WCAs compared to cPPFs due to the high fluxes of radicals diffusing to the surface. The increases over time in the rPPF WCAs correspond to the energy differences between the strongly polar, reactive radicals diffusing to the rPPF surface from within the coating post-deposition and the more stable polar groups formed through their autoxidation [270, 354]. Wettability, as measured by WCA, has major effects on protein adsorption and subsequent biological response to a surface. Dowling *et al.* [374] demonstrated that MG63 cell line attachment was optimised for WCA in the range 57˚- 64˚ on both rough and smooth polymeric surfaces. Therefore, the formation of polar groups from autoxidation and the transition from a highly hydrophilic to a mildly hydrophilic state suggests that the aged rPPF would present a more beneficial surface for cells.

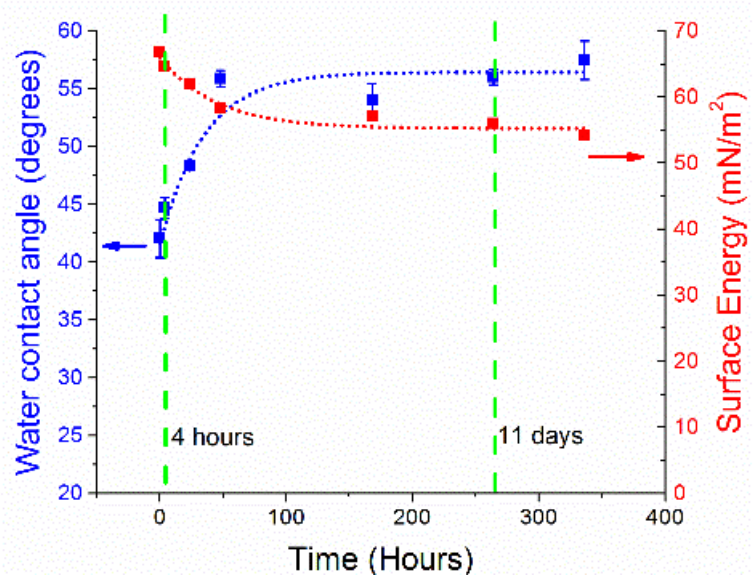

Figure 4.4. Surface energy and water contact angle for rPPF deposited on Ti foils as a function of time after deposition. The graph demonstrates a decrease in total surface energy corresponding to an increase in water contact angle, caused by plasma polymer autoxidation, radical recombination, and polymer chain migration. The green lines indicate the 4-hours and 11 days time points selected for cell assays in this study. Error bars correspond to standard deviations.

The quantification of unpaired electrons associated with radicals within the rPPF was performed via EPR. **Figure 4.5.a** shows the unprocessed spectra of rPPFs after 4 hours (fresh) and 11 days (aged) compared to the polystyrene control. The peaks are symmetrical and centred around 3505 G consistent with the radicals being predominantly carbon-centred (G-Factor = 2.002). The broadness of the peaks could show that there are a variety of carbon-centred radical species within the rPPF [58], and may also reflect that the radicals appear at the rPPF surface, which would also cause anisotropic spectra. A comparison of the two rPPF spectra shows a 27.1 ± 3.6 % reduction in signal intensity. The radical densities for the rPPF conditions calculated, following the double integration of the EPR spectra and comparison to the weak pitch (WP) standard, are plotted over 14 days **(Figure 4.5.b)**. The resulting curve follows the double exponential decay previously observed for other plasma immersion ion implanted polymeric substrates [269, 385, 397]. The rPPFs demonstrate a rapid initial loss of radicals between the first reading at approximately 30 minutes and 24 hours, in-keeping with the trend of surface oxidation, after which the radical density loss tails-off.

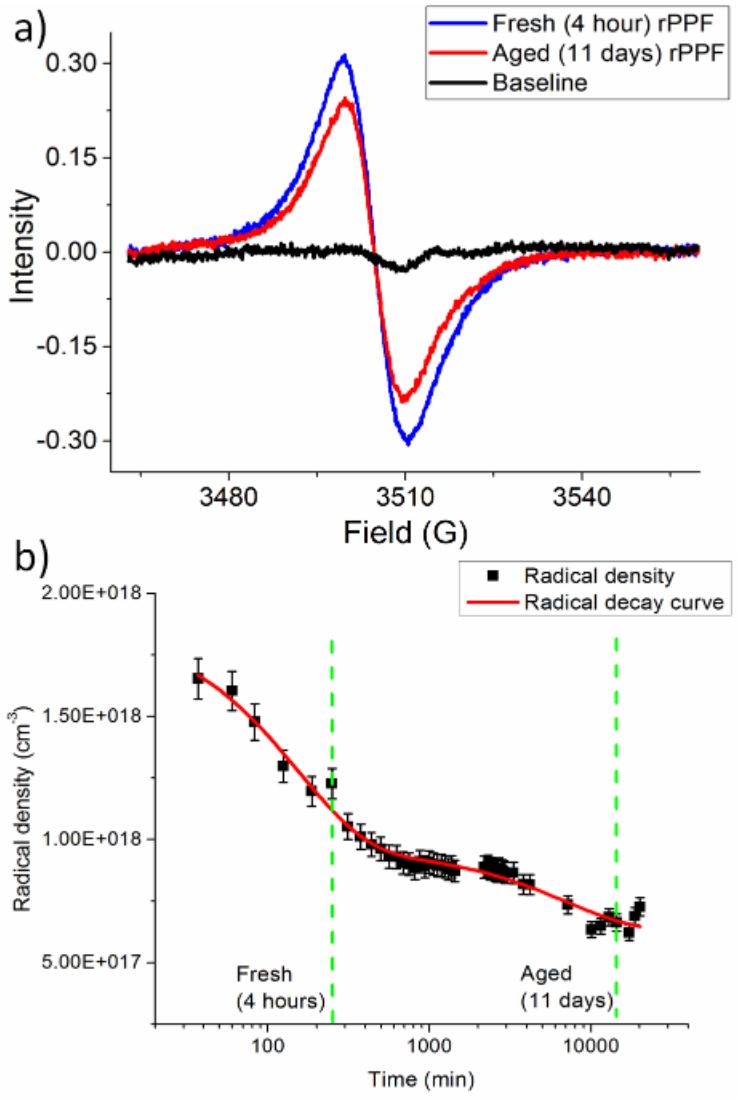

Figure 4.5. a) The EPR spectrum of fresh and aged rPPF deposited on polystyrene. Double integration of the resulting spectra after background subtraction and scaling to the control, revealed a 27.1 ± 3.6 % loss in unpaired radical electrons between the 4 hours and 11 days time points. **b)** The radical density decay curve fitted to the double exponential trend, $Y=A_0 + A_1*\exp(-x/t_1) + A_2*\exp(-x/t_2)$ [269].The total radical loss from the initial measurement to the 14 days of examination demonstrates an approximately 60% reduction in radical density.

The radical decay kinetics demonstrate a double exponential decay curve; $Y=A_0 + A_1*\exp(-x/t_1) + A_2*\exp(-x/t_2)$. The coefficients derived from the radical decay curve are $A_0 = 6.297 \pm 0.256 \times 10^{17}$, $A_1 = 3.236 \pm 0.202 \times 10^{17}$, $t_1 = 6974 \pm 1675$, $A_2 = 9.130 \pm 0.699 \times 10^{17}$, and $t_2 = 152.2 \pm 18.1$; where A_1 and A_2 are the multiplying constants, t_1 and t_2 are the respective time constants. These coefficients align with other plasma immersion ion implanted polymeric substrates treated for 240 seconds [269]. Overlaying

the data for the fresh and aged conditions, the fresh rPPFs fall into the radical ageing region governed by rapid surface oxidation, and hence, possess a higher flux of reactive radicals than the aged rPPF which is governed by slower kinetics (lower radical flux). The rPPFs showed a radical density of 1-2 orders of magnitude greater than conventional cPPFs deposited in the absence of enhanced ion-bombardment [58, 353, 398]. The significantly increased radical density enables rPPFs to covalently immobilise biomolecules even after extended ageing times [283], meaning that the radicals described by the slower decay kinetics provided sufficient radical flux to the surface for biomolecule functionalisation. The high flux of rapidly decaying autoxidative radicals at early time points highlighted the potential for radical-derived cytotoxicity and warranting investigation.

4.3.2 Cellular probing of rPPF surfaces

The response of primary osteoblasts (OBs) (**Figure 4.6**) and MG63 cells (**Figure 4.7**) to the two rPPF samples aged for 4 hours (fresh) and 11 days (aged), as marked in **Figures 4.2-5**, were examined. These assays were performed to determine if the observed differences in surface chemistry, radical density, and surface energy would affect the immediate cell attachment and longer-term proliferation. Primary osteoblasts revealed no statistical difference in attached cell quantity between the two rPPF surfaces, with the average cell density of 89 ± 26 cells per field of view (x5 magnification) for the fresh and 100 ± 17 cells per field of view for aged surfaces, as shown in **Figure 4.6.a**. The cell attachment observed on the aged rPPF surface was significantly greater that of the bare titanium (75 ± 20 cells per field of view). **Figure 4.6.b** shows that the spreading of the OBs on fresh and aged rPPF surfaces, 1209 ± 58 μm^2 and 1099 ± 199 μm^2 respectively, were significantly larger than that on titanium alone, 774 ± 58 μm^2. No significant difference was observed between the two rPPF surfaces. Representative fluorescence microscopy images of the cell attachment and spreading are presented in **Figures 4.6.c-e**. The elevated cell attachment and spreading observed on fresh and aged rPPFs

compared to bare Ti can be attributed to the presence of organic carbon and nitrogen groups, which have previously been shown to enhance cellular attachment and proliferation [243].

The MTS assay results, as shown in **Figure 4.6.f**, demonstrated no significant difference between the surfaces after 3 days of proliferation. The detected absorption signals for the Ti, fresh, and aged rPPF surfaces were 0.79 ± 0.11, 0.70 ± 0.11, and 0.66 ± 0.13, respectively. No significant difference was observed between the proliferation results of the two rPPF surfaces with absorbances for the fresh and aged surfaces being 1.05 ± 0.05 and 0.99 ± 0.04 for 7 days, 1.16 ± 0.03 and 1.19 ± 0.06 for 11 days, and 1.31 ± 0.12 and 1.22 ± 0.10 for 14 days, respectively. This behaviour is consistent with the attachment and spreading data presented in **Figure 4.6.a-b.** The Ti absorbances were 1.19 ± 0.09, 1.32 ± 0.07, and 1.44 ± 0.14 for the 7 days, 11 days, and 14 days time points, respectively. Overall, no significant difference was observed between the attachment and spreading or proliferation behaviour of the fresh and aged rPPF surfaces. These results indicate that the increased radical flux at the surface does not significantly alter cell metabolic activity compared to non-treated surfaces.

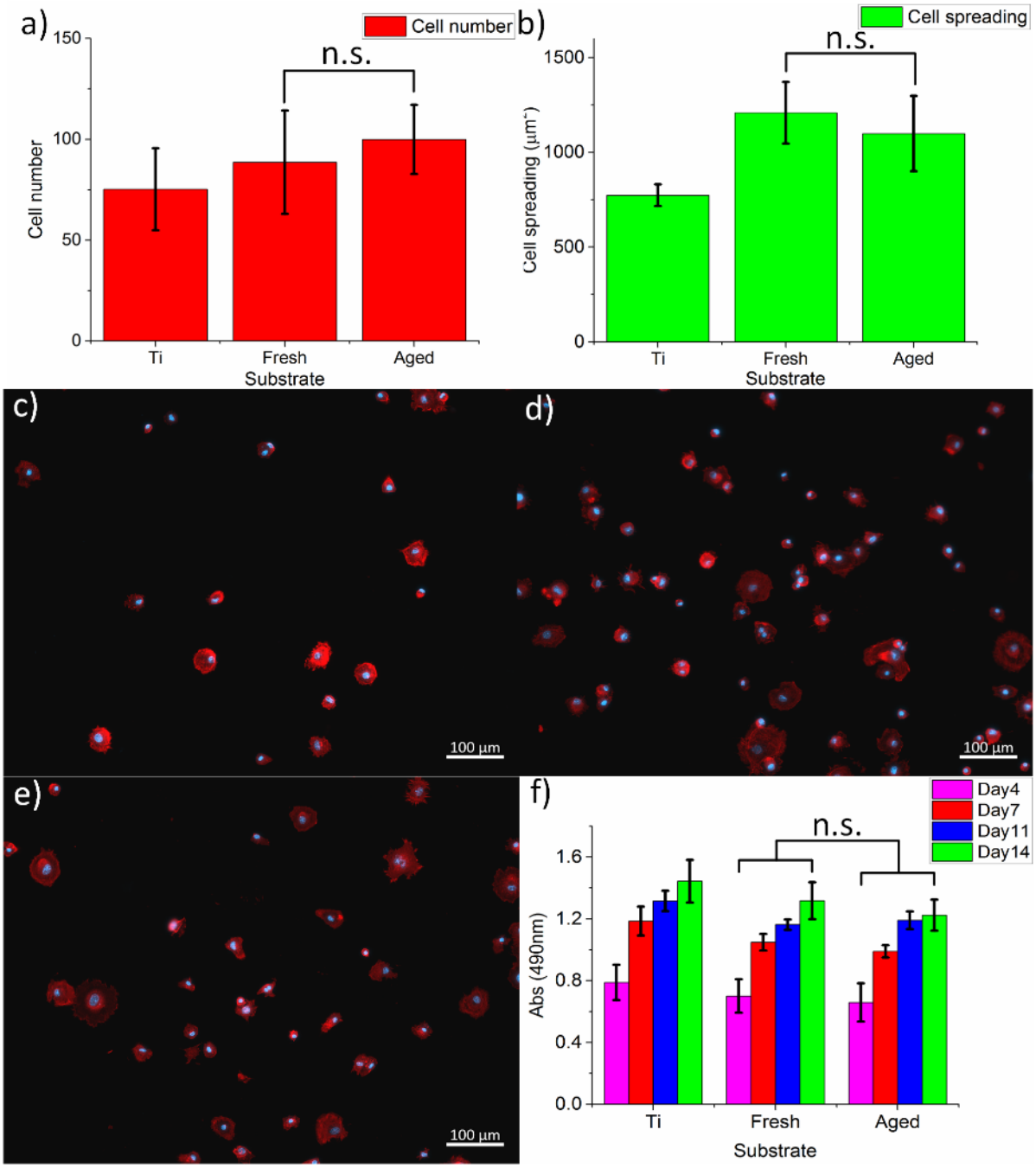

Figure 4.6. Osteoblast cell attachment (**a**) and spreading (**b**) on Ti, fresh rPPF, and aged rPPF. No significant difference (n.s.) was observed between the results for the fresh and aged rPPF surfaces. Fluorescence microscopy images of OBs stained with actinRED555 (red) and DAPI (blue) at 10x magnifications for Ti (**c**), fresh (**d**), and aged (**e**) rPPFs. No significant differences were observed between the two rPPF surfaces for cellular proliferation (**f**).

MG63 osteosarcoma cells were used to further probe the attachment and proliferation trends observed for the primary osteoblasts. The cell attachment and spreading results are shown in **Figure 4.7. a,b**, with representative images for Ti, fresh rPPF, and aged rPPF in **Figure 4.7.c-e**. The attached cell numbers for fresh and aged rPPFs were 652 ± 108 and 742 ± 119 cells per field of view (x5 magnification), respectively. These values are significantly higher than that of the Ti control (456 ± 116 cells per field of view). The MG63 cells were significantly more spread on the rPPFs with average cell sizes of 696 ± 18 μm^2 and 619 ± 62 μm^2 for the fresh and aged surfaces respectively, compared to the Ti control, 489 ± 45 μm^2. Again, the cells showed no preference for either the fresh or aged surface suggesting that the difference in radical flux between the surfaces does not affect the cellular responses.

The AlamarBlue (AB) proliferation assays (**Figure 4.7.f**) produced absorbances of 67 ± 10, 98 ± 33, and 284 ± 28 for Ti on day 1, 3, and 7, respectively. Fresh rPPFs produced values of 66 ± 9, 95 ± 25, and 314 ± 43, while aged rPPFs had absorbances of 80 ± 7, 111 ± 31, and 358 ± 17. No statistical difference was observed between the fresh and aged rPPFs as predicted by the attachment and spreading. The cells reached confluence by day 7 and commenced mineralisation on all surfaces. Significance was seen between the day 7 Ti and aged sheets. This reflects the previously seen increase in cell attachment and spreading, given that the proliferation rates were equal across all samples. Overall, no significant differences were observed between the rPPF surfaces. Both surfaces increased cell affinity, and no radical-induced cytotoxicity was observed. The MG63 assays confirm the results observed in the primary osteoblasts; that rPPFs do not demonstrate radical-derived cytotoxicity.

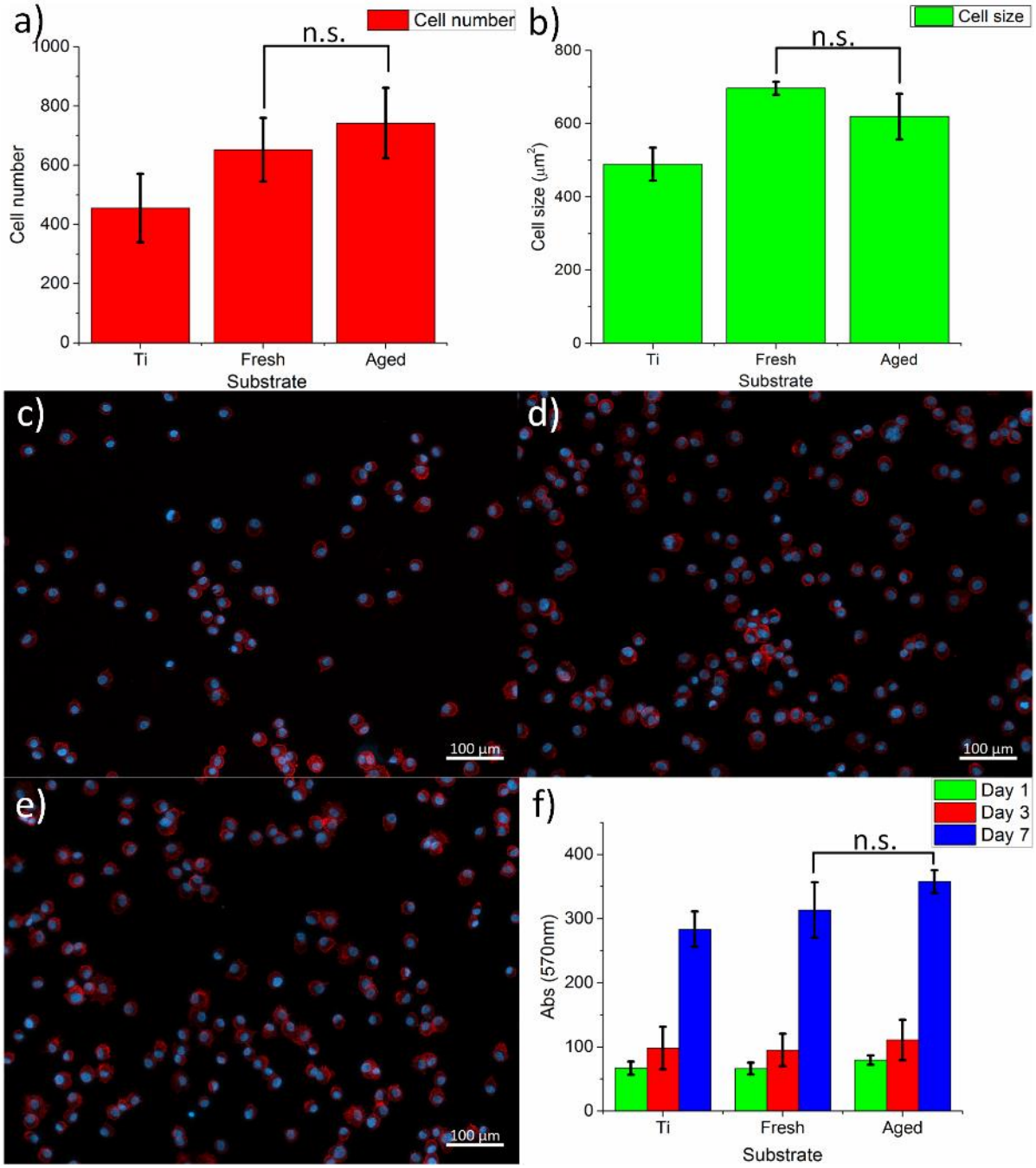

Figure 4.7. MG63 Cell attachment and proliferation on untreated Ti, and the fresh and aged rPPF surfaces. The average cell number (**a**) and spreading (**b**) was increased significantly on the rPPFs compared to the Ti foils, where $P < 0.05$. However, no significance was observed between the rPPF surfaces. The elevated cell number can be visually observed by fluorescence microscopy. The images show cells on Ti (**c**), fresh (**d**), and aged (**e**) rPPFs. The proliferation as determined by AlamarBlue metabolism assays show a statistically significant increase between the aged rPPF compared to Ti sheets, but no significance between the two rPPF conditions (**f**).

4.4 Discussion

Biomolecule-functionalisation utilising radical-functionalised plasma polymers represents a promising method of providing biological cues on the surfaces of biomedical devices which is readily translatable into manufacturing [288]. The functionalisability of rPPFs is derived from radicals in the form of unpaired electrons, whose density is highest immediately after polymerisation. The non-specific covalent binding of macromolecules upon contact and reaction with emerging radicals allows for simple, single-step surface functionalisation with antimicrobial and osteogenic biomolecules [58, 376]. However, a high flux of radicals in biological systems is known to generate oxidative stress in cells, and hence, there is a potential that fresh rPPF surfaces could elicit radical-induced cytotoxicity. An investigation of fresh and aged rPPFs with primary osteoblasts and MG63 osteosarcoma cells revealed that the higher flux of radicals in the fresh rPPFs produces no detrimental effects on either bone lineage cell type. The biocompatibility of the rPPFs was shown to be similar to that of titanium, with significant increases in initial cell attachment and spreading observed on both rPPF surfaces compared to titanium alone.

The improvements in attachment and spreading observed on the rPPFs is believed to stem from the favourable oxidation and wettability of the coatings, and the lack of cytotoxicity is attributed to the inability of radicals to propagate through the biomolecule backbones [399]. When the rPPFs are placed in *in vitro* cell culture medium, the surface becomes coated with biomolecules from the medium that are covalently immobilised upon contact via reactions with radicals that have propagated to the surface from within the rPPF [264, 269, 386]. The unpaired electrons preferentially react with side chain groups [400, 401]. Reactions with the protein backbone may occur at the α-carbon sites [400], but do not propagate through the peptide bonds along the protein backbone [399]. Cells then interact with the surface according to the biomolecules presented and their conformations [48, 50]. If the surface is favourable, the cells will establish an extracellular matrix (ECM) for proliferation and other biological functions. Should any free products of radical reactions at the

protein-surface interface penetrate through the cell wall into the cytoplasm, there are antioxidative enzymes, such as superoxide dismutase (SOD) and catalase. These enzymes regulate and remove reactive oxygen species and oxidative stress produced through metabolic functions [402]. The results demonstrate that the radical fluxes to the surface of freshly prepared rPPFs have minimal negative effects on the biological affinity and proliferation of bone lineage cells, suggesting that rPPFs, and other radical functionalised PP products [390], are appropriate for biological applications at any ageing time. Their ease of functionalisation makes them attractive platforms for the creation of simultaneously antibacterial and osteogenic implant surfaces.

4.5 Conclusion

Biomolecule functionalisation of medical devices, especially load bearing orthopaedics, represents the potential for vastly improving the quality of life for patients and the longevity of implanted biomedical devices through optimal tissue integration. The functionalisation potential of radical-functionalised plasma polymer films (rPPFs) was shown to be unaffected by ageing, but concerns existed regarding the potential for radical-induced cytotoxicity. The rPPFs were examined over 2 weeks of ageing. The potential for radical-induced cytotoxicity due to the higher radical flux of the fresh samples was examined with primary osteoblasts and the MG63 cell line. Enhanced cell attachment and spreading, as well as proliferation equivalent to titanium, was observed for both cell lineages on all rPPFs, regardless of ageing time. The biocompatibility is attributed to the mild hydrophilicity of the oxidised surfaces and the retention of native protein conformations. Radical-induced damage to cells is limited by the inability of radicals to propagate along the peptide backbones of immobilised biomolecules. In conclusion, rPPFs demonstrate cellular affinity even when radical fluxes through the surface are at their highest. Their inherent ease of biomolecule functionalisation suggests a translatable approach for surface engineering of implantable orthopaedic devices.

Chapter 5: Quantification of protein-functionalised rPPF surfaces and the development of multi-protein interfaces.

This chapter reports the development of radical-functionalised plasma polymer film (rPPF) based multifunctional and multi-protein interfaces. Enzyme-linked immunosorbent assays (ELISAs), derived from specific peptide sequence detection, were optimised for the proteins of interest and used to determine the optimum incubation concentrations for surface functionalisation. The monolayer protein solution concentrations for fibronectin, osteocalcin, and the fusion protein containing functional fragments of both fibronectin and osteocalcin were determined to be 15 µg/mL. The fraction of covalently bonded surface protein was found to be between 60% and 80% of the monolayer ELISA signal, depending on the protein. A series of rPPF surfaces co-immobilised with ratios of fibronectin: osteocalcin were developed and compared with the fusion protein functionalised surfaces.

The results from this chapter are reported in "Multifunctional protein-immobilized plasma polymer coatings for orthopedic applications." by Callum A.C. Stewart, Behnam Akhavan, Juichien Hung, Shisan Bao, Jun-Hyeog Jang, Steven G Wise, and Marcela M.M. Bilek (Accepted; ACS Biomaterials Science and Engineering).

5.1 Introduction

Protein-functionalisation of surfaces stemmed from peptide functionalisation, with only a few publications appearing through the early 1990's [103, 167, 168, 403]. Since then, protein-functionalisation has expanded into many interdisciplinary fields involving biological and medical applications, including titanium-based orthopaedics. Surface immobilisation of proteins and peptides through adsorption, chemical covalent linking, or physical covalent methods, allows for the bestowment of specific biological functions to titanium orthopaedic surfaces to overcome their biologically inert nature. A comprehensive evaluation of these surface immobilisation approaches can

be found in Chapter 1. Protein-functionalisation can reduce the potential for post-operative complications that require revision surgeries to correct [1], such as antibiotic-resistant biofilm formation [7, 404-406] or fibrotic encapsulation of the implant from negative foreign body reactions (FBR) [3-5].

The single protein approach to biomolecule functionalisation has shown some success [57, 407, 408], but a deeper understanding of the osseointegration process reveals that a multifunctional protein-coated surface is required. The synergistic combination of biological functionalities would allow for increased cellular attachment in conjunction with more rapid bone formation, leading to greater osseointegration. A few avenues have been explored for the multifunctionalisation of biointerfaces. One approach investigated the immobilisation of an incomplete monolayer of protein onto a biologically-active linker molecule, thereby expressing properties from both the linker molecule and the protein [145-147]. Another avenue to multi-functionalisation is the immobilisation of cocktail solutions containing multiple proteins onto a single surface through physical adsorption or chemical methodologies [316, 409-412]. However, immobilisation from protein cocktails faces the same hurdles as immobilisation from single protein solutions, namely displacement by the Vroman effect for physically adsorbed proteins or the need to control complicated wet chemical reactions to achieve covalent attachment. The ratio of the proteins on the functionalised surface is difficult to control and does not reflect that in the solution due to differences in the relative protein surface affinities and protein-protein complexing. An alternative approach is to use a series of multiple protein solution exposures to achieve a multi-protein functionalised surface, but unfortunately, this approach is not feasible for most immobilisation methodologies, due to protein displacement when the layers are physically adsorbed, or the potential for reagent incompatibilities and reversible or side reactions in chemical linker methodologies. However, the on-contact covalent immobilisation capability of radical-functionalised plasma polymer films (rPPFs) may enable controllable multi-functionalisation using multiple single protein exposures to form successive covalently immobilised partial monolayers.

An alternative direction to multi-functionalisation involves the immobilisation of synthetic multifunctional biomolecules, known as fusion proteins [316, 411]. Fusion proteins are synthesised through recombinant processes to incorporate multiple peptide sequences responsible for various cellular interactions into a single protein [413], allowing for surface functionalisation via simpler single molecule immobilisation methodologies. A few fusion biomolecules have been utilised for orthopaedic applications such as a branched antibacterial/attachment protein [414], a composite attachment protein [124, 415], and an attachment/signalling protein (fibronectin/BMP-2 fusion) [416].

In this study, the non-specific bonding capacity of the radical-functionalised plasma polymer films (rPPFs) were optimised for the immobilisation of the extracellular matrix (ECM) protein fibronectin (FN) (440 kDa), the bone-signalling osteocalcin (OCN) protein (5.9 kDa), and a fusion protein containing the FN9,10 domains and the OCN22-49 sequence (FN-OCN/ Fusion protein) (40 kDa) produced by our collaborators at Inha University, Korea [287, 316]. For comparison, a co-immobilised FN and OCN multi-protein interface was developed through the sequential exposure of the rPPF surface to multiple protein solutions. These optimised surfaces were examined for their *in vitro* osteogenic potency in Chapter 6.

5.2 Method

5.2.1 Substrate preparation and analysis

rPPFs were deposited on nitric acid cleaned Ti foils following the procedure and deposition conditions for 20%N rPPFs outlined in Chapters 2 and 3. Briefly, the foils were nitric acid cleaned to remove surface contaminants. The surface was argon plasma cleaned, and the 20%N rPPF was deposited. The rPPF- coated foils were allowed to age for 5 - 7 days before use.

Surface characterisation of the 20%N coatings was performed via X-ray photoelectron spectroscopy (XPS), contact angle measurements, and electron paramagnetic resonance (EPR) spectroscopy following the protocols previously described in Chapter 2. Briefly, the surface composition of the rPPF was examined using XPS survey spectrum collected in the energy range of 0 – 1000 eV with a resolution of 0.5 eV. High-resolution (0.1 eV) C 1s spectra were collected at a pass energy of 20 eV. The contact angles of water (polar) and diiodomethane (non-polar) droplets (≈ 50 µl) were measured (n = 5). The angles were used to calculate the total, dispersive, and polar surface energies via the Owens–Wendt–Rabel–Kaelble (OWRK) model. The radical density of the rPPFs was measured via EPR on polystyrene films (7 cm × 7 cm). The EPR spectrometer was calibrated using a weak pitch sample (~1 × 10^{13} spins/cm) before measuring the rPPF. Ten scans were averaged per sample and the radical density calculated per cm^3. The surface characterisation of 20%N rPPFs has also been previously reported by Martin *et al* [356].

5.2.2 Fusion protein synthesis and purification

The FN-OCN fusion protein was produced by Jang *et al*. as previously described [287, 316] and outlined in Chapter 2. Briefly, protein synthesis was initiated via polymerase chain reaction (PCR) amplification of the OCN-FN genetic sequence. The amplified PCR products were digested, ligated, and transfected into E.coli for overnight expression of the protein. The bacteria were harvested and the supernatant collected and purified. The final protein was measured to be approximately 40 kDa via western plotting [316].

5.2.3 Proteins, antibodies, and reagents

Antibodies were acquired for the detection of FN, OCN, and FN-OCN proteins. Fibronectin (F2006, Sigma Aldrich) was detected with a rabbit-anti-FN primary antibody (F3648, Sigma Aldrich).

Osteocalcin (O5761, Sigma Aldrich) was detected using three primary antibodies corresponding to the N-terminal, C-terminal, and an internal sequence of the protein. The N-terminal and internal sequence were rabbit-derived antibodies (ab14173 and ab93876, respectively), while the C-terminal antibody was derived from goat (ab175453). The FN-OCN fusion protein was detected using the OCN internal sequence and a rabbit-derived 6x histidine (6His) tag primary antibody (ab125262). The rabbit primary antibodies were coupled to a goat-anti-rabbit secondary antibody (ab6721) and the goat-derived primary was coupled with a donkey-anti-goat secondary (ab205723) Both secondary antibodies were conjugated with horseradish peroxidase (HRP) for colourimetric detection of 3, 3', 5, 5', -tetramethylbenzidine (TMB), purchased as 1-Step™ Ultra TMB - ELISA Substrate (cat. 34022, Thermofisher Scientific).

5.2.4 ELISA calibration and protein quantification

5.2.4.1 Calibration

The principles of ELISA detection and the general procedure of the biochemical protein quantification technique are explained in Chapter 2. Calibration of each ELISA for the optimal specific signal was performed in a 96 well plate. 150 µL of 10 µg/mL protein solution was aliquoted into the wells according to the grid setup presented in **Figures 5.2.a,b, 5.3.a,b ,** and **5.4.a,b.** The well plate was incubated in the protein solution overnight at 4˚C. The protein solution was removed and the wells were gently washed with PBS. A BSA solution was added into the protein-incubated and non-incubated wells for 1 hr at room temperature. Following the removal of BSA, primary Ig dilutions of 1:1000, 1:2000, 1:5000, and 1:10,000 were dispensed into their corresponding column positions and incubated. The primary Ig was replaced with secondary Ig dilutions of 1:10,000, 1:20,000, 1:50,000, and 1:100,000 in their corresponding rows. The wells were then incubated with TMB for 30 min and the HRP-substrate reaction stopped with 0.2 M H_2SO_4. The absorbance of the 96 well plate was measured at 450 nm. A negative control consisting of TMB and 0.2 M H_2SO_4 only was measured to

account for TMB oxidation in the absence of HRP. The protein-specific signal was calculated by background subtraction of the BSA blocked wells from their protein coated counterparts. The signal to noise ratio (protein: blocked) was calculated for each condition.

5.2.4.2 Protein detection and quantification via ELISA

All protein dilutions were done under sterile conditions so as not to contaminate the protein stocks for cell culturing. The desired protein was equilibrated to 37˚C and transferred into a sterilised Biological safety cabinet (BSC). A series of protein solutions between 1 – 30 µg/mL were diluted from the stock solutions according to the dilution equation (Eqn 2.1):

$$C_1V_1 = C_2V_2 \qquad \textit{Equation 2.1}$$

The 20%N rPPF foils were cut into 0.8 cm x 0.6 cm rectangles and the top right-hand corner was removed to indicate coating-side-up orientation. The foils were transferred into a 48 well plate, and 75 µL of protein solution was deposited on the substrates via droplet deposition. This method was chosen to conserve the expensive and limited supplies of osteocalcin and fusion proteins. The foils were incubated with the protein solution overnight at 4˚C. The excess protein solution was removed the next day and the substrates were gently washed with PBS. The ELISA procedure was carried out with the optimised conditions. The absorbance values for each protein solution concentration were plotted to produce a titration curve and indicate the solution concentration of protein at which a full monolayer was attached to the rPPF.

To determine the covalently immobilised proportion of protein, bare Ti and rPPF samples were incubated overnight in the protein solution concentration that yielded a monolayer. The samples were then transferred into an Eppendorf tube containing 1 mL of 5% sodium dodecyl sulphate (SDS) solution and incubated at 90˚C for 15 min [58, 354]. SDS is a surfactant that disrupts physical interactions

leaving only covalently bonded protein. Pre- and post- SDS washing samples were then examined together in ELISAs. The ratio of signals between the background subtracted values indicated the relative amount of covalently immobilised protein.

5.3 Results

5.3.1 Material characterisation

The 20%N rPPF coatings were used for the protein immobilisation and primary cell studies (reported in Chapter 6). The rPPF surface chemistry was analysed using XPS, and a typical survey spectrum is shown in **Figure 5.1.a**. The atomic composition was 71 ± 4 % carbon, 20 ± 1 % nitrogen, and 9 ± 1 % oxygen. The large concentration of carbon is typical of amorphous carbon deposited from carbon-based monomers, such as acetylene, that have been highly cross-linked through ion bombardment. The nitrogen was incorporated into the gas mixture to promote sp^2 bonding and relieve internal stresses in the deposited film [361, 362]. The presence of 9 ± 1 % of oxygen suggests that the rPPF has undergone autoxidation reactions between carbon-centred radicals and atmospheric oxygen [207, 292, 363]. The C1s high-resolution peak was curve-fitted with binding energies corresponding to C−C/C−H (284.6 ± 0.5 eV), C−O/C−N (286.5 ± 0.5 eV), C=O/N−C=O (287.5 ± 0.5 eV), and COOH (289 ± 0.5 eV) [309, 353, 364]. The peak fitting further illustrates autoxidation with the presence of single and double bonded carbon-oxygen groups (blue and magenta curves in **Figure 5.1.b**, respectively) and the minor formation of carboxylic acid functionalities (cyan peak at 289 ± 0.5 eV). The organic polar groups formed as autoxidative products are known to be beneficial for cellular attachment and proliferation [243]. Unlike for chemical-functionalised PPFs, the formation of autoxidative products does not diminish the protein immobilisation potential of the rPPFs [58, 264, 283, 357].

The water contact angle (WCA) of the rPPF surface, measured one week after deposition, was approximately 59.4˚ (**Figure 5.1.c**) and that diiodomethane contact angle was 31.4˚. The total surface energy was 56.2 $mJ.m^{-2}$ with dispersive and polar components of 43.6 and 12.6 $mJ.m^{-2}$, respectively [356]. The hydrophilic nature of the rPPF is derived from the free energy of radicals and polar oxidative products formed by exposure to atmospheric oxygen [58, 343, 357]. The WCA shows the surface has a mildly hydrophilic range (WCA < 90) [65, 66] and, therefore, allows proteins to retain a native conformation and biological activity [68]. The 59.4˚ WCA places the rPPF within the optimal wettability range for bone lineage cell attachment [374].

The unpaired electrons representing radicals contained in the rPPF were detected using EPR (**Figure 5.1.d)**. The spectrum contains a symmetrical peak centred at a g-value of 2.003 indicating the presence of surface-embedded radicals. The broadness of the peak indicates a variety of carbon-centred radicals and/or signal anisotropy due to the radicals appearing at the rPPF surface [58, 279, 343]. The rPPFs have been shown to possess radical densities 1-2 orders of magnitude greater than conventional PPFs deposited in the absence of enhanced ion-bombardment [58, 353, 398].

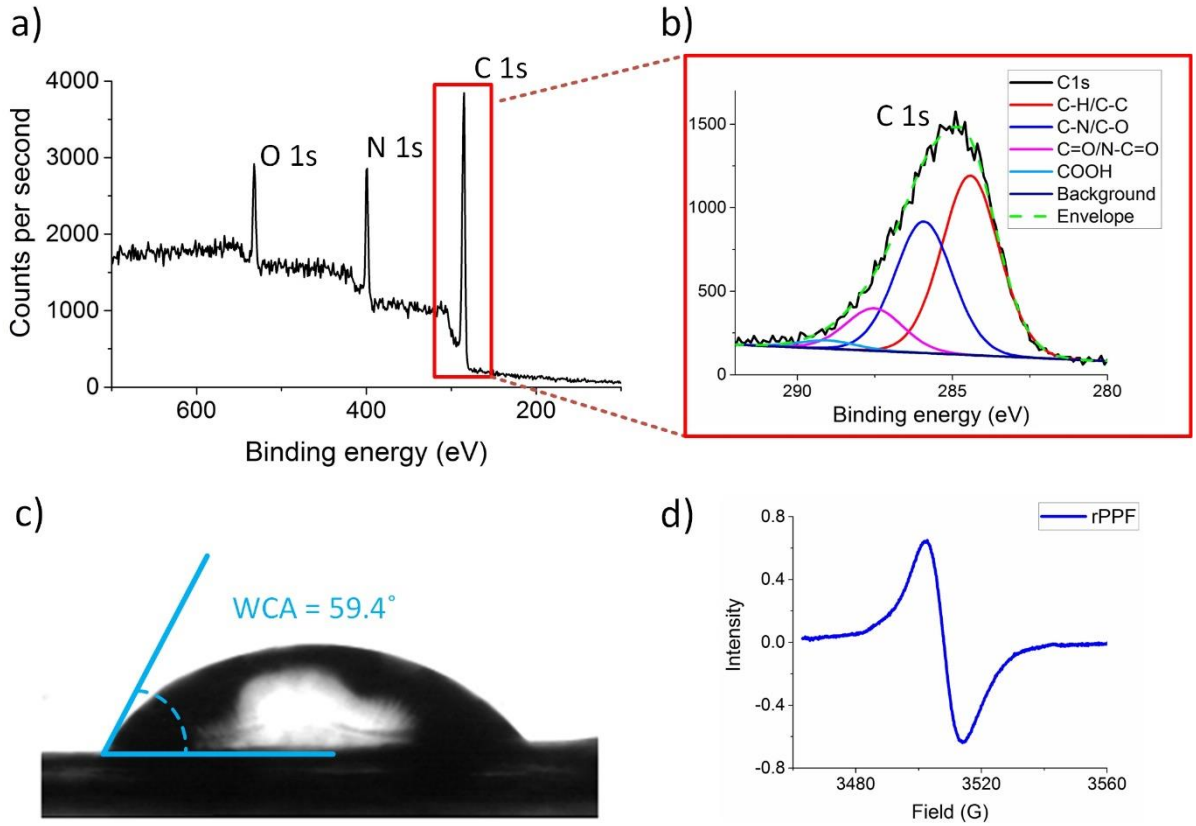

Figure 5.1. Characterisation of the rPPF surface. (**a**) The elemental composition was 71 ± 4 % carbon, 20 ± 1 % nitrogen, and 9 ± 1 % oxygen as calculated from the XPS survey spectrum. **(b)** The high resolution C1s spectrum was curve-fitted with components at binding energies (284.6 ± 0.5 eV (C−C/C−H), 286.5 ± 0.5 eV (C−O/C−N), 287.5 ± 0.5 eV (C=O/N−C=O), and 289 ± 0.5 eV (COOH). (**c**) A representative image of the water drop placed on the rPPF-coated Ti showing a water contact angle (WCA) of 59.4°. **d)** A representative EPR spectrum of the rPPF deposited on polystyrene. Signal broadening originates from a variety of carbon-centred radicals and/or anisotropic signal due to the presences of surface radicals.

5.3.2 Optimisation and characterisation of fibronectin- functionalised rPPF surfaces

The absorbance signal from the FN-ELISA calibration assay increased proportionally to the concentration of the primary and secondary antibodies (**Figure 5.2.a**). The maximum protein-specific signal was observed at the concentration of primary 1:2000/ secondary 1:10,000, followed by primary 1:5000/ secondary 1: 10,000, and primary 1:5000/ secondary 1:20,000. An examination of the signal to noise ratios (S:N) showed that the signal sensitivity was maximised using the primary 1:5000/ secondary 1:20,000 conditions (S:N = 3.3)(**Figure 5.2.b**). These dilutions were selected as they

provided a strong protein-specific signal and the highest signal sensitivity, according to the signal-to-noise ratio. The titration curve showed a monolayer formation at approximately 15 µg/mL solution concentration (3.4 x 10^{-8} M), as indicated by the signal plateau in **Figure 5.2.c**.

SDS washing of surface with immobilised FN demonstrated significant differences in the covalent binding capacities. The rPPF surfaces produced a significant increase in initial absorbance compared to the bare titanium, most likely due to changes in adsorption-desorption equilibrium dynamics. The rPPF surfaces demonstrated a protein retention ratio of 79 ± 7% after SDS washing. The post-SDS washed rPPF surfaces demonstrated an absorbance equivalent to the pre-SDS washing Ti surfaces. A significant reduction of surface protein concentration was observed on the bare Ti with only 15 ± 6% of the adsorbed protein retention after SDS washing.

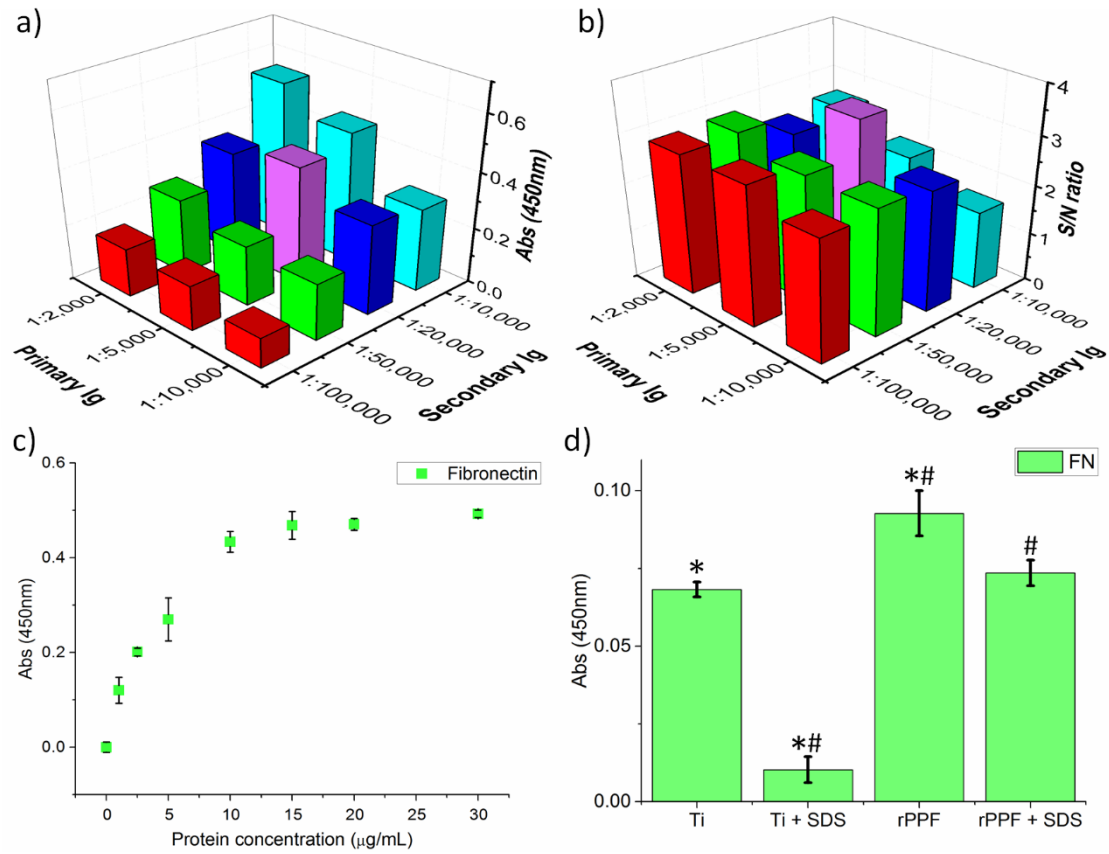

Figure 5.2. Fibronectin ELISA surface quantification. **a)** The calibration of the FN-ELISA conditions showed a general signal increase proportional to the concentration of the primary and secondary antibodies. **b)** The signal to noise ratio was calculated for each condition and the optimum is highlighted in purple (S/N = 3.3). **c)** The titration curve of FN suggests that a monolayer of protein is immobilised at a solution concentration of

approximately 15 µg/mL. **d)** SDS washing of FN immobilised on Ti and rPPF show that 79 ± 7% of the adsorbed protein on rPPFs is retained after SDS washing while only 15 ± 6% on Ti. Significant differences ($p < 0.01$) compared to non-SDS washed Ti (*) and non-SDS rPPF (#) are indicated.

Many FN-functionalisation concentrations have been reported in the literature for a variety of materials and processes. A FN solution concentration of 5 - 10 µg/mL was reported for cyanate-modified PEEK [87], 20 µg/mL for ion implanted polymers, 50 µg/mL for the ligation of FN to chemical brushes via EDC/NHS chemistry [215], while 100 µg/mL was reported for the tresylation process [108, 109] and silanisation [417]. Concentrations ranging from 500 – 1000 µg/mL have also been reported for more complex protein immobilisation processes [185, 214]. The monolayer concentration of 15 µg/mL required for the functionalisation of rPPF surfaces is placed at the lower end of these reported concentrations. The post-SDS FN retention also aligns with the previously reported approximately 80% FN retention on cyanate-modified PEEK [87]. Overall, the FN-functionalised rPPFs demonstrate significant improvements in protein immobilisation and retention quantities compared to Ti without the need for extensive chemical modification.

5.3.3 Optimisation and characterisation of osteocalcin- functionalised rPPF surfaces

Characterisation of the osteocalcin (OCN)-functionalised surfaces via ELISA experienced complications due to primary antibody selection. The OCN protein is predominately detected in solution via an orientation-independent sandwich ELISA [418, 419] and no information regarding attachment to non-bone tissue surfaces was available. Three antibodies aligning with the amino acid (AA) sequences for the N-terminal (AA 1-21), mid-sequence (AA 22-35), and C-terminal (AA 36-49) were sourced.

The N-terminal ELISA calibration assay showed elevated baseline absorbance signals of 0.8-0.9. A protein-specific signal of 0.12 was found at primary 1:1000/ secondary 1:10,000 concentrations. However, no other combination produced any signal above the baseline. Further testing with blocker proteins showed that the absorbances on OCN-functionalised rPPF surfaces were lower than the baseline. The consistently elevated baseline signal indicated that the N-terminal primary Ig could be interacting non-specifically with the BSA blocking protein. As such, the N-terminal antibody was replaced with the mid-sequence and C-terminal primary Igs.

The mid-sequence OCN-ELISA calibration array was performed. A maximum protein-specific absorbance signal of 0.15 was found at the primary 1:2000/ secondary 1:10,000 dilution, as shown in **Figure 5.3.a.** The maximum signal was the most sensitive with a signal to noise ratio (S:N) of 2.7 (**Figure 5.3.b**)**.** The titration curve demonstrated a protein-specific signal maximum at 20 µg/mL, but the 30 µg/mL signal decreased to be level with the 15 µg/mL concentration. This signal decrease, in combination with the uncertainty, indicated that the 20 µg/mL might be artificially increased, and the 15 µg/mL (2.5×10^{-6} M) concentration was taken to be the monolayer concentration (**Figure 5.3.c**). No previous surface immobilisation work could be found to compare with the experimental values. The ELISA examination of immobilised protein concentration after SDS washing showed that the rPPFs immobilised and retained a significantly greater quantity of protein compared to the bare Ti (**Figure 5.3.d**). The rPPF surfaces retained 62 ± 8% of the physically adsorbed OCN. By comparison, the OCN was almost completely removed on the bare Ti surfaces.

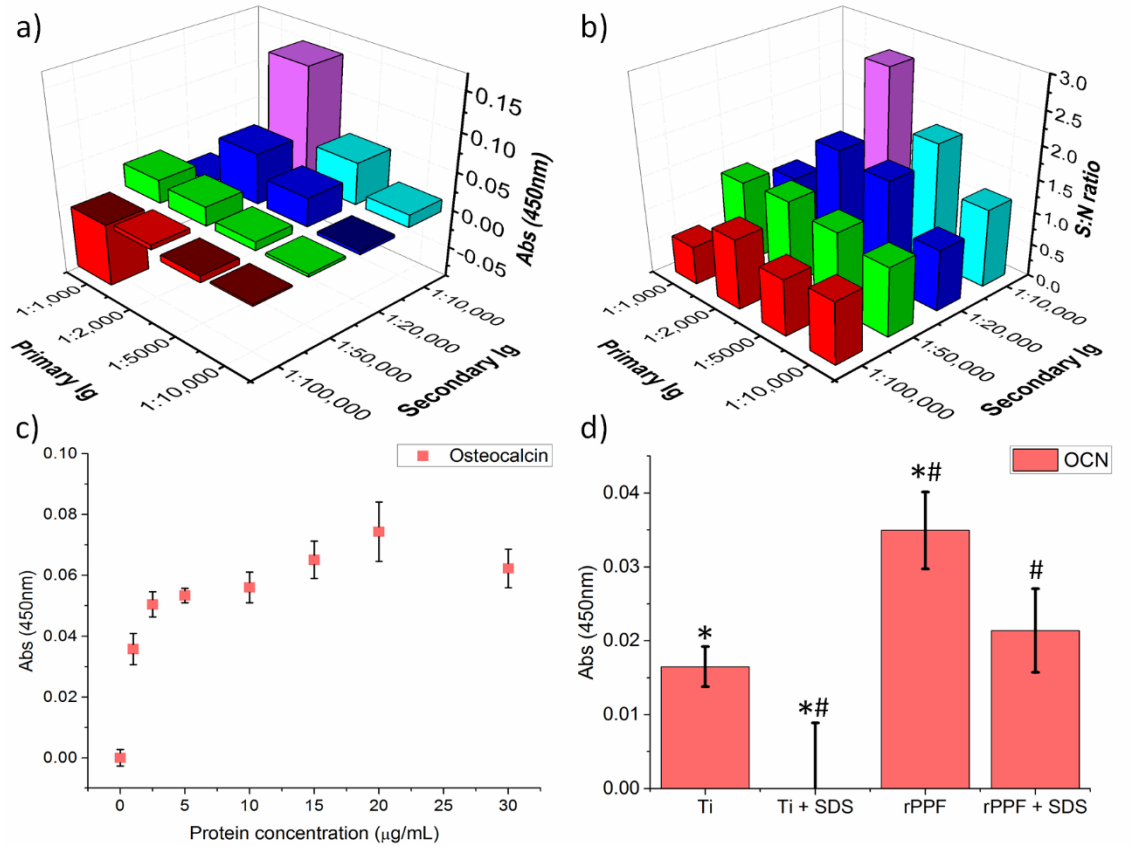

Figure 5.3. OCN mid-sequence ELISA quantification. **(a)** The calibration of the mid sequence OCN-ELISA antibody dilution conditions showed a general signal increase proportional to the secondary Ig concentration. The optimal signal is highlighted in purple. **(b)** The signal to noise ratio was calculated for each condition and the optimum is highlighted in purple (S:N = 2.7). **(c)** The titration curve of OCN produced a monolayer at a protein solution concentration of approximately 15 µg/mL. **(d)** SDS treatment of monolayer OCN surfaces showed SDS resistant fractions of 62 ± 8% on rPPF surfaces and near complete removal on Ti. Statistical significance ($p < 0.05$) is shown for absorbances compared to non-SDS washed Ti (*) and rPPF (#).

The C-terminal ELISA system was calibrated, demonstrating a maximum signal at the primary 1:1000 /secondary 1:10,000 dilution conditions, with an absorbance signal of 0.76 and a signal to noise ratio of S:N ≈7.3. The optimised ELISA dilution conditions were used to obtain an OCN titration curve. The protein titration curve produced signal strengths that were independent of the protein solution concentration over the range of 1 - 30 µg/mL. The absorbance plateau of Abs = 0.09 - 0.1 was thought to be due to over-saturation of the secondary-HRP antibody and a rapid reaction of the TMB substrate solution. The two surrounding conditions of primary 1:1000/ secondary 1:20,000, and primary 1:2000/

secondary 1:10,000 were used to examine rPPF surfaces with 0 µg/mL, 1 µg/mL, and 15 µg/mL immobilised OCN to determine if a difference in protein signal could be produced. However, no difference was found between the protein conditions with either ELISA condition. The signal saturation across all protein concentrations for the three sets of antibody concentrations suggests that the OCN surface is fully saturated by the c-terminal ELISA antibodies. The primary Igs for the ELISAs are generally ≈ 10-12 kDa while the secondary Igs conjugated with HRP are ≈ 37-42 kDa (as stated on the product information). The difference in the produced absorbance signal between individual ELISA systems can be attributed to the catalysed TMB reduction kinetics, given the protein functionalised surfaces and the Ig molecular weights are consistent.

The inability to accurately detect the N-terminal of OCN above the large background was unexpected. OCN attaches to the positively charged Ca^{+} minerals in bone through the negatively charged Gla side chains in the 1-22 AA sequence at physiological pH [420]. The net negative charge at the 20%N rPPF surface at physiological pH [356] should orient the 1-22 AA sequence away from the surface. However, given the protein detection by the C-terminal and mid-sequence antibodies, the assays suggest that the pyramidal conformation of OCN was oriented predominately with the N-terminal contacting the rPPF surface and C-terminal exposed the aqueous environment.

5.3.4 Optimisation and characterisation of fusion protein - functionalised rPPF surfaces

The FN-OCN fusion protein was initially examined with a 6x histidine (6His) primary Ig to detect the 6His tag inserted at the N-terminal. No significant trend was observed in the ELISA calibration performed on the 96 well plates (**Figure 5.4.a**). The maximum signal was produced at the primary 1:5,000/ secondary 1:20,000 dilution conditions and possessed a S:N ≈ 2 (**Figure 5.4.b**). The titration curve was performed using the optimised 6His ELISA conditions, but no significant signal beyond the

baseline fluctuations could be observed, with the largest signal of Abs = 0.005 ± 0.004 being detected on the 10 µg/mL concentration (**Figure 5.4.c**). Further repetitions confirmed the lack of protein-specific signal. The inability to detect protein signal could come from the orientation of the protein on the tissue culture plastic wells compared to the rPPF surfaces. The 6xhistidine sequence is positively charged at physiological pH due to the imidazole side chains on the individual amino acids and could influence the fusion protein orientation when in close proximity to the negatively charged rPPF surface. However, there are also other factors that influence surface protein orientation as discussed in Chapter 1.2. Overall, the 6xhis primary antibody ELISA did not produce sufficient absorbance signals for quantification.

The fusion protein-coated surfaces were examined with the optimised FN and mid-sequence OCN ELISAs to determine which of the component protein ELISAs produced the optimal protein-specific signal. The OCN and FN ELISAs demonstrated protein-specific signals of 0.091 ± 0.003 and 0.058 ± 0.002, and S:N ratios 0f 2.02 ± 0.11 and 1.34 ± 0.04, respectively (**Figure 5.4.d**). The mid-sequence OCN ELISA was selected for the titration curve (**Figure 5.4.e**) and the SDS washing experiments (**Figure 5.4.f**). The titration curve showed that the protein concentration signal plateaued between 10 - 15 µg/mL and plateaued within variation for the greater protein solution concentrations. The optimal protein concentration for the FN-OCN proteins was previously reported as 20 µg/mL, so 15 µg/mL (3.8×10^{-7} M) concentration was selected as a suitable solution concentration to form an adsorbed monolayer. The results after SDS washing showed 5 ± 7% protein retention on the Ti, and 73 ± 13% on the rPPF surfaces.

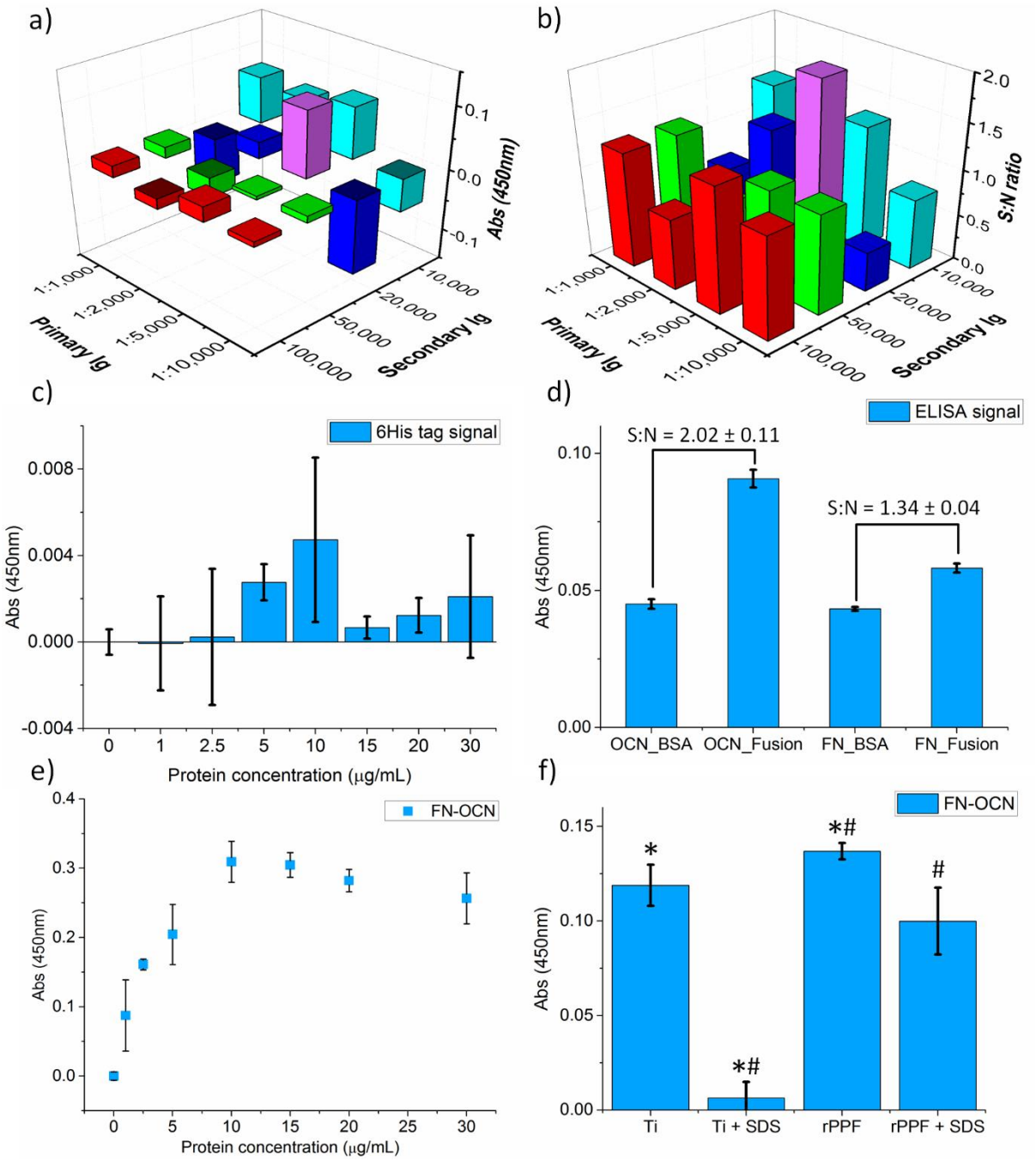

Figure 5.4. ELISA optimisation and quantification of FN-OCN fusion protein-coated surfaces. The calibration of the 6His-ELISA conditions showed an inconsistent relationship between the primary and secondary antibodies **(a)**. The signal to noise ratio **(b)** produced a S:N ≈ 2 for the optimised condition highlighted. **(c)** The 6xhistidine titration curve produced no significant signal after background subtraction. **d)** The fusion protein surface showed considerable signal on both the optimised FN- and OCN- ELISAs. The OCN-mid sequence ELISA was selected due to the greater S:N. **e)** The fusion titration via OCN-ELISA demonstrated a signal saturation at 10 – 15 µg/mL. **f)** SDS washing of monolayers on Ti and rPPF showed fractions of 5 ± 7% and 73 ± 13% were retained, respectively. Statistical significance ($p < 0.05$) is shown for absorbance signals compared to non-SDS washed Ti (*) and rPPF (#).

5.3.5 Synthesis, optimisation, and characterisation of co-immobilised fibronectin: osteocalcin rPPF surfaces

Surfaces comprising of co-immobilised FN and OCN were developed for comparison with the FN-OCN fusion protein. The potential for cross-reaction between the ELISAs and their non-target proteins needed to be investigated before the quantification of the co-immobilised FN:OCN ratios could proceed. FN and OCN surfaces were exposed to the opposite ELISA system to gauge for non-specific signal that might influence the co-immobilisation results. The assays showed marginal increases in signal compared to the corresponding BSA controls**.** The FN surface examined with the OCN-ELISA produced an absorbance of 0.212 ± 0.025, a significant increase ($p < 0.05$) over the BSA control value of 0.172 ± 0.012. The OCN surface examined with FN-ELISA demonstrated a slight increase (0.085 ± 0.006) over the BSA control signal 0.068 ± 0.008 ($p > 0.05$). The relative increases in signal on the OCN or FN compared to their controls could be due to the difference in non-specific binding affinities of the primary Igs. A comparison of primary antibody targeted genetic sequences to the full FN and OCN proteins using the web-based Pairwise sequence alignment "Needle" software (EMBOSS) showed no correlation between the OCN and FN-primary Ig. However, a strong partial match was found between the FN protein and the OCN-primary Ig, which could account for the significant increase on the FN-functionalised surface. Overall, the cross-reactivity ELISAs revealed that the slightly elevated signals on the OCN surfaces compared to their respective controls is due to non-specific binding, while the cross-reactivity of the FN surface can be taken into account for the co-immobilisation results.

A sequential 2-step exposure was used to co-immobilised FN and OCN in various ratios. The first incubation was carried out with OCN and the FN was then adsorbed onto the OCN fractionally coated surface. The solution concentrations used were determined according to the desired monolayer fraction as per their individual titration curves. A series of ratios were examined pre- and post- SDS

washing with the FN and OCN ELISAs, as shown in **Figure 5.5.a**. The 100% protein surfaces show similar post-SDS proportional retentions as in **Figures 5.2.d** and **5.3.d**, indicative of covalent immobilisation. The same conditions resulted in near complete removal of the corresponding protein layers on Ti surfaces (**Figure 5.5.b**). When co-immobilised, the signals of OCN and FN decrease compared to their 100% controls, most noticeably for OCN prior to SDS washing. The transition from a 100% to 90% OCN surface with FN produced a signal reduction resembling SDS washing due to competitive adsorption-desorption of OCN. The OCN immobilisation follows the expected trends, while the FN shows minimal variation across the given ratios. The co-immobilisation sequential 2-step approach accounts for the reduction in ELISA signal from competitive adsorption-desorption and the titration trend for the OCN, but not the FN behaviour.

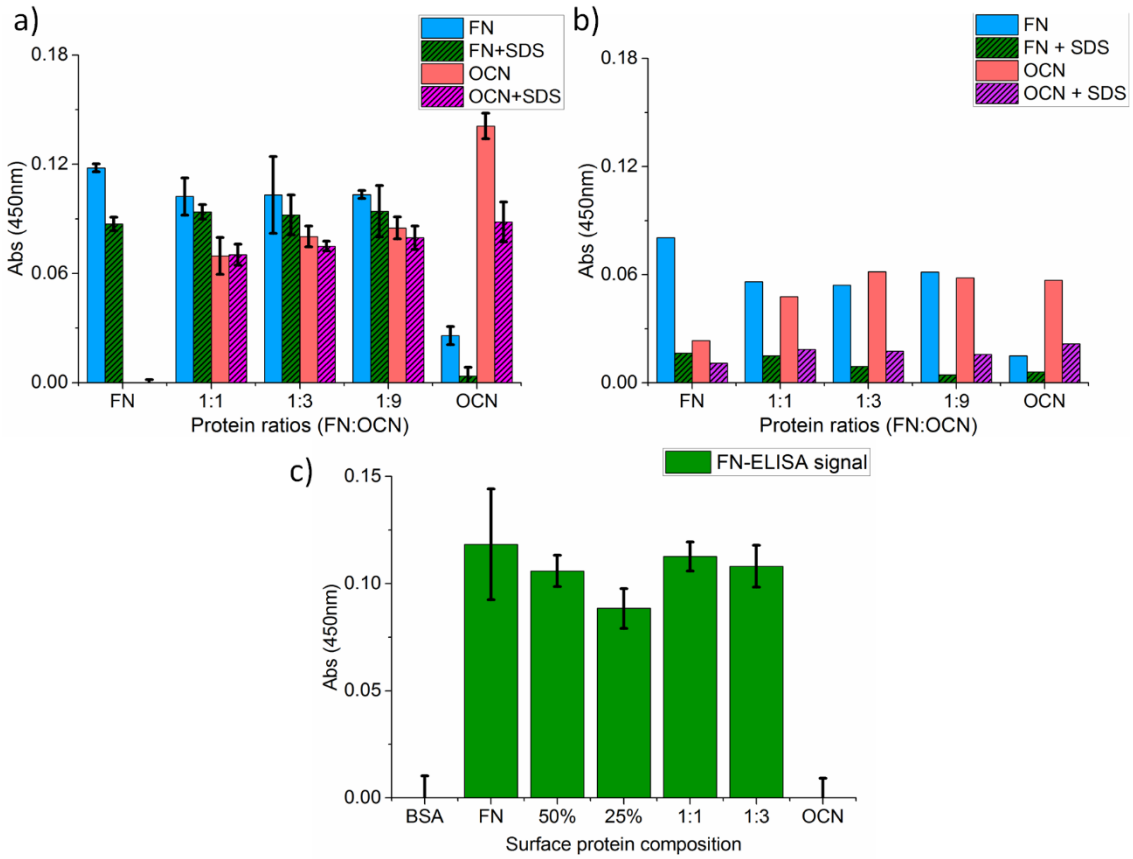

Figure 5.5. ELISA quantification of the co-immobilised rPPF surfaces. **a)** The rPPF surfaces, both pre- and post-SDS washing, show a non-linear correlation between the OCN and FN concentrations and signal strength. The FN signal maintained a near-monolayer signal, while a titration trend was observed in the OCN. **b)** Ti surface showed the drastic removal of the adsorbed proteins under the same SDS washing conditions. **c)** SDS washed

co-immobilised surfaces were compared to their FN concentration equivalent, demonstrating a non-titration like signal generation.

The unusual FN-ELISA signal was initially thought to result from adsorbed FN occupying the surface. However, the behaviour remained unchanged post-SDS treatment. As such, the observed plateau in the FN-ELISA may originate from FN reorientation. For comparison, the immobilisation ratios and their monolayer concentration counterparts were investigated side-by-side. The 100%FN, 50%FN, and 25%FN monolayers appears to produce a signal reduction resembling the titration curve (**Figure 5.2.c**), however, the difference in values is not significant. The 1:1 and 1:3 FN:OCN ratios produced equivalent signal (**Figure 5.5.c**) and showed no significant changes from the 100% monolayer signal. The preliminary test suggests that in the co-immobilisation process, changes the FN protein conformation or orientation due to altered surface conditions by the presence of the incomplete OCN layers. Overall, the 1:3 ratio of FN:OCN was selected for cellular examination as it provided optimal signals from both ELISAs, while expressing a substantial difference in surface protein composition.

5.4 Discussion

In this study, protein-specific ELISAs were used to optimise the protein immobilisation conditions for fibronectin (FN), osteocalcin (OCN), and the custom fusion protein that combined functional domains from both of these proteins. The quantities of adsorbed and immobilised proteins on the 20%N rPPF surfaces was increased over the bare Ti in all cases. The information derived from the titration curves and the relative size difference of FN and OCN was used to develop a multi-protein interface.

The quantity of proteins on the Ti and rPPF surfaces, via single or sequential exposures, is determined by a competitive adsorption-desorption equilibrium [71, 113, 421]. Proteins will adsorb

to the exposed surface based on hydrophobic and electrostatic interactions and become displaced by incoming proteins through transitional complexes with the rearrangement driven by relative solution partial concentrations and surface affinity [111-113]. The effective monolayer for any given surface occurs when the adsorption-desorption dynamic has reached equilibrium. The protein adsorption-desorption equilibrium on rPPFs is influenced by the probability of covalent bond formation between a surface migrating radical and the adsorbed proteins, thus preventing desorption. The competitive exchange of proteins will continue but with a reducing effective surface area, as depicted in **Figure 5.6**. This mechanism accounts for the observed increase in protein specific signal from the rPPFs compared to the Ti, and the significantly different protein retention values [280].

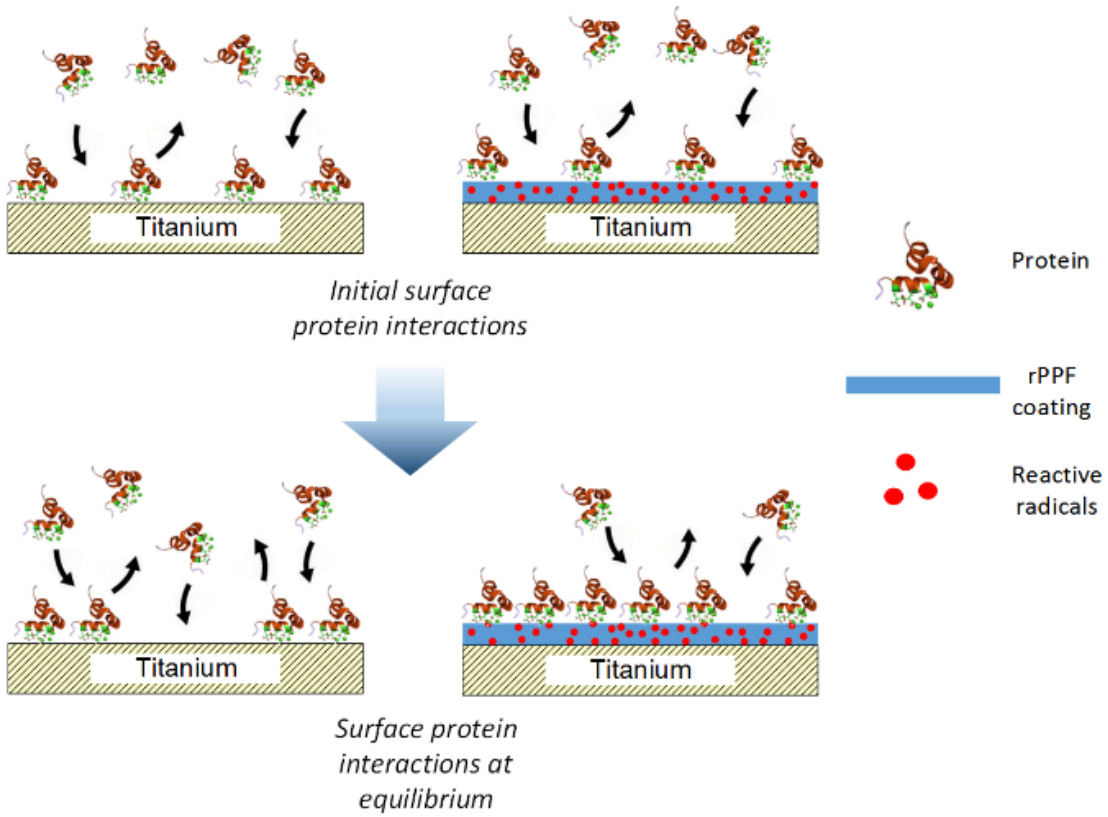

Figure 5.6. A visual representation of protein equilibrium on Ti and rPPF surfaces. The proteins initially adsorb onto the Ti and rPPF surfaces. The adsorbed surface proteins will undergo competitive adsorption-desorption dynamics as the system reaches equilibrium and the on-rates equal off-rates for each type of protein. The adsorbed proteins on the rPPF surfaces form covalent bonds with the surface migrating radicals preventing desorption and leading to greater surface protein retention.

The differences in mobilities and binding affinities between proteins makes it difficult to translate the single protein titration results into a mixed solution yielding the desired surface coverage ratios post immobilisation [113]. Thus, the co-immobilisation of fibronectin and osteocalcin was performed by sequential protein solution exposures to allow for greater control of the competitive adsorption–desorption dynamics and surface composition. In principle, the covalently bound proportions of OCN would reduce the effective area, limiting the available sites for FN immobilisation at the surface. The rPPF surfaces must have sufficient protein exposure time to ensure the optimal covalent attachment. The osteocalcin, immobilised in various ratios, reproduced a concentration behaviour consistent with the titration curve, as expected for the first incubated protein solution. During the subsequent incubation, the FN bonded to the available surface and displaced the non-covalently bonded OCN [111-113]. This explains why the ELISA signal was equivalent to that obtained post-SDS washing in the initial OCN retention experiments (**Figure 5.5.a**). The observed fibronectin signal plateau across all protein concentration ratios, both pre- and post SDS washing, contradicts the expected titration curve behaviour (**Figure 5.2.c, 5.5.a**). The uniform signal strength suggests a change in FN adsorption dynamics that could invoke a protein reorientation or refolding in response to the partially OCN-functionalized rPPF surfaces. A reorientation of the bi-polypeptide FN structure (2x 220kDa polypeptide units [422]) could potentially double the availability of the primary antibody targeted genetic sequence presented in solution. The ELISA signal would then increase by a fraction equivalent to the proportion of reoriented FN present. Such unexpected increases in target sequence presentation reduce the reliability of ELISA detection for the quantification of immobilised protein ratios.

The examination of protein ratios is a time and resource-intensive process. The quantification of multi-protein surfaces via ELISA requires the examination of each protein ratio with all the required ELISA systems to determine the concentrations of the individual proteins. Thus, the samples required

increase exponentially as more different proteins are included onto the surface. In addition to the signal discrepancies from protein reorientation or refolding, the ELISA technique can also introduce effective area discrepancies related to the size differences between the proteins and the antibodies (Igs). The ELISA signal produced is considered representative of the protein quantity if the target protein is larger than the primary (≈ 10 – 12 kDa) and secondary (≈ 37 – 42 kDa) antibodies, e.g., fibronectin. However, smaller proteins and peptides can experience an ELISA detection limit based on steric hindrance due to the large footprint of the antibodies, which understates the surface protein quantity. In contrast, the multi-functionalisation of an implant surface with fusion proteins reduces the number of samples required for the characterisation of an immobilisation protocol and increases the ELISA accuracy. For example, the combination of the FN9,10 and OCN 22-49 sequences in a single protein allows for protein quantification via a single ELISA using an antibody targeting either of the sequences. The fusion protein in this study is reported to be approximately 40 kDa [287, 316] which reduces the potential for misrepresentation via ELISA antibody steric hindrance. Overall, the utilisation of the fusion protein allows for simpler and more accurate ELISA quantification and greatly simplify surface immobilisation protocols.

ELISAs are one of the most widely used methods of protein quantification being used to detect a vast number of proteins both surface bound and in free solution [331]. However, other physical techniques can be used for determining the concentrations of immobilised proteins through the detection of distinctive heavier elements, such as Br, F, or Cl. Alternatively, the inclusion of fluorescent or radionucleotide markers allow for the direct examination of protein quantity and adsorption-deposition kinetics. Typically, these approaches require the chemical modification of the proteins before surface immobilisation. These modifications may alter the protein conformations and, therefore, the adsorption-desorption behaviours. The ELISA methodology provides a reproducible and reliable approach for protein quantification of both single and co-immobilised protein surfaces.

5.5 Conclusions

The optimisation of fibronectin, osteocalcin, and FN-OCN fusion protein-functionalised rPPF surfaces was performed with protein-specific, enzyme-linked immunosorbent assays (ELISAs). Protein concentrations required to form a saturated monolayer during the 4˚C overnight incubation was determined to be approximately 15 µg/mL. Covalent binding ratios after this length of incubation were between 60-80% depending on the protein. A 2-step sequential exposure approach was used for the co-immobilisation of OCN and FN to rPPF surfaces to better control the competitive adsorption-desorption dynamics compared to multiple protein solutions. The subsequently incubated FN demonstrated different binding behaviours from the expected single protein behaviour established on rPPF surfaces due to the FN interactions with the partially OCN-functionalised surface. Overall, it was demonstrated that i) rPPF coated surfaces present a simple and reproducible platform for producing single and multifunctional biointerfaces and ii) the optimisation of multi-protein biointerfaces is substantially more complex relative that required for multifunctional fusion protein biointerfaces.

Chapter 6: *In vitro* investigation of protein-functionalised rPPF surfaces to determine osteogenic potential

This chapter reports the osteogenic potency of the protein-functionalised surfaces, as characterised in chapter 5, with primary osteoblasts (OBs) and mesenchymal stem cells (MSC). The OB attachment, proliferation, and mineralisation were investigated. The fibronectin-osteocalcin fusion protein functionalised surfaces demonstrating high levels of cellular attachment and increased mineralisation compared to those functionalised with the component proteins. The MSC differentiation was shown to be on par with the osteocalcin functionalised signalling surfaces.

The results from this chapter are reported in "Multifunctional protein-immobilized plasma polymer coatings for orthopedic applications." by Callum A.C. Stewart, Behnam Akhavan, Juichien Hung, Shisan Bao, Jun-Hyeog Jang, Steven G Wise, and Marcela M.M. Bilek (Accepted; ACS Biomaterials Science and Engineering).

6.1 Introduction

Protein and peptide surface functionalisation provides a versatile approach to improve the osseointegration of orthopaedics. The goal of protein functionalisation is to increase the beneficial interactions between the implant surface and the biological environment, thereby, leading to more optimised osseointegration, as outlined in chapter 1. An increased degree of cellular recruitment and bone formation on implant surfaces can reduce the potential for adverse non-integration conditions, such as biofilm formation [6, 7, 423] and fibrotic encapsulation [3-5], which require revision surgery to correct [2, 3]. Biomolecule-functionalisation may also mitigate the long-term effects of bone resorption caused by the lack of mechanotransductive forces (Wolff's Law) [29-32]. Thus, modifying orthopaedic devices to promote osseointegration with the body has the potential to increase patient quality of life and implant longevity.

The plethora of proteins and peptides investigated to improve osseointegration can be broadly classified into three main categories: i) anti-microbial, ii) adhesive extracellular matrix (ECM), and iii) bone signalling proteins. Anti-microbial functionalised surfaces focus on the prevention of bacterial and fungal infections at the implant site [249, 424]. The biomolecules investigated include bacitracin [156, 425], caspofungin [349, 357, 426, 427], and the linker molecule chitosan [136, 145-147, 428-430], along with hundreds of antimicrobial peptide sequences [431, 432]. The approaches to anti-microbial surfaces have been reviewed elsewhere [433, 434]. ECM proteins are involved in the recruitment and establishment of osteoblasts and stem cells at the surface of the implant. Fibronectin and collagen, for example, contain the canonical RGD cell binding motif that interacts with a range of cell-surface integrins, including α5β1, α2β1, and αvβ3, to adhere the cells to the protein-functionalised surface [411]. Bone formation at the ECM-functionalised surface occurs through natural mineralisation processes and is typically increased due to the greater cell coverage rather than enhanced mineralisation activity [435, 436]. The signalling proteins, for example BMP-2 [409], and other signalling molecules, such as Simvastatin [95, 437, 438], increase the rate of bone formation by accelerating the differentiation and mineralisation of the adherent cells through the upregulation of osteogenic metabolic products, e.g. osteocalcin (OCN/BGlaP), osteopontin (OPN), and alkaline phosphatase (ALP) [287, 439, 440]. Osteogenic proteins that promote cell attachment and bone formation resemble the natural physiological environment more closely and stimulate native tissue to win the 'race for the surface' [441, 442], outcompeting bacteria. Osteogenic protein-functionalisation, therefore, addresses both biofilm and foreign body reactions as well as providing functional integration of the implant.

The single protein approach to biomolecule functionalisation has shown some success, but a deeper understanding of the osseointegration process reveals that a multifunctional protein-coated surface is required. The synergistic combination of biological functionalities would allow for increased cellular attachment in conjunction with more rapid bone formation, leading to greater osseointegration. In this chapter, the osteogenic potency of the multifunctional protein surfaces

developed in chapter 5 were comparatively investigated against the single component proteins: FN and OCN. The osteoblast (OB) cell affinity for the surfaces were examined through short-term attachment and spreading, the longer-term biocompatibility through proliferation, and the osteogenic potential through the OB calcium deposition. The protein-functionalised surfaces were examined for their differentiation potential with mesenchymal stem cells (MSCs).

6.2 Methods

6.2.1 Substrate preparation

Ti and the biologically favourable 20%N rPPF coated foils were prepared as previously described in Chapter 2. In short, the Ti foils were cut to size and cleaned with nitric acid before the deposition of the 20%N rPPF. The surfaces were left for 5-7 days before use to ensure the surface chemical and physical properties had stabilised (see Chapter 4). An examination of their surface chemical composition, wettability, and radical density is outlined in Chapter 5.

6.2.2 Primary cell harvesting and culturing

Primary osteoblasts (OBs) and mesenchymal stem cells (MSCs) were utilised in this study. The experiments were conducted in accordance with the Australian Code of Practice for the Care and Use of Animals for Scientific Purposes. All personnel involved in the animal procedures have completed an approved animal care and ethics course. Primary OBs were harvested from mouse long bones and the cultured as described in Chapter 2 [333, 334]. Briefly, mouse long bones were collected, cleaned, and cut into 1-2mm^2 pieces before being placed in non-differentiating cell media to allow for OB outgrowth. The cells were expanded into working cultures and monitored for cell health.

MSC harvesting and culturing were performed as described in the standard protocol [341] and Chapter 2.2.7. Long bones were collected from 7-week-old mice and washed with 70% EtOH. The ends

of the bone were removed as for the primary osteoblast extraction. The bone marrow was flushed out with DMEM solution and collected. The marrow solution was resuspended and filtered through a 70 µm cell sieve before being transferred to a well plate for culturing. The cells were cultured in complete DMEM without ascorbic acid as not to stimulate osteoblast differentiation and the media changed every 3 days. The cells were expanded to working stocks and closely monitored for differentiation or ingrowth of other cell types.

In vitro cell assays play a necessary screening role in the overall biomedical evaluation process [443]. Primary cells were chosen to investigate the biological efficacy of the protein-functionalised surfaces over their cell line equivalents, like the MC3T3 transformed rat pre-osteoblast cell line [108, 134, 139, 444-449], as they are more sensitive to chemical cues. Overall, primary cells should be more representative of the *in vivo* environment [332].

6.2.3 Cell attachment and spreading

The cell attachment and spreading assay was performed on the protein functionalised surfaces as described in Chapter 2. Briefly, the 20%N rPPF-coated Ti foils were cut to 0.8 cm x 1 cm to fit the 8-well chamber slides and protein-functionalised as described in Chapter 2 and 5. The OBs were seeded at 10,000 cells per well. The OB seeding media was removed after 1 hr and the surfaces fixed with 70%EtOH. After washing the samples in a 0.1% Triton solution, the cell cytoskeleton and nucleus were stained with ActinRED555™ and DAPI, respectively, and mounted between two glass slides. The cell number and spreading on the different surfaces were examined under 5x (≈ 4 mm^2) and 10x (≈ 1 mm^2) magnification (n > 9) on a fluorescence microscope at the corresponding wavelengths. The images were analysed with ImageJ.

6.2.4 Proliferation assay

The samples for the 3-(4,5-dimethylthiazol-2-yl)-5-(3-carboxymethoxyphenyl)-2-(4-sulfophenyl)-2H-tetrazolium (MTS) proliferation assay were prepared according to the protocol in Chapter 2 and 4. The OBs were seeded at 4,000 cells per well and allowed to grow for 14 days. The proliferation was measured at day 3, day 6, day 11, and day 14 post seeding, with the media being replaced every 3 days. At the stated examination time points, the media was removed, and the samples were incubated in 40 mM MTS in DMEM solution for 2 hr under dark conditions. 150 µL aliquots were taken after the incubation time and the absorbance measured at 490 nm.

6.2.5 Alizarin red mineralisation assays

The mineralisation capacity of the different protein conditions was examined with the AlizarinRed stain (ARS) as described in Chapter 2. The Ti, rPPF, and protein-functionalised surfaces were prepared as previously described in Chapters 2 and 5, and primary osteoblasts were seeded at 10,000 cells per well. The cells were maintained for 1 month washed in PBS, and stained with ARS for 2 hr. The excess was removed, and the samples washed gently before being transferred into individual Eppendorf tubes. 400 µL of 10% (v/v) acetic acid was added before vortexing and heating to 85˚C for 10 min. The samples were then centrifuged at 16000 g for 15 min, and 50 µL of ammonia hydroxide added to each sample. 200 µL aliquots were transferred to a 96 well plate, and the absorbance read at 405 nm.

6.2.6 Mesenchymal stem cell differentiation

ALP production in MSCs was measured via fluorescent microscopy as outlined in Chapter 2. MSCs were seeded at 8000 cells/well on the protein-functionalised rPPF surfaces in an 8-well chamber slide. The media was changed every 3 days to ensure sufficient nutrients. After 10 and 20 days, the cells

were fixed to the foils with EtOH and washed in 0.1% Triton solution. The surfaces were stained with Vector Red Alkaline Phosphatase dye (Vector) and DAPI fluorescent mounting media (Agilent). The surfaces were then examined with a Zeiss Axio Imager.Z2 fluorescence microscope at 365/560 nm for the ALP dye and 358⁄461 nm for the DAPI. The images were analysed with the 'ImageJ' software. The degree of differentiation was determined by dividing the total area of the Vector Red (μm^2) by the number of cells (blue nuclei).

6.3 Results

6.3.1 Primary osteoblast attachment and spreading

Osteoblast attachment and spreading were analysed via fluorescence microscopy. The average cell number, shown in **Figure 6.1.a**, revealed that the FN-OCN fusion protein-coated surfaces had the highest cell average of 174 ± 35 cells/field of view, followed by the FN and FN:OCN coated surfaces, 157 ± 35 and 149 ± 38, respectively. All three demonstrate cell attachments significantly greater than the 73 ± 25 cells/field of view observed for uncoated titanium surfaces. The OCN and rPPF surfaces had cell attachments of 78 ± 30 and 97 ± 25, respectively, showing no significant increase over Ti. The average cell size of the OBs (**Figure 6.1.b**) on the FN, FN:OCN, and fusion protein-coated surfaces were 2664 ± 421, 2569 ± 529, and 1999 ± 278 μm^2, respectively, showing a significant increase in spreading over cells on Ti alone (912 ± 203 μm^2). The rPPF surfaces also induced a significant increase in cell spreading (2213 ± 331 μm^2), while OCN (1214 ± 345 μm^2) produced a slight, but not significant, increase in size compared to Ti. The cell population and spreading for each surface can be observed in the corresponding representative fluorescence image panels in **Figure 6.1.c.**

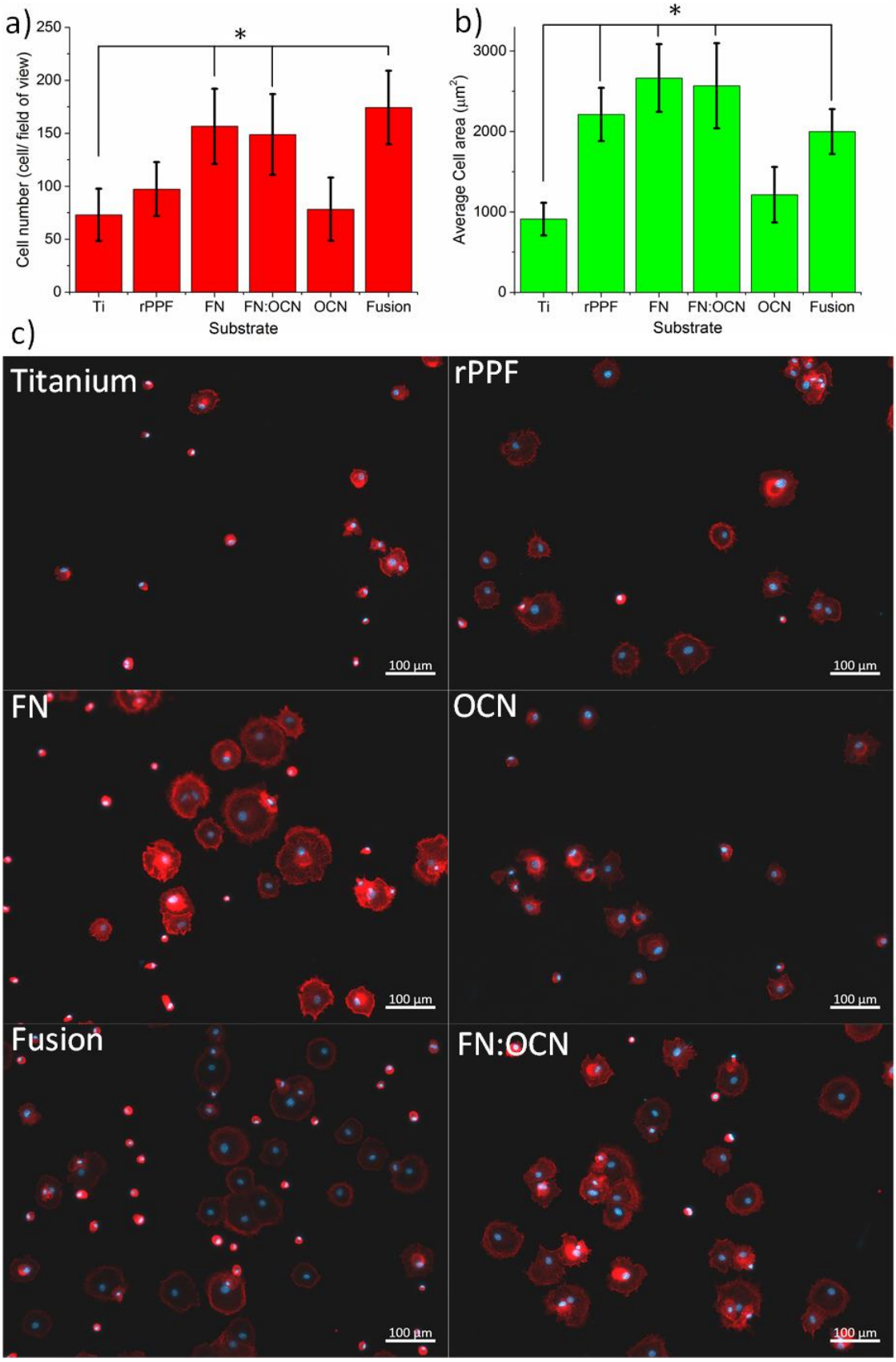
a)
Cell number (cell/ field of view)
250
200
150
100
50
0
*
Ti
rPPF
FN
FN:OCN
OCN
Fusion
Substrate
b)
Average Cell area (μm²)
3000
2000
1000
0
*
Ti
rPPF
FN
FN:OCN
OCN
Fusion
Substrate
c)
Titanium
rPPF
FN
OCN
Fusion
FN:OCN
100 μm

Figure 6.1. Average osteoblast cell quantity (**a**) and cell size (**b**) after 1-hour incubation as determined by fluorescence cell staining with DAPI/ActinRED. Uncertainties are determined from the standard deviation between samples (n = 9). (c) Representative 10x magnification fluorescence microscope images of osteoblast cell attachment on bare titanium, rPPF coatings, fibronectin-functionalised (FN), osteocalcin-functionalised (OCN), FN-OCN fusion protein-functionalised, and FN:OCN ratio-functionalised surfaces. The cell viability was determined by staining with DAPI (blue - nuclei) and cell spreading was determined by staining with ActinRED (red - cytoskeletons).

The increased cell number and spreading on the FN, FN:OCN, and fusion surfaces is attributed to the presence of the RGD binding sequence in the FN (9, 10) domains. The RGD sequence is one of the primary binding sequences in ECM proteins responsible for cellular attachment [124, 414]. Both multi-functionalised protein-coated surfaces demonstrated cell attachment and spreading on par with the FN-functionalised surface, indicating that the RGD sequence was well presented and accessible to the cells. OCN and rPPF surfaces provided equivalent cell attachment to Ti as they do not possess binding motifs. The cell spreading was significantly increased on the rPPF compared to Ti, possibly due to the presence of nitrogen- and oxygen-containing carbon groups at the interface [450]. An examination of the overall cellular affinity for the surfaces agrees with the expected trends: the RGD containing surfaces (the fusion, FN, and FN:OCN) are favoured most for cell attachment and spreading, followed by the organic surfaces (rPPF and OCN), and the inorganic Ti surfaces being least favoured; i.e.

RGD motif (FN, FN:OCN, fusion) > organic non-binding (OCN, rPPF) > inorganic (Ti)

6.3.2 Osteoblast proliferation

The proliferation of OBs on the proteins functionalised surfaces was determined with MTS. The absorbances were observed on day 3, 6, 11, and 14 as shown in **Figure 6.2**. On day 3, the Ti (0.87 ± 0.04), FN (1.00 ± 0.21), and FN:OCN (0.96 ± 0.18) surfaces demonstrated elevated absorbance compared to the rPPF (0.74 ± 0.01), OCN (0.74 ± 0.04), and fusion (0.78 ± 0.07) protein-functionalised

surfaces. The Ti, rPPF, FN, and FN:OCN surfaces showed steady growth through the day 6 and day 11 time points. Unfortunately, the day 6 and day 11 samples for OCN and fusion, shown with black strips, were compromised due to media leakage and fungal contamination, respectively. The day 14 MTS absorbances demonstrate equal proliferation on the Ti (1.20 ± 0.04) and rPPF (1.19 ± 0.05), with the FN (1.32 ± 0.09) and FN: OCN (1.33 ± 0.13) surfaces remaining slightly elevated. The OCN (1.10 ± 0.14) and fusion (1.01 ± 0.11) protein-functionalised surfaces produced less proliferation signal relative to the rPPF and Ti. The osteoblast growth rates showed insignificant variations across all samples.

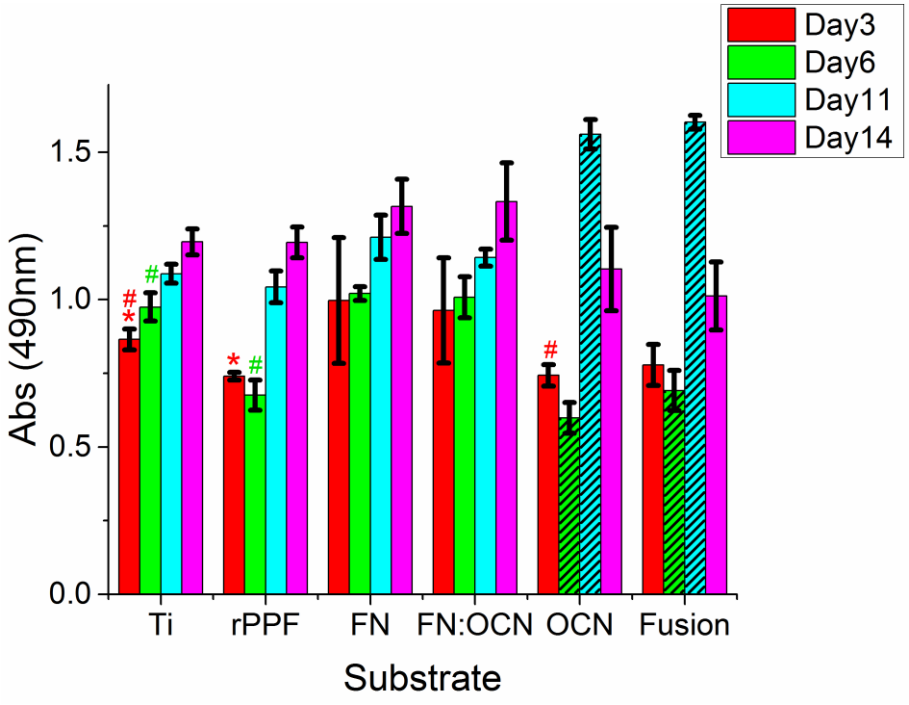

Figure 6.2. MTS proliferation signal for OBs on Ti, rPPF, FN, Ratio, OCN, and fusion surfaces at day 3, day 6, day 11, and day 14 post seeding. Analysis of the growth ratios showed no difference between the surfaces. The day 6 and 11 OCN and FN-OCN (black striped) experienced contamination and media leakage. The osteoblasts demonstrated steady growth across the time points. The observed statistical significances compared to Ti are shown in their representative colours ($p < 0.05$ - *, $p < 0.01$ - #). Uncertainty comes from the standard deviation ($n = 3$).

The OB proliferation is correlated with the extent of cell attachment and spreading. The general trend of the FN-containing surfaces producing more MTS signal than the OCN and rPPF is based on the elevated cell numbers at the attachment stage (**figure 6.1. a,b**), as the proliferation rates are similar. The FN-OCN fusion protein batch utilised in this assay was stored frozen upon delivery by mistake. A repeating assay was unsuccessfully attempted due to failed OB surface establishment and premature culture apoptosis. The mineralisation assays were prioritised to make most effective use of the remaining fusion protein. Primary osteoblasts were unavailable after completion of the mineralisation assays due to time constraints. Overall, the Ti, rPPF, and the protein-functionalised surfaces supported the attachment, spreading, and proliferation of osteoblasts.

6.3.3 Osteoblast mineralisation

The mineralisation potency of the multifunctional surfaces, as determined by the calcium concentration, was probed with an Alizarin Red stain (ARS) (**Figure 6.3**). The first ARS assay on the day 17 fusion-protein coated surface (Abs = 0.47 ± 0.04) showed a significant increase in calcium ($p < 0.05$) compared to the OCN-functionalised and rPPF surfaces, Abs = 0.32 ± 0.04 and 0.28 ± 0.10, respectively. The fusion-functionalised surfaces also produced a highly significant increase ($p < 0.01$) compared to Ti (Abs = 0.25 ± 0.03) (**Figure 6.3.a**). The following day 25 and day 32 ARS results showed that the calcium content of rPPF and protein-functionalised surfaces were equal to or greater than the bare Ti surface.

The second mineralisation assay (**Figure 6.3.b**) showed some variation on the previous trends. The day 20 ARS results showed a considerable increase across all surfaces compared to the Ti, with FN producing a significant increase ($P < 0.05$). The day 26 assay results demonstrated a significant calcium increase on the OCN and rPPF surfaces compared to Ti and non-statistical increases on the remaining

surfaces. The day 32 mineralisation measurements showed statistically significant increases on the protein-functionalised surfaces except for the rPPF and OCN surfaces.

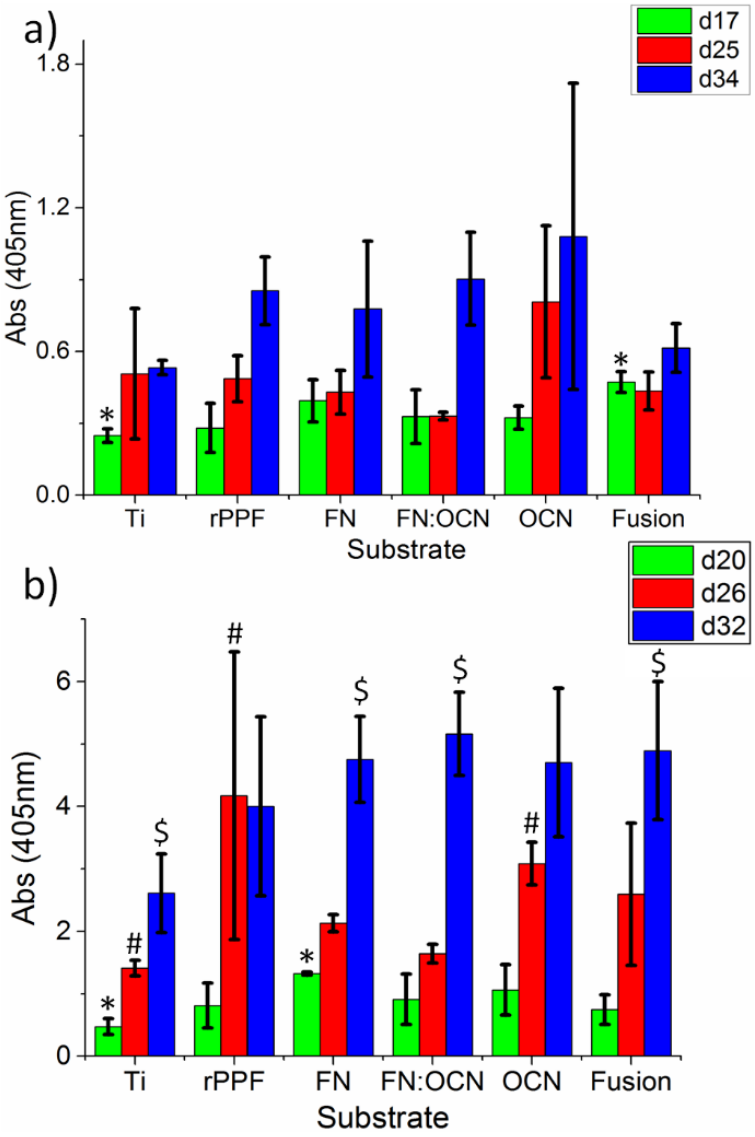

Figure 6.3. The calcium content deposited by primary osteoblasts on the protein-functionalised surfaces was determined by the alizarin red assays. Variations in mineralisation trends were observed at the earlier time points between the two individual tests performed. The commonalities between the two tests show that: i) the protein-functionalised surfaces substantially increase mineralisation compared to Ti, and ii) Signalling surfaces (fusion and OCN) induce larger degrees of mineralisation at earlier time points. Statistical significance ($p < 0.05$) compared to Ti is shown for the first (*), second (#), and third ($) time points. Uncertainty comes from the standard deviation between samples (n = 3).

The mineralisation observed on the single protein-functionalised surfaces is derived from the increased cell quantity for the FN and the enhanced mineralisation rate due to OCN signalling, as shown by comparing their attachment and mineralisation assays. The two multifunctional surfaces, FN: OCN and fusion, presented different mineralisation behaviours related to the nature of the multi-functionalisation. The FN:OCN ratio surfaces did not demonstrate an enhancement beyond the single protein surfaces, potentially due to the inhomogeneous presentation of the two proteins. In contrast, the fusion protein-coated surfaces accelerated calcium deposition as the protein is designed to uniformly present both signalling and attachment motifs by combining the adhesive FN9-10 domain with the signalling capability of the OCN (22-49 amino acid sequence) in a single molecule [287, 316]. Overall, the fusion protein demonstrated the greatest mineralisation potential in shorter time frames, indicating the significant benefits of its application in orthopaedic implants.

6.3.4 Differentiation of mesenchymal stem cells

The specific fluorescence (SF) of alkaline phosphatase (ALP), as calculated by the total fluorescence area per cell quantity (μm^2/cell), was used to quantify the differentiation of MSCs into osteoblasts under non-differentiating conditions. The samples were examined at day 10 and day 20 (**Figure 6.4)**. The day 10 SF results demonstrated three statically distinct bands. Titanium produced the most ALP with an SF of 592 ± 166 and constituted the statistically increased band relative to the rPPF surfaces. The rPPFs (SF = 376 ± 112), fusion-functionalised surfaces (SF = 353 ± 86), OCN-functionalised surfaces (392 ± 94), and OB conditioning media controls (SF = 323 ± 41) formed the middle band. The FN (SF = 224 ± 22) and FN:OCN (SF = 243 ± 24) surfaces demonstrate a significantly reduced SF. The day 20 SF results show that the middle band results from day 10 had equalised with the titanium. The FN and FN:OCN functionalised surfaces had increased slightly but demonstrated significantly less differentiation than the other surfaces.

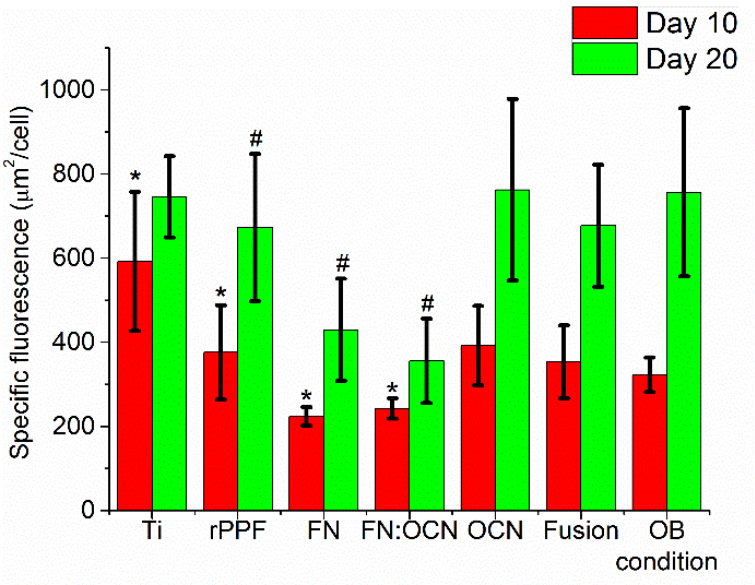

Figure 6.4. Specific fluorescence (SF) indicating the alkaline phosphatase (ALP) production of mesenchymal stem cells (MSCs) via fluorescence microscopy. Statistical significance ($p < 0.05$) between the rPPF and other surfaces are shown for day 10 (*) and day 20 (#). Uncertainty comes from the standard deviation (n = 3).

The ALP quantification assay further examined the osteogenic potential of the protein-functionalised surfaces through their capacity for signalling MSC differentiation. This is an important function for orthopaedic surfaces as the osseointegration process involves interactions with undifferentiated and pre-osteoblastic cells, as well as fully differentiated osteoblasts. The FN-functionalised surfaces produced less MSC differentiation overall as FN is known to be non-differentiating [451]. The equivalent values for the FN:OCN and FN surfaces confirmed the trends observed in the OB mineralisation assays, suggesting that the biological responses to the FN:OCN surfaces are dominated by the FN proteins. However, the expected increase in ALP production on the OCN and fusion protein surfaces relative to the uncoated Ti was not observed. MSC differentiation is governed by the cellular response to the surface topology and chemistry [241, 244, 366, 452] and through biological cues from neighbouring cells and the extracellular matrix [366, 453-455]. The day 10 results showed that the specific fluorescence of the fusion protein surfaces was on par with the OCN and rPPF, but the cell number was significantly lower than those for the other surfaces ($p < 0.01$). The drastic reduction in MSC population would greatly impact the intercellular signalling and rates of

differentiation relative to the other surfaces. The cell population was equalised across all surfaces by the day 20 time point. Further examinations would assist in clarifying the differentiation potential of the fusion protein surfaces.

6.4 Discussion

The functionalisation of orthopaedic implants with biological cues for rapid osseointegration is essential for reducing the post-operative complications associated with fibrotic encapsulation and biofilm formation [4, 356]. This biofunctionalisation strategy requires the development of easily reproducible, multifunctional surfaces that encourage rapid cellular attachment and accelerate mineralisation. Protein and biomolecule immobilisation represents one direction for producing multifunctional orthopaedic interfaces through the co-immobilisation of multiple proteins. Alternatively, the benefits may be more practically achieved through the utilisation of synthetic multifunctional biomolecules. In this chapter, the osteogenic potential of a surface with co-immobilised fibronectin and osteocalcin (1:3 FN:OCN) was compared with that of a multifunctional fusion protein surface. Both protein surfaces utilised radical-functionalised plasma polymer films (rPPFs) to achieve direct covalent bonding of the proteins to the Ti surfaces.

The most critical component of both multi-functionalisation approaches is the presentation of the desired motifs to the biological environment. The primary osteoblasts demonstrated that both multifunctional surfaces presented the RGD sequence by the observed increase in cellular attachment and spreading (**Figure 6.1**). However, a significant increase in mineralisation was observed only on the fusion protein surfaces **(Figure 6.3)**. This suggests that the OCN signalling sequence in the fusion protein is freely available to the biological environment, whereas, the OCN proteins on the FN:OCN surfaces are inefficiently presented, whether through obstruction by the FN or below a critical concentration. The difference in cellular response was also confirmed in the MSC differentiation assay, which showed that the FN:OCN surfaces exhibited non-differentiating effects while the fusion protein

surfaces signalled ALP production at lower cell populations. Similar observations of the effectiveness of co-immobilised vs fusion protein surfaces were noted in other biomolecule functionalisation work [124, 415], where a composite attachment fusion peptide outperformed the 50:50 mixture of the component peptides on the surface. The compromised performance was attributed to the inhomogeneity of the surface biomolecule layer [124, 415]. The 1:3 FN:OCN ratio selected is a close approximation to the 50:50 surface ratio but with a more inhomogeneous surface coverage due to the significant size difference between the FN (440 kDa) and the OCN (5.9 kDa) proteins. In contrast, the FN-OCN fusion protein surfaces presented the required densities of both the RGD cell binding sequence and the OCN signalling sequence homogenously across the surface, resulting in significantly greater osteogenic potency. Overall, the multifunctional fusion protein coated rPPF surfaces presented the most significant potential for osseointegrating orthopaedic implants based on the simplicity of the protein functionalisation and the homogenous availability of cell adhesive RGD and mineralisation signalling OCN sequences [124, 415, 416].

6.5 Conclusions

The functionalisation of titanium orthopaedics with proteins or peptides is a versatile approach to improve osseointegration, allowing for the bestowment of active biological functionality onto inert implant surfaces. While the current single protein-functionalisation approach has shown success, a multifunctional surface is often required for optimal implant osseointegration. In this chapter, the osteogenic potential of the two multi-functionalisation surfaces was comparatively examined with their single protein counterparts. Osteoblast attachment, spreading, proliferation, and mineralisation of the FN-OCN fusion protein surfaces were shown to be equal or greater than the FN and OCN single component proteins, while, the cellular responses on the co-immobilised FN:OCN ratio surfaces were similar to those on the FN-functionalised surfaces. The differentiation of MSCs on the fusion protein surfaces was on par with the OCN protein surfaces, whereas, the ratio surfaces portrayed the non-

differentiation behaviour of FN. Overall, the findings indicated that the FN-OCN fusion-protein coated rPPF surfaces hold significant potential for improving the osseointegration of implantable orthopaedic devices.

Chapter 7: Concluding summary and Future directions

7.1 Conclusions

Titanium orthopaedic devices are becoming increasingly common with the demand for load-bearing implants growing annually. However, the biochemical inertness of the devices leads to complications requiring additional surgeries. This thesis focussed on developing novel protein-functionalised plasma polymer biointerfaces to provide a robust, biologically active surface that stimulates bone-integration of the devices in a process that is translatable to an industrial context. Plasma polymer films (PPFs) are of great interest for biomaterial applications because of their versatility and substrate-independence. Conventional PPFs bind proteins through chemical reactions with surface chemical functionalities such as amine and carboxyl groups, which require specific reagents and complex monitoring. In contrast, the radical-functionalised PPFs (rPPFs) utilised in this thesis are able to immobilise multiple proteins onto a surface without the need for chemical reagents. Such radical-functionalised coatings were investigated as platforms to biologically functionalise titanium for orthopaedic applications.

A series of rPPFs with varied nitrogen atomic concentrations were investigated to determine the optimum coating for titanium surfaces based on the mechanical stability and cellular responses. The SEM images of rPPF coatings demonstrated that the 20%N and 30%N coatings were more robust under the mechanical stresses of cellular proliferation, aqueous swelling, and dehydration. A slight advantage in mechanical stability was observed on the 30%N rPPF. The proliferation assays showed a non-significant increase in cell quantity for the 20%N coating over the 30%N based on the day 1 and day 3 proliferation results, potentially deriving from a relatively elevated cellular attachment. Both rPPF coatings demonstrated the required mechanical stability and stimulated beneficial cellular

responses. Hence, these two rPPF-coatings were selected for continued material and biological examinations.

The relatively large quantity of radical electrons and radical flux to the surface of the rPPF coatings [217, 264] represent potential complications for biological applications through radical-induced cytotoxicity [381, 382]. The changes in surface properties of the 30%N rPPF, observed over 2 weeks, followed radical decay dynamics similar to plasma immersion ion implantation (PIII) treated polymers [269]. The fluorescence microscopy analysis and proliferation assays of bone lineage cells demonstrated no significant biological differences between the high radical flux (aged for only 4 hr) and low radical flux (aged for 11 days) rPPFs. The inability of the radical electrons to propagate through the peptide bonds in protein backbones is believed to protect cells at the interface from the detrimental effects of excess radicals. Thus, rPPF biointerfaces can be used in timeframes favouring the desired physical or chemical surface properties, such as wettability for protein attachment, without concerns over radical-induced cytotoxicity.

The 20%N rPPFs were functionalised with fibronectin (FN), osteocalcin (OCN), and a custom-made FN-OCN fusion protein. Full monolayer functionalisation was achieved at protein solution concentrations of 15 μg/mL, lower than the previously published studies using wet chemical methods. The majority of this monolayer (60-80%) was retained even when subject to rigorous SDS washing. The surfaces possessed greater protein quantities than bare Ti due to covalent binding through surface migrating radicals in the adsorption-desorption equilibrium dynamics. The rPPFs were also shown to permanently immobilise multiple proteins through a sequential incubations approach not possible with chemical or adsorption-based techniques. An unusual FN absorption signal behaviour was observed on the ratio surfaces potentially due to the altered surface conditions of the partially OCN functionalised interfaces. A 1:3 ratio of FN:OCN was selected for comparative osteogenic examination against a multifunctional fusion protein and the individual component proteins. Finally, a simple and effective methodology to create multifunctional protein surfaces was demonstrated.

A deepening understanding of the osseointegration process revealed that a multifunctional surface, that stimulates cell attachment and bone formation simultaneously, is required for optimal osseointegration. Primary mouse osteoblasts demonstrated significantly increased cell attachment on both multifunctional surfaces; however, only the fusion protein surfaces demonstrated accelerated calcium deposition. The considerable difference in osteogenic potency was due to the presentation and availability of the canonical RGD and the OCN 22-49 motifs. The homogenous presentation of both motifs across the fusion protein surfaces resulted in greater cellular attachment and signalling for bone formation. In contrast, the inhomogeneity derived from the random protein immobilisation and size difference presented by the co-immobilised ratio surface stimulated cell attachment only. The osteogenic potency of the co-immobilised surfaces was also confirmed by a mesenchymal stem cell differentiation on par with the non-differentiating FN. This thesis was an initial investigation focussing on the rPPF coating properties and examining the protein functionalised surfaces to determine the optimal combination. *In vivo* examination of the optimised surfaces is planned for future projects. Overall, the fusion protein-functionalised rPPFs present a highly osteogenic and scalable approach for the biofunctionalisation of orthopaedic devices.

7.2 Future directions

This thesis investigated the development of protein-functionalised biointerfaces based on radical-functionalised plasma polymer films (rPPFs) for orthopaedic titanium implants. The project covered the optimisation of the rPPFs, the characterisation of the multifunctional biointerfaces, and the *in vitro* biological studies to demonstrate their efficacy. The research performed opens multiple avenues for further exploration.

The rPPFs produced in this thesis provide a foundation for other 2D biointerface research [58, 356, 357]. The non-specific protein-functionalisation capacity of rPPFs provides a versatile platform to

investigate the efficacy on a surface of other untested osteogenic biomolecules, such as osteopontin or periostin [214, 456-464]. The incorporation of micro-patterning techniques into protein-functionalisation could be explored to determine if biomolecule patterning improves the osteogenic potential of orthopaedics. Alternatively, rPPFs could be transferred to microarray and biosensing technologies. The chemical tailoring of rPPFs could also be investigated through the addition of reagent monomers containing elements or compounds for specific applications, e.g. strontium, calcium, or phosphate groups, to improve bone formation [465].

The interdisciplinary field of biomaterials and tissue engineering has been transitioning from 2D surfaces towards more complex 3D structures, such as those produced through additive manufacturing [466-468]. The coating of 3D structures via plasma deposition processes is difficult especially when shadowed cavities, such as internal porosity, are present. The coating stability is a major issue because of the chemically and mechanically aggressive nature of the *in vivo* environment, and the long-term stability required. The importance of coating stability is further elevated by the medical consequences of a delamination event. The rPPF coatings address the stability issues through the formation of carbide bonds on the Ti substrates and a high degree of crosslinking created by employing more energetic deposition conditions during early stages of the plasma polymerisation [285, 309]. Research into the homogenous deposition of rPPFs throughout complex 3D scaffolds and the subsequent biomolecule functionalisation would further improve the osseointegration of porous 3D orthopaedic implants [469].

In vivo examination of potential biomedical products, including implantable biointerfaces, is a requirement for clinical certification. *In vivo* animal models provide information that cannot be accurately obtained through current 2D *in vitro* testing, e.g. regarding bone formation rates, foreign body reactions, the effects of nutrient and oxygen gradients, and cell 'cross talk' [470]. The disparity between *in vitro* and *in vivo* is an ongoing issue for all forms of biomedical and pharmacological research [471] as a significant increase in effectiveness *in vitro* does not guarantee transfer to the

animal model. A significant osseointegration increase *in vivo* for mouse, rabbit or large animal models for protein-functionalised rPPFs would ease the transition of this research into the clinic.

Plasma polymerisation, unlike wet chemistry methods, has the capacity to be easily scaled and incorporated into manufacturing processes, as evident by the application of plasma enhanced chemical vapour deposition processes in optics, electronics, and solar cells [288, 289]. The post-production modification of orthopaedic devices with rPPFs would allow for the transfer of protein-functionalisation into an implantable device [288, 289]. The unique non-specific immobilisation of rPPFs has a greater degree of versatility in the application of proteins; permitting the surfaces to be functionalised as part of the manufacturing process or to be functionalised onsite before implantation. Previous work has shown at least a 4.5 month longevity for biomolecule functionalisation of rPPFs in air [264], allowing for feasible storage and transportation times. The process of implant fabrication, rPPF deposition, and device storage will need to be optimised but the potential advantages for improved osseointegration and implant lifetime could significantly increase patient quality of life. In conclusion, the substrate-independent nature of rPPF surfaces and the scalability of plasma deposition techniques allow for the transfer of these easily-producible, multifunctional biointerfaces into the next generation of implantable devices.

References

[1] D. Davidson, R. DeSteiger, S. Graves, A. Tomkins, A.O. Association, National Joint Replacement Registry, Annual Report, ISSN 1445-3657, 2015.
[2] S.B. Goodman, Z. Yao, M. Keeney, F. Yang, The future of biologic coatings for orthopaedic implants, Biomaterials 34(13) (2013) 3174-3183.
[3] J.M. Anderson, A. Rodriguez, D.T. Chang, Foreign body reaction to biomaterials, Seminars in Immunology 20(2) (2008) 86-100.
[4] R. Trindade, T. Albrektsson, P. Tengvall, A. Wennerberg, Foreign Body Reaction to Biomaterials: On Mechanisms for Buildup and Breakdown of Osseointegration, Clinical Implant Dentistry and Related Research 18(1) (2016) 192-203.
[5] T. Albrektsson, C. Dahlin, T. Jemt, L. Sennerby, A. Turri, A. Wennerberg, Is Marginal Bone Loss around Oral Implants the Result of a Provoked Foreign Body Reaction?, Clinical Implant Dentistry and Related Research 16(2) (2014) 155-165.
[6] B. Zhao, H.C. van der Mei, G. Subbiahdoss, J. de Vries, M. Rustema-Abbing, R. Kuijer, H.J. Busscher, Y. Ren, Soft tissue integration versus early biofilm formation on different dental implant materials, Dental Materials 30(7) (2014) 716-727.
[7] A. Cochis, B. Azzimonti, C. Della Valle, R. Chiesa, C.R. Arciola, L. Rimondini, Biofilm formation on titanium implants counteracted by grafting gallium and silver ions, Journal of biomedical materials research. Part A 103(3) (2015) 1176-1187.
[8] A.M. Dottore, P.Y. Kawakami, K. Bechara, J.A. Rodrigues, A. Cassoni, L.C. Figueiredo, A. Piattelli, J.A. Shibli, Stability of Implants Placed in Augmented Posterior Mandible after Alveolar Osteotomy Using Resorbable Nonceramic Hydroxyapatite or Intraoral Autogenous Bone: 12-Month Follow-Up, Clinical Implant Dentistry and Related Research 16(3) (2014) 330-336.
[9] J. Hao, A. Acharya, K. Chen, J. Chou, S. Kasugai, N. Lang, Novel bioresorbable strontium hydroxyapatite membrane for guided bone regeneration, Clin. Oral Implants Res. 26(1) (2015) 1-7.
[10] L. Tan, X. Yu, P. Wan, K. Yang, Biodegradable Materials for Bone Repairs: A Review, Journal of Materials Science & Technology 29(6) (2013) 503-513.
[11] D.W. Weisgerber, K. Erning, C.L. Flanagan, S.J. Hollister, B.A.C. Harley, Evaluation of multi-scale mineralized collagen–polycaprolactone composites for bone tissue engineering, Journal of the Mechanical Behavior of Biomedical Materials 61 (2016) 318-327.
[12] P.S.P. Poh, D.W. Hutmacher, B.M. Holzapfel, A.K. Solanki, M.M. Stevens, M.A. Woodruff, In vitro and in vivo bone formation potential of surface calcium phosphate-coated polycaprolactone and polycaprolactone/bioactive glass composite scaffolds, Acta Biomaterialia 30 (2016) 319-333.
[13] L. Pruitt, J. Furmanski, Polymeric biomaterials for load-bearing medical devices, JOM 61(9) (2009) 14-20.
[14] S.M. Kurtz, J.N. Devine, PEEK biomaterials in trauma, orthopedic, and spinal implants, Biomaterials 28(32) (2007) 4845-4869.
[15] X. Liu, F. Han, P. Zhao, C. Lin, X. Wen, X. Ye, Layer-by-layer self-assembled multilayers on PEEK implants improve osseointegration in an osteoporosis rabbit model, Nanomedicine: Nanotechnology, Biology and Medicine 13(4) (2017) 1423-1433.
[16] A.H.C. Poulsson, D. Eglin, S. Zeiter, K. Camenisch, C. Sprecher, Y. Agarwal, D. Nehrbass, J. Wilson, R.G. Richards, Osseointegration of machined, injection moulded and oxygen plasma modified PEEK implants in a sheep model, Biomaterials 35(12) (2014) 3717-3728.
[17] W.R. Walsh, N. Bertollo, C. Christou, D. Schaffner, R.J. Mobbs, Plasma-sprayed titanium coating to polyetheretherketone improves the bone-implant interface, The Spine Journal 15(5) (2015) 1041-1049.
[18] Q. Chen, G.A. Thouas, Metallic implant biomaterials, Mater Sci Eng R Rep 87 (2015) 1-57.

[19] R. Bothe, L. Beaton, H. Davenport, Reaction of bone to multiple metallic implants, Surg Gynecol Obstet 71(6) (1940) 598-602.
[20] M. Niinomi, Mechanical properties of biomedical titanium alloys, Materials Science and Engineering: A 243(1–2) (1998) 231-236.
[21] Y. Kirmanidou, M. Sidira, A. Bakopoulou, M.-E. Drosou, V. Bennani, A. Tsouknidas, N. Michailidis, K. Michalakis, New Ti-Alloys and Surface Modifications to Improve the Mechanical Properties and the Biological Response to Orthopedic and Dental Implants: A Review, Biomed Res Int 2016 (2016) 2908570.
[22] Y. Li, C. Yang, H. Zhao, S. Qu, X. Li, Y. Li, New developments of Ti-based alloys for biomedical applications, Materials 7(3) (2014) 1709-1800, 92 pp.
[23] A. Cheng, D.J. Cohen, A. Kahn, R.M. Clohessy, K. Sahingur, J.B. Newton, S.L. Hyzy, B.D. Boyan, Z. Schwartz, Laser Sintered Porous Ti–6Al–4V Implants Stimulate Vertical Bone Growth, Annals of Biomedical Engineering (2017) 1-11.
[24] H. Li, S.M. Oppenheimer, S.I. Stupp, D.C. Dunand, L.C. Brinson, Effects of pore morphology and bone ingrowth on mechanical properties of microporous titanium as an orthopaedic implant material, Mater. Trans. 45(4) (2004) 1124-1131.
[25] C. Zou, E. Zhang, M. Li, S. Zeng, Preparation, microstructure and mechanical properties of porous titanium sintered by Ti fibres, Journal of materials science. Materials in medicine 19(1) (2008) 401-5.
[26] M. Geetha, A.K. Singh, R. Asokamani, A.K. Gogia, Ti based biomaterials, the ultimate choice for orthopaedic implants – A review, Progress in Materials Science 54(3) (2009) 397-425.
[27] J. Currey, Chapter A1 Cortical Bone, Handbook of Biomaterial Properties, Springer2016, pp. 3-13.
[28] C.A. Grant, L.J. Wilson, C. Langton, D. Epari, Comparison of mechanical and ultrasound elastic modulus of ovine tibial cortical bone, Medical Engineering & Physics 36(7) (2014) 869-874.
[29] M. Niinomi, M. Nakai, Titanium-Based Biomaterials for Preventing Stress Shielding between Implant Devices and Bone, International Journal of Biomaterials 2011 (2011) 10.
[30] Q.-H. Zhang, A. Cossey, J. Tong, Stress shielding in periprosthetic bone following a total knee replacement: Effects of implant material, design and alignment, Medical Engineering & Physics 38(12) (2016) 1481-1488.
[31] D.R. Sumner, Long-term implant fixation and stress-shielding in total hip replacement, Journal of Biomechanics 48(5) (2015) 797-800.
[32] S. Samiezadeh, P. Tavakkoli Avval, Z. Fawaz, H. Bougherara, On optimization of a composite bone plate using the selective stress shielding approach, Journal of the Mechanical Behavior of Biomedical Materials 42 (2015) 138-153.
[33] A.H. Glassman, J.D. Bobyn, M. Tanzer, New Femoral Designs: Do They Influence Stress Shielding?, Clinical orthopaedics and related research 453(December) (2006) 10.
[34] B. O'Brien, W. Carroll, M. Kelly, Passivation of nitinol wire for vascular implants—a demonstration of the benefits, Biomaterials 23(8) (2002) 1739-1748.
[35] A. Sidambe, Biocompatibility of Advanced Manufactured Titanium Implants—A Review, Materials 7(12) (2014) 8168.
[36] M.H. Fathi, M. Salehi, A. Saatchi, V. Mortazavi, S.B. Moosavi, In vitro corrosion behavior of bioceramic, metallic, and bioceramic–metallic coated stainless steel dental implants, Dental Materials 19(3) (2003) 188-198.
[37] V. Sansone, D. Pagani, M. Melato, The effects on bone cells of metal ions released from orthopaedic implants. A review, Clin Cases Miner Bone Metab 10(1) (2013) 34-40.
[38] K.L. Wapner, Implications of metallic corrosion in total knee arthroplasty, Clinical orthopaedics and related research (271) (1991) 12-20.
[39] N.J. Hallab, C. Vermes, C. Messina, K.A. Roebuck, T.T. Glant, J.J. Jacobs, Concentration- and composition-dependent effects of metal ions on human MG-63 osteoblasts, Journal of biomedical materials research 60(3) (2002) 420-33.

[40] B. Moretti, V. Pesce, G. Maccagnano, G. Vicenti, P. Lovreglio, L. Soleo, P. Apostoli, Peripheral neuropathy after hip replacement failure: is vanadium the culprit?, The Lancet 379(9826) 1676.
[41] K. Narita, M. Niinomi, M. Nakai, Effects of micro- and nano-scale wave-like structures on fatigue strength of a beta-type titanium alloy developed as a biomaterial, Journal of the Mechanical Behavior of Biomedical Materials 29(0) (2014) 393-402.
[42] X. Song, L. Wang, M. Niinomi, M. Nakai, Y. Liu, M. Zhu, Microstructure and fatigue behaviors of a biomedical Ti–Nb–Ta–Zr alloy with trace CeO2 additions, Materials Science and Engineering: A 619(0) (2014) 112-118.
[43] K. Narita, M. Niinomi, M. Nakai, J. Hieda, K. Oribe, Development of thermo-mechanical processing for fabricating highly durable -type Ti–Nb–Ta–Zr rod for use in spinal fixation devices, Journal of the Mechanical Behavior of Biomedical Materials 9(0) (2012) 207-216.
[44] K. Narita, M. Niinomi, M. Nakai, J. Hieda, K. Oribe, Specific characteristics of mechanically and biologically compatible titanium alloy rods for use in spinal fixation applications, Materials Letters 86(0) (2012) 178-181.
[45] N. Sumitomo, K. Noritake, T. Hattori, K. Morikawa, S. Niwa, K. Sato, M. Niimoni, Experiment study on fracture fixation with low rigidity titanium alloy, Journal of Materials Science: Materials in Medicine 19(4) (2008) 6.
[46] A. Shukla, R. Balasubramaniam, Effect of surface treatment on electrochemical behavior of CP Ti, Ti–6Al–4V and Ti–13Nb–13Zr alloys in simulated human body fluid, Corrosion Science 48(7) (2006) 1696-1720.
[47] J.-H. Xing, H. Li, Z.-B. Xia, J.-F. Hu, Y.-H. Zhang, L. Zhong, Formation and crystallization of anodic oxide films on sputter-deposited titanium in potentiostatic and potential-sweep modes, Journal of The Electrochemical Society 160(10) (2013) C503-C510.
[48] S.C. Cosma, N. Balc, M. Moldovan, C.S. Miron-Borzan, Surface treatments applied on titanium implants, Ovidius Univ. Ann. Chem. 26(1) (2015) 41-48.
[49] P. Sevilla, K.V. Vining, J. Dotor, D. Rodriguez, F.J. Gil, C. Aparicio, Surface immobilization and bioactivity of TGF-β1 inhibitor peptides for bone implant applications, J. Biomed. Mater. Res. Part B Appl. Biomater. 104(2) (2016) 385-394.
[50] H. Chen, L. Yuan, W. Song, Z. Wu, D. Li, Biocompatible polymer materials: Role of protein–surface interactions, Progress in Polymer Science 33(11) (2008) 1059-1087.
[51] S.P. Massia, J.A. Hubbell, Covalent surface immobilization of Arg-Gly-Asp- and Tyr-Ile-Gly-Ser-Arg-containing peptides to obtain well-defined cell-adhesive substrates, Anal. Biochem. 187(2) (1990) 292-301.
[52] K.C. Dee, D.C. Rueger, T.T. Andersen, R. Bizios, Conditions which promote mineralization at the bone-implant interface: a model in vitro study, Biomaterials 17(2) (1996) 209-215.
[53] T.W. Axelrad, T.A. Einhorn, Bone morphogenetic proteins in orthopaedic surgery, Cytokine & Growth Factor Reviews 20(5–6) (2009) 481-488.
[54] M. Suk, Use of recombinant human BMP-2 in orthopedic trauma, in: S. Vukicevic, K.T. Sampath (Eds.), Bone Morphogenetic Proteins: From Local to Systemic Therapeutics, Birkhäuser Basel, Basel, 2008, pp. 25-42.
[55] F.-Y. Teng, W.-C. Chen, Y.-L. Wang, C.-C. Hung, C.-C. Tseng, Effects of osseointegration by bone morphogenetic protein-2 on titanium implants in vitro and in vivo, Bioinorg. Chem. Appl. (2016) 1-10.
[56] S.E. Kim, C.-S. Kim, Y.-P. Yun, D.H. Yang, K. Park, S.E. Kim, C.-M. Jeong, J.-B. Huh, Improving osteoblast functions and bone formation upon BMP-2 immobilization on titanium modified with heparin, Carbohydr. Polym. 114 (2014) 123-132.
[57] L. Han, H. Lin, X. Lu, W. Zhi, K.f. Wang, F.z. Meng, O. Jiang, BMP2-encapsulated chitosan coatings on functionalized Ti surfaces and their performance in vitro and in vivo, Materials Science and Engineering: C 40 (2014) 1-8.

[58] G.C. Yeo, M. Santos, A. Kondyurin, J. Liskova, A.S. Weiss, M.M.M. Bilek, Plasma-Activated Tropoelastin Functionalization of Zirconium for Improved Bone Cell Response, ACS Biomaterials Science & Engineering 2(4) (2016) 662-676.
[59] Z. Zhang, Y. Qu, X. Li, S. Zhang, Q. Wei, Y. Shi, L. Chen, Electrophoretic deposition of tetracycline modified silk fibroin coatings for functionalization of titanium surfaces, Applied Surface Science 303 (2014) 255-262.
[60] Z. Zhang, T. Jiang, K. Ma, X. Cai, Y. Zhou, Y. Wang, Low temperature electrophoretic deposition of porous chitosan/silk fibroin composite coating for titanium biofunctionalization, Journal of Materials Chemistry 21(21) (2011) 7705-7713.
[61] S. Nayak, T. Dey, D. Naskar, S.C. Kundu, The promotion of osseointegration of titanium surfaces by coating with silk protein sericin, Biomaterials 34(12) (2013) 2855-2864.
[62] P.W. Atkins, J. De Paula, Atkins' physical chemistry, Oxford University Press, Oxford

New York, 2010.
[63] D.L. Nelson, D.L. Nelson, A.L. Lehninger, M.M. Cox, Lehninger principles of biochemistry, W.H. Freeman, New York, 2008.
[64] K. Cai, M. Frant, J. Bossert, G. Hildebrand, K. Liefeith, K.D. Jandt, Surface functionalized titanium thin films: Zeta-potential, protein adsorption and cell proliferation, Colloids and Surfaces B: Biointerfaces 50(1) (2006) 1-8.
[65] R.A. Gittens, L. Scheideler, F. Rupp, S.L. Hyzy, J. Geis-Gerstorfer, Z. Schwartz, B.D. Boyan, A review on the wettability of dental implant surfaces II: Biological and clinical aspects, Acta Biomaterialia 10(7) (2014) 2907-2918.
[66] F. Rupp, R.A. Gittens, L. Scheideler, A. Marmur, B.D. Boyan, Z. Schwartz, J. Geis-Gerstorfer, A review on the wettability of dental implant surfaces I: Theoretical and experimental aspects, Acta Biomaterialia 10(7) (2014) 2894-2906.
[67] L.-C. Xu, C.A. Siedlecki, Effects of surface wettability and contact time on protein adhesion to biomaterial surfaces, Biomaterials 28(22) (2007) 3273-3283.
[68] R.A. Latour, Perspectives on the simulation of protein–surface interactions using empirical force field methods, Colloids and Surfaces B: Biointerfaces 124 (2014) 25-37.
[69] C. Leng, H.-C. Hung, S. Sun, D. Wang, Y. Li, S. Jiang, Z. Chen, Probing the Surface Hydration of Nonfouling Zwitterionic and PEG Materials in Contact with Proteins, ACS Appl. Mater. Interfaces 7(30) (2015) 16881-16888.
[70] N. Zhang, J. Ma, M.A.S. Melo, M.D. Weir, Y. Bai, H.H.K. Xu, Protein-repellent and antibacterial dental composite to inhibit biofilms and caries, Journal of Dentistry 43(2) (2015) 225-234.
[71] A. Sanfeld, C. Royer, A. Steinchen, Thermodynamic, kinetic and conformational analysis of proteins diffusion–sorption on a solid surface, Advances in Colloid and Interface Science 222 (2015) 639-660.
[72] V.B. Damodaran, N.S. Murthy, Bio-inspired strategies for designing antifouling biomaterials, Biomaterials Research 20(1) (2016) 18.
[73] R. Tejero, E. Anitua, G. Orive, Toward the biomimetic implant surface: Biopolymers on titanium-based implants for bone regeneration, Progress in Polymer Science 39(7) (2014) 1406-1447.
[74] C. Guo, S. Wang, H. Liu, L. Feng, Y. Song, L. Jiang, Wettability Alteration of Polymer Surfaces Produced by Scraping, Journal of Adhesion Science and Technology 22(3-4) (2008) 395-402.
[75] R.A. Gittens, T. McLachlan, R. Olivares-Navarrete, Y. Cai, S. Berner, R. Tannenbaum, Z. Schwartz, K.H. Sandhage, B.D. Boyan, The effects of combined micron-/submicron-scale surface roughness and nanoscale features on cell proliferation and differentiation, Biomaterials 32(13) (2011) 3395-3403.
[76] A.B. Faia-Torres, S. Guimond-Lischer, M. Rottmar, M. Charnley, T. Goren, K. Maniura-Weber, N.D. Spencer, R.L. Reis, M. Textor, N.M. Neves, Differential regulation of osteogenic differentiation of stem cells on surface roughness gradients, Biomaterials 35(33) (2014) 9023-9032.
[77] F. Grizon, E. Aguado, G. Hure, M. Baslé, D. Chappard, Enhanced bone integration of implants with increased surface roughness: a long term study in the sheep, Journal of dentistry 30(5) (2002) 195-203.

[78] J.E. Davies, E. Ajami, R. Moineddin, V.C. Mendes, The roles of different scale ranges of surface implant topography on the stability of the bone/implant interface, Biomaterials 34(14) (2013) 3535-3546.
[79] G.P. Rockwell, L.B. Lohstreter, J.R. Dahn, Fibrinogen and albumin adsorption on titanium nanoroughness gradients, Colloids and Surfaces B: Biointerfaces 91 (2012) 90-96.
[80] K. Rechendorff, M.B. Hovgaard, M. Foss, V.P. Zhdanov, F. Besenbacher, Enhancement of Protein Adsorption Induced by Surface Roughness, Langmuir 22(26) (2006) 10885-10888.
[81] K. Cai, J. Bossert, K.D. Jandt, Does the nanometre scale topography of titanium influence protein adsorption and cell proliferation?, Colloids Surf., B 49(2) (2006) 136-144.
[82] E.M. Blanco, M.A. Horton, P. Mesquida, Simultaneous Investigation of the Influence of Topography and Charge on Protein Adsorption Using Artificial Nanopatterns, Langmuir 24(6) (2008) 2284-2287.
[83] D.D. Deligianni, N. Katsala, S. Ladas, D. Sotiropoulou, J. Amedee, Y.F. Missirlis, Effect of surface roughness of the titanium alloy Ti–6Al–4V on human bone marrow cell response and on protein adsorption, Biomaterials 22(11) (2001) 1241-1251.
[84] X. Liu, P.K. Chu, C. Ding, Surface modification of titanium, titanium alloys, and related materials for biomedical applications, Materials Science and Engineering: R: Reports 47(3–4) (2004) 49-121.
[85] K. Anselme, M. Bigerelle, Topography effects of pure titanium substrates on human osteoblast long-term adhesion, Acta Biomaterialia 1(2) (2005) 211-222.
[86] A. Bagno, C. Di Bello, Surface treatments and roughness properties of Ti-based biomaterials, Journal of materials science. Materials in medicine 15(9) (2004) 935-49.
[87] O. Noiset, Y.-J. Schneider, J. Marchand-Brynaert, Fibronectin adsorption or/and covalent grafting on chemically modified PEEK film surfaces, Journal of Biomaterials Science, Polymer Edition 10(6) (1999) 657-677.
[88] O. Noiset, Y.-J. Schneider, J. Marchand-Brynaert, Adhesion and growth of CaCo2 cells on surface-modified PEEK substrata, Journal of Biomaterials Science, Polymer Edition 11(7) (2000) 767-786.
[89] J. van der Stok, D. Lozano, Y.C. Chai, S. Amin Yavari, A.P. Bastidas Coral, J.A. Verhaar, E. Gomez-Barrena, J. Schrooten, H. Jahr, A.A. Zadpoor, P. Esbrit, H. Weinans, Osteostatin-coated porous titanium can improve early bone regeneration of cortical bone defects in rats, Tissue engineering. Part A 21(9-10) (2015) 1495-506.
[90] L. Jia, X. Peng, T. Jie, J. Zhaojun, C. Hong, L. Zhongjun, Enhanced angiogenesis and osteogenesis in critical bone defects by the controlled release of BMP-2 and VEGF: implantation of electron beam melting-fabricated porous Ti 6 Al 4 V scaffolds incorporating growth factor-doped fibrin glue, Biomedical Materials 10(3) (2015) 035013.
[91] U. Fischer, U. Hempel, D. Becker, S. Bierbaum, D. Scharnweber, H. Worch, K.W. Wenzel, Transforming growth factor β1 immobilized adsorptively on Ti6Al4V and collagen type I coated Ti6Al4V maintains its biological activity, Biomaterials 24(15) (2003) 2631-2641.
[92] T. Hanawa, A comprehensive review of techniques for biofunctionalization of titanium, J. Periodontal Implant Sci. 41(6) (2011) 263-272.
[93] T. Vermonden, R. Censi, W.E. Hennink, Hydrogels for Protein Delivery, Chemical Reviews 112(5) (2012) 2853-2888.
[94] A.B. Lovati, S. Lopa, G. Talo, S. Previdi, C. Recordati, D. Mercuri, F. Segatti, L. Zagra, M. Moretti, In vivo evaluation of bone deposition in macroporous titanium implants loaded with mesenchymal stem cells and strontium-enriched hydrogel, Journal of biomedical materials research. Part B, Applied biomaterials 103(2) (2015) 448-56.
[95] L. Hao, L. Wei, L. Can, T. Jie, W. Hong, H. Bao, C. Hong, L. Hui-Jie, L. Zhong-Jun, S. Chun-Li, Incorporating simvastatin/poloxamer 407 hydrogel into 3D-printed porous Ti 6 Al 4 V scaffolds for the promotion of angiogenesis, osseointegration and bone ingrowth, Biofabrication 8(4) (2016) 045012.

[96] S.D. Nath, N.T. Linh, A. Sadiasa, B.T. Lee, Encapsulation of simvastatin in PLGA microspheres loaded into hydrogel loaded BCP porous spongy scaffold as a controlled drug delivery system for bone tissue regeneration, Journal of Biomaterials Applications 28(8) (2014) 1151-1163.
[97] B. Wen, L. Kuhn, L. Charles, D. Pendrys, D. Shafer, M. Freilich, Comparison of bone morphogenetic protein-2 delivery systems to induce supracrestal bone guided by titanium implants in the rabbit mandible, Clin. Oral Implants Res. 27(6) (2016) 676-685.
[98] S.-H. Lee, H. Shin, Matrices and scaffolds for delivery of bioactive molecules in bone and cartilage tissue engineering, Advanced Drug Delivery Reviews 59(4–5) (2007) 339-359.
[99] D.M.R. Gibbs, C.R.M. Black, J.I. Dawson, R.O.C. Oreffo, A review of hydrogel use in fracture healing and bone regeneration, Journal of Tissue Engineering and Regenerative Medicine 10(3) (2016) 187-198.
[100] T. Amemiya, Y. Fukayo, K. Nakaoka, Y. Hamada, T. Hayakawa, Tissue response of surface-modified three-dimensional titanium fiber structure, J. Hard Tissue Biol. 23(2) (2014) 137-148.
[101] T. Hayakawa, Biochemical surface modifications to titanium implants using the tresyl chlorideactivated method, Dental materials journal 34(6) (2015) 725-739.
[102] K. Nilsson, K. Mosbach, [3] Tresyl chloride-activated supports for enzyme immobilization, Methods in Enzymology, Academic Press1987, pp. 65-78.
[103] D.A. Puleo, Biochemical surface modification of Co・Cr・Mo, Biomaterials 17(2) (1996) 217-222.
[104] T. Hayakawa, M. Yoshinari, K. Nemoto, Direct attachment of fibronectin to tresyl chloride-activated titanium, J. Biomed. Mater. Res., Part A 67A(2) (2003) 684-688.
[105] T. Hayakawa, M. Yoshinari, K. Nemoto, Quartz-crystal microbalance-dissipation technique for the study of initial adsorption of fibronectin onto tresyl chloride-activated titanium, J. Biomed. Mater. Res., Part B 73B(2) (2005) 271-276.
[106] H. Sheng, Y. Wang, T. Jiang, H. Xia, Study of binding fibronectin to tresyl chloride-activated titanium, Xiandai Kouqiang Yixue Zazhi 20(4) (2006) 378-381.
[107] T. Suzuki, T. Hayakawa, T. Kawamoto, K. Gomi, Bone response of TGF-β2 immobilized titanium in a rat model, Dent. Mater. J. 33(2) (2014) 233-241.
[108] T. Hayakawa, E. Yoshida, Y. Yoshimura, M. Uo, M. Yoshinari, MC3T3-E1 Cells on Titanium Surfaces with Nanometer Smoothness and Fibronectin Immobilization, International Journal of Biomaterials 2012 (2012) 6.
[109] M. Hirota, H. Shimpo, C. Ohkubo, T. Umegaki, T. Toyama, T. Hayakawa, Bone Adaptation of Fibronectin-Immobilized Titanium Implants Using a Tresyl Chloride-Activated Method, Journal of Hard Tissue Biology 24(4) (2015) 341-346.
[110] T. Suzuki, T. Hayakawa, T. Kawamoto, K. Gomi, Bone response of TGF-β2 immobilized titanium in a rat model, Dental materials journal 33(2) (2014) 233-241.
[111] L. Vroman, A.L. Adams, G.C. Fischer, P.C. Munoz, Interaction of high molecular weight kininogen, factor XII, and fibrinogen in plasma at interfaces, Blood 55(1) (1980) 156-159.
[112] S.L. Hirsh, D.R. McKenzie, N.J. Nosworthy, J.A. Denman, O.U. Sezerman, M.M. Bilek, The Vroman effect: competitive protein exchange with dynamic multilayer protein aggregates, Colloids and Surfaces B: Biointerfaces 103 (2013) 395-404.
[113] H. Noh, E.A. Vogler, Volumetric interpretation of protein adsorption: Competition from mixtures and the Vroman effect, Biomaterials 28(3) (2007) 405-422.
[114] W. Wang, N.W. Woodbury, Selective protein–peptide interactions at surfaces, Acta Biomaterialia 10(2) (2014) 761-768.
[115] O. Noiset, Y.J. Schneider, J. Marchand–Brynaert, Surface modification of poly(aryl ether ether ketone) (PEEK) film by covalent coupling of amines and amino acids through a spacer arm, Journal of Polymer Science Part A: Polymer Chemistry 35(17) (1997) 3779-3790.
[116] F. Wang, J. Roovers, Functionalization of poly(aryl ether ether ketone) (PEEK): synthesis and properties of aldehyde and carboxylic acid substituted PEEK, Macromolecules 26(20) (1993) 5295-5302.

[117] Y. Zheng, C. Xiong, X. Li, L. Zhang, Covalent attachment of cell-adhesive peptide Gly-Arg-Gly-Asp (GRGD) to poly(etheretherketone) surface by tailored silanization layers technique, Applied Surface Science 320 (2014) 93-101.
[118] K. Endo, Chemical modification of metallic implant surfaces with biofunctional proteins. Part 2. Corrosion resistance of a chemically modified NiTi alloy, Dent. Mater. J. 14(2) (1995) 199-210.
[119] K. Endo, Chemical modification of metallic implant surfaces with biofunctional proteins. Part 1. Molecular structure and biological activity of a modified NiTi alloy surface, Dent. Mater. J. 14(2) (1995) 185-98.
[120] H. Ao, Y. Xie, H. Tan, X. Wu, G. Liu, A. Qin, X. Zheng, T. Tang, Improved hMSC functions on titanium coatings by type I collagen immobilization, Journal of Biomedical Materials Research Part A 102(1) (2014) 204-214.
[121] S. Altmann, J. Pfeiffer, The hydrolysis/condensation behaviour of methacryloyloxyalkylfunctional alkoxysilanes: Structure-reactivity relations, Monatshefte Fur Chemie 134(8) (2003) 1081-1092.
[122] G. Voggenreiter, K. Hartl, S. Assenmacher, M. Chatzinikolaidou, H. Rumpf, H. Jennissen, Assessment of the biological activity of chemically immobilized rhBMP-2 on titanium surfaces in vivo, Materialwissenschaft und Werkstofftechnik 32(12) (2001) 942-948.
[123] B.e. Nie, T. Long, H. Ao, T. Tang, B. Yue, J. Zhou, B. Yue, Covalent immobilisation of enoxacin onto Ti implant surfaces for inhibiting multiple bacteria species infection and in vivo MRSA infection prophylaxis, Antimicrob Agents Chemother (2016).
[124] R. Fraioli, K. Dashnyam, J.-H. Kim, R.A. Perez, H.-W. Kim, J. Gil, M.-P. Ginebra, J.M. Manero, C. Mas-Moruno, Surface guidance of stem cell behavior: Chemically tailored co-presentation of integrin-binding peptides stimulates osteogenic differentiation in vitro and bone formation in vivo, Acta Biomaterialia 43 (2016) 269-281.
[125] Y. Tanaka, Y. Matsuo, T. Komiya, Y. Tsutsumi, H. Doi, T. Yoneyama, T. Hanawa, Characterization of the spatial immobilization manner of poly(ethylene glycol) to a titanium surface with immersion and electrodeposition and its effects on platelet adhesion, Journal of Biomedical Materials Research Part A 92A(1) (2010) 350-358.
[126] Y. Tanaka, H. Doi, E. Kobayashi, T. Yoneyama, T. Hanawa, Determination of the Immobilization Manner of Amine-Terminated Poly(Ethylene Glycol) Electrodeposited on a Titanium Surface with XPS and GD-OES, Mater. Trans. 48(3) (2007) 287-292.
[127] G.L. Kenausis, J. Vörös, D.L. Elbert, N. Huang, R. Hofer, L. Ruiz-Taylor, M. Textor, J.A. Hubbell, N.D. Spencer, Poly(l-lysine)-g-Poly(ethylene glycol) Layers on Metal Oxide Surfaces: Attachment Mechanism and Effects of Polymer Architecture on Resistance to Protein Adsorption, The Journal of Physical Chemistry B 104(14) (2000) 3298-3309.
[128] L. Yuan, Q. Yu, D. Li, H. Chen, Surface Modification to Control Protein/Surface Interactions, Macromol. Biosci. 11(8) (2011) 1031-1040.
[129] J. Buxadera-Palomero, C. Calvo, S. Torrent-Camarero, F.J. Gil, C. Mas-Moruno, C. Canal, D. Rodríguez, Biofunctional polyethylene glycol coatings on titanium: An in vitro-based comparison of functionalization methods, Colloids and Surfaces B: Biointerfaces 152 (2017) 367-375.
[130] S. Krishnan, Biofilm Formation on Medical Devices and Infection: Preventive Approaches, in: H. Kanematsu, D.M. Barry (Eds.), Biofilm and Materials Science, Springer International Publishing, Cham, 2015, pp. 93-108.
[131] Y. Tanaka, H. Doi, Y. Iwasaki, S. Hiromoto, T. Yoneyama, K. Asami, H. Imai, T. Hanawa, Electrodeposition of amine-terminatedpoly(ethylene glycol) to titanium surface, Materials Science and Engineering: C 27(2) (2007) 206-212.
[132] E. Byun, J. Kim, S.M. Kang, H. Lee, D. Bang, H. Lee, Surface PEGylation via native chemical ligation, Bioconjugate Chemistry 22(1) (2011) 4-8.
[133] C.-J. Pan, Y.-H. Hou, H.-Y. Ding, Y.-X. Dong, Enhancing anticoagulation and endothelial cell proliferation of titanium surface by sequential immobilization of poly(ethylene glycol) and collagen, Applied Surface Science 287 (2013) 443-450.

[134] X. Yu, J. Walsh, M. Wei, Covalent immobilization of collagen on titanium through polydopamine coating to improve cellular performances of MC3T3-E1 cells, RSC Adv. 4(14) (2014) 7185-7192.
[135] S.E. Kim, Y.P. Yun, J.Y. Lee, K. Park, D.H. Suh, Osteoblast activity of MG-63 cells is enhanced by growth on a lactoferrin-immobilized titanium substrate, Colloids and Surfaces B: Biointerfaces 123 (2014) 191-198.
[136] Z. Shi, K.G. Neoh, E.T. Kang, C.K. Poh, W. Wang, Surface Functionalization of Titanium with Carboxymethyl Chitosan and Immobilized Bone Morphogenetic Protein-2 for Enhanced Osseointegration, Biomacromolecules 10(6) (2009) 1603-1611.
[137] J. Lahann, D. Klee, W. Pluester, H. Hoecker, Bioactive immobilization of r-hirudin on CVD-coated metallic implant devices, Biomaterials 22(8) (2001) 817-826.
[138] S.E. Sakiyama-Elbert, 4.420 - Drug Delivery via Heparin Conjugates, in: P. Ducheyne (Ed.), Comprehensive Biomaterials, Elsevier, Oxford, 2011, pp. 333-338.
[139] E.-C. Kim, T.-H. Kim, J.-H. Jung, S.O. Hong, D.-W. Lee, Enhanced osteogenic differentiation of MC3T3-E1 on rhBMP-2-immobilized titanium via click reaction, Carbohydr. Polym. 103 (2014) 170-178.
[140] X. Fan, L. Lin, J.L. Dalsin, P.B. Messersmith, Biomimetic Anchor for Surface-Initiated Polymerization from Metal Substrates, J. Am. Chem. Soc. 127(45) (2005) 15843-15847.
[141] C. Xu, K. Xu, H. Gu, R. Zheng, H. Liu, X. Zhang, Z. Guo, B. Xu, Dopamine as A Robust Anchor to Immobilize Functional Molecules on the Iron Oxide Shell of Magnetic Nanoparticles, Journal of the American Chemical Society 126(32) (2004) 9938-9939.
[142] C.-Y. Chien, W.-B. Tsai, Poly(dopamine)-Assisted Immobilization of Arg-Gly-Asp Peptides, Hydroxyapatite, and Bone Morphogenic Protein-2 on Titanium to Improve the Osteogenesis of Bone Marrow Stem Cells, ACS Appl. Mater. Interfaces 5(15) (2013) 6975-6983.
[143] J. Kang, S. Tada, T. Kitajima, T.I. Son, T. Aigaki, Y. Ito, Immobilization of bone morphogenetic protein on DOPA- or dopamine-treated titanium surfaces to enhance osseointegration, BioMed Research International 2013 (2013).
[144] A.W.G. Nijhuis, J.J.J.P. van den Beucken, O.C. Boerman, J.A. Jansen, S.C.G. Leeuwenburgh, 1-Step Versus 2-Step Immobilization of Alkaline Phosphatase and Bone Morphogenetic Protein-2 onto Implant Surfaces Using Polydopamine, Tissue Eng., Part C 19(8) (2013) 610-619.
[145] B.L. Foss, N. Ghimire, R. Tang, Y. Sun, Y. Deng, Bacteria and osteoblast adhesion to chitosan immobilized titanium surface: A race for the surface, Colloids and Surfaces B: Biointerfaces 134 (2015) 370-376.
[146] N. Ghimire, J. Luo, R. Tang, Y. Sun, Y. Deng, Novel anti-infective activities of chitosan immobilized titanium surface with enhanced osteogenic properties, Colloids and Surfaces B: Biointerfaces 122 (2014) 126-133.
[147] D. Zheng, K.G. Neoh, E.-T. Kang, Bifunctional coating based on carboxymethyl chitosan with stable conjugated alkaline phosphatase for inhibiting bacterial adhesion and promoting osteogenic differentiation on titanium, Applied Surface Science 360, Part A (2016) 86-97.
[148] D. Depan, R.D.K. Misra, The interplay between nanostructured carbon-grafted chitosan scaffolds and protein adsorption on the cellular response of osteoblasts: Structure–function property relationship, Acta Biomaterialia 9(4) (2013) 6084-6094.
[149] J. Zhang, G. Liu, Q. Wu, J. Zuo, Y. Qin, J. Wang, Novel Mesoporous Hydroxyapatite/Chitosan Composite for Bone Repair, Journal of Bionic Engineering 9(2) (2012) 243-251.
[150] S.K. Shukla, A.K. Mishra, O.A. Arotiba, B.B. Mamba, Chitosan-based nanomaterials: A state-of-the-art review, International Journal of Biological Macromolecules 59 (2013) 46-58.
[151] G. Li, G. Cheng, H. Xue, S. Chen, F. Zhang, S. Jiang, Ultra low fouling zwitterionic polymers with a biomimetic adhesive group, Biomaterials 29(35) (2008) 4592-4597.
[152] H. Lee, S.M. Dellatore, W.M. Miller, P.B. Messersmith, Mussel-inspired surface chemistry for multifunctional coatings, Science (Washington, DC, U. S.) 318(5849) (2007) 426-430.

[153] H. Lee, J. Rho, P.B. Messersmith, Facile conjugation of biomolecules onto surfaces via mussel adhesive protein inspired coatings, Adv. Mater. (Weinheim, Ger.) 21(4) (2009) 431-434.
[154] A.W.G. Nijhuis, J.J.J.P. van den Beucken, J.A. Jansen, S.C.G. Leeuwenburgh, In vitro response to alkaline phosphatase coatings immobilized onto titanium implants using electrospray deposition or polydopamine-assisted deposition, J. Biomed. Mater. Res., Part A 102A(4) (2014) 1102-1109.
[155] D.H. Yang, S.W. Moon, G. Jang, K. Park, Y. Yoo, D.-W. Lee, Surface modification of titanium with β-CD/polydopamine for a controlled release of lovastatin, and its effect on the enhanced osteogenic activity, Journal of Industrial and Engineering Chemistry 49 (2017) 158-167.
[156] B.e. Nie, H. Ao, T. Long, J. Zhou, T. Tang, B. Yue, Immobilizing bacitracin on titanium for prophylaxis of infections and for improving osteoinductivity: An in vivo study, Colloids and Surfaces B: Biointerfaces 150 (2017) 183-191.
[157] R. Biran, D. Pond, Heparin coatings for improving blood compatibility of medical devices, Advanced Drug Delivery Reviews 112 (2017) 12-23.
[158] G. Li, P. Yang, X. Guo, N. Huang, R. Shen, An in vitro evaluation of inflammation response of titanium functionalized with heparin/fibronectin complex, Cytokine 56(2) (2011) 208-217.
[159] S. Suliman, Z. Xing, X. Wu, Y. Xue, T.O. Pedersen, Y. Sun, A.P. Døskeland, J. Nickel, T. Waag, H. Lygre, A. Finne-Wistrand, D. Steinmüller-Nethl, A. Krueger, K. Mustafa, Release and bioactivity of bone morphogenetic protein-2 are affected by scaffold binding techniques in vitro and in vivo, J. Control. Release 197 (2015) 148-157.
[160] S.-Y. Lee, Y.-P. Yun, H.-R. Song, H.J. Chun, D.H. Yang, K. Park, S.E. Kim, The effect of titanium with heparin/BMP-2 complex for improving osteoblast activity, Carbohydrate Polymers 98(1) (2013) 546-554.
[161] D.H. Yang, S.W. Moon, D.-W. Lee, Surface Modification of Titanium with BMP-2/GDF-5 by a Heparin Linker and Its Efficacy as a Dental Implant, Int. J. Mol. Sci. 18(1) (2017).
[162] C. Mateo, V. Grazu, J.M. Palomo, F. Lopez-Gallego, R. Fernandez-Lafuente, J.M. Guisan, Immobilization of enzymes on heterofunctional epoxy supports, Nat. Protocols 2(5) (2007) 1022-1033.
[163] E. Casero, M.D. Petit-Domínguez, L. Vázquez, I. Ramírez-Asperilla, A.M. Parra-Alfambra, F. Pariente, E. Lorenzo, Laccase biosensors based on different enzyme immobilization strategies for phenolic compounds determination, Talanta 115 (2013) 401-408.
[164] L.E. Englade-Franklin, C.K. Saner, J.C. Garno, Spatially selective surface platforms for binding fibrinogen prepared by particle lithography with organosilanes, Interface Focus 3(3) (2013) 20120102.
[165] G. Clayden, Warren & Wothers, 2008, Organic Chemistry 279-303.
[166] J. McMurry, E. Simanek, Fundamentals of organic chemistry, Thomson-Brooks/Cole2003.
[167] D.A. Puleo, Retention of enzymic activity immobilized on silanized Co-Cr-Mo and Ti-6Al-4V, J. Biomed. Mater. Res. 37(2) (1997) 222-228.
[168] A. Nanci, J.D. Wuest, L. Peru, P. Brunet, V. Sharma, S. Zalzal, M.D. McKee, Chemical modification of titanium surfaces for covalent attachment of biological molecules, J. Biomed. Mater. Res. 40(2) (1998) 324-335.
[169] W. Khan, M. Kapoor, N. Kumar, Covalent attachment of proteins to functionalized polypyrrole-coated metallic surfaces for improved biocompatibility, Acta Biomaterialia 3(4) (2007) 541-549.
[170] M. Alagem-Shafir, E. Kivovich, I. Tzchori, N. Lanir, M. Falah, M.Y. Flugelman, U. Dinnar, R. Beyar, N. Lotan, S.S. Sivan, The formation of an anti-restenotic/anti-thrombotic surface by immobilization of nitric oxide synthase on a metallic carrier, Acta Biomaterialia 10(5) (2014) 2304-2312.
[171] K. Fang, W. Song, L. Wang, S. Jia, H. Wei, S. Ren, X. Xu, Y. Song, Immobilization of chitosan film containing semaphorin 3A onto a microarc oxidized titanium implant surface via silane reaction to improve MG63 osteogenic differentiation, Int. J. Nanomed. 9 (2014) 4649-4657.

[172] J. Kang, S. Tada, T. Kitajima, T.I. Son, T. Aigaki, Y. Ito, Immobilization of bone morphogenetic protein on DOPA-or dopamine-treated titanium surfaces to enhance osseointegration, BioMed research international 2013 (2013).
[173] M.J.B. Wissink, R. Beernink, J.S. Pieper, A.A. Poot, G.H.M. Engbers, T. Beugeling, W.G. van Aken, J. Feijen, Immobilization of heparin to EDC/NHS-crosslinked collagen. Characterization and in vitro evaluation, Biomaterials 22(2) (2001) 151-163.
[174] Y.J. Weng, F. Qi, N. Huang, J. Wang, J.Y. Cheng, Y.X. Leng, Photochemical immobilization of bovine serum albumin on Ti–O and evaluations in vitro and in vivo, Applied Surface Science 255(2) (2008) 489-493.
[175] A. Mahapatro, Bio-functional nano-coatings on metallic biomaterials, Mater. Sci. Eng. C 55 (2015) 227-251.
[176] N. Metoki, L. Liu, E. Beilis, N. Eliaz, D. Mandler, Preparation and characterization of alkylphosphonic acid self-assembled monolayers on titanium alloy by chemisorption and electrochemical deposition, Langmuir 30(23) (2014) 6791-6799.
[177] A. Mahapatro, Bio-functional nano-coatings on metallic biomaterials, Materials Science and Engineering: C 55 (2015) 227-251.
[178] C. Lorenz, A. Hoffmann, G. Gross, H. Windhagen, P. Dellinger, K. Möhwald, W. Dempwolf, H. Menzel, Coating of Titanium Implant Materials with Thin Polymeric Films for Binding the Signaling Protein BMP2, Macromol. Biosci. 11(2) (2011) 234-244.
[179] L. Tack, K. Schickle, F. Böke, H. Fischer, Immobilization of specific proteins to titanium surface using self-assembled monolayer technique, Dental Materials 31(10) (2015) 1169-1179.
[180] P. Innocenzi, C. Figus, T. Kidchob, M. Valentini, B. Alonso, M. Takahashi, Sol-gel reactions of 3-glycidoxypropyltrimethoxysilane in a highly basic aqueous solution, Dalton Trans. (42) (2009) 9146-9152.
[181] R. Müller, J. Abke, E. Schnell, F. Macionczyk, U. Gbureck, R. Mehrl, Z. Ruszczak, R. Kujat, C. Englert, M. Nerlich, P. Angele, Surface engineering of stainless steel materials by covalent collagen immobilization to improve implant biocompatibility, Biomaterials 26(34) (2005) 6962-6972.
[182] R. Müller, J. Abke, E. Schnell, D. Scharnweber, R. Kujat, C. Englert, D. Taheri, M. Nerlich, P. Angele, Influence of surface pretreatment of titanium- and cobalt-based biomaterials on covalent immobilization of fibrillar collagen, Biomaterials 27(22) (2006) 4059-4068.
[183] K. Zhang, J.-y. Chen, W. Qin, J.-a. Li, F.-x. Guan, N. Huang, Constructing bio-layer of heparin and type IV collagen on titanium surface for improving its endothelialization and blood compatibility, Journal of Materials Science: Materials in Medicine 27(4) (2016) 81.
[184] D. Yang, S. Moon, D.-W. Lee, Surface Modification of Titanium with BMP-2/GDF-5 by a Heparin Linker and Its Efficacy as a Dental Implant, Int. J. Mol. Sci. 18(1) (2017) 229.
[185] E. Vanderleyden, S. Van Bael, Y.C. Chai, J.P. Kruth, J. Schrooten, P. Dubruel, Gelatin functionalised porous titanium alloy implants for orthopaedic applications, Materials Science and Engineering: C 42(0) (2014) 396-404.
[186] A. Simchi, F. Pishbin, A.R. Boccaccini, Electrophoretic deposition of chitosan, Materials Letters 63(26) (2009) 2253-2256.
[187] T.Y. Lim, W. Wang, Z. Shi, C.K. Poh, K.G. Neoh, Human bone marrow-derived mesenchymal stem cells and osteoblast differentiation on titanium with surface-grafted chitosan and immobilized bone morphogenetic protein-2, Journal of Materials Science: Materials in Medicine 20(1) (2008) 1.
[188] K. Shin, C.S. Kim, Application of EQCN for quantitative analysis of alkanethiol adsorbed on modified Ti surfaces, Mater. Sci. Eng., C C23(3) (2003) 407-411.
[189] X. Han, X. Sun, T. He, S. Sun, Formation of Highly Stable Self-Assembled Alkyl Phosphonic Acid Monolayers for the Functionalization of Titanium Surfaces and Protein Patterning, Langmuir 31(1) (2015) 140-148.
[190] P.K. Chu, J.Y. Chen, L.P. Wang, N. Huang, Plasma-surface modification of biomaterials, Materials Science and Engineering: R: Reports 36(5–6) (2002) 143-206.

[191] S. Eliezer, Y. Eliezer, The fourth state of matter: an introduction to plasma science, CRC Press2001.
[192] M.A. Lieberman, A.J. Lichtenberg, Principles of plasma discharges and materials processing, John Wiley & Sons2005.
[193] N. Inagaki, Plasma surface modification and plasma polymerization, CRC Press1996.
[194] J. Friedrich, The plasma chemistry of polymer surfaces: advanced techniques for surface design, John Wiley & Sons2012.
[195] A. Michelmore, D.A. Steele, J.D. Whittle, J.W. Bradley, R.D. Short, Nanoscale deposition of chemically functionalised films via plasma polymerisation, RSC Advances 3(33) (2013) 13540-13557.
[196] R. Messier, S. Trolier-McKinstry, Thin-film Processes A2 - Buschow, K.H. Jürgen, in: R.W. Cahn, M.C. Flemings, B. Ilschner, E.J. Kramer, S. Mahajan, P. Veyssière (Eds.), Encyclopedia of Materials: Science and Technology (Second Edition), Elsevier, Oxford, 2001, pp. 9306-9313.
[197] D.M. Vranceanu, C.M. Cotrut, M. Bramowicz, I. Titorencu, S. Kulesza, A. Kiss, A. Berbecaru, V. Pruna, M. Branzei, A. Vladescu, Osseointegration of sputtered SiC-added hydroxyapatite for orthopaedic applications, Ceramics International 42(8) (2016) 10085-10093.
[198] M.A. Surmeneva, E.A. Chudinova, I.Y. Grubova, O.S. Korneva, I.A. Shulepov, A.D. Teresov, N.N. Koval, J. Mayer, C. Oehr, R.A. Surmenev, Effect of pulsed electron beam treatment on the physico-mechanical properties of hydroxyapatite-coated titanium, Ceramics International 42(1) (2016) 1470-1475.
[199] M. Bramowicz, L. Braic, F.A. Azem, S. Kulesza, I. Birlik, A. Vladescu, Mechanical properties and fractal analysis of the surface texture of sputtered hydroxyapatite coatings, Applied Surface Science 379 (2016) 338-346.
[200] J.N. Yewle, Y. Wei, D.A. Puleo, S. Daunert, L.G. Bachas, Oriented Immobilization of Proteins on Hydroxyapatite Surface Using Bifunctional Bisphosphonates as Linkers, Biomacromolecules 13(6) (2012) 1742-1749.
[201] S.V. Dorozhkin, Calcium orthophosphate deposits: Preparation, properties and biomedical applications, Materials Science and Engineering: C 55 (2015) 272-326.
[202] P.H. Li, P.K. Chu, 1 - Thin film deposition technologies and processing of biomaterials A2 - Griesser, Hans J, Thin Film Coatings for Biomaterials and Biomedical Applications, Woodhead Publishing2016, pp. 3-28.
[203] M.A. Surmeneva, R.A. Surmenev, A.I. Tyurin, T.M. Mukhametkaliyev, A.D. Teresov, N.N. Koval, T.S. Pirozhkova, I.A. Shuvarin, C. Oehr, Comparative study of the radio-frequency magnetron sputter deposited CaP films fabricated onto acid-etched or pulsed electron beam-treated titanium, Thin Solid Films 571 (2014) 218-224.
[204] I. Castellini, L. Andreani, P.D. Parchi, E. Bonicoli, N. Piolanti, F. Risoli, M. Lisanti, Hydroxyapatite in total hip arthroplasty. Our experience with a plasma spray porous titanium alloy/hydroxyapatite double-coated cementless stem, Clinical Cases in Mineral and Bone Metabolism 13(3) (2016) 221-227.
[205] J.E. Biemond, T.S. Eufrásio, G. Hannink, N. Verdonschot, P. Buma, Assessment of bone ingrowth potential of biomimetic hydroxyapatite and brushite coated porous E-beam structures, Journal of materials science. Materials in medicine 22(4) (2011) 917-925.
[206] D.M. Mattox, Handbook of Physical Vapor Deposition (Pvd) Processing, Elsevier, London, 2010.
[207] F. Khelifa, S. Ershov, Y. Habibi, R. Snyders, P. Dubois, Free-Radical-Induced Grafting from Plasma Polymer Surfaces, Chemical Reviews 116(6) (2016) 3975-4005.
[208] B.R. Coad, M. Jasieniak, S.S. Griesser, H.J. Griesser, Controlled covalent surface immobilisation of proteins and peptides using plasma methods, Surface and Coatings Technology 233 (2013) 169-177.
[209] M. Morra, C. Cassinelli, G. Cascardo, P. Cahalan, L. Cahalan, M. Fini, R. Giardino, Surface engineering of titanium by collagen immobilization. Surface characterization and in vitro and in vivo studies, Biomaterials 24(25) (2003) 4639-4654.

[210] M. Yoshinari, T. Hayakawa, K. Matsuzaka, T. Inoue, Y. Oda, M. Shimono, T. Ide, T. Tanaka, Oxygen plasma surface modification enhances immobilization of simvastatin acid, Biomed. Res. 27(1) (2006) 29-36.
[211] B. Finke, F. Luethen, K. Schroeder, P.D. Mueller, C. Bergemann, M. Frant, A. Ohl, B.J. Nebe, The effect of positively charged plasma polymerization on initial osteoblastic focal adhesion on titanium surfaces, Biomaterials 28(30) (2007) 4521-4534.
[212] B. Thierry, M. Jasieniak, L.C.P.M. de Smet, K. Vasilev, H.J. Griesser, Reactive Epoxy-Functionalized Thin Films by a Pulsed Plasma Polymerization Process, Langmuir 24(18) (2008) 10187-10195.
[213] T. He, Z. Yang, R. Chen, J. Wang, Y. Leng, H. Sun, N. Huang, Enhanced endothelialization guided by fibronectin functionalized plasma polymerized acrylic acid film, Materials Science and Engineering: C 32(5) (2012) 1025-1031.
[214] M. Heller, P.W. Kaemmerer, B. Al-Nawas, M.-A. Luszpinski, R. Foerch, J. Brieger, The effect of extracellular matrix proteins on the cellular response of HUVECS and HOBS after covalent immobilization onto titanium, J. Biomed. Mater. Res., Part A 103(6) (2015) 2035-2044.
[215] X. Ren, Y. Wu, Y. Cheng, H. Ma, S. Wei, Fibronectin and Bone Morphogenetic Protein-2-Decorated Poly(OEGMA-r-HEMA) Brushes Promote Osseointegration of Titanium Surfaces, Langmuir 27(19) (2011) 12069-12073.
[216] K.S. Siow, L. Britcher, S. Kumar, H.J. Griesser, Plasma methods for the generation of chemically reactive surfaces for biomolecule immobilization and cell colonization - a review, Plasma Processes Polym. 3(6/7) (2006) 392-418.
[217] M.M.M. Bilek, Biofunctionalization of surfaces by energetic ion implantation: Review of progress on applications in implantable biomedical devices and antibody microarrays, Applied Surface Science 310 (2014) 3-10.
[218] D.A. Puleo, R.A. Kissling, M.S. Sheu, A technique to immobilize bioactive proteins, including bone morphogenetic protein-4 (BMP-4), on titanium alloy, Biomaterials 23(9) (2002) 2079-2087.
[219] B.R. Coad, T. Bilgic, H.-A. Klok, Polymer brush gradients grafted from plasma-polymerized surfaces, Langmuir 30(28) (2014) 8357-8365.
[220] S. Ershov, F. Khelifa, P. Dubois, R. Snyders, Derivatization of free radicals in an isopropanol plasma polymer film: The first step toward polymer grafting, ACS Applied Materials and Interfaces 5(10) (2013) 4216-4223.
[221] S. Ershov, F. Khelifa, V. Lemaur, J. Cornil, D. Cossement, Y. Habibi, P. Dubois, R. Snyders, Free radical generation and concentration in a plasma polymer: The effect of aromaticity, ACS Applied Materials and Interfaces 6(15) (2014) 12395-12405.
[222] J.J. Keating, J. Imbrogno, G. Belfort, Polymer Brushes for Membrane Separations: A Review, ACS Applied Materials and Interfaces 8(42) (2016) 28383-28399.
[223] M. Krishnamoorthy, S. Hakobyan, M. Ramstedt, J.E. Gautrot, Surface-initiated polymer brushes in the biomedical field: Applications in membrane science, biosensing, cell culture, regenerative medicine and antibacterial coatings, Chemical Reviews 114(21) (2014) 10976-11026.
[224] Z. Qu, K. Chen, H. Gu, H. Xu, Covalent Immobilization of Proteins on 3D Poly(acrylic acid) Brushes: Mechanism Study and a More Effective and Controllable Process, Bioconjugate Chemistry 25(2) (2014) 370-378.
[225] O. Hollmann, C. Czeslik, Characterization of a Planar Poly(acrylic acid) Brush as a Materials Coating for Controlled Protein Immobilization, Langmuir 22(7) (2006) 3300-3305.
[226] A.L.S. Burzava, M. Jasieniak, M.P. Cockshell, C.S. Bonder, F.J. Harding, H.J. Griesser, N.H. Voelcker, Affinity Binding of EMR2 Expressing Cells by Surface-Grafted Chondroitin Sulfate B, Biomacromolecules (2017) Ahead of Print.
[227] S. Babaei, P.-L. Girard-Lauriault, Tuning the Surface Properties of Oxygen-Rich and Nitrogen-Rich Plasma Polymers: Functional Groups and Surface Charge, Plasma Chemistry and Plasma Processing 36(2) (2016) 651-666.

[228] A. Manakhov, M. Michlíček, D. Nečas, J. Polčák, E. Makhneva, M. Eliáš, L. Zajíčková, Carboxyl-rich coatings deposited by atmospheric plasma co-polymerization of maleic anhydride and acetylene, Surface and Coatings Technology 295 (2016) 37-45.
[229] X. Gong, H.J. Griesser, Excitation Frequency Dependence of the Surface Properties and Composition of Plasma Polymers from Aldehyde Monomers, Plasmas and Polymers 2(4) (1997) 261-276.
[230] A. Hadjizadeh, Acetaldehyde plasma polymer-coated PET fibers for endothelial cell patterning: chemical, topographical, and biological analysis, J. Biomed. Mater. Res., Part B 94B(1) (2010) 11-21.
[231] S.W. Myung, H.S. Choi, Chemical structure and surface morphology of plasma polymerized-allylamine film, Korean Journal of Chemical Engineering 23(3) (2006) 505-511.
[232] F. Basarir, N. Cuong, W.K. Song, T.H. Yoon, Surface modification via plasma polymerization of allylamine for antibody immobilization, Macromolecular symposia, Wiley Online Library, 2007, pp. 61-66.
[233] A. Abbas, C. Vivien, B. Bocquet, D. Guillochon, P. Supiot, Preparation and Multi-Characterization of Plasma Polymerized Allylamine Films, Plasma Processes and Polymers 6(9) (2009) 593-604.
[234] J.C. Ruiz, A. St-Georges-Robillard, C. Thérésy, S. Lerouge, M.R. Wertheimer, Fabrication and Characterisation of Amine-Rich Organic Thin Films: Focus on Stability, Plasma Processes and Polymers 7(9-10) (2010) 737-753.
[235] H. Yasuda, C.R. Wang, Plasma polymerization investigated by the substrate temperature dependence, Journal of Polymer Science: Polymer Chemistry Edition 23(1) (1985) 87-106.
[236] D. Hegemann, E. Koerner, S. Guimond, Plasma polymerization of acrylic acid revisited, Plasma Processes and Polymers 6(4) (2009) 246-254.
[237] A. Manakhov, M. Landová, J. Medalová, M. Michlíček, J. Polčák, D. Nečas, L. Zajíčková, Cyclopropylamine plasma polymers for increased cell adhesion and growth, Plasma Processes and Polymers 14(7) (2017) 1600123-n/a.
[238] H.J. Griesser, R.C. Chatelier, T.R. Gengenbach, G. Johnson, J.G. Steele, Growth of human cells on plasma polymers: Putative role of amine and amide groups, Journal of Biomaterials Science, Polymer Edition 5(6) (1994) 531-554.
[239] L. Štrbková, A. Manakhov, L. Zajíčková, A. Stoica, P. Veselý, R. Chmelík, The adhesion of normal human dermal fibroblasts to the cyclopropylamine plasma polymers studied by holographic microscopy, Surface & Coatings Technology (295) (2016) 70-77.
[240] B. Finke, H. Rebl, F. Hempel, J. Schäfer, K. Liefeith, K.-D. Weltmann, J.B. Nebe, Aging of Plasma-Polymerized Allylamine Nanofilms and the Maintenance of Their Cell Adhesion Capacity, Langmuir 30(46) (2014) 13914-13924.
[241] P.-Y. Wang, L.R. Clements, H. Thissen, W.-B. Tsai, N.H. Voelcker, Screening rat mesenchymal stem cell attachment and differentiation on surface chemistries using plasma polymer gradients, Acta Biomaterialia 11 (2015) 58-67.
[242] K. Schröder, B. Finke, A. Ohl, F. Lüthen, C. Bergemann, B. Nebe, J. Rychly, U. Walschus, M. Schlosser, K. Liefeith, H.G. Neumann, K.D. Weltmann, Capability of Differently Charged Plasma Polymer Coatings for Control of Tissue Interactions with Titanium Surfaces, Journal of Adhesion Science and Technology 24(7) (2010) 1191-1205.
[243] S.-C. Jung, K. Lee, B.-H. Kim, Biocompatibility of plasma polymerized sandblasted large grit and acid titanium surface, Thin Solid Films 521 (2012) 150-154.
[244] X. Liu, Q. Feng, A. Bachhuka, K. Vasilev, Surface modification by allylamine plasma polymerization promotes osteogenic differentiation of human adipose-derived stem cells, ACS Appl. Mater. Interfaces 6(12) (2014) 9733-9741.
[245] K.R. Diener, S.N. Christo, S.S. Griesser, G.T. Sarvestani, K. Vasilev, H.J. Griesser, J.D. Hayball, Solid-state capture and real-time analysis of individual T cell activation via self-assembly of binding multimeric proteins on functionalized materials surfaces, Acta Biomaterialia 8(1) (2012) 99-107.

[246] B.R. Coad, T. Scholz, K. Vasilev, J.D. Hayball, R.D. Short, H.J. Griesser, Functionality of proteins bound to plasma polymer surfaces, ACS Appl. Mater. Interfaces 4(5) (2012) 2455-2463.
[247] X. Deng, J. Lahann, A Generic Strategy for Co-Presentation of Heparin-Binding Growth Factors Based on CVD Polymerization, Macromolecular Rapid Communications 33(17) (2012) 1459-1465.
[248] T.M. Blättler, S. Pasche, M. Textor, H.J. Griesser, High salt stability and protein resistance of poly (L-lysine)-g-poly (ethylene glycol) copolymers covalently immobilized via aldehyde plasma polymer interlayers on inorganic and polymeric substrates, Langmuir 22(13) (2006) 5760-5769.
[249] B.R. Coad, S.J. Lamont-Friedrich, L. Gwynne, M. Jasieniak, S.S. Griesser, A. Traven, A.Y. Peleg, H.J. Griesser, Surface coatings with covalently attached caspofungin are effective in eliminating fungal pathogens, Journal of Materials Chemistry B 3(43) (2015) 8469-8476.
[250] N. Inagaki, S. Tasaka, Y. Horikawa, Durable, hydrophilic surface modification of polypropylene films by plasma graft polymerization of glycidyl methacrylate, Polymer Bulletin 26(3) (1991) 283-289.
[251] C. Oehr, M. Müller, B. Elkin, D. Hegemann, U. Vohrer, Plasma grafting — a method to obtain monofunctional surfaces, Surface and Coatings Technology 116–119 (1999) 25-35.
[252] C. Tarducci, E.J. Kinmond, J.P.S. Badyal, S.A. Brewer, C. Willis, Epoxide-Functionalized Solid Surfaces, Chemistry of Materials 12(7) (2000) 1884-1889.
[253] L.-Q. Chu, W. Knoll, R. Förch, Plasma polymerized epoxide functional surfaces for DNA probe immobilization, Biosensors and Bioelectronics 24(1) (2008) 118-122.
[254] G. Camporeale, M. Moreno-Couranjou, S. Bonot, R. Mauchauffé, N.D. Boscher, C. Bebrone, C.V.d. Weerdt, H.M. Cauchie, P. Favia, P. Choquet, Atmospheric-Pressure Plasma Deposited Epoxy-Rich Thin Films as Platforms for Biomolecule Immobilization—Application for Anti-Biofouling and Xenobiotic-Degrading Surfaces, Plasma Processes and Polymers 12(11) (2015) 1208-1219.
[255] K. Vasilev, Nanoengineered Plasma Polymer Films for Biomaterial Applications, Plasma Chemistry and Plasma Processing 34(3) (2014) 545-558.
[256] G.S. Shin, B.H. Kim, Y.H. Hwang, Y.M. Ko, Plasma Polymerization of 1,2-Diaminocyclohexane for Covalent Bonding of Bone Morphogenic Protein-2 on Titanium Surface, Journal of nanoscience and nanotechnology 15(8) (2015) 5624.
[257] P. Rivolo, S.M. Severino, S. Ricciardi, F. Frascella, F. Geobaldo, Protein immobilization on nanoporous silicon functionalized by RF activated plasma polymerization of Acrylic Acid, Journal of Colloid and Interface Science 416 (2014) 73-80.
[258] L. O'Toole, A.J. Beck, R.D. Short, Characterization of Plasma Polymers of Acrylic Acid and Propanoic Acid, Macromolecules 29(15) (1996) 5172-5177.
[259] A. Choukourov, I. Gordeev, J. Ponti, C. Uboldi, I. Melnichuk, M. Vaidulych, J. Kousal, D. Nikitin, L. Hanyková, I. Krakovský, D. Slavínská, H. Biederman, Microphase-Separated PE/PEO Thin Films Prepared by Plasma-Assisted Vapor Phase Deposition, ACS Appl. Mater. Interfaces 8(12) (2016) 8201.
[260] N.J. Nosworthy, J.P.Y. Ho, A. Kondyurin, D.R. McKenzie, M.M.M. Bilek, The attachment of catalase and poly-l-lysine to plasma immersion ion implantation-treated polyethylene, Acta Biomaterialia 3(5) (2007) 695-704.
[261] H. Hajian, S.G. Wise, D.V. Bax, A. Kondyurin, A. Waterhouse, L.L. Dunn, C.M. Kielty, Y. Yu, A.S. Weiss, M.M.M. Bilek, P.G. Bannon, M.K.C. Ng, Immobilisation of a fibrillin-1 fragment enhances the biocompatibility of PTFE, Colloids and Surfaces B: Biointerfaces 116 (2014) 544-552.
[262] H. Main, J. Radenkovic, E. Kosobrodova, D. McKenzie, M. Bilek, U. Lendahl, Cell surface antigen profiling using a novel type of antibody array immobilised to plasma ion-implanted polycarbonate, Cellular and Molecular Life Sciences 71(19) (2014) 3841-3857.
[263] S.L. Hirsh, M.M.M. Bilek, N.J. Nosworthy, A. Kondyurin, C.G. dos Remedios, D.R. McKenzie, A Comparison of Covalent Immobilization and Physical Adsorption of a Cellulase Enzyme Mixture, Langmuir 26(17) (2010) 14380-14388.
[264] M.M.M. Bilek, D.V. Bax, A. Kondyurin, Y. Yin, N.J. Nosworthy, K. Fisher, A. Waterhouse, A.S. Weiss, C.G. dos Remedios, D.R. McKenzie, Free radical functionalization of surfaces to prevent adverse responses to biomedical devices, Proceedings of the National Academy of Sciences 108(35) (2011) 14405-14410.

[265] A. Waterhouse, S.G. Wise, Y. Yin, B. Wu, B. James, H. Zreiqat, D.R. McKenzie, S. Bao, A.S. Weiss, M.K.C. Ng, M.M.M. Bilek, In vivo biocompatibility of a plasma-activated, coronary stent coating, Biomaterials 33(32) (2012) 7984-7992.
[266] A. Waterhouse, Y. Yin, S.G. Wise, D.V. Bax, D.R. McKenzie, M.M.M. Bilek, A.S. Weiss, M.K.C. Ng, The immobilization of recombinant human tropoelastin on metals using a plasma-activated coating to improve the biocompatibility of coronary stents, Biomaterials 31(32) (2010) 8332-8340.
[267] Y. Yin, S.G. Wise, N.J. Nosworthy, A. Waterhouse, D.V. Bax, H. Youssef, M.J. Byrom, M.M.M. Bilek, D.R. McKenzie, A.S. Weiss, M.K.C. Ng, Covalent immobilisation of tropoelastin on a plasma deposited interface for enhancement of endothelialisation on metal surfaces, Biomaterials 30(9) (2009) 1675-1681.
[268] A. Kondyurin, M. Bilek, 9 - Biological and medical applications, Ion Beam Treatment of Polymers, Elsevier, Amsterdam, 2008, pp. 205-241.
[269] E. Wakelin, G. Yeo, A. Kondyurin, M. Davies, D. McKenzie, A. Weiss, M. Bilek, Bio-functionalisation of polyether ether ketone using plasma immersion ion implantation, SPIE Micro+ Nano Materials, Devices, and Applications, International Society for Optics and Photonics, 2015, pp. 96685R-96685R-9.
[270] A. Kondyurin, P. Naseri, K. Fisher, D.R. McKenzie, M.M.M. Bilek, Mechanisms for surface energy changes observed in plasma immersion ion implanted polyethylene: The roles of free radicals and oxygen-containing groups, Polymer Degradation and Stability 94(4) (2009) 638-646.
[271] E. Kosobrodova, R.T. Jones, A. Kondyurin, W. Chrzanowski, P.J. Pigram, D.R. McKenzie, M.M.M. Bilek, Orientation and conformation of anti-CD34 antibody immobilised on untreated and plasma treated polycarbonate, Acta Biomaterialia 19 (2015) 128-137.
[272] C.H. Yang, Y.C. Li, W.F. Tsai, C.F. Ai, H.H. Huang, Oxygen plasma immersion ion implantation treatment enhances the human bone marrow mesenchymal stem cells responses to titanium surface for dental implant application, Clin. Oral Implants Res. 26(2) (2015) 166-175.
[273] S. Qiao, H. Cao, X. Zhao, H. Lo, L. Zhuang, Y. Gu, J. Shi, X. Liu, H. Lai, Ag-plasma modification enhances bone apposition around titanium dental implants: An animal study in labrador dogs, International Journal of Nanomedicine 10 (2015) 653-664.
[274] M. Cheng, Y. Qiao, Q. Wang, G. Jin, H. Qin, Y. Zhao, X. Peng, X. Zhang, X. Liu, Calcium Plasma Implanted Titanium Surface with Hierarchical Microstructure for Improving the Bone Formation, ACS Applied Materials and Interfaces 7(23) (2015) 13053-13061.
[275] J. Fang, J. Zhao, Y. Sun, H. Ma, X. Yu, Y. Ma, Y. Ni, L. Zheng, Y. Zhou, Biocompatibility and antibacterial properties of zinc-ion implantation on titanium, Journal of Hard Tissue Biology 23(1) (2014) 35-43.
[276] S. Han, H. Kim, Y. Lee, J. Lee, S.-G. Kim, Plasma source ion implantation of nitrogen, carbon and oxygen into Ti-6Al-4V alloy, Surface and Coatings Technology 82(3) (1996) 270-276.
[277] P. Vlcak, F. Cerny, J. Drahokoupil, J. Sepitka, Z. Tolde, The microstructure and surface hardness of Ti6Al4V alloy implanted with nitrogen ions at an elevated temperature, Journal of Alloys and Compounds 620 (2015) 48-54.
[278] F. Hempel, B. Finke, C. Zietz, R. Bader, K.D. Weltmann, M. Polak, Antimicrobial surface modification of titanium substrates by means of plasma immersion ion implantation and deposition of copper, Surface and Coatings Technology 256 (2014) 52-58.
[279] A. Meyer-Plath, Identification of Surface Radicals on Polymers, Vakuum in Forschung und Praxis 17(S1) (2005) 40-46.
[280] A. Kondyurin, O. Polonskyi, N. Nosworthy, J. Matousek, P. Hlidek, H. Biederman, M.M.M. Bilek, Covalent Attachment and Bioactivity of Horseradish Peroxidase on Plasma-Polymerized Hexane Coatings, Plasma Processes and Polymers 5(8) (2008) 727-736.
[281] M.I. Jamesh, R.L. Boxman, N.J. Nosworthy, I.S. Falconer, P.K. Chu, M.M.M. Bilek, A. Kondyurin, R. Ganesan, D.R. McKenzie, Graded metal carbon protein binding films prepared by hybrid cathodic arc — Glow discharge plasma assisted chemical vapor deposition, Surface and Coatings Technology 265 (2015) 222-234.

[282] Y. Yin, N.J. Nosworthy, H. Youssef, B. Gong, M.M.M. Bilek, D.R. McKenzie, Acetylene plasma coated surfaces for covalent immobilization of proteins, Thin Solid Films 517(17) (2009) 5343-5346.
[283] Y. Yin, N.J. Nosworthy, B. Gong, D. Bax, A. Kondyurin, D.R. McKenzie, M.M. Bilek, Plasma polymer surfaces compatible with a CMOS process for direct covalent enzyme immobilization, Plasma Processes and Polymers 6(1) (2009) 68-75.
[284] Y. Yin, M.M. Bilek, K. Fisher, C. Guo, D.R. McKenzie, An integrated solution for rapid biosensing with robust linker free covalent bindingsurfaces, Biosensors and Bioelectronics 42 (2013) 447-452.
[285] Y. Yin, K. Fisher, N.J. Nosworthy, D. Bax, S. Rubanov, B. Gong, A.S. Weiss, D.R. McKenzie, M.M.M. Bilek, Covalently Bound Biomimetic Layers on Plasma Polymers with Graded Metallic Interfaces for in vivo Implants, Plasma Processes and Polymers 6(10) (2009) 658-666.
[286] B. Akhavan, S.G. Wise, M.M.M. Bilek, Substrate-Regulated Growth of Plasma-Polymerized Films on Carbide-Forming Metals, Langmuir 32(42) (2016) 10835-10843.
[287] W. Chrzanowski, J.H. Lee, A. Kondyurin, M.S. Lord, J.-H. Jang, H.-W. Kim, M.M.M. Bilek, Nano-Bio-Chemical Braille for Cells: The Regulation of Stem Cell Responses using Bi-Functional Surfaces, Advanced Functional Materials 25(2) (2015) 193-205.
[288] H. Yasuda, Y. Matsuzawa, Economical advantages of low-pressure plasma polymerization coating, Plasma Processes and Polymers 2(6) (2005) 507-512.
[289] A. Belkind, S. Gershman, Plasma cleaning of surfaces, Vacuum Coating and Technology November (2008) 46-57.
[290] J. Friedrich, Mechanisms of Plasma Polymerization – Reviewed from a Chemical Point of View, Plasma Processes and Polymers 8(9) (2011) 783-802.
[291] B. Akhavan, K. Jarvis, P. Majewski, Evolution of Hydrophobicity in Plasma Polymerised 1, 7-Octadiene Films, Plasma Processes and Polymers 10(11) (2013) 1018-1029.
[292] T.R. Gengenbach, R.C. Chatelier, H.J. Griesser, Characterization of the Ageing of Plasma-deposited Polymer Films: Global Analysis of X-ray Photoelectron Spectroscopy Data, Surface and Interface Analysis 24(4) (1996) 271-281.
[293] B. Akhavan, K. Jarvis, P. Majewski, Tuning the hydrophobicity of plasma polymer coated silica particles, Powder technology 249 (2013) 403-411.
[294] T.R. Gengenbach, Z.R. Vasic, S. Li, R.C. Chatelier, H.J. Griesser, Contributions of restructuring and oxidation to the aging of the surface of plasma polymers containing heteroatoms, Plasmas and Polymers 2(2) (1997) 91-114.
[295] D. Hegemann, E. Lorusso, M.-I. Butron-Garcia, N.m.E. Blanchard, P. Rupper, P. Favia, M. Heuberger, M. Vandenbossche, Suppression of hydrophobic recovery by plasma polymer films with vertical chemical gradients, Langmuir 32(3) (2016) 651-654.
[296] C. López-Santos, F. Yubero, J. Cotrino, A.n.R. González-Elipe, Surface functionalization, oxygen depth profiles, and wetting behavior of PET treated with different nitrogen plasmas, ACS Appl. Mater. Interfaces 2(4) (2010) 980-990.
[297] E. Bormashenko, G. Chaniel, R. Grynyov, Towards understanding hydrophobic recovery of plasma treated polymers: Storing in high polarity liquids suppresses hydrophobic recovery, Applied Surface Science 273 (2013) 549-553.
[298] E. Bormashenko, G. Chaniel, O. Gendelman, Hydrophilization and hydrophobic recovery in polymers obtained by casting of polymer solutions on water surface, Journal of Colloid and Interface Science 435 (2014) 192-197.
[299] N.L. Burns, K. Holmberg, C. Brink, Influence of Surface Charge on Protein Adsorption at an Amphoteric Surface: Effects of Varying Acid to Base Ratio, Journal of Colloid and Interface Science 178(1) (1996) 116-122.
[300] S. Swaraj, U. Oran, A. Lippitz, J.F. Friedrich, W.E.S. Unger, Aging of Plasma-Deposited Films Prepared from Organic Monomers, Plasma Processes and Polymers 4(S1) (2007) S784-S789.
[301] B. Akhavan, B. Menges, R. Förch, Inhomogeneous Growth of Micrometer Thick Plasma Polymerized Films, Langmuir 32(19) (2016) 4792-4799.

[302] A. Michelmore, P. Martinek, V. Sah, R.D. Short, K. Vasilev, Surface Morphology in the Early Stages of Plasma Polymer Film Growth from Amine-Containing Monomers, Plasma Processes and Polymers 8(5) (2011) 367-372.
[303] K. Vasilev, A. Michelmore, P. Martinek, J. Chan, V. Sah, H.J. Griesser, R.D. Short, Early Stages of Growth of Plasma Polymer Coatings Deposited from Nitrogen- and Oxygen-Containing Monomers, Plasma Processes and Polymers 7(9-10) (2010) 824-835.
[304] K. Vasilev, A. Michelmore, H.J. Griesser, R.D. Short, Substrate influence on the initial growth phase of plasma-deposited polymer films, Chemical communications (24) (2009) 3600-3602.
[305] R.T. Chen, B.W. Muir, L. Thomsen, A. Tadich, B.C. Cowie, G.K. Such, A. Postma, K.M. McLean, F. Caruso, New insights into the substrate–plasma polymer interface, The Journal of Physical Chemistry B 115(20) (2011) 6495-6502.
[306] K. Furuya, R. Nakanishi, H. Okumura, M. Makita, A. Harata, Influence of substrate type on surface structure of polymeric perfluorocarbon in the initial stage of deposition in Ar/c-C 4 F 8 plasmas, Thin Solid Films 516(18) (2008) 6028-6032.
[307] W. Asghar, M. Yuksekkaya, H. Shafiee, M. Zhang, M.O. Ozen, F. Inci, M. Kocakulak, U. Demirci, Engineering long shelf life multi-layer biologically active surfaces on microfluidic devices for point of care applications, Scientific Reports 6 (2016) 21163.
[308] B. Akhavan, K. Jarvis, P. Majewski, Plasma polymerization of sulfur-rich and water-stable coatings on silica particles, Surface and Coatings Technology 264 (2015) 72-79.
[309] P. Rupper, M. Vandenbossche, L. Bernard, D. Hegemann, M. Heuberger, Composition and Stability of Plasma Polymer Films Exhibiting Vertical Chemical Gradients, Langmuir 33(9) (2017) 2340-2352.
[310] Y. Kusano, Atmospheric Pressure Plasma Processing for Polymer Adhesion: A Review, The Journal of Adhesion 90(9) (2014) 755-777.
[311] S. Lerouge, J. Barrette, J.-C. Ruiz, M. Sbai, H. Savoji, B. Saoudi, M. Gauthier, M.R. Wertheimer, Nitrogen-Rich Plasma Polymer Coatings for Biomedical Applications: Stability, Mechanical Properties and Adhesion Under Dry and Wet Conditions, Plasma Processes and Polymers 12(9) (2015) 882-895.
[312] K. Schroeder, B. Finke, A. Ohl, F. Luethen, C. Bergemann, B. Nebe, J. Rychly, U. Walschus, M. Schlosser, K. Liefeith, H.G. Neumann, K.D. Weltmann, Capability of differently charged plasma polymer coatings for control of tissue interactions with titanium surfaces, J. Adhes. Sci. Technol. 24(7) (2010) 1191-1205.
[313] D.E. Robinson, D.J. Buttle, J.D. Whittle, K.L. Parry, R.D. Short, D.A. Steele, The Substrate and Composition Dependence of Plasma Polymer Stability, Plasma Processes and Polymers 7(2) (2010) 102-106.
[314] S. Zanini, R. Ziano, C. Riccardi, Stable Poly(Acrylic Acid) Films from Acrylic Acid/Argon Plasmas: Influence of the Mixture Composition and the Reactor Geometry on the Thin Films Chemical Structures, Plasma Chemistry and Plasma Processing 29(6) (2009) 535.
[315] A. Tarasova, P. Hamilton-Brown, T. Gengenbach, H.J. Griesser, L. Meagher, Colloid Probe AFM and XPS Study of Time-Dependent Aging of Amine Plasma Polymer Coatings in Aqueous Media, Plasma Processes and Polymers 5(2) (2008) 175-185.
[316] S.G. Kim, D.S. Lee, S. Lee, J.H. Jang, Osteocalcin/fibronectin-functionalized collagen matrices for bone tissue engineering, Journal of Biomedical Materials Research Part A 103(6) (2015) 2133-2140.
[317] D. Schild, X-ray Photoelectron Spectroscopy, Hydrogen Technology, Springer2008, pp. 575-601.
[318] S. Hüfner, Photoelectron spectroscopy: principles and applications, Springer Science & Business Media2013.
[319] S.E. Glassford, B. Byrne, S.G. Kazarian, Recent applications of ATR FTIR spectroscopy and imaging to proteins, Biochimica et Biophysica Acta (BBA) - Proteins and Proteomics 1834(12) (2013) 2849-2858.
[320] S.G. Kazarian, K.L.A. Chan, ATR-FTIR spectroscopic imaging: recent advances and applications to biological systems, Analyst 138(7) (2013) 1940-1951.

[321] D.Y. Kwok, A.W. Neumann, Contact angle measurement and contact angle interpretation, Advances in Colloid and Interface Science 81(3) (1999) 167-249.
[322] T. Young, III. An essay on the cohesion of fluids, Philosophical Transactions of the Royal Society of London 95 (1805) 65-87.
[323] D.K. Owens, R. Wendt, Estimation of the surface free energy of polymers, Journal of applied polymer science 13(8) (1969) 1741-1747.
[324] J.A. Weil, J.R. Bolton, Electron paramagnetic resonance: elementary theory and practical applications, John Wiley & Sons2007.
[325] K. Danyal, Z.-Y. Yang, L.C. Seefeldt, Electron Paramagnetic Resonance Spectroscopy, in: M.W. Ribbe (Ed.), Nitrogen Fixation: Methods and Protocols, Humana Press, Totowa, NJ, 2011, pp. 191-205.
[326] J.-H. Kwon, H. Shahbaz, J.-J. Ahn, Advanced Electron Paramagnetic Resonance Spectroscopy for the Identification of Irradiated Food, 2014.
[327] A. Michelmore, P. Martinek, V. Sah, R.D. Short, K. Vasilev, Surface Morphology in the Early Stages of Plasma Polymer Film Growth from Amine-Containing Monomers, Plasma Processes and Polymers 8(5) (2011) 367-372.
[328] D. Alsteens, H.E. Gaub, R. Newton, M. Pfreundschuh, C. Gerber, D.J. Müller, Atomic force microscopy-based characterization and design of biointerfaces, Nature Reviews Materials 2 (2017) 17008.
[329] G. Dan, X. Guoxin, L. Jianbin, Mechanical properties of nanoparticles: basics and applications, Journal of Physics D: Applied Physics 47(1) (2014) 013001.
[330] I. Horcas, R. Fernández, J. Gomez-Rodriguez, J. Colchero, J. Gómez-Herrero, A. Baro, WSXM: a software for scanning probe microscopy and a tool for nanotechnology, Review of scientific instruments 78(1) (2007) 013705.
[331] S. Hosseini, P. Vázquez-Villegas, M. Rito-Palomares, S.O. Martinez-Chapa, Step by Step with ELISA: Mechanism of Operation, Crucial Elements, Different Protocols, and Insights on Immobilization and Detection of Various Biomolecular Entities, Enzyme-linked Immunosorbent Assay (ELISA): From A to Z, Springer Singapore, Singapore, 2018, pp. 31-56.
[332] E.M. Czekanska, M.J. Stoddart, J.R. Ralphs, R.G. Richards, J.S. Hayes, A phenotypic comparison of osteoblast cell lines versus human primary osteoblasts for biomaterials testing, Journal of Biomedical Materials Research Part A 102(8) (2014) 2636-2643.
[333] A.D. Bakker, J. Klein-Nulend, Osteoblast Isolation from Murine Calvaria and Long Bones, in: M.H. Helfrich, S.H. Ralston (Eds.), Bone Research Protocols, Humana Press, Totowa, NJ, 2012, pp. 19-29.
[334] H. Zhu, Z.-K. Guo, X.-X. Jiang, H. Li, X.-Y. Wang, H.-Y. Yao, Y. Zhang, N. Mao, A protocol for isolation and culture of mesenchymal stem cells from mouse compact bone, Nature protocols 5 (2010) 550.
[335] V. Borsari, G. Giavaresi, M. Fini, P. Torricelli, M. Tschon, R. Chiesa, L. Chiusoli, A. Salito, A. Volpert, R. Giardino, Comparative in vitro study on a ultra-high roughness and dense titanium coating, Biomaterials 26(24) (2005) 4948-4955.
[336] Y. Zhang, P. Liu, Y.n. Liang, B. Tao, Y. He, Y. Hao, W. Yang, Y. Hu, K. Cai, Investigation of osteogenic responses of Fe-incorporated micro/nano-hierarchical structure on titanium surface, J. Mater. Chem. B (2018) Ahead of Print.
[337] G. Wang, Y. Wan, B. Ren, T. Wang, Z. Liu, Surface Functionalization of Micro/Nanostructured Titanium with Bioactive Ions to Regulate the Behaviors of Murine Osteoblasts, Advanced Engineering Materials 19(11) (2017) 1700299-n/a.
[338] N. Dubey, K. Ellepola, F.E.D. Decroix, J.L.P. Morin, A. Castro Neto, C.J. Seneviratne, V. Rosa, Graphene onto medical grade titanium: an atom-thick multimodal coating that promotes osteoblast maturation and inhibits biofilm formation from distinct species, Nanotoxicology (2018) Ahead of Print.

[339] J. Shi, X. Zhang, S. Qiao, J. Ni, J. Mo, Y. Gu, H. Lai, Enhanced osteointegration of tantalum-modified titanium implants with micro/nano-topography, RSC Adv. 7(73) (2017) 46472-46479.
[340] M. Martínez-Ibáñez, N.S. Murthy, Y. Mao, J. Suay, M. Gurruchaga, I. Goñi, J. Kohn, Enhancement of plasma protein adsorption and osteogenesis of hMSCs by functionalized siloxane coatings for titanium implants, J. Biomed. Mater. Res. Part B Appl. Biomater. (2017).
[341] S.V. Boregowda, V. Krishnappa, D.G. Phinney, Isolation of Mouse Bone Marrow Mesenchymal Stem Cells, in: M. Gnecchi (Ed.), Mesenchymal Stem Cells: Methods and Protocols, Springer New York, New York, NY, 2016, pp. 205-223.
[342] S.K. Nishimoto, M. Nishimoto, S.-W. Park, K.-M. Lee, H.-S. Kim, J.-T. Koh, J.L. Ong, Y. Liu, Y. Yang, The effect of titanium surface roughening on protein absorption, cell attachment, and cell spreading, International Journal of Oral & Maxillofacial Implants 23(4) (2008).
[343] C.A.C. Stewart, B. Akhavan, M. Santos, J. Hung, C.L. Hawkins, B. Bao, S.G. Wise, M.M.M. Bilek, Cellular responses to radical propagation from ion-implanted plasma polymer surfaces, Applied Surface Science.
[344] Y. Su, Y. Zheng, L. Tang, Y.-X. Qin, D. Zhu, Calcium Phosphate Coatings for Metallic Orthopedic Biomaterials, in: B. Li, T. Webster (Eds.), Orthopedic Biomaterials: Advances and Applications, Springer International Publishing, Cham, 2017, pp. 167-183.
[345] S.B. Goodman, Wear particles, periprosthetic osteolysis and the immune system, Biomaterials 28(34) (2007) 5044-5048.
[346] S.R. Paital, N.B. Dahotre, Calcium phosphate coatings for bio-implant applications: Materials, performance factors, and methodologies, Materials Science and Engineering: R: Reports 66(1) (2009) 1-70.
[347] M.E. W., H. A., A. U., Severe osteolysis after third-body wear due to hydroxyapatite particles from acetabular cup coating, The Journal of Bone and Joint Surgery. British volume 80-B(2) (1998) 267-272.
[348] C.A. St. Pierre, M. Chan, Y. Iwakura, D.C. Ayers, E.A. Kurt-Jones, R.W. Finberg, Periprosthetic osteolysis: Characterizing the innate immune response to titanium wear-particles, Journal of Orthopaedic Research 28(11) (2010) 1418-1424.
[349] T.D. Michl, C. Giles, A.T. Cross, H.J. Griesser, B.R. Coad, Facile single-step bioconjugation of the antifungal agent caspofungin onto material surfaces via an epoxide plasma polymer interlayer, RSC Adv. (2017) Ahead of Print.
[350] J. Dorst, M. Vandenbossche, M. Amberg, L. Bernard, P. Rupper, K.-D. Weltmann, K. Fricke, D. Hegemann, Improving the stability of amino-containing plasma polymer films in aqueous environments, Langmuir (2017) Ahead of Print.
[351] K.S. Beckwith, S.P. Cooil, J.W. Wells, P. Sikorski, Tunable high aspect ratio polymer nanostructures for cell interfaces, Nanoscale 7(18) (2015) 8438-8450.
[352] M.-J. Kim, B. Lee, K. Yang, J. Park, S. Jeon, S.H. Um, D.-I. Kim, S.G. Im, S.-W. Cho, BMP-2 peptide-functionalized nanopatterned substrates for enhanced osteogenic differentiation of human mesenchymal stem cells, Biomaterials 34(30) (2013) 7236-7246.
[353] M. Santos, E.C. Filipe, P.L. Michael, J. Hung, S.G. Wise, M.M.M. Bilek, Mechanically Robust Plasma-Activated Interfaces Optimized for Vascular Stent Applications, ACS Appl. Mater. Interfaces 8(15) (2016) 9635-9650.
[354] S.G. Wise, P.L. Michael, A. Waterhouse, M. Santos, E. Filipe, J. Hung, A. Kondyurin, M.M.M. Bilek, M.K.C. Ng, Immobilization of bioactive plasmin reduces the thrombogenicity of metal surfaces, Colloids and Surfaces B: Biointerfaces 136 (2015) 944-954.
[355] M. Santos, M.M.M. Bilek, S.G. Wise, Plasma-synthesised carbon-based coatings for cardiovascular applications, Biosurface and Biotribology 1(3) (2015) 146-160.
[356] L.J. Martin, B. Akhavan, M.M.M. Bilek, Electric fields control the orientation of peptides irreversibly immobilized on radical-functionalized surfaces, Nature Communications 9(1) (2018) 357.

[357] B. Akhavan, T.D. Michl, C. Giles, K. Ho, L. Martin, O. Sharifahmadian, S.G. Wise, B.R. Coad, N. Kumar, H.J. Griesser, M.M. Bilek, Plasma activated coatings with dual action against fungi and bacteria, Applied Materials Today 12 (2018) 72-84.
[358] M.J. Son, T.F. Zhang, Y.J. Jo, K.H. Kim, Enhanced electrochemical properties of the DLC films with an arc interlayer, nitrogen doping and annealing, Surface and Coatings Technology 329 (2017) 77-85.
[359] J. Corona-Gomez, S. Shiri, M. Mohammadtaheri, Q. Yang, Adhesion enhancement of DLC on CoCrMo alloy by diamond and nitrogen incorporation for wear resistant applications, Surface and Coatings Technology 332 (2017) 120-127.
[360] T.F. Zhang, Q.Y. Deng, B. Liu, B.J. Wu, F.J. Jing, Y.X. Leng, N. Huang, Wear and corrosion properties of diamond like carbon (DLC) coating on stainless steel, CoCrMo and Ti6Al4V substrates, Surface and Coatings Technology 273 (2015) 12-19.
[361] S. Flege, R. Hatada, M. Hoefling, A. Hanauer, A. Abel, K. Baba, W. Ensinger, Modification of diamond-like carbon films by nitrogen incorporation via plasma immersion ion implantation, Nuclear Instruments and Methods in Physics Research Section B: Beam Interactions with Materials and Atoms 365 (2015) 357-361.
[362] P. Yang, N. Huang, Y.X. Leng, Z.Q. Yao, H.F. Zhou, M. Maitz, Y. Leng, P.K. Chu, Wettability and biocompatibility of nitrogen-doped hydrogenated amorphous carbon films: Effect of nitrogen, Nuclear Instruments and Methods in Physics Research Section B: Beam Interactions with Materials and Atoms 242(1) (2006) 22-25.
[363] B. Akhavan, K. Jarvis, P. Majewski, Evolution of hydrophobicity in plasma polymerised 1,7-octadiene films, Plasma Processes and Polymers 10(11) (2013) 1018-1029.
[364] B. Akhavan, K. Jarvis, P. Majewski, Development of oxidized sulfur polymer films through a combination of plasma polymerization and oxidative plasma treatment, Langmuir 30(5) (2014) 1444-1454.
[365] D. Melilli, N. Mauceri, Surface treatments for titanium implants, Int. J. Clin. Dent. 8(2) (2015) 139-149.
[366] R. McBeath, D.M. Pirone, C.M. Nelson, K. Bhadriraju, C.S. Chen, Cell Shape, Cytoskeletal Tension, and RhoA Regulate Stem Cell Lineage Commitment, Developmental Cell 6(4) (2004) 483-495.
[367] P. Mazón, D. García-Bernal, L. Meseguer-Olmo, F. Cragnolini, P.N. De Aza, Human mesenchymal stem cell viability, proliferation and differentiation potential in response to ceramic chemistry and surface roughness, Ceramics International 41(5, Part A) (2015) 6631-6644.
[368] T. Hanawa, Research and development of metals for medical devices based on clinical needs, Science and Technology of Advanced Materials 13(6) (2012) 064102.
[369] M. Fischer, M.F. Maitz, C. Werner, 7 - Coatings for biomaterials to improve hemocompatibility A2 - Siedlecki, Christopher A, Hemocompatibility of Biomaterials for Clinical Applications, Woodhead Publishing2018, pp. 163-190.
[370] J. Lahann, D. Klee, H. Thelen, H. Bienert, D. Vorwerk, H. Hocker, Improvement of haemocompatibility of metallic stents by polymer coating, Journal of materials science. Materials in medicine 10(7) (1999) 443-8.
[371] Z. Yang, Y. Yang, K. Xiong, X. Li, P. Qi, Q. Tu, F. Jing, Y. Weng, J. Wang, N. Huang, Nitric oxide producing coating mimicking endothelium function for multifunctional vascular stents, Biomaterials 63(Supplement C) (2015) 80-92.
[372] P. Qi, Y. Yang, S. Zhao, J. Wang, X. Li, Q. Tu, Z. Yang, N. Huang, Improvement of corrosion resistance and biocompatibility of biodegradable metallic vascular stent via plasma allylamine polymerized coating, Materials & Design 96 (2016) 341-349.
[373] M. Mortazavi, M. Nosonovsky, A model for diffusion-driven hydrophobic recovery in plasma treated polymers, Applied Surface Science 258(18) (2012) 6876-6883.

[374] D.P. Dowling, I.S. Miller, M. Ardhaoui, W.M. Gallagher, Effect of Surface Wettability and Topography on the Adhesion of Osteosarcoma Cells on Plasma-modified Polystyrene, Journal of Biomaterials Applications 26(3) (2011) 327-347.
[375] M. Vandenbossche, D. Hegemann, Recent approaches to reduce aging phenomena in oxygen- and nitrogen-containing plasma polymer films: An overview, Current Opinion in Solid State and Materials Science (2018).
[376] B. Akhavan, T.D. Michl, C. Giles, K. Ho, L. Martin, O. Sharifahmadian, S.G. Wise, B.R. Coad, N. Kumar, H.J. Griesser, Plasma activated coatings with dual action against fungi and bacteria, Appl. Mater. Today 12 (2018) 72-84.
[377] Y. Yin, K. Fisher, N.J. Nosworthy, D. Bax, R.J. Clarke, D.R. McKenzie, M.M.M. Bilek, Comparison on protein adsorption properties of diamond-like carbon and nitrogen-containing plasma polymer surfaces, Thin Solid Films 520(7) (2012) 3021-3025.
[378] T. Fukai, M. Ushio-Fukai, Superoxide Dismutases: Role in Redox Signaling, Vascular Function, and Diseases, Antioxidants & Redox Signaling 15(6) (2011) 1583-1606.
[379] G. Filomeni, D. De Zio, F. Cecconi, Oxidative stress and autophagy: the clash between damage and metabolic needs, Cell Death & Differentiation 22(3) (2015) 377-388.
[380] K. Sinha, J. Das, P.B. Pal, P.C. Sil, Oxidative stress: the mitochondria-dependent and mitochondria-independent pathways of apoptosis, Archives of Toxicology 87(7) (2013) 1157-1180.
[381] B. Halliwell, J.M. Gutteridge, Free radicals in biology and medicine, Oxford University Press, USA2015.
[382] F. Wauquier, L. Leotoing, V. Coxam, J. Guicheux, Y. Wittrant, Oxidative stress in bone remodelling and disease, Trends in Molecular Medicine 15(10) (2009) 468-477.
[383] M.J. Jackson, J. Kopac, M. Balazic, D. Bombac, M. Brojan, F. Kosel, Titanium and Titanium Alloy Applications in Medicine, in: W. Ahmed, M.J. Jackson (Eds.), Surgical Tools and Medical Devices, Springer International Publishing, Cham, 2016, pp. 475-517.
[384] S. Ferraris, A. Vitale, E. Bertone, S. Guastella, C. Cassinelli, J. Pan, S. Spriano, Multifunctional commercially pure titanium for the improvement of bone integration: Multiscale topography, wettability, corrosion resistance and biological functionalization, Materials Science and Engineering: C 60 (2016) 384-393.
[385] E. Kosobrodova, A. Kondyurin, D.R. McKenzie, M.M.M. Bilek, Kinetics of post-treatment structural transformations of nitrogen plasma ion immersion implanted polystyrene, Nuclear Instruments and Methods in Physics Research Section B: Beam Interactions with Materials and Atoms 304 (2013) 57-66.
[386] E.A. Wakelin, M.J. Davies, M.M.M. Bilek, D.R. McKenzie, Temperature Activated Diffusion of Radicals through Ion Implanted Polymers, ACS Appl. Mater. Interfaces 7(47) (2015) 26340-26345.
[387] G.L. Pierre-Luc, D.P. M., G. Thomas, W. Thomas, U.W.E. S., Chemical Characterization of the Long-Term Ageing of Nitrogen-Rich Plasma Polymer Films under Various Ambient Conditions, Plasma Processes and Polymers 10(4) (2013) 388-395.
[388] F. Truica-Marasescu, P.-L. Girard-Lauriault, A. Lippitz, W.E.S. Unger, M.R. Wertheimer, Nitrogen-rich plasma polymers: Comparison of films deposited in atmospheric- and low-pressure plasmas, Thin Solid Films 516(21) (2008) 7406-7417.
[389] J. Coates, Interpretation of infrared spectra, a practical approach, Encyclopedia of analytical chemistry (2000).
[390] M. Santos, P.L. Michael, E.C. Filipe, A.H.P. Chan, J. Hung, R.P. Tan, B.S.L. Lee, M. Huynh, C. Hawkins, A. Waterhouse, M.M.M. Bilek, S.G. Wise, Plasma Synthesis of Carbon-Based Nanocarriers for Linker-Free Immobilization of Bioactive Cargo, ACS Applied Nano Materials (2018).
[391] A. Choukourov, H. Biederman, D. Slavinska, L. Hanley, A. Grinevich, H. Boldyryeva, A. Mackova, Mechanistic Studies of Plasma Polymerization of Allylamine, The Journal of Physical Chemistry B 109(48) (2005) 23086-23095.

[392] A. Manakhov, P. Kiryukhantsev-Korneev, M. Michlicek, E. Permyakova, E. Dvorakova, J. Polcak, Z. Popov, M. Visotin, D.V. Shtansky, Grafting of carboxyl groups using CO2/C2H4/Ar pulsed plasma: Theoretical modeling and XPS derivatization, Appl. Surf. Sci. 435 (2018) 1220-1227.
[393] M. Vandenbossche, D. Hegemann, Recent approaches to reduce aging phenomena in oxygen- and nitrogen-containing plasma polymer films: An overview, Current Opinion in Solid State and Materials Science 22(1) (2018) 26-38.
[394] E. Sardella, R. Gristina, A. Milella, R. d'Agostino, P. Favia, Functionalization of Biomedical Polymers by Means of Plasma Processes: Plasma Treated Polymers with Limited Hydrophobic Recovery and PE-CVD of -COOH Functional Coatings, Journal of Photopolymer Science and Technology 15(2) (2002) 341-350.
[395] V. Jokinen, P. Suvanto, S. Franssila, Oxygen and nitrogen plasma hydrophilization and hydrophobic recovery of polymers, Biomicrofluidics 6(1) (2012) 016501-016501-10.
[396] J. Dorst, M. Vandenbossche, M. Amberg, L. Bernard, P. Rupper, K.D. Weltmann, K. Fricke, D. Hegemann, Improving the Stability of Amino-Containing Plasma Polymer Films in Aqueous Environments, Langmuir 33(40) (2017) 10736-10744.
[397] E.A. Kosobrodova, A.V. Kondyurin, K. Fisher, W. Moeller, D.R. McKenzie, M.M.M. Bilek, Free radical kinetics in a plasma immersion ion implanted polystyrene: Theory and experiment, Nuclear Instruments and Methods in Physics Research Section B: Beam Interactions with Materials and Atoms 280 (2012) 26-35.
[398] M. Haupt, J. Barz, C. Oehr, Creation and Recombination of Free Radicals in Fluorocarbon Plasma Polymers: An Electron Spin Resonance Study, Plasma Processes and Polymers 5(1) (2008) 33-43.
[399] W.A. Prütz, F. Siebert, J. Butler, E.J. Land, A. Menez, T. Montenay-Garestier, Charge transfer in peptides: Intramolecular radical transformations involving methionine, tryptophan and tyrosine, Biochimica et Biophysica Acta (BBA) - Protein Structure and Molecular Enzymology 705(2) (1982) 139-149.
[400] C.L. Hawkins, M.J. Davies, Generation and propagation of radical reactions on proteins, Biochimica et Biophysica Acta (BBA) - Bioenergetics 1504(2) (2001) 196-219.
[401] Y. Yin, M.M.M. Bilek, D.R. McKenzie, Direct Evidence of Covalent Immobilisation of Microperoxidase-11 on Plasma Polymer Surfaces, Plasma Processes and Polymers 7(8) (2010) 708-714.
[402] B.M. Scicchitano, L. Pelosi, G. Sica, A. Musarò, The physiopathologic role of oxidative stress in skeletal muscle, Mechanisms of Ageing and Development (2017).
[403] E. Vandenberg, H. Elwing, A. Askendal, I. Lundström, Protein immobilization of 3-aminopropyl triethoxy silaneglutaraldehyde surfaces: Characterization by detergent washing, Journal of Colloid and Interface Science 143(2) (1991) 327-335.
[404] W. Zimmerli, P. Sendi, Orthopaedic biofilm infections, APMIS 125(4) (2017) 353-364.
[405] L. Drago, Modern Approach to Biofilm-related Orthopaedic Implant Infections, Springer2017.
[406] S. Cometa, M.A. Bonifacio, F. Baruzzi, S. de Candia, M.M. Giangregorio, L.C. Giannossa, M. Dicarlo, M. Mattioli-Belmonte, L. Sabbatini, E. De Giglio, Silver-loaded chitosan coating as an integrated approach to face titanium implant-associated infections: analytical characterization and biological activity, Analytical and Bioanalytical Chemistry 409(30) (2017) 7211-7221.
[407] M. Sartori, G. Giavaresi, A. Parrilli, A. Ferrari, N.N. Aldini, M. Morra, C. Cassinelli, D. Bollati, M. Fini, Collagen type I coating stimulates bone regeneration and osteointegration of titanium implants in the osteopenic rat, International Orthopaedics 39(10) (2015) 2041-2052.
[408] H.P. Felgueiras, A. Decambron, M. Manassero, L. Tulasne, M.D.M. Evans, V. Viateau, V. Migonney, Bone tissue response induced by bioactive polymer functionalized Ti6Al4V surfaces: In vitro and in vivo study, Journal of Colloid and Interface Science 491 (2017) 44-54.
[409] I. Brigaud, R. Agniel, J. Leroy-Dudal, S. Kellouche, A. Ponche, T. Bouceba, N. Mihailescu, M. Sopronyi, E. Viguier, C. Ristoscu, F. Sima, I.N. Mihailescu, A.C.O. Carreira, M.C. Sogayar, O. Gallet, K.

Anselme, Synergistic effects of BMP-2, BMP-6 or BMP-7 with human plasma fibronectin onto hydroxyapatite coatings: A comparative study, Acta Biomaterialia 55 (2017) 481-492.
[410] X. Chen, P. Sevilla, C. Aparicio, Surface biofunctionalization by covalent co-immobilization of oligopeptides, Colloids and Surfaces B: Biointerfaces 107 (2013) 189-197.
[411] C. Mas-Moruno, 3 - Surface functionalization of biomaterials for bone tissue regeneration and repair A2 - Barbosa, Mário A, in: M.C.L. Martins (Ed.), Peptides and Proteins as Biomaterials for Tissue Regeneration and Repair, Woodhead Publishing2018, pp. 73-100.
[412] R. Fraioli, K. Dashnyam, J.H. Kim, R.A. Perez, H.W. Kim, J. Gil, M.P. Ginebra, J.M. Manero, C. Mas-Moruno, Surface guidance of stem cell behavior: Chemically tailored co-presentation of integrin-binding peptides stimulates osteogenic differentiation in vitro and bone formation in vivo, Acta Biomaterialia 43 (2016) 269-281.
[413] K. Yu, C. Liu, B.-G. Kim, D.-Y. Lee, Synthetic fusion protein design and applications, Biotechnology Advances 33(1) (2015) 155-164.
[414] M. Hoyos-Nogués, F. Velasco, M.-P. Ginebra, J.M. Manero, F.J. Gil, C. Mas-Moruno, Regenerating Bone via Multifunctional Coatings: The Blending of Cell Integration and Bacterial Inhibition Properties on the Surface of Biomaterials, ACS Appl. Mater. Interfaces 9(26) (2017) 21618-21630.
[415] C. Mas-Moruno, R. Fraioli, F. Albericio, J.M. Manero, F.J. Gil, Novel Peptide-Based Platform for the Dual Presentation of Biologically Active Peptide Motifs on Biomaterials, ACS Appl. Mater. Interfaces 6(9) (2014) 6525-6536.
[416] S. Lee, D.-S. Lee, I. Choi, L. Pham, J.-H. Jang, Design of an Osteoinductive Extracellular Fibronectin Matrix Protein for Bone Tissue Engineering, Int. J. Mol. Sci. 16(4) (2015) 7672.
[417] C. Pan, Y. Hu, Y. Hou, T. Liu, Y. Lin, W. Ye, Y. Hou, T. Gong, Corrosion resistance and biocompatibility of magnesium alloy modified by alkali heating treatment followed by the immobilization of poly (ethylene glycol), fibronectin and heparin, Materials Science and Engineering: C 70 (2017) 438-449.
[418] M. Ferron, J. Wei, T. Yohizawa, P. Ducy, G. Karsenty, AN ELISA-BASED METHOD TO QUANTIFY OSTEOCALCIN CARBOXYLATION IN MICE, Biochemical and biophysical research communications 397(4) (2010) 691-696.
[419] H.J. Kim, J.S. Park, S.W. Yi, H.J. Oh, J.-H. Kim, K.-H. Park, Sequential transfection of RUNX2/SP7 and ATF4 coated onto dexamethasone-loaded nanospheresenhances osteogenesis, Scientific Reports 8 (2018) 1447.
[420] S.L. Booth, A. Centi, S.R. Smith, C. Gundberg, The role of osteocalcin in human glucose metabolism: marker or mediator?, Nature Reviews Endocrinology 9 (2012) 43.
[421] P. Huetz, V. Ball, J.C. Voegel, P. Schaaf, Exchange Kinetics for a Heterogeneous Protein System on a Solid Surface, Langmuir 11(8) (1995) 3145-3152.
[422] V.E. Koteliansky, M.A. Glukhova, M.V. Benjamin, V.N. Smirnov, V.V. Filimonov, O.M. Zalite, S.Y. Venyaminov, A Study of the Structure of Fibronectin, European Journal of Biochemistry 119(3) (1981) 619-624.
[423] C.R. Arciola, D. Campoccia, G.D. Ehrlich, L. Montanaro, Biofilm-Based Implant Infections in Orthopaedics, in: G. Donelli (Ed.), Biofilm-based Healthcare-associated Infections: Volume I, Springer International Publishing, Cham, 2015, pp. 29-46.
[424] Y. Li, S. Wei, J. Wu, J. Jasensky, C. Xi, H. Li, Y. Xu, Q. Wang, E.N.G. Marsh, C.L. Brooks, Z. Chen, Effects of Peptide Immobilization Sites on the Structure and Activity of Surface-Tethered Antimicrobial Peptides, The Journal of Physical Chemistry C 119(13) (2015) 7146-7155.
[425] B.e. Nie, H. Ao, J. Zhou, T. Tang, B. Yue, Biofunctionalization of titanium with bacitracin immobilization shows potential for anti-bacteria, osteogenesis and reduction of macrophage inflammation, Colloids and Surfaces B: Biointerfaces 145 (2016) 728-739.
[426] S. Kucharíková, E. Gerits, K. De Brucker, A. Braem, K. Ceh, G. Majdič, T. Španič, E. Pogorevc, N. Verstraeten, H. Tournu, N. Delattin, F. Impellizzeri, M. Erdtmann, A. Krona, M. Lövenklev, M. Knezevic, M. Fröhlich, J. Vleugels, M. Fauvart, W.J. de Silva, K. Vandamme, J. Garcia-Forgas, B.P.A.

Cammue, J. Michiels, P. Van Dijck, K. Thevissen, Covalent immobilization of antimicrobial agents on titanium prevents Staphylococcus aureus and Candida albicans colonization and biofilm formation, Journal of Antimicrobial Chemotherapy 71(4) (2016) 936-945.
[427] A. Braem, K. De Brucker, N. Delattin, M.S. Killian, M.B.J. Roeffaers, T. Yoshioka, S. Hayakawa, P. Schmuki, B.P.A. Cammue, S. Virtanen, K. Thevissen, B. Neirinck, Alternating Current Electrophoretic Deposition for the Immobilization of Antimicrobial Agents on Titanium Implant Surfaces, ACS Appl. Mater. Interfaces 9(10) (2017) 8533-8546.
[428] T.E.L. Douglas, S. Kumari, K. Dziadek, M. Dziadek, A. Abalymov, P. Cools, G. Brackman, T. Coenye, R. Morent, M.K. Mohan, A.G. Skirtach, Titanium surface functionalization with coatings of chitosan and polyphenol-rich plant extracts, Materials Letters 196 (2017) 213-216.
[429] S. Zeng, J. Ye, Z. Cui, J. Si, Q. Wang, X. Wang, K. Peng, W. Chen, Surface biofunctionalization of three-dimensional porous poly(lactic acid) scaffold using chitosan/OGP coating for bone tissue engineering, Materials Science and Engineering: C 77 (2017) 92-101.
[430] M. Li, D. Mitra, E.-T. Kang, T. Lau, E. Chiong, K.G. Neoh, Thiol-ol Chemistry for Grafting of Natural Polymers to Form Highly Stable and Efficacious Antibacterial Coatings, ACS Appl. Mater. Interfaces 9(2) (2017) 1847-1857.
[431] R.R. Silva, K.Y. Avelino, K.L. Ribeiro, O.L. Franco, M.D. Oliveira, C.A. Andrade, Chemical immobilization of antimicrobial peptides on biomaterial surfaces, Frontiers in bioscience (Scholar edition) 8 (2016) 129-42.
[432] G. Wang, X. Li, Z. Wang, APD3: the antimicrobial peptide database as a tool for research and education, Nucleic Acids Res 44(D1) (2016) D1087-93.
[433] M. Cloutier, D. Mantovani, F. Rosei, Antibacterial Coatings: Challenges, Perspectives, and Opportunities, Trends in Biotechnology 33(11) (2015) 637-652.
[434] J. Gallo, M. Holinka, C. Moucha, Antibacterial Surface Treatment for Orthopaedic Implants, Int. J. Mol. Sci. 15(8) (2014) 13849.
[435] C. Linsley, B. Wu, B. Tawil, The Effect of Fibrinogen, Collagen Type I, and Fibronectin on Mesenchymal Stem Cell Growth and Differentiation into Osteoblasts, Tissue Engineering Part A 19(11-12) (2013) 1416-1423.
[436] J. Folkert, A. Meresta, T. Gaber, K. Miksch, F. Buttgereit, J. Detert, N. Pischon, K. Gurzawska, Nanocoating with plant-derived pectins activates osteoblast response in vitro, International Journal of Nanomedicine 12 (2017) 239-249.
[437] W. Fang, S. Zhao, F. He, L. Liu, G. Yang, Influence of Simvastatin-Loaded Implants on Osseointegration in an Ovariectomized Animal Model, BioMed Research International 2015 (2015) 831504.
[438] Z.G. Karaji, B. Houshmand, S. Abbasi, S. Shafiei, S. Faghihi, Biofunctionalization of Titanium Granules with Simvastatin for Improving Osteogenic Activity and Antibacterial Properties (Ex Vivo Study), INTERNATIONAL JOURNAL OF ORAL & MAXILLOFACIAL IMPLANTS 32(6) (2017) 1266-1272.
[439] M.-H. Ho, C.-J. Yao, M.-H. Liao, P.-I. Lin, S.-H. Liu, R.-M. Chen, Chitosan nanofiber scaffold improves bone healing via stimulating trabecular bone production due to upregulation of the Runx2/osteocalcin/alkaline phosphatase signaling pathway, International Journal of Nanomedicine 10 (2015) 5941-5954.
[440] F. Ruan, Q. Zheng, J. Wang, Mechanisms of bone anabolism regulated by statins, Bioscience Reports 32(6) (2012) 511-519.
[441] A.G. Gristina, P. Naylor, Q. Myrvik, Infections from biomaterials and implants: a race for the surface, Med Prog Technol 14(3-4) (1988) 205-224.
[442] V.T.H. Pham, V.K. Truong, A. Orlowska, S. Ghanaati, M. Barbeck, P. Booms, A.J. Fulcher, C.M. Bhadra, R. Buividas, V. Baulin, C.J. Kirkpatrick, P. Doran, D.E. Mainwaring, S. Juodkazis, R.J. Crawford, E.P. Ivanova, “Race for the Surface”: Eukaryotic Cells Can Win, ACS Appl. Mater. Interfaces 8(34) (2016) 22025-22031.
[443] W. Li, J. Zhou, Y. Xu, Study of the in vitro cytotoxicity testing of medical devices, Biomedical Reports 3(5) (2015) 617-620.

[444] P. Rezvanian, R. Daza, P.A. López, M. Ramos, D. González-Nieto, M. Elices, G.V. Guinea, J. Pérez-Rigueiro, Enhanced Biological Response of AVS-Functionalized Ti-6Al-4V Alloy through Covalent Immobilization of Collagen, Scientific Reports 8(1) (2018) 3337.
[445] J. Ran, H. Zeng, J. Cai, P. Jiang, P. Yan, L. Zheng, Y. Bai, X. Shen, B. Shi, H. Tong, Rational design of a stable, effective, and sustained dexamethasone delivery platform on a titanium implant: An innovative application of metal organic frameworks in bone implants, Chem. Eng. J. (Amsterdam, Neth.) 333 (2018) 20-33.
[446] C.J. da Costa Fernandes, M.R. Ferreira, F.J.B. Bezerra, W.F. Zambuzzi, Zirconia stimulates ECM-remodeling as a prerequisite to pre-osteoblast adhesion/proliferation by possible interference with cellular anchorage, Journal of Materials Science: Materials in Medicine 29(4) (2018) 41.
[447] Z. Gorgin Karaji, M. Speirs, S. Dadbakhsh, J.P. Kruth, H. Weinans, A.A. Zadpoor, S. Amin Yavari, Additively Manufactured and Surface Biofunctionalized Porous Nitinol, ACS Appl. Mater. Interfaces 9(2) (2017) 1293-1304.
[448] H.P. Felgueiras, M.D.M. Evans, V. Migonney, Contribution of fibronectin and vitronectin to the adhesion and morphology of MC3T3-E1 osteoblastic cells to poly(NaSS) grafted Ti6Al4V, Acta Biomaterialia 28 (2015) 225-233.
[449] E. Yoshida, Y. Yoshimura, M. Uo, M. Yoshinari, T. Hayakawa, Influence of nanometer smoothness and fibronectin immobilization of titanium surface on MC3T3-E1 cell behavior, Journal of Biomedical Materials Research Part A 100A(6) (2012) 1556-1564.
[450] M. Lu, D. Shao, P. Wang, D. Chen, Y. Zhang, M. Li, J. Zhao, Y. Zhou, Enhanced osteoblast adhesion on amino-functionalized titanium surfaces through combined plasma enhanced chemical vapor deposition (PECVD) method, RSC Advances 6(86) (2016) 82688-82697.
[451] F. Asghari Sana, M. Çapkın Yurtsever, G. Kaynak Bayrak, E.Ö. Tunçay, A.S. Kiremitçi, M. Gümüşderelioğlu, Spreading, proliferation and differentiation of human dental pulp stem cells on chitosan scaffolds immobilized with RGD or fibronectin, Cytotechnology 69(4) (2017) 617-630.
[452] K.A. Kilian, B. Bugarija, B.T. Lahn, M. Mrksich, Geometric cues for directing the differentiation of mesenchymal stem cells, Proceedings of the National Academy of Sciences 107(11) (2010) 4872.
[453] G.C. Reilly, A.J. Engler, Intrinsic extracellular matrix properties regulate stem cell differentiation, Journal of Biomechanics 43(1) (2010) 55-62.
[454] Q.P. Pham, F. Kurtis Kasper, L. Scott Baggett, R.M. Raphael, J.A. Jansen, A.G. Mikos, The influence of an in vitro generated bone-like extracellular matrix on osteoblastic gene expression of marrow stromal cells, Biomaterials 29(18) (2008) 2729-2739.
[455] M. Baroncelli, B.C. van der Eerden, Y.-Y. Kan, R.D. Alves, J.A. Demmers, J. van de Peppel, J.P. van Leeuwen, Comparative proteomic profiling of human osteoblast-derived extracellular matrices identifies proteins involved in mesenchymal stromal cell osteogenic differentiation and mineralization, Journal of Cellular Physiology 233(1) (2018) 387-395.
[456] F. Kahles, H.M. Findeisen, D. Bruemmer, Osteopontin: A novel regulator at the cross roads of inflammation, obesity and diabetes, Molecular Metabolism 3(4) (2014) 384-393.
[457] G. Karsenty, M. Ferron, The contribution of bone to whole-organism physiology, Nature 481(7381) (2012) 314-320.
[458] A. Mizokami, T. Kawakubo-Yasukochi, M. Hirata, Osteocalcin and its endocrine functions, Biochemical pharmacology (2017).
[459] S. Takeshita, R. Kikuno, K. Tezuka -i, E. Amann, Osteoblast-specific factor 2: Cloning of a putative bone adhesion protein with homology with the insect protein fasciclin I, BIOCHEM. J. 294(1) (1993) 271-278.
[460] K. Horiuchi, N. Amizuka, S. Takeshita, H. Takamatsu, M. Katsuura, H. Ozawa, Y. Toyama, L.F. Bonewald, A. Kudo, Identification and Characterization of a Novel Protein, Periostin, with Restricted Expression to Periosteum and Periodontal Ligament and Increased Expression by Transforming Growth Factor β, Journal of Bone and Mineral Research 14(7) (1999) 1239-1249.

[461] N. Bonnet, S.J. Conway, S.L. Ferrari, Regulation of beta catenin signaling and parathyroid hormone anabolic effects in bone by the matricellular protein periostin, Proceedings of the National Academy of Sciences 109(37) (2012) 15048-15053.
[462] M. Nagaoka, H.-L. Jiang, T. Hoshiba, T. Akaike, C.-S. Cho, Application of Recombinant Fusion Proteins for Tissue Engineering, Annals of Biomedical Engineering 38(3) (2010) 683-693.
[463] S. Gomes, I.B. Leonor, J.F. Mano, R.L. Reis, D.L. Kaplan, Spider silk-bone sialoprotein fusion proteins for bone tissue engineering, Soft Matter 7(10) (2011) 4964-4973.
[464] A. Groß, C. Hashimoto, H. Sticht, J. Eichler, Synthetic Peptides as Protein Mimics, Frontiers in Bioengineering and Biotechnology 3 (2015) 211.
[465] R.V.F. Paulino, S. Saboohi, A. Michelmore, The chemistry of organophosphate thin film coatings from low pressure plasma and the effect of the substrate on adhesion, Plasma Processes Polym. (2017) Ahead of Print.
[466] H. Fukuda, Additive Manufacturing Technology for Orthopedic Implants, in: M. Niinomi, T. Narushima, M. Nakai (Eds.), Advances in Metallic Biomaterials: Processing and Applications, Springer Berlin Heidelberg, Berlin, Heidelberg, 2015, pp. 3-26.
[467] K. Pałka, R. Pokrowiecki, Porous Titanium Implants: A Review, Advanced Engineering Materials 20(5) (2018) 1700648.
[468] H. Attar, S. Ehtemam-Haghighi, D. Kent, M.S. Dargusch, Recent developments and opportunities in additive manufacturing of titanium-based matrix composites: A review, International Journal of Machine Tools and Manufacture 133 (2018) 85-102.
[469] G. Stevenson, S. Rehman, E. Draper, E. Hernández-Nava, J. Hunt, J.W. Haycock, Combining 3D human in vitro methods for a 3Rs evaluation of novel titanium surfaces in orthopaedic applications, Biotechnology and Bioengineering 113(7) (2016) 1586-1599.
[470] L. Vi, G.S. Baht, H. Whetstone, A. Ng, Q. Wei, R. Poon, S. Mylvaganam, M. Grynpas, B.A. Alman, Macrophages Promote Osteoblastic Differentiation In Vivo: Implications in Fracture Repair and Bone Homeostasis, Journal of Bone and Mineral Research 30(6) (2015) 1090-1102.
[471] J.W. Haycock, 3D Cell Culture: A Review of Current Approaches and Techniques, in: J.W. Haycock (Ed.), 3D Cell Culture: Methods and Protocols, Humana Press, Totowa, NJ, 2011, pp. 1-15.

Appendix

Permission/ licences to reprint

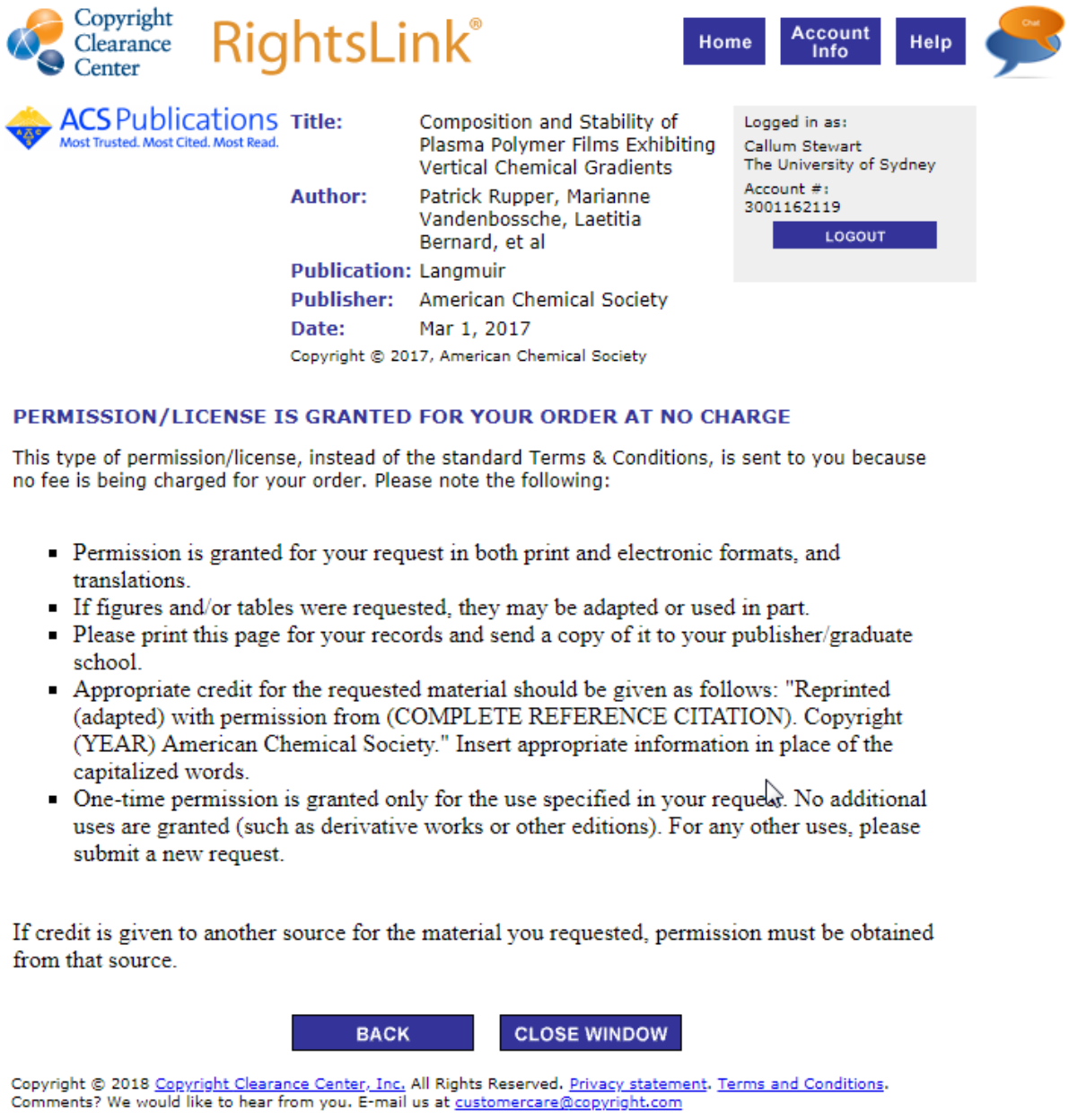

Copyright Clearance Center RightsLink®

Home | Account Info | Help

ACS Publications
Most Trusted. Most Cited. Most Read.

Title: Composition and Stability of Plasma Polymer Films Exhibiting Vertical Chemical Gradients
Author: Patrick Rupper, Marianne Vandenbossche, Laetitia Bernard, et al
Publication: Langmuir
Publisher: American Chemical Society
Date: Mar 1, 2017
Copyright © 2017, American Chemical Society

Logged in as:
Callum Stewart
The University of Sydney
Account #:
3001162119
LOGOUT

PERMISSION/LICENSE IS GRANTED FOR YOUR ORDER AT NO CHARGE

This type of permission/license, instead of the standard Terms & Conditions, is sent to you because no fee is being charged for your order. Please note the following:

- Permission is granted for your request in both print and electronic formats, and translations.
- If figures and/or tables were requested, they may be adapted or used in part.
- Please print this page for your records and send a copy of it to your publisher/graduate school.
- Appropriate credit for the requested material should be given as follows: "Reprinted (adapted) with permission from (COMPLETE REFERENCE CITATION). Copyright (YEAR) American Chemical Society." Insert appropriate information in place of the capitalized words.
- One-time permission is granted only for the use specified in your request. No additional uses are granted (such as derivative works or other editions). For any other uses, please submit a new request.

If credit is given to another source for the material you requested, permission must be obtained from that source.

BACK | CLOSE WINDOW

Copyright © 2018 Copyright Clearance Center, Inc. All Rights Reserved. Privacy statement. Terms and Conditions.
Comments? We would like to hear from you. E-mail us at customercare@copyright.com

Title: Plasma-Activated Tropoelastin Functionalization of Zirconium for Improved Bone Cell Response

Author: Giselle C. Yeo, Miguel Santos, Alexey Kondyurin, et al

Publication: ACS Biomaterials Science & Engineering

Publisher: American Chemical Society

Date: Apr 1, 2016

PERMISSION/LICENSE IS GRANTED FOR YOUR ORDER AT NO CHARGE

This type of permission/license, instead of the standard Terms & Conditions, is sent to you because no fee is being charged for your order. Please note the following:

- Permission is granted for your request in both print and electronic formats, and translations.
- If figures and/or tables were requested, they may be adapted or used in part.
- Please print this page for your records and send a copy of it to your publisher/graduate school.
- Appropriate credit for the requested material should be given as follows: "Reprinted (adapted) with permission from (COMPLETE REFERENCE CITATION). Copyright (YEAR) American Chemical Society." Insert appropriate information in place of the capitalized words.
- One-time permission is granted only for the use specified in your request. No additional uses are granted (such as derivative works or other editions). For any other uses, please submit a new request.

If credit is given to another source for the material you requested, permission must be obtained from that source.